Development of a Novel Interim Bulk Fuel Storage Facility for the PBMR

W.F. Fuls M. Eng

A thesis submitted in fulfilment of the requirements for the degree Philisophiae Doctor in Engineering at the University of the North West

Supervisor : Prof. M. Kleingeld

November 2004

Potchefstroom

ABSTRACT

The PBMR is the first High Temperature Reactor being designed for commercial power generation in South Africa. It makes use of spherical fuel elements, containing coated uranium oxide particles encapsulated in a graphite matrix. The spent fuel generated from the reactor is stored in a storage system before final disposal.

Such storage systems are called interim storage facilities, and normally make use of small transportable containers. The PBMR design makes use of bulk storage containers, capable of holding more than half a million spent fuel spheres. This is a unique concept for nuclear spent fuel storage. Also, most nuclear reactors make use of an intermediate cooling pool before the fuel is transferred to the storage facility. For the PBMR, the spent fuel is discharged directly into the interim storage facility, thus eliminating the intermediate cooling pool.

All interim storage facilities have to comply with five basic requirements, namely: fuel sub-criticality; decay heat removal; radioactive material containment; fuel integrity protection; and radiation protection of the workers and the public. The solution for each requirement depends upon the type of fuel, as well as the philosophical criteria of the reactor design. For the PBMR, it involves a storage life of 80 years, passive cooling and bulk storage tanks. In addition to the basic requirements, the PBMR storage facility should also be able to store used fuel during reactor maintenance, and to transfer it back to the reactor or to another storage tank when required.

During the four years of the development of the storage system, the design has undergone several changes. These changes were brought on by changes of the reactor design, and also due to developments and improvements on immature areas. The result is an integrated solution, retaining virtually none of the original concept, but still complying with all requirements.

The containment design solution is a vertically suspended ASME VIII pressure vessel (or storage tank) with a loading point and an unloading device. All radioactive material is captured inside the pressure boundary, and the tank is completely sealed off when not in use. New devices were developed to systematically load the tank, and to remove the spheres from the tank. Scale tests were done to verify the performance of the new devices and to ensure proper sphere flow inside the tank.

Sub-criticality of the fuel volume is achieved by adding hollow tubes to the inside of the storage tank, thereby creating a sub-critical geometry. Burn-up credit is also taken for the fuel at 20% below the average core burn-up. The fuel is therefore passively safe even if the full contents of the reactor is transferred into a storage tank.

In order to ensure that the tank lasts for 80 years in a cost-effective manner, the tanks are cooled in a closed loop system. The closed loop air is continuously dried to a very low relative humidity, which minimises corrosion on even normal carbon steel. Corrosion tests have been performed to investigate the effect of radiolysis products that may build up in the closed loop. These tests are still under way.

The decay heat is removed from the fuel spheres by means of air convection around the tank surface. The tubes inside the tank also allow air to pass through, creating a very strong chimney effect. A new method was developed to calculate the fuel temperatures for a given cooling flow. The technique makes use of FEA and analytical equations. Solutions are obtained at a fraction of the time it takes to perform a full CFD analysis, and within 5% compared to CFD results. Full-scale tests are planned to measure and verify the heat

transfer properties of the cooling tubes in order to boost the credibility of the FEA and CFD analyses.

The storage tank design is integrated into a storage unit, which performs all the nuclear functions. The storage unit can operate in four different cooling modes, namely closed loop active cooling; open loop passive cooling; open loop active cooling and closed loop conditioning. There is an automatic fallback from the active cooling mode to a passive cooling mode. The active cooling is thus only needed to prevent excessive corrosion of the tanks. A scale model has been built to demonstrate the passive cooling ability of a storage unit, and the results agree well with CFD analyses. Also, a new method was developed to calculate the passive cooling characteristics using pipe network simulation software. This method is significantly faster than CFD analyses, and allows one to easily incorporate fan characteristics and to perform sensitivity studies.

Twelve storage units make up the Sphere Storage System of the PBMR. An intricate sphere pipe system allows one to transfer fuel spheres from the reactor to any tank, from any tank back to the reactor or to another tank, or to a decommissioning cask. All maintenance intensive components are placed at accessible areas, thus protecting the workers from the radiation coming from the tanks. Measures are incorporated to detect any contamination leakage, and also to enable the IAEA to verify the nuclear inventory of the storage system.

The Sphere Storage System is a fully integrated, yet modular design that complies with all nuclear and process requirements. It presents a unique solution to the interim fuel storage of the PBMR, and is believed to be a cost-effective solution for 80 years of storage. Some future tests and developments are required to finalise immature areas, but overall, the system is sufficiently engineered such that detail design can continue.

SAMEVATTING

Die PBMR is die eerste Hoë Temperatuur Reaktor wat ontwikkel word vir kommersiële elektrisiteitsgenerasie in Suid Afrika. Dit maak gebruik van sferiese brandstofelemente met bedekte uraanoksied partikels, vasgevang in 'n grafiet matriks. Die verbruikte brandstof wat deur die reaktor gegenereer word, word in 'n stoorstelsel gehou tot met finale wegdoening.

Sulke stoorstelsels word interim stoorstelsels genoem, en maak normaalweg gebruik van vervoerbare houers. Die PBMR ontwerp maak gebruik van grootmaat stoortenks wat elk meer as 'n half miljoen verbruikte brandstof kan stoor. Hierdie is 'n unieke konsep vir die stoor van verbruikte kernbrandstof. Meeste ander kernreaktore gebruik 'n afkoelpoel voordat die brandstof geskuif word na die stoorstelsel. Die verbruikte brandstof van die PBMR gaan egter direk na die interim stoorfasiliteit, en skakel daardeur die afkoelpoel stap uit.

Alle interim stoorfasiliteite moet aan vyf basiese vereistes voldoen, naamlik: brandstof sub-kritikaliteit; verval-hitte verwydering; radio-aktiewe materiaal inperking; behoud van die brandstof integriteit; en stralingsbeskerming van die werkers en die publiek. Die oplossing vir elke vereiste hang van die tipe brandstof af, asook filosofiese kriteria aangaande die ontwerp van die reaktor. Dit behels vir die PBMR 'n stoortyd van 80 jaar, passiewe verkoeling en grootmaat stoortenks. Saam met die basiese vereistes moet die PBMR stoorstelsel ook gebruikte brandstof kan stoor tydens reaktor-instandhouding, en moet dit dan kan terugstuur na die reaktor of 'n ander tenk indien nodig.

Die stoorstelsel het verskeie veranderinge ondergaan gedurende die vier jaar van ontwikkeling. Hierdie veranderinge is veroorsaak deur veranderinge in die reaktor ontwerp, asook ontwikkelinge en verbeteringe van onryp areas. Die resultaat is 'n geïntegreerde ontwerp wat feitlik niks oorgehou het van die oorspronklike konsep nie, maar wat steeds aan al die vereistes voldoen.

Die ontwerpsoplossing vir die inperking is 'n vertikaal gesuspendeerde ASME VIII drukhouer (of stoortenk) met 'n laaipunt en ontlaaitoestel. Alle radio-aktiewe materiaal word vasgevang binne die drukgrens, en die tenk word volledig afgesëel wanneer nie in gebruik nie. Nuwe toestelle is ontwikkel om die sfere sistematies in die tenk te laai, en uit die tenk te verwyder. Skaaltoetse is gedoen om die toestelle se werkverrigting te verifieer en om behoorlike sfeervloei in die tenk te verseker.

Sub-kritikaliteit van die brandstof word verkry met hol buise binne-in die tenk wat daardeur 'n sub-kritiese geometrie skep. Krediet vir die afbrand word geneem op 20% laer as die gemiddelde reaktor hart afbrand. Die brandstof is dus passief veilig selfs al word die volle inhoud van die reaktor in die stoortenk gelaai.

Ten einde 'n tenkleeftyd van 80 jaar op 'n koste-effektiewe manier te kry, word die tenks in 'n geslote lus verkoel. Die lug in die geslote lus word kontinu uitgedroog tot 'n baie lae relatiewe humiditeit, wat die korrosie op selfs gewone koolstofstaal minimeer. Korrosietoetse is gedoen om die effek van die radiolise produkte wat in die lug vorm te ondersoek. Hierdie toetse is steeds aan die gang.

Die verval-hitte word verwyder deur lugkonveksie rondom die tenk oppervlak. Die buise deur die tenk laat ook lug deur wat dan 'n baie sterk skoorsteen-effek veroorsaak. 'n Nuwe metode is ontwikkel om die brandstoftemperature in die tenk te bereken vir 'n gegewe verkoelingsvloei. Die tegniek maak gebruik van EEA en analitiese tegnieke. Antwoorde word verkry in 'n fraksie van die tyd wat dit volledige CFD analises neem, en binne 5% akkuraatheid van die CFD resultate. Volskaalse toetse word beplan om die hitteoordrag eienskappe van die verkoelingsbuise te meet en te verifieer en sodoende die vertroue in die EEA en CFD analises te verhoog.

Die stoortenk ontwerp is geïntegreer in 'n stooreenheid wat al die kernveiligheidsfunksies verrig. Die stooreenheid kan in vier verskillende verkoelingsmodusse bedryf word, naamlik: geslote lus aktiewe verkoeling; oop lus passiewe verkoeling; oop lus aktiewe verkoeling; en geslote lus kondisionering. Daar is 'n outomatiese terugval vanaf aktiewe verkoeling na passiewe verkoeling. Die aktiewe verkoeling is dus slegs nodig om oormatige hoeveelheid korrosie op die tenks te beperk. 'n Skaalmodel is gebou om die passiewe verkoelingsvermoë van die stooreenheid te demonstreer, en die resultate vergelyk goed met CFD analises. Daar is ook 'n nuwe metode ontwikkel om die passiewe verkoeling van die tenks te bereken met behulp van pypnetwerk simulasie sagteware. Hierdie metode is aansienlik vinniger as CFD en dis maklik om waaier karakterestieke by te voeg en sensitiwiteit studies te doen.

Die Sfeer Stoor Stelsel van die PBMR bevat twaalf stooreenhede. 'n Spesiale sfeerpypstelsel maak dit moontlik om sfere na enige tenk toe te stuur, vanaf enige tenk na die reaktor of 'n ander tenk toe, of selfs na 'n wegdoeningshouer. Alle instandhoudingsintensiewe komponente is op toeganklike areas geplaas, wat sodoende die werkers beskerm teen die straling van die tenks. Daar is voorsorg getref om enige lekkasie te kan monitor, asook vir die IAEA om te verifieer wat die kern-inventaris van die stoorstel is.

Die Sfeer Stoor Stelsel is 'n volledig geïntegreerde, dog modulêre ontwerp wat voldoen aan alle kernkrag en proses vereistes. Dit is 'n unieke oplossing vir die interim stoor van die PBMR brandstof, en word as 'n koste-effektiewe oplossing geag vir 'n 80 jaar stoortydperk. Daar is 'n paar toekomstige toetse en ontwikkelings nog nodig om onryp areas te finaliseer, maar oor die algemeen is die stelsel volledig genoeg ontwerp dat detail ontwerp kan voortgaan.

PREFACE

The PBMR project is one of the few massive high technology projects currently in South Africa. I have been involved with the design of the spent fuel and used fuel storage from 2000. As with many projects of this scale, it has undergone several twists and turns in the last four years.

These four years have been a very enriching experience for me, as I was required to learn a vast amount of new technologies. The work I did probably involved the most disciplines any engineer could wish for. I had to deal with nuclear physics; chemistry; structural design; *metallurgy*; electronics and instrumentation; air conditioning; pressure vessel technology; particle and granular flow; thermo hydraulics; numerical mathematics; civil structures; finite element analyses; experimental techniques; manufacturing; systems engineering and project management. All of these had to be integrated into a synergistic final solution.

I am a strong believer in the PBMR technology and hope that it will become the norm for future power generation of the world. I also believe that the interim storage solution that I present in this thesis could revolutionise the way spent fuel will be stored in the world in future.

To be part of the design team of the PBMR is a great privilege. My thanks go out to all the people who have put their trust in me to come up with a feasible cost-effective storage solution. I acknowledge the contributions of all the people from PBMR and IST who assisted me in some way or another in the development of the design, especially:

Carel Viljoen who performed most of the CFD analyses for me;

Chris Koch who provided guidance on the corrosion design and tests;

Coenie Stoker who performed the criticality analyses;

Andre Stander who modelled the designs in CAD and assisted me in building the various experiments;

and Evert Schlünz who taught me how to convey my opinions and designs in a diplomatic yet assertive manner to the client.

Wim F. Fuls

TABLE OF CONTENTS

LIST OF FIGURES

LIST OF TABLES

ABBREVIATIONS, DEFINITIONS AND ACRONYMS

Abbreviations And Acronyms

Abbreviation or Acronym	Explanation
2D	Two Dimensional
3D	Three Dimensional
A/D	Analogue to Digital
ALARA	As Low As Reasonably Achievable
ASHRAE	American Society of Heating, Refrigeration and Air-Conditioning Engineers
ASME	American Society of Mechanical Engineers
CAD	Computer Aided Design
CCU	Cooling & Conditioning Unit
CFD	Computational Fluid Dynamics
CSIR	Council for Scientific and Industrial Research
FEA	Finite Element Analysis
FHSS	Fuel Handling and Storage System
GR	Graphite (sphere)
GRSU	Graphite Storage Unit
GRT	Graphite Tank
HICS	Helium Inventory Control System
HVAC	Heating, Ventilation and Air Conditioning
IAEA	International Atomic Energy Agency
ID	Internal Diameter
NC	Numerically Controlled
OD	Outer Diameter
PCD	Pitch Circle Diameter
PLC	Programmable Logic Controller
RH	Relative Humidity
SCADA	Supervisory Control and Data Acquisition
SCC	Stress Corrosion Cracking
SCS	Sphere Circulating System
SF	Spent Fuel (sphere)
SFSU	Spent Fuel Storage Unit
SFT	Spent Fuel Tank
SSS	Sphere Storage System
TUD	Tank Unloading Device
UF	Used Fuel (sphere)
UFSU	Used Fuel Storage Unit
UFT	Used Fuel Tank

Definitions

Definition	Explanation
Burn-up	This is the term used to describe the amount of nuclear energy that has been released by a fuel sphere. Burn-up is measured in GWd/tu. It is expressed as Gigawatt-day per tonne initial uranium.
Criticality	Criticality is a measure to quantify the sustainability of a nuclear fission reaction. It is expressed in an effective multiplication factor k_{eff}, which is the ratio of one generation neutrons over the previous generation. A volume is said to be sub-critical if $k_{eff} < 1.0$
Defence-in-Depth	A design principle followed in nuclear engineering to ensure there are sufficient protection barriers to mitigate an accident.
Fresh Fuel	A fuel sphere that has not undergone nuclear fission yet. It is in its fabricated form, and is not radioactive, but contain sufficient fissile material to partake in the nuclear reaction when introduced in the reactor.
Grashof number	A dimensionless number used to characterize buoyancy driven flow. It represents the ratio of the buoyancy forces to the viscous forces. It is generally written as: $Gr = \frac{\beta \cdot \Delta T \cdot L^3 \cdot g}{\nu^2}$
Packing Factor or Packing Density	Spheres stored in a closed volume do not occupy the total available volume. There are voids between the spheres. The packing factor (PF) is the ratio between the stored sphere volume and the available volume. The maximum theoretical packing factor is 0.74, but values ranging from 0.60 to 0.64 is more often found in practice. The void factor is also often reported, which is 1-PF.
Passive Cooling	Passive cooling is the heat removal (cooling) of a volume without the aid of any additional energy source. The implication is that the heat to be removed drives the cooling flow through natural convection. Natural convection is the phenomena through which all materials tend to cool down to the ambient temperature through convective heat transfer.
Reactivity potential	In pure nuclear reactor theory, reactivity is defined as: $\rho = \frac{k_{eff} - 1}{k_{eff}}$ However, in the context of this document, the word reactivity potential is used to describe the potential of a fuel volume to become critical when placed in a certain geometry.
Reynolds Number	A dimensionless number used to characterise fluid flow. It represents the ratio of the kinematic forces to the viscous forces. It is generally written as: $Re = \frac{\rho \cdot V \cdot D}{\mu}$
Spent Fuel	A fuel sphere, which has undergone the required amount of burn-up and is no longer producing sufficient energy in the core. A spent fuel sphere is replaced by a fresh fuel sphere.
Used Fuel	A used fuel sphere is the average sphere found inside the reactor. The reactor is filled with a mixture of fresh to spent fuel, with various sphere burn-ups in between. A used fuel sphere has sufficient fissile material left to still partake in the nuclear reaction.

Chapter 1 : Introduction

1. BACKGROUND TO THE PBMR PROJECT

The Pebble Bed Modular Reactor (PBMR) is a new generation nuclear power plant developed in South Africa. The reactor is based upon High Temperature Reactor (HTR) technology conceived in Germany some forty years ago. The PBMR relies on the experience and proof of safety established in Germany with two HTR research reactors, the THTR and the AVR [1].

In recent years there have been a revival of nuclear energy in the world due to the increasing energy demand and the air pollution associated with coal-fired power stations. Several countries have established research projects to develop new generation nuclear power reactors which are inherently safe and hence catastrophe free. Of the various types of reactors being studied, the HTR is becoming more and more favourable due to its inherent passive safety and cogeneration of potable water from sea water and hydrogen production.

The PBMR started its concept phase in the early 1990's at IST Holdings (Pty) Ltd., but only gained momentum at the beginning of 2000. The company PBMR (Pty) Ltd. was established in 2000 and is responsible for the overall development of the reactor. Their major shareholders are Eskom, the Industrial Development Corporation (IDC) and British Nuclear Fuel (BNFL) [1]. The South African Government has identified the PBMR project as an important project for the development of the country, and has included it as part of its five-year infrastructure investment program [2]. Table 1 summarises some of the major characteristics of the PBMR.

Table 1: Major characteristics of the PBMR (from references [3] and [4])

Characteristic	Value
Thermal Power	400 MW
Electrical Power Output	165 MW
Power conversion cycle	Direct, closed-circuit Brayton cycle
Coolant	Helium
Moderation	Graphite
Operating pressure	9 MPa
Core inlet temperature	490°C
Core outlet temperature	900°C
Fuel	60mm Spherical graphite with TRISO particles inside
Enrichment	9.6% ^{235}U
Heavy metal per sphere	9 g
Target burn-up	92 GWg/tu
Spheres in core	± 500 000

IST Nuclear, a Division of IST Holdings (Pty) Ltd. holds the contract for the design and supply of three major support systems of the PBMR. They are the Fuel Handling and Storage System (FHSS), the Reactivity Control and Shutdown System (RCCS) and various gas support systems such as the Helium Inventory Control System (HICS), the Start-up Blower System (SBS) and the Core Barrel Conditioning System (CBCS).

A subsystem of the FHSS is the Sphere Storage System (SSS). This system can also be named the Interim Storage Facility as this is where all the spent fuel will be stored for the interim period before final disposal.

2. PURPOSE OF THIS WORK

This thesis describes the design for the interim spent fuel storage for the PBMR. This design is unique in the world as it makes use of bulk storage containers. Also, the cost involved in interim storage of spent fuel of traditional reactors was deemed too high. A new solution was required to solve the problem of spent fuel storage.

In developing a spent fuel storage system, there are various challenges, which have to be overcome. For example, all the nuclear safety functions have to be retained, meaning the spent fuel must stay sub-critical, all the decay heat should be safely and reliably removed, and the fuel must be protected from damage. The handling of the fuel inside the storage system also poses problems such as how to load it into the storage container, and getting it out at a later stage. A cost effective solution was also required to ensure that the fuel could be stored for a long duration – up to 80 years without significant corrosion damage.

Other aspects such as installation, operation, maintenance, reliability and inspect ability had to be addressed. At the same time, the solution had to fit in with the current module building layout and other external design constraints. Changes to the PBMR concept also had to be accommodated throughout the design.

All of the above challenges (including many other minor issues) had to be addressed in an integrated design. This required work on a systems level, as well as development of minute details to ensure proper functioning of the complete system.

3. CONTRIBUTIONS OF THIS STUDY

The primary contribution of this study is the development and design of a unique solution for the interim storage of the PBMR's spent fuel. Within this integrated solution lies a vast amount of new and novel designs, alternative methods or techniques and experimental results. It is a combination of several engineering and scientific disciplines, all integrated into a synergistic final solution. The individual contributions with references to the detailed description are summarized below:

a. **First of its kind spent fuel storage**: This study presents a spent fuel storage system that makes use of bulk storage containers, holding more than 500 000 fuel elements per container (Chapter 1, §2). Normally spent fuel is stored in transportable containers or in a water pool (Chapter 3, §2 and §4). This is the first time dry spent fuel storage is proposed for bulk containers. The study presents an integrated solution that complies with all nuclear and process requirements. It is also believed to be the most cost-effective solution for an 80 year interim storage facility of PBMR fuel.

b. **Unique storage tank design**: The design of the storage tank is a unique approach to spent fuel storage (Chapter 5, §2). Never before has PBMR-type fuel been stored in pressure vessels that stand six stories high. The tank acts as large heat exchanger

that enables one to even store the full contents of the reactor (used fuel) without overheating. Previously, it was proposed that the used fuel be stored in an annular tank, cooled with water (Chapter 4, §3).

c. **Novel tank loading device**: A novel device was developed and tested, called the mechanical brake, that ensures the spheres do not get damaged as they are loaded into the tank (Chapter 5, §3.4). It is a passive device with virtually no possibility to fail. This design has been adopted by PBMR for the reactor loading device as well due to its intrinsic passive features and reliability.

d. **Novel tank unloading device**: To remove the spheres from the tank, a novel device was developed and tested that has a highly reliable and controllable unloading characteristic (Chapter 6, §1 and §2). Although the principle of a tank unloading device is not new, none of the various concepts studied for the last 10 years worked as reliable as the one proposed in this study.

e. **A fresh look at criticality**: The traditional method to attain fuel sub-criticality is with neutron absorbing material. This study presents a fresh look at criticality with sub-critical geometries only (Chapter 7, §6). This is a much more passive and cost-effective solution. Also, the way burn-up credit is defined is also new to the nuclear industry (Chapter 7, §3). The advantage is that a new license is not required every time the fuel changes.

f. **A new absorber rod spacing algorithm**: A new algorithm was developed that allows one to optimise absorber rod spacing for criticality without the need for numerous criticality analyses (Chapter 7, §5). Although the algorithm was not used to determine the final geometry, it is still a valuable new tool for the nuclear engineer.

g. **A novel 80 year life solution**: One of the most challenging requirements was that of 80 years storage (Chapter 8, §1). This has been solved through a novel solution for the cooling design that incorporates a closed loop dry air cooling, but with a passive cooling fallback (Chapter 8, §9). This way a low cost material can be used for the tank, without requiring a safety related active cooling system. This solution requires a dogmatic shift from the traditional solution of dry storage containers that have very thick stainless steel or even concrete walls.

h. **New corrosion test results**: New corrosion tests were performed for steel in air exposed to radiolysis (Chapter 8, §12). Although still preliminary, it showed that minimal corrosion occur on carbon steel containing a certain amount of chrome in a dry environment, even at high radiolysis concentrations.

i. **Fast new thermal analysis technique**: A new technique was developed to calculate the temperature distribution of the fuel inside the tank (Chapter 9, §3). It uses a combination of FEA and analytical techniques, and made it possible to analyse a large range of scenarios at a fraction of the time it takes CFD analyses. This is a continuation of a novel technique that used a Finite Difference solving algorithm instead of FEA, which has been published[1].

j. **Novel multi-mode cooling design**: The cooling design of the tanks is done with a novel multi-mode cooling design (Chapter 10, §2). This design allows for various cooling modes to operate, depending upon the heat load of the tank. At the heart of the design is a Cooling & Conditioning Unit that can be configured in the various modes with minimal effort (Chapter 10, §4).

---

[1] Transient Thermal Analysis of a PBMR Spent Fuel Tank Using Finite Differences; W.F. Fuls, E.H. Mathews; R&D Journal; 2004; pages 8-15.

k. **Fast new passive cooling analysis technique**: A technique was developed to solve the passive cooling characteristics of the integrated design in a much shorter time than CFD (Chapter 10, §8). It is a simulation of the tank and other geometry as a network of pipes, which is then solved using the Flownex software. It is also the only feasible way to solve pressure transients and investigate the effect of fan and heat exchanger characteristics.

l. **Novel passive cooling demonstrator**: A novel test has been developed to demonstrate the passive cooling of the storage tanks (Chapter 10, §9). This test was simple, yet helped to convince sceptics about the feasibility of passive cooling, and also confirmed some unexpected phenomena seen from CFD analyses. It is currently often used as a demonstrator to the public of how the tank's cooling will work.

m. **Unique sphere distribution**: A unique and very flexible solution is proposed for the distribution of the spheres to and from the storage tanks (Chapter 11, §4). It makes use of simple sphere pipe spool pieces that are moved around to define a certain sphere route, similar to what happens in a railroad shunting yard.

n. **Patented design**: The overall principles developed and described in this thesis have been deemed so unique and commercially valuable that a patent has been registered by PBMR [86]. This patent covers the principle design and layout of the modular storage unit, which could easily be used for other storage system designs.

o. **International publications**: The integrated storage design has been presented at an international conference on High Temperature Reactors in 2004[2]. There was a large audience, showing the interest of the nuclear engineering community in the work presented. A similar paper has been submitted to the Annals of Nuclear Energy Journal during March 2005[3]. The paper is still being reviewed. Two more papers will be presented in coming conferences during 2005, one pertaining the criticality design of the tanks[4], and one about the passive cooling of the tanks[5].

In conclusion it can with confidence be said that this thesis contains several contributions to the nuclear engineering industry. Many of the new designs or techniques are not restricted to the PBMR only, but can be further expanded for use in other nuclear reactor designs.

---

[2] The Interim Fuel Storage Facility of the PBMR; WF Fuls et. al.; 2nd International Topical Meeting on HIGH TEMPERATURE REACTOR TECHNOLOGY; Beijing; China; September 22-24, 2004; Paper D13

[3] The Interim Fuel Storage Facility of the PBMR; WF Fuls et. al.; Annals of Nuclear Energy; paper 3.02.05 still under peer review.

[4] PBMR Fuel Storage Design Criticality Analysis; C.C. Stoker, F. Reitsma, F. Albornoz, W.F. Fuls; Nuclear Criticality Safety Division Topical Meeting; Knoxville; Tennessee; September 19-22, 2005.

[5] Passive Cooling of the PBMR Spent and Used Fuel Tanks; W.F. Fuls; 18th International Conference on Structural Mechanics in Reactor Technology; Beijing, China, August 7-12, 2005; paper S05_5.

4. STRUCTURE OF THIS THESIS

The structure of this thesis is shown schematically in the diagram below.

Chapter 2 presents the design requirements for the Sphere Storage System. They are categorised into nuclear requirements, system functions and design criteria. These requirements form the basis of the work done, and is used to measure the validity of the design.

In order to get an appreciation for this work, Chapter 3 describes the current trends of spent fuel storage in the world. A differentiation is made between traditional water reactors and high temperature reactors. The principle of dry storage is discussed, with a short discussion about the problem of final disposal.

The design of the Sphere Storage System was done over a period of four years. However, the design reached maturity during the last two years. The first two years was marked by various changes to the PBMR concept, as well as several concept studies. This history is briefly described in Chapter 4.

Chapters 5 to 11 present the current design of the SSS. They present the solutions to the specific nuclear requirements: containment of radioactivity (Chapters 5 and 6); sub-criticality of the fuel (Chapter 7); corrosion protection (Chapter 8); and decay heat removal (Chapter 9). Each solution is carried over to the next, thereby resulting in a total solution for all the requirements, and culminating in an integrated storage unit design (Chapter 10). As the solutions are presented, the level of detail increases in order to fully define the design. Finally the solutions are integrated into a complete functioning system (Chapter 11) to fulfil the functional requirements.

Chapter 12 contains conclusions about the design. It summarises aspects such as nuclear safety, performance, cost efficiency, design maturity and risks.

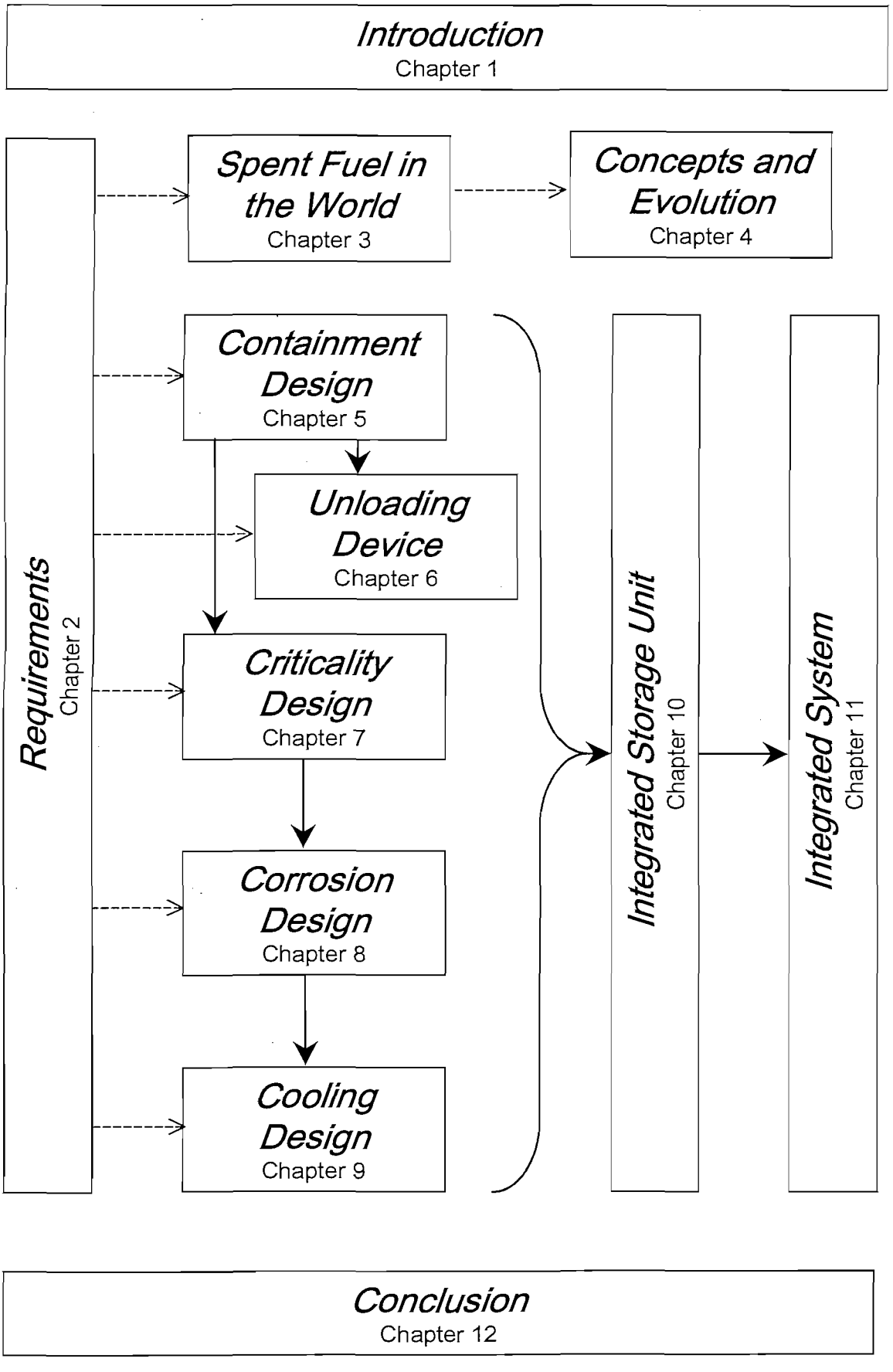
Introduction
Chapter 1
Requirements
Chapter 2
Spent Fuel in the World
Chapter 3
Concepts and Evolution
Chapter 4
Containment Design
Chapter 5
Unloading Device
Chapter 6
Criticality Design
Chapter 7
Corrosion Design
Chapter 8
Cooling Design
Chapter 9
Integrated Storage Unit
Chapter 10
Integrated System
Chapter 11
Conclusion
Chapter 12

Chapter 2 : Fuel Storage Requirements

1. INTRODUCTION

For any engineering project, the starting point is the requirements that are often compiled in a system requirement specification. Unfortunately, this specification is hardly ever precisely what the client really wants, and may contain several "nice-to-have's" or overly-ambitious values.

In order to define the boundaries of the storage design, the requirements were grouped into three categories. The first one is the nuclear requirements. They are internationally seen as what is needed for any storage system, and does not change for any nuclear facility. The second requirement is plant specific and has to do with the functional operation of the storage facility in the plant. Lastly there are design criteria that are often not cast in concrete, and sometimes not even written down. They contain guidelines originating from past experience as well as fundamental design philosophies.

The process followed in this study was to satisfy the nuclear requirements first but taking cognisance of the design criteria and the overall system functions. Finally, the solution was integrated to meet all the functional requirements, and in the process some of the design criteria may have been bent a bit. The following paragraphs list the various requirements that drove the solution as it is presented in this thesis.

2. NUCLEAR REQUIREMENTS

According to the IAEA Safety Standard Series [5] and [6] the following five fundamental safety functions must be fulfilled for any storage facility:

a. Confine all radioactive substances: Uncontrolled release of radioactive material can pose a health and environmental risk and must be prevented. This requirement is the most difficult one to prove compliance in a final disposal repository. Achieving confinement above ground is fairly simple through properly engineered barriers and structures of which the integrity can be monitored and maintained.

b. Maintain sub-criticality of the fuel: Although the fuel is deemed "spent", there is still an amount of fissile material left, which, when placed in the right arrangement can result in an uncontrolled nuclear reaction. Spent fuel systems should therefore be designed to ensure with sufficient margins of safety and conservatism that the fuel cannot reach criticality.

c. Remove residual heat from the fuel: Due to the radioactive decay of the fission products, an amount of heat is still being generated inside the fuel. This heat needs to be removed continuously to prevent overheating of the containment, which may lead to large geometric changes and possible criticality. The preferable method of heat removal is passive cooling via natural convection, although active cooling is not excluded.

d. Protect workers from radiation exposure: Although the radioactive material is confined in the storage container, there is a high flux of gamma radiation emanating from the spent fuel. It is therefore paramount that sufficient shielding be provided between the fuel and the workers to limit the radiation dose. This is often achieved through thick concrete or steel barriers.

e. Maintain fuel integrity: In the PBMR case, this means that one should prevent excessive damage to the spheres during handling, and also protect them from corrosion or oxidation.

3. PRIMARY SYSTEM FUNCTIONS

The Sphere Storage System performs a support role for the rest of Fuel Handling and Storage System during plant operation [7]. It is therefore required to perform other functions than simply store the fuel. The SSS needs to perform three main functions, namely:

a. Store all spheres: Apart form the spent fuel generated in the reactor, the SSS should also store an amount of pure graphite spheres used for the initial loading and start-up of the core. It should be able to store a full core contents of used fuel when maintenance on the reactor core is required. The SSS can store a total of more than 6 million spheres. During storage, all the nuclear requirements have to be met, for the first forty years during plant operation, and an additional forty years thereafter. This result in a total design life of 80 years.

b. Return used fuel or graphite to the core: The PBMR has the ability to completely empty the reactor when maintenance on the core internals is required. The SSS has to receive the fuel and safely store it until it has to be returned to the reactor. Also, before used fuel can be returned to the core, it has to be filled with pure graphite spheres, also coming from the SSS.

c. Distribute the spheres: It should be possible to distribute the spheres stored in one tank to another tank in order to perform maintenance on the first tank. Also, after the 80 years interim storage, the spheres have to be transferred to a transport cask located outside the building for final disposal.

4. GENERAL DESIGN CRITERIA

The following design criteria have been accumulated from various sources. Some of these are fundamental design philosophies, while others are guidelines obtained from experience of the THTR operation. The requirements relating to the licensing of the PBMR [8] are also encapsulated by the list below.

a. Bulk storage: The storage tanks must be bulk storage containers, rather than small movable casks as those traditionally used for spent fuel storage. This is the most significant design criterion for the SSS and makes the system unique amongst all other nuclear fuel storage systems.

b. Extensive use of THTR designs and expertise: A lot of the design principles used for the THTR could not be used due to the bulk storage criterion. However, the sphere conveying, and process element insert design was used.

c. Gravity sphere lines minimum incline of 10°: This is a guideline from THTR experience in order to reduce the possibility of a sphere blockage. This rule was followed as much as possible.

d. Minimum sphere gap of 6 diameters: All granular material has the tendency to block the exit hole if the hole is less than a certain diameter. This diameter is often related to the average grain diameter. From the THTR experience, it was found that the probability of a sphere blockage in a hole of more than 6 diameters is very low. All apertures where spheres need to pass through should therefore be more than 6 diameters wide.

e. Minimise sphere damage: This criterion is implemented by means of limited sphere velocities, bend radii of 650mm where possible, and a loading mechanism inside the tank to limit the impact velocity the spheres.

f. Follow the principles of ALARA: The principle of As Low As Reasonably Achievable is often used in measuring the design in terms of radiation exposure. The designer has to show the Nuclear Regulator and the public that he has made all reasonable attempts to reduce the risk to the public and the environment [9].

g. Employ the principles Defence-in-depth: This means that a design should have multiple layers of safety or barriers to prevent an accident from escalating to a catastrophe [10]. A simplistic example is to apply a locking agent such as Lock-Tight on the thread of a nut, even though there is a locking wire. If for some reason the lock wire gets detached, the Lock-Tight will reduce the possibility of the nut falling off.

h. Minimise capital and operational cost: Trade-off studies have to be performed in order to choose the most cost-effective design. This criterion is often in direct conflict with the ALARA principle, as the question always arises: What is reasonably low? An easy way to reduce cost is to reduce material thickness, but that will then increase the radiation exposure. It is also in conflict with nuclear safety, since high margins of safety and conservatism results in an increased cost.

Chapter 3 : Nuclear Spent Fuel Storage in the World

1. INTRODUCTION

Commercial nuclear power reactors have been in operation for more than forty years all over the world. There are currently about 440 reactors in operation, generating 16% of the global electricity [11]. About 230 000 tons heavy metal of nuclear spent fuel has been generated by 2000 [12]. All of this is currently stored in the reactor building, or at special storage facilities above ground.

The problem with spent fuel is that it contains radioactive by-products formed in the nuclear fission process, which are highly hazardous to any organic organism. Also, these elements are present in the fuel for thousands of years. The safe storage and management of spent fuel is therefore of utmost importance to the future of nuclear power generation. In fact, with the introduction of passively-safe and catastrophe-free reactor designs (such as the PBMR), the spent fuel generation is the only valid argument left against the use of nuclear power.

Unfortunately, there is currently no proven method to dispose of the spent fuel so that it may not be a problem for future generations thousands of years from now. The problem of final disposal will be discussed in more detail later in this chapter. Due to the lack of a final solution, all spent fuel is currently stored in interim storage facilities for a period of 30 to even 100 years [12]. This is to allow enough time to develop a final storage solution, and also to reduce the radioactivity of the fuel.

There are various storage solutions implemented over the world. Only some general types will be discussed in order to put the design of the PBMR interim storage into perspective.

2. TRADITIONAL WATER REACTOR SPENT FUEL STORAGE

Most of the spent fuel currently in storage in the world originates from water reactors. There are a number of different types of water reactors all using water as primary coolant. The reactor fuel design also looks similar. A single fuel element is in the form of a long bundle, about 4m long (see Figure 1). Inside this bundle are a number of small cylindrical fuel pellets, enclosed in a metal cladding. The nuclear reaction occurs inside this pellet. All radioactive by-products are retained inside the pellet by the metal cladding.

When the fuel has reached its target burn-up value, it is classified as spent fuel, and is removed from the reactor. Removing spent fuel from a water reactor requires that the reactor be shut down and opened up. The spent fuel element is then removed with an overhead crane and placed in a spent fuel water pool. To reduce the frequency of spent fuel removal, an excessive amount of fresh fuel is loaded into the core. The nuclear reaction is then suppressed with control rods and absorber material. These are active control measures and are required to ensure the safe operation of the reactor.

Because of the amount of fission products inside the spent fuel, there is a large amount of decay heat, which has to be removed. This is why the spent fuel is stored in a water pool. The spent fuel has to stay in the pool until the decay heat has dropped sufficiently to allow

dry storage of the fuel. In some reactors, the spent fuel is kept in a water pool until final disposal.

Storage of spent fuel in a water pool is a proven technique, and is used extensively throughout the world. However, the operational cost of such a facility is extremely high [14]. A more cost-effective solution is that of dry storage.

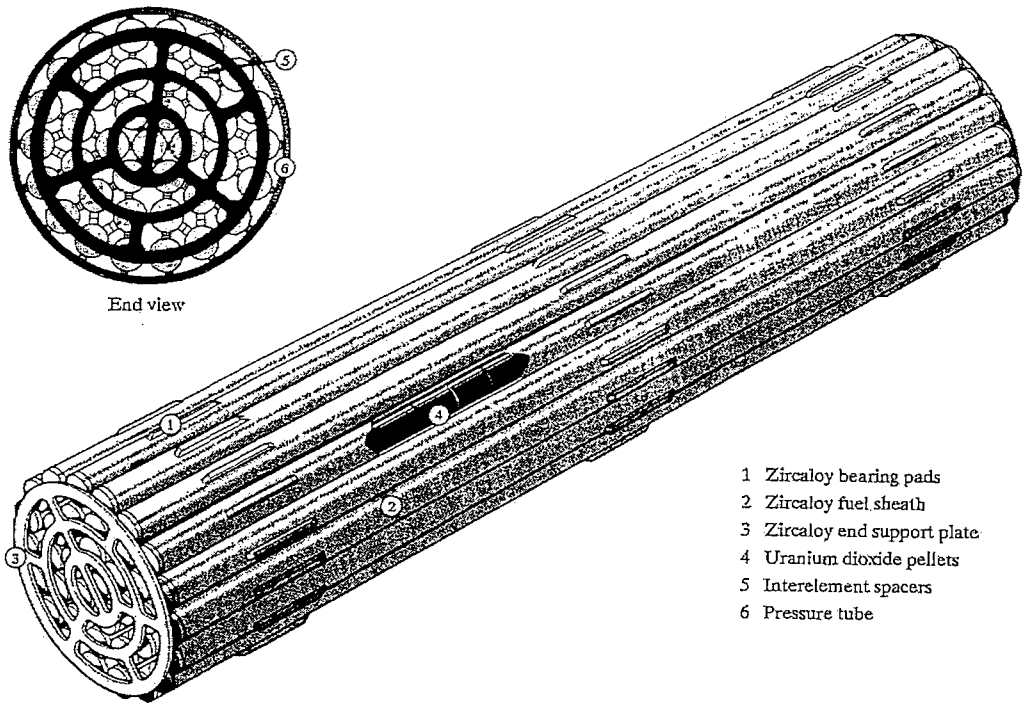

Figure 1: Typical layout of a water reactor fuel element or assembly [13].

3. THE PRINCIPLE OF DRY STORAGE

The term "Dry Storage" implies that the spent fuel decay heat is not removed by water, but by a gas and often through natural convection. A dry storage cask is a thick-walled cylinder in which a number of spent fuel elements may be stored (see Figure 2). A water reactor spent fuel element has to decay for a few years before it can be stored in a dry cask. This is due to the poor heat transfer from the fuel to the cylinder, and then through the thick wall to the outside.

The storage casks are often placed in ambient air to allow for natural convection to take place. A life of up to 100 years is predicted for some casks. The casks are transportable, and can weigh anything from 30 tons to 130 tons [15]. Although the casks may be cheaper over the complete life cycle when compared to a water pool, it is still an expensive way to store the spent fuel and the initial capital cost is extremely high.

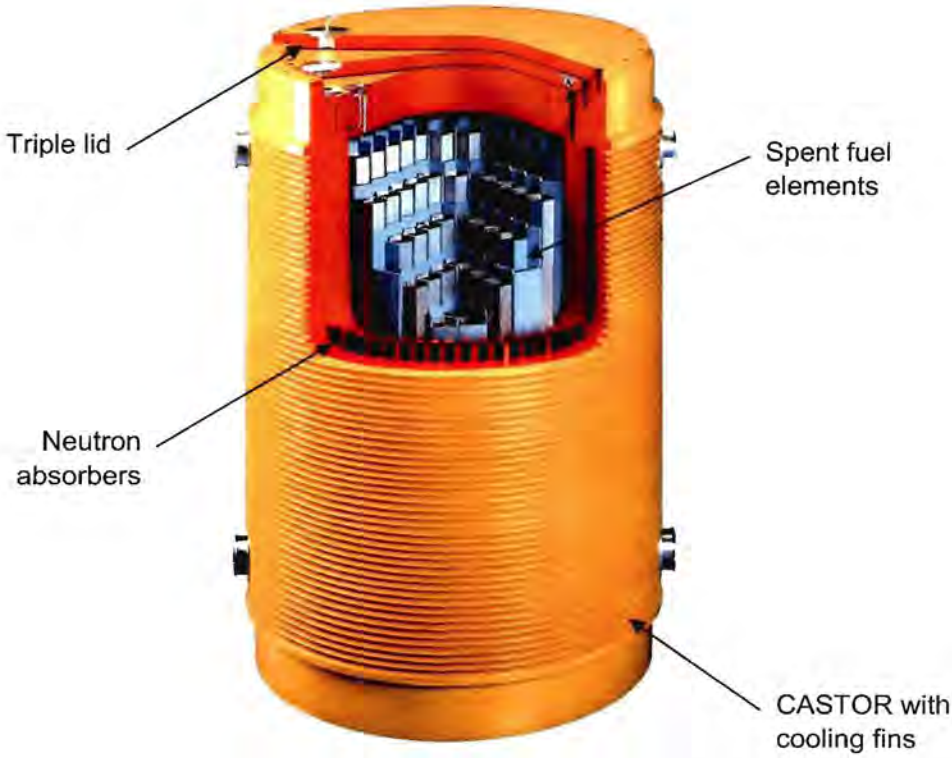

Figure 2: Typical dry storage and transport cask for water reactor fuel elements (Courtesy GNB [15]).

4. HIGH TEMPERATURE REACTOR SPENT FUEL STORAGE

HTRs, or better-named High Temperature Gas Cooled Reactors make use of a gas (often Helium) as its primary coolant. Where water reactors are often limited to 370°C, HTRs operate at 900°C or higher. This high temperature requires a different type of fuel design. It consists of small coated particles with a ceramic shell (often Silicon Carbide). These particles are then encapsulated in a graphite matrix to form a fuel element (see Figure 3). The nuclear fission products are retained inside the particles, with the Silicon Carbide forming the pressure boundary.

The fuel elements can be in the form of a hexagonal block (such as that of Japan's HTTR [16], and the shut down Fort St. Vrain and Peach Bottom reactors [17]), or as spherical elements (such as that of the THTR, AVR and the PBMR). Block fuel requires the same type of handling as that of water reactors, but spherical fuel can be handled like granular material. This means that the fuel can be extracted from the bottom of the core while the reactor is in operation. The fuel is then measured, and if spent, discharged to the spent fuel storage. For every spent fuel element discharged, a fresh fuel element is introduced at the top of the core. In other words, the reactor is continuously fuelled.

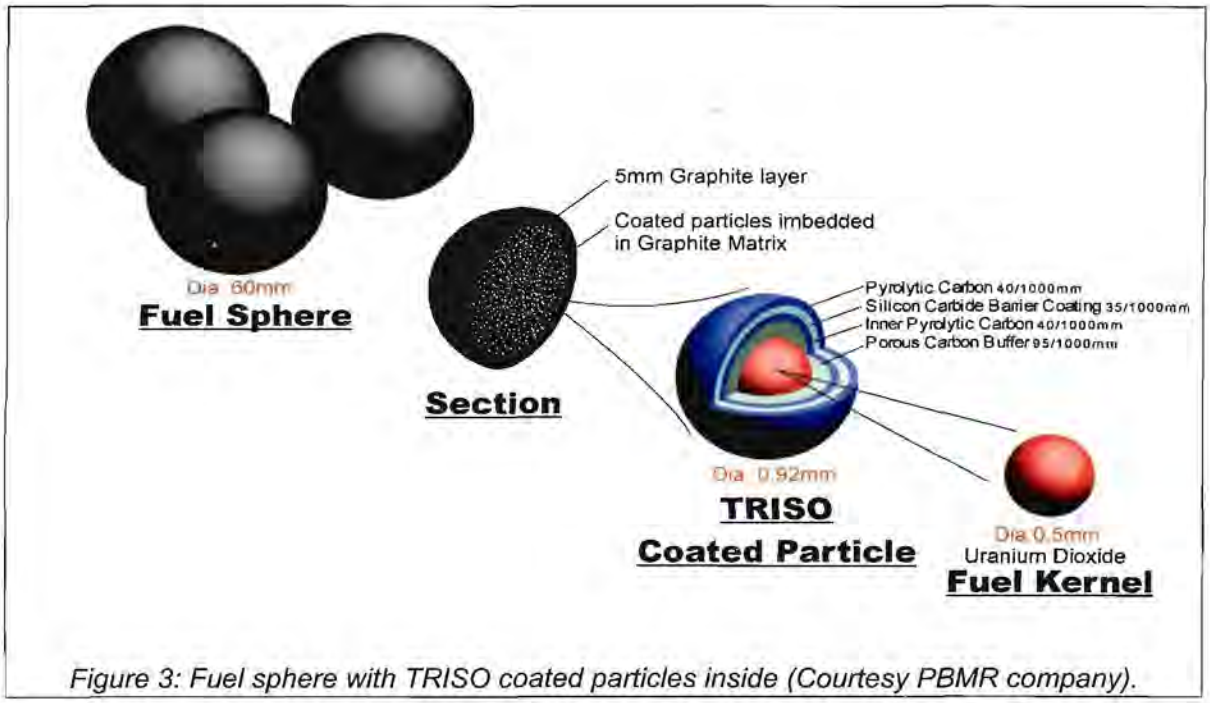

Figure 3: Fuel sphere with TRISO coated particles inside (Courtesy PBMR company).

Because of this continuous fuelling, it is not necessary to introduce excessive amount of fuel into the core, hence there are no systems required to suppress the nuclear reactor for safe operation. This is the passive safety of the PBMR. Also, when as much fuel as possible is loaded into a water reactor, the power density per fuel element becomes quite high leading to very high spent fuel decay heat. The PBMR's power density is much lower, hence the decay heat per sphere is significantly lower than that of a water reactor.

To date, there are three research reactors making use of spherical fuel elements. Two of these, the AVR and THTR have been shut down due to political changes in Germany, but the HTR10 of China is still in operation [18]. The spent fuel of all three reactors is stored in small transportable containers. The containers are air-cooled and are located inside a spent fuel storage building. This building acts as the "spent fuel pool" for the reactor. For both the AVR and THTR, the fuel has been removed from the small casks and placed into larger storage and transport casks, similar to what is used for the water reactors. The spent fuel of the THTR has been transported to the interim storage facility at Ahaus, Germany [12].

The problem with the above spent fuel storage methods is that they require a number of sophisticated handling and sealing equipment for the casks. Figure 4 shows such equipment for the THTR. Also, because of the lower power density of HTR fuel, the volume of spent fuel is much more than that of water reactors. Interim storage of HTR fuel in the same way as water reactor fuel is thus more expensive.

It was for these reasons that it was decided to store the PBMR's spent fuel in large storage containers for the full interim storage period, without any intermediate storage.

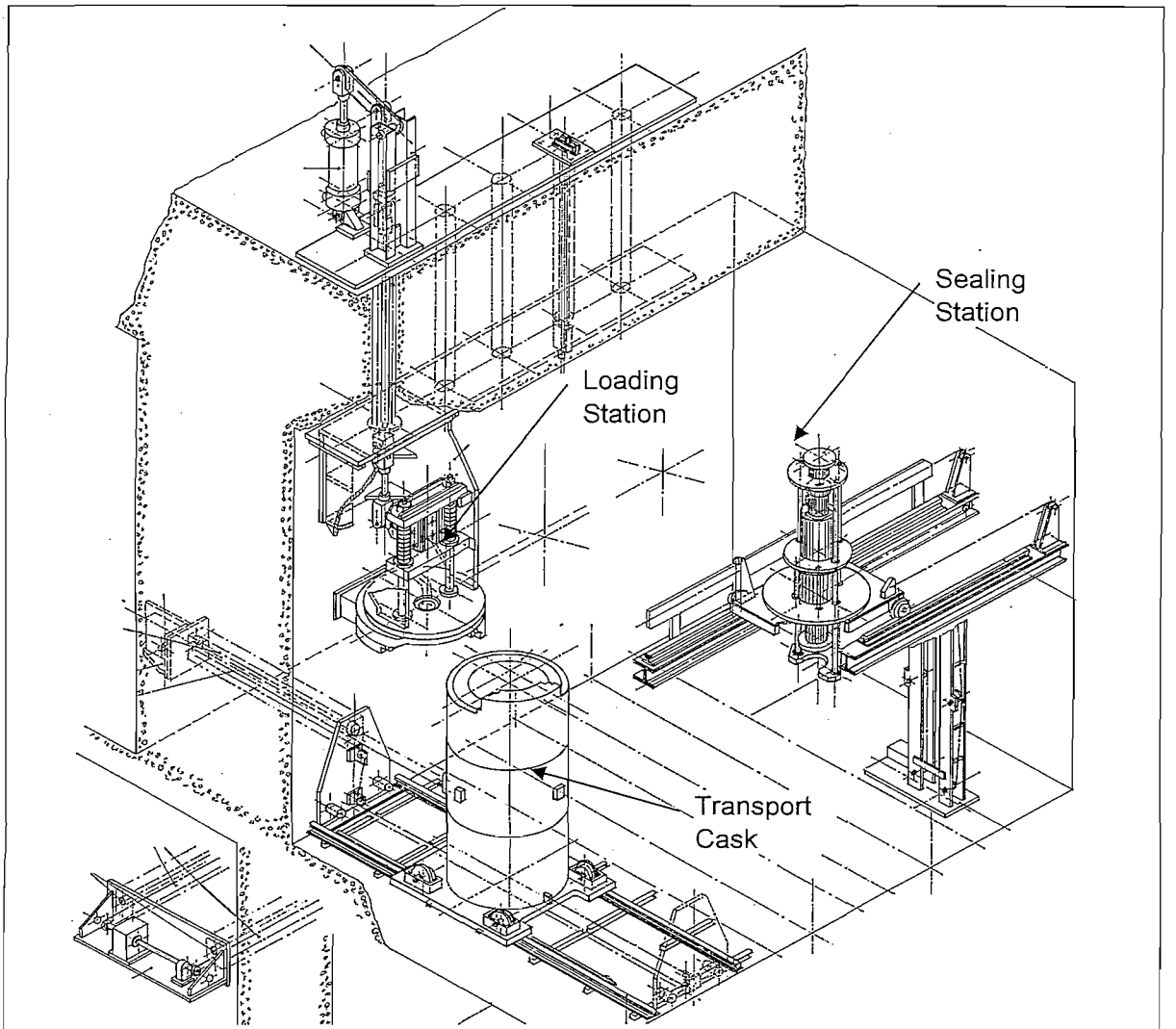

Figure 4: THTR Spent fuel cask loading & sealing facility [19].

5. THE PROBLEM WITH FINAL DISPOSAL

It was mentioned in paragraph 1 that the storage of spent fuel is the only valid issue left against nuclear power. The problem lies with the requirement that the waste be stored for thousands of years out of the reach of the environment.

The most favourable option currently is to store the fuel in deep geological depositories (100m or deeper below the ground). The location is very important, since it should not have any water movement through the depository. Candidates are inter alia clay, volcanic rock, or salt deposits [20]. A vast amount of research has been done to locate a suitable storage site in the world, and many countries have identified candidate locations. However, only the Unites Sates has recently made the decision that all its spent fuel will be disposed in the Yucca Mountain in the Nevada desert [12][21]. The storage site is currently under construction, and will receive spent fuel in 2010.

A big cost driver for final disposal is the storage volume required. This is because only a small percentage of the total volume of a spent fuel element is radioactive and hazardous. For the PBMR, this amounts to less than 7%.

The method of reprocessing is often used to separate the hazardous material from the rest,

thereby reducing the volume. However, reprocessing introduces the possibility that malicious groups may extract the plutonium to make nuclear weapons. Hence, reprocessing is only employed in a few countries such as France and the United Kingdom.

Even though reprocessing reduces the volume of waste to be disposed of, it does not reduce the amount of radioactive material. A technique that is gaining more and more attention is that of deep burn transmutation. In essence it involves placing the radioactive material in a neutron field, thereby forcing the material to undergo faster decay and decomposition into a less hazardous material [22].

To make transmutation cost-effective, reprocessing is required to separate the still useable nuclear material from the waste and make it into two types of fuel elements. These elements are then mixed in a certain way in the reactor to simultaneously generate power, and transmute the waste. This process is also called a closed fuel cycle. The alternative is to place the spent fuel in an accelerator that simply bombards the fuel with neutrons. Little energy is recovered from the fuel, but at least it eliminates the need for reprocessing.

Reprocessing can reduce the trans-uranic elements by 90%, and virtually destroy all weapons grade plutonium. Gas-cooled reactors using coated particles, such as the PBMR, are good candidates for deep burn transmutation. What's left after the process can then be disposed of in deep geological sites.

The question is: Is it fair to the future generations to leave them with graveyards of radioactive waste? Should it not be better for us to store the fuel above ground so that future generations can employ new technology to properly dispose of or disintegrate the waste? Why do we keep the waste on earth, when the sun is the ideal incinerator for the relative minute amount of waste we generate? Surely if it took less than sixty years from the beginning of human flight to the first space walk, why should it not be possible for future generations 80 years from now to safely transport radioactive waste out of the earth's atmosphere?

On the other hand, many believe in the principle of "polluter pays", and that one generation should not leave their waste problems for the next generation to solve. Therefore, one should bury the waste as soon as possible.

The question of whether to store the waste above ground for the future generation to dispose of, or to bury it as soon as possible will probably never be answered. However, public acceptance of above ground storage is much better than underground, as it has been proven to be safe, and no-one would like a radioactive grave in their backyard.

PBMR has opted to store the spent fuel above ground for a period of 80 years. This is to provide future generations a chance to better dispose of the waste. Also the spent fuel is not packaged in final disposal casks (as some critics would propose), since it is most likely that the fuel will undergo some form of volume reduction or reprocessing before final disposal. The spent fuel of the PBMR is stored in large tanks above ground to be packaged into disposal form only 80 years later.

Chapter 4 : Concept Studies and Design Evolution

1. INTRODUCTION

This chapter contains a short description of the history of the design. Because the work presented in this thesis was done over four years, many changes have caused the design to evolve in a certain direction. Also, a number of concept studies and cost reduction exercises were performed during the four years.

The first year consisted mainly of concept studies and is briefly discussed in the next paragraph. The result was a basic design baseline for the PBMR with a thermal power of 268MW. The diagram in Figure 5 depicts the progression of the Sphere Storage System as it evolved from the 268MW basic design baseline to the current 400MW detail design baseline. During this course of about three years, there were six major events (indicated in grey), which steered the design into the direction taken. These events were either initiated by design changes from PBMR, or they were the result of the resolution of outstanding issues of the design at that stage.

Although the actual values changed during the design progression, the overall functions remained the same. The result was a completely new design, retaining virtually nothing of the original 268MW baseline, whilst still performing all the required functions in a much more integrated and optimised design.

2. BULK STORAGE CONCEPTS

The initial PBMR concept had three distinct types of storage tanks, a Spent Fuel Tank (SFT), a Used Fuel Tank (UFT) and a Graphite Tank (GRT). All three of these tanks adopted the bulk storage principle as they could store in the order of 500 000 spheres each. The tanks were at that stage seen as three separate designs.

A study was performed to change the SFTs from cylindrical steel vessels to rectangular concrete regions inside the building. The concept failed because of the cost and complexity involved to ensure a leak-tight concrete structure.

Significant problems were experienced with the cooling design of the used fuel tank. Various concepts, like a long thin tank, several small tanks and annular tanks were investigated. A water-cooled annular tank was chosen at that stage for the UFT.

The GRT never posed a problem since it did not require any cooling or sub-criticality measures. It was simply a cylindrical pressure vessel, which had to fit in the building and store the required amount of spheres.

These bulk storage designs formed the basic design baseline for the 268MW PBMR.

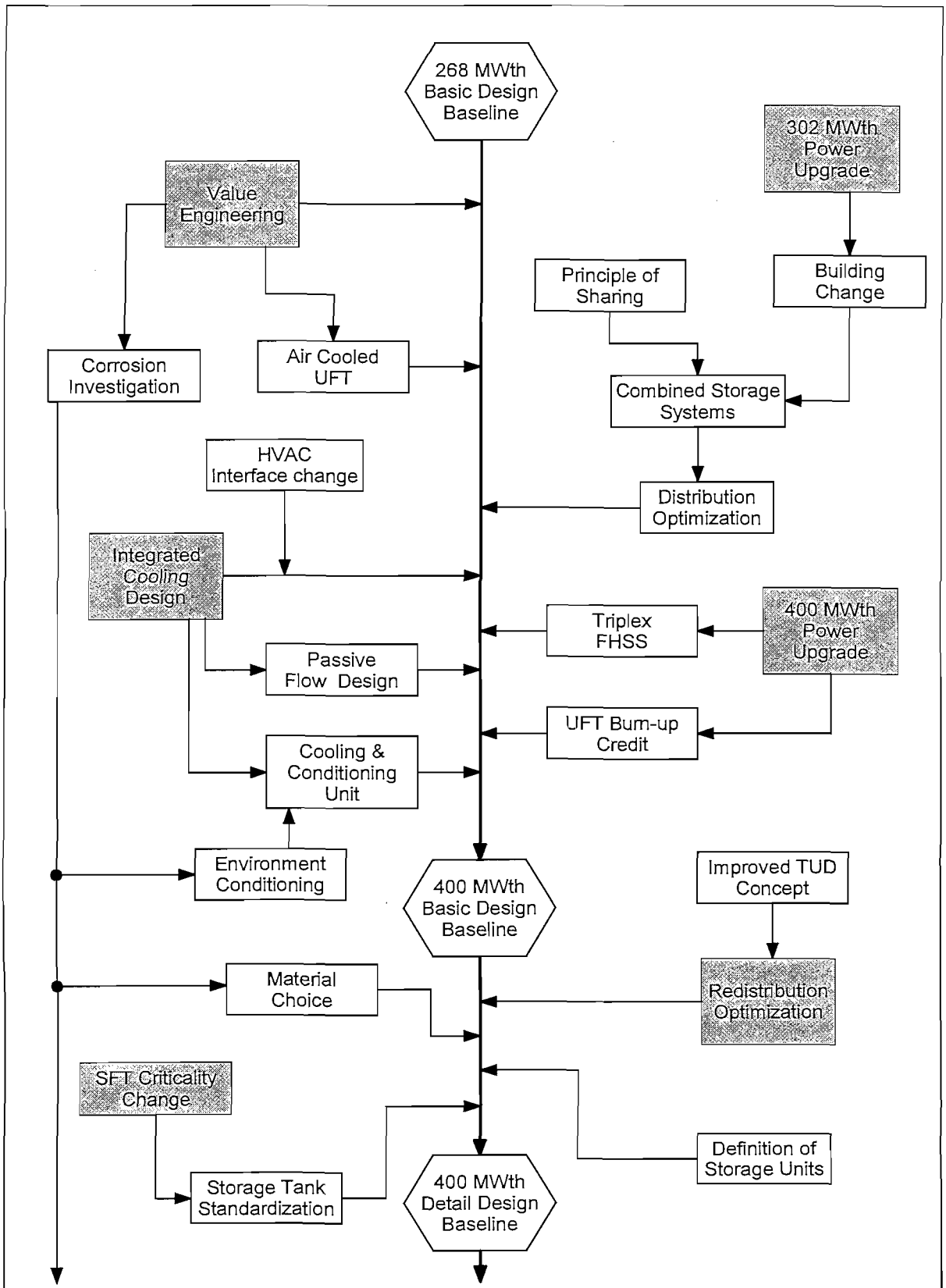

Figure 5: SSS design progression diagram.

3. 268MW BASIC DESIGN

The 268MW basic design baseline consisted of a Spent Fuel Storage System and a Used Fuel and Graphite Storage and Feed System with the three bulk storage tanks as shown in Figure 6.

The SFT was a cylindrical pressure vessel with a number of neutron absorber rods inside the tank, suspended from the top. The tanks were sub-critical with a full load of fresh fuel and cooling was done by the plant HVAC system. There were ten tanks, loaded two at a time. Change-over to the next two tanks were done by manually rotating diverter valves.

The UFT consisted of an annular pressure vessel, submerged in a water tank. Cooling was done by the Active Cooling System of the module, and there was sufficient water to boil off for retention purposes if the active cooling fails. Sub-criticality was achieved by means of the annular geometry and water, for a tank filled with fresh fuel. The UFT was situated above the rest of the FHSS process blocks, next to the reactor. The tank had two unloading points.

The GRT was a cylindrical pressure vessel with no neutron absorbers inside. It had no cooling requirements, and also had two unloading points. The tank was also situated above the FHSS process blocks, on the opposite side of the reactor.

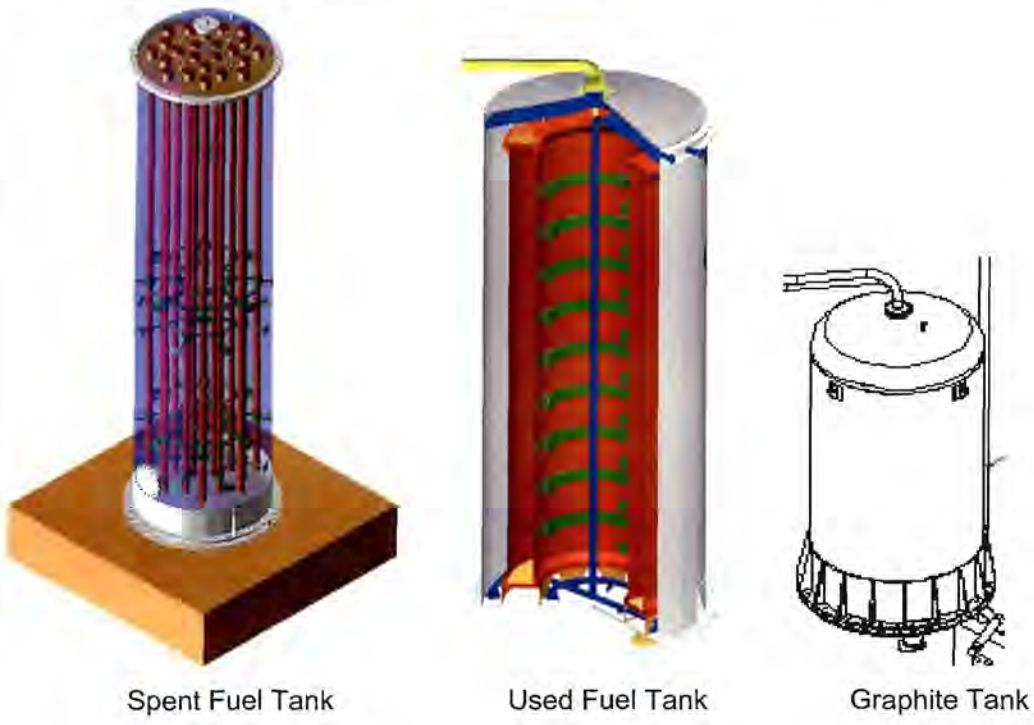

Figure 6: 268MW baseline storage tanks.

4. VALUE ENGINEERING

The value engineering exercise was initiated to reduce the capital cost of the Spent Fuel Tanks. The study and its conclusions are documented in detail in reference [23]. The tank and the neutron absorber material were put under the spotlight. From the study it was found that stainless steel is not a suitable material for the tanks due to its susceptibility for stress corrosion cracking. This initiated a corrosion study which was aimed at finding a cost effective 80-year life solution for the tank materials. Recent results of the study indicated that

still ongoing.

Whilst investigating a number of various absorber materials, as well as sub-critical designs, it was realised that steel in itself can be used to achieve sub-criticality. The result was a tank with sufficient steel internals to create sub-critical geometries. The amount of steel required was further reduced by introducing burn-up credit for the storage of spent fuel. The requirement was changed from fresh fuel, to 40GWd/tu, which is sufficient to hold an equilibrium core.

The final choice of tank geometry was based upon the tank with the best natural convection ability. The result was a long, cylindrical tank with four hollow tubes running from the bottom to the top of the tank situated at a specific pitch circle. These tubes ensure that the fuel volume is sub-critical, and allows cooling air to pass through it. CFD analyses indicated this geometry had a very good passive cooling ability.

As a final structural optimisation, the tank support was changed from a bottom support to a top support. This eliminates the buckling loads on the tank shell, and simplifies installation and airflow.

With the successful implementation of the value engineering results, analyses were initiated to investigate the feasibility to change the UFT also to an air-cooled tank. The result was a tank of similar dimensions to the SFT, but containing 8 tubes on one PCD and four smaller tubes on a smaller PCD.

5. 302MW POWER UPGRADE

The 302MW power upgrade was initiated by PBMR as a result of an optimisation study on the cost efficiency of the reactor. With this upgrade came a number of building changes. These changes made more space available in the spent fuel area, while the area where the UFT and GRT were situated became less. Also, the total spent fuel capacity was increased from 5 million to 6 million spheres.

At the same time, it became clear that some of the functions performed by the Spent Fuel Storage System are exactly the same as those of the Used Fuel and Graphite Storage and Feed System. Also, the two systems are never required to operate at the same time and can thus share the same sphere lines. It was therefore possible to integrate the two systems into one single system called the Sphere Storage System. With the newly air-cooled UFT and more space available in the spent fuel area, it was proposed to move the UFT and GRT to the spent fuel area.

Because of the shared functions of the two previous systems, it was necessary to re-configure the sphere distribution. This resulted in the philosophy that tanks shall be connected to sphere lines only when required, and then by means of bolted flanges. This eliminated a large number of isolation valves and diverter components previously required.

6. INTEGRATED COOLING DESIGN

One of the outstanding issues of the 268MW baseline was the cooling design which includes a feasible passive cooling mode. With the new UFT and SFT being air-cooled with a good passive cooling ability, an integrated cooling design was proposed. From the corrosion study it became evident that the most cost effective solution was to condition the cooling air to such an extent so as to limit corrosion on the tank. This resulted in a closed loop cooling flow with a heat exchanger needed to transfer the heat to the external cooling air.

Flow paths inside the tank cubicle and around the tank were optimised to ensure proper heat removal and minimise heat radiation to the concrete. It also allowed for passive cooling of the tanks.

A Cooling & Conditioning Unit was introduced which performs all the required cooling operations. It can operate in four different cooling modes, with an automatic transfer from active to passive cooling mode. The cooling design for the UFT and SFT could then be made similar.

The GRT design was made exactly the same as that of an SFT. It can therefore act as a spare tank if needed.

The cooling is now done by the storage system itself, with no interface to the module HVAC. This decision increased the reliability of the passive cooling ability, and it is felt to be a more cost-effective solution, especially since the tank cooling needs to be operational for 40 years after plant operation.

7. 400MW POWER UPGRADE

A further power upgrade to 400MW was initiated by PBMR in 2003. The two primary changes which affected the Sphere Storage System, was the change to three unloading devices from the reactor, and the increase in fuel enrichment. The three unloading devices on the reactor prompted the FHSS to change from a duplex system to a triplex system (three parallel process lines).

The best solution to discharge three spent fuel buffers to the storage tanks was to discharge *all spheres into* one tank. This means the loading changed from two tanks at a time, to one tank only with an increase in heat load of the specific tank. An additional cooling tube was needed in the centre of the SFT to accommodate the increased heat load.

The triplex FHSS also required three lines into and out of the UFT and GRT. This resulted in a complex pipe and block arrangement at the bottom to be able to distribute the UFT contents to an SFT, since it has only one inlet line.

The increase in fuel enrichment required an increase in the number of tubes needed to achieve sub-criticality of a volume of fresh fuel. The increase was so significant that it was not possible to arrive at a feasible UFT geometry (within the current tank concept) without compromising sphere flow. Hence it was decided to implement burn-up credit for the UFT as well.

8. REDISTRIBUTION OPTIMIZATION

The complex layout at the bottom of the tanks prompted a re-examination of the Tank Unloading Device. A new concept was developed which eliminated all the previous problems that led to the complex pipe layout. The new concept can unload from one or three positions, has built-in counters and discharges spheres at fixed intervals.

9. SFT CRITICALITY CHANGE

With the UFT now also having burn-up credit to achieve sub-criticality, it was decided to standardise all the storage tanks to that of the UFT. This led to an even lower criticality of the SFT, because the UFT geometry had a larger centre tube, and eight outer tubes. The total storage capacity was reduced to 530 000 spheres per tank, which still fall within the

expected spent fuel consumption.

The only difference between the three types of tanks is that the UFT and GRT have three loading and unloading points, while the SFT has only one. In fact, the names GRT and UFT were kept more for historical purpose and process definition than to differentiate between the designs since they now look exactly the same.

10. 400MW DETAIL DESIGN BASELINE

As part of the completion of the basic design phase, the product hierarchy of the Sphere Storage System was rearranged into functioning units. This lead to the definition of a generic storage unit that contains all the equipment necessary to perform its storage functions. Three types of units are defined, depending upon whether it contains an SFT, UFT or GRT.

The following chapters will present the details of the SSS design as it currently stands for the 400MW Detail Design Baseline.

Chapter 5 : Containment Design

1. CONTAINMENT REQUIREMENT

Containment of radioactive material is the most important function any storage system should perform. Failure of the other functions such as heat removal or sub-criticality could eventually also lead to a loss of containment. In turn this will expose the public and environment to the hazardous elements inside the fuel.

The PBMR fuel design has an extremely good containment ability on its own. This is because virtually all fission products are retained in the ceramic shell of the fuel kernels [24] and [25]. Only a small amount of radioactive gasses diffuse through the kernels, but is then mostly trapped in the surrounding graphite matrix of the fuel sphere. The result is that the helium inside the reactor has very low concentrations of radioactivity. In fact, the majority of radioactivity in the helium comes from irradiated impurities in the fuel graphite [26].

Another important aspect of the fuel is that it can sustain temperatures in excess of 1600°C without significant contamination release from the fuel kernels [24]. The only prerequisite is that the fuel is not exposed to oxygen. Above 400°C, the graphite undergoes an exothermal oxidation reaction that could expose the fuel kernels inside [27].

In the light of the above information, one could argue that no further containment barrier is needed to store the fuel in. This is true, but it will not be As Low As Reasonably Achievable. Also, although the gas around the spheres is virtually "clean", there is a large amount of sub-micron graphite dust particles amongst the spheres. This dust is contaminated with radioactive impurities and could be lethal to a person if it is inhaled. Therefore, one only needs to have a dust-tight container, but with a bit of additional engineering and quality control effort, the container can be made gas tight, i.e. a pressure vessel design. There is then an additional high quality containment barrier around the fuel spheres. This complies with the ALARA principle.

To conclude, the storage tanks are pressure vessel designs, forming the final containment barrier for any radioactive material that may have escaped from the fuel, as well as containment of the dust. The additional advantage of designing the tank as a pressure vessel is that it allows spheres to be pneumatically conveyed with Helium to and from the tank. It was established that a pressure of 1MPa is required to convey the spheres in a controllable manner, hence the design pressure is set at 1MPa.

2. A UNIQUE STORAGE TANK DESIGN

As described in the previous chapter, there are three types of storage tanks that have evolved into one single geometric design. The only difference is that the UFT and GRT have three sphere loading lines and three outlets, while the SFT has only a single loading and outlet line.

The storage tank is a 1MPa pressure vessel, to be designed and built according to the ASME VIII Boiler and Pressure Vessel Code [28]. The choice of ASME VIII rather than ASME III [29] (which is the code for nuclear pressure vessels) may be strange. The argument proposed by PBMR is that the spent fuel can be classified as radioactive waste, in which

case, the ASME VIII code is valid. This choice has a significant reduction in material and manufacturing cost. Also, there is currently no ASME III certified pressure vessel manufacturer in South Africa. It will cost a few million Rands for a company to attain the ASME III certification, and this cost will then be discounted into the price of the storage tanks.

Figure 7 shows a schematic layout of the storage tank with its main components. The primary components are the pressure vessel that contains the cooling tubes and forms the pressure boundary. It has a ring support at the top and is therefore suspended from above. This eliminates any buckling modes experienced by bottom-supported vessels. The Tank Unloading Device (TUD) connects at the bottom of the tank via a special interface welded to the pressure vessel. Figure 8 shows a pictorial view of the tank. In the next paragraphs, the main components will be discussed in more detail.

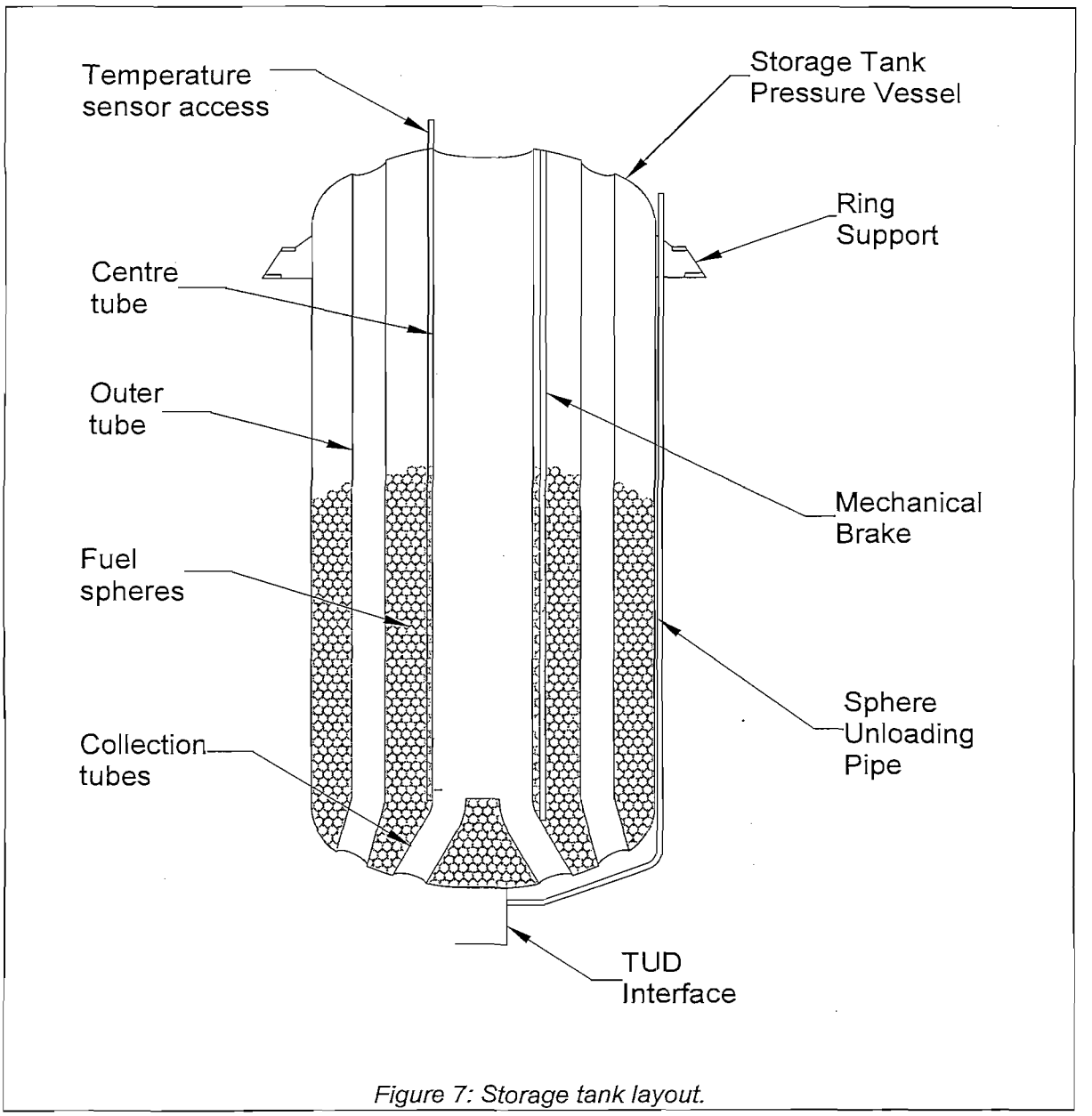

Figure 7: Storage tank layout.

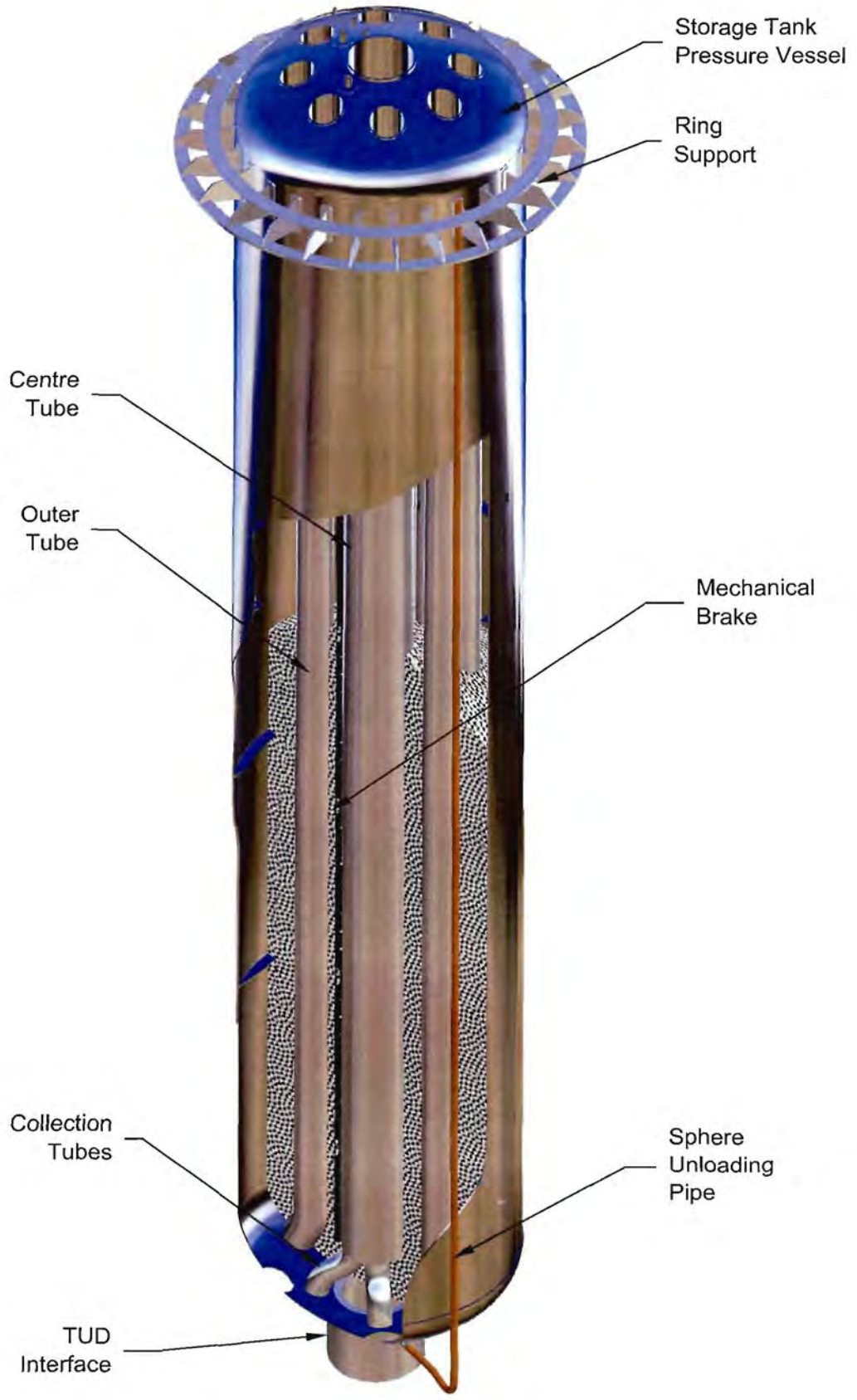

Figure 8: Picture of the storage tank.

3. STORAGE TANK MAIN COMPONENTS

3.1 STORAGE TANK PRESSURE VESSEL

This component defines the fuel storage volume. It is a 3.1m ID cylindrical pressure vessel with semi-ellipsoidal dish ends at the top and bottom. The vessel is nominally 18m long from end to end. The top dish end has a number of small tube nozzles where sphere, gas and inspection pipes are welded to during installation. The shell is 16mm thick and the dish ends 18mm after forming.

In the centre is a cooling tube of 762mm (30inches) OD running from the top and splits into four smaller collection tubes at the bottom.

There are also 8 outer tubes running from the top of the tank to the bottom. The tubes are situated at a pitch circle of 1800mm and all have an OD of 406mm (16inches). The tubes are open at both ends to allow airflow through. At the bottom, the tubes bend slightly outwards to make room for the centre collection tubes.

The nominal wall thickness of all tubes is 16mm, although the closest standard size for the tubes will be used.

At the top of each cooling tube, just below the dish end, is a linear expansion bellow. This bellow prevents thermal stresses due to the differential expansion. The bellows are however stiff enough in the radial direction to prevent major lateral displacements.

There are four stiffening rings on the inside of the pressure vessel shell to protect it from collapsing under full vacuum. The stiffener rings have a 10° sloping upper surface to prevent stationary spheres.

3.2 RING SUPPORT

The ring support is welded to the top of the pressure vessel, just below the joint between the dish end and the shell. The tank is supported vertically by this component. It consists of 27 gussets, welded to com-pads onto the pressure vessel shell. An upper and lower ring is also welded to all gussets. The support is designed in such a fashion to allow airflow to pass through the support. The support is shown pictorially in Figure 9.

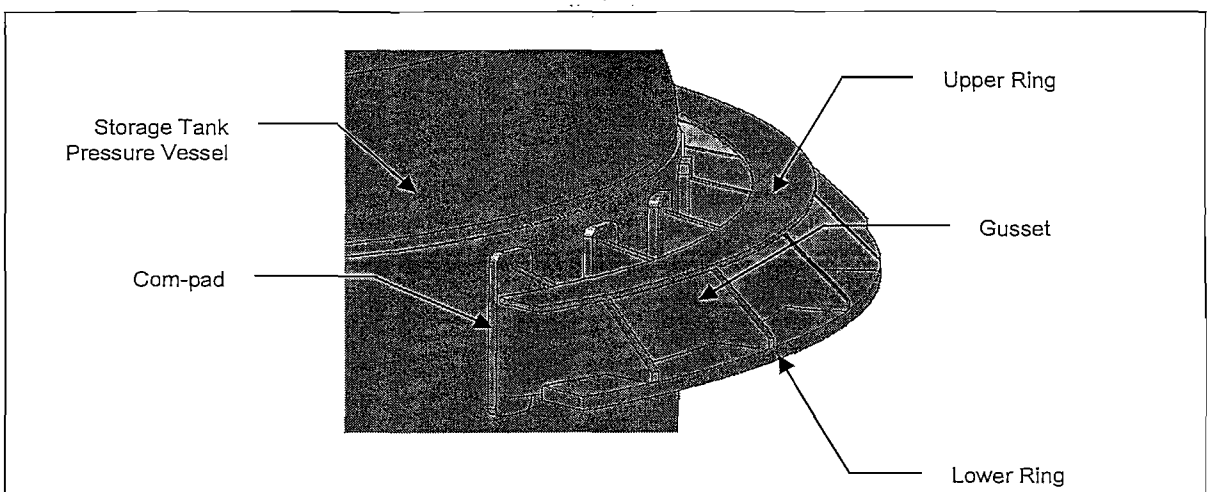

Figure 9: Tank ring support.

Finite element analyses of the support have been done for a full tank under a 2g vertical load. The stress contours are displayed in Figure 10. A small stress concentration of 100MPa can be seen at the base of interface between the gusset and bottom ring. This would be the place where fatigue cracking would start, and needs to be monitored during the life of the tank. More detailed analyses are needed to verify the structural integrity according to the ASME code requirements, however, there is ample room to increase the strength by using thicker gussets.

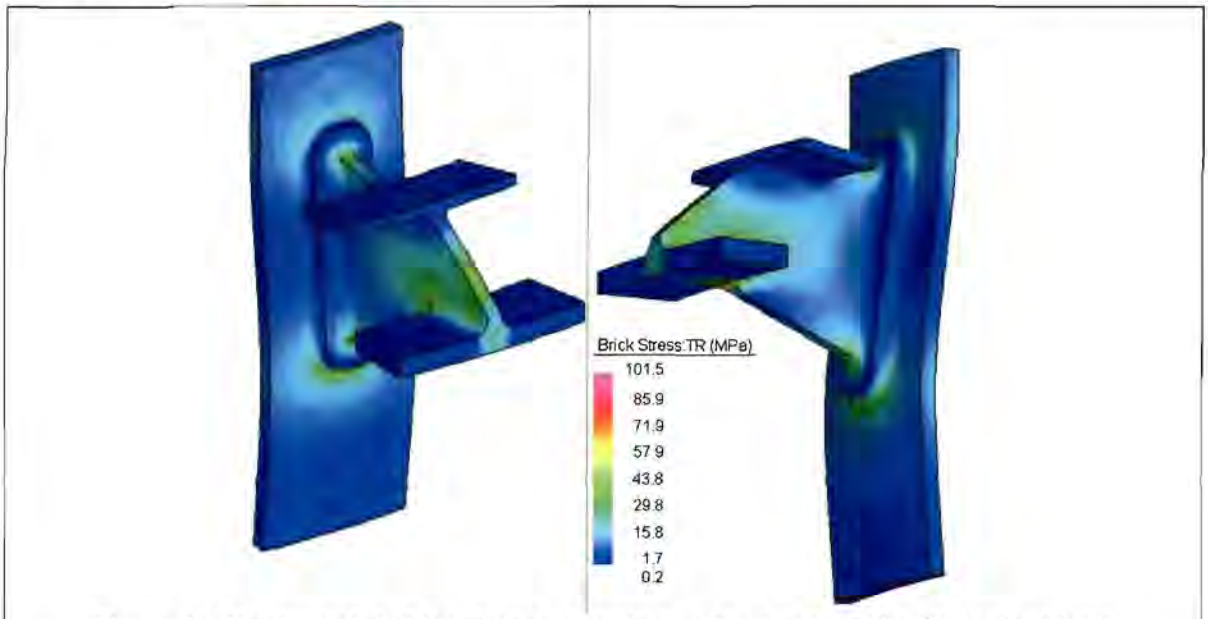

Figure 10: Contour plot of the Tresca stresses on the support at a 2g vertical load.

3.3 TANK UNLOADING DEVICE INTERFACE

In the centre of the bottom dished end is the TUD interface. This is a specially machined "flange" into which the functional components of the Tank Unloading Device (TUD) are installed. The tank is also supported radially onto this component. There are two types of TUD Interfaces, one has a single outlet, and the other has three outlets. The SFT has a single outlet interface, and the UFT and GRT have triple outlet interfaces. The TUD is described in more detail in the next chapter. When the TUD is not installed, the opening is large enough so that it can also function as the access hole to the inside of the tank. The storage tank therefore does not have an additional access hole.

3.4 PASSIVE MECHANICAL BRAKE

The mechanical brake limits the sphere velocity as it drops down inside the tank. This is necessary to prevent significant damage to the spheres. It is a passive device, having no moving components.

The brake consists of an 80mm ID pipe with a number of obstructions along the length of the pipe. The obstructions are placed in such a fashion that it is not possible for a sphere to fall down the pipe without hitting any obstruction. The sphere therefore continuously hits the obstructions as it moves down. These impacts reduce the kinetic energy of the sphere, thus limiting its maximum velocity. The obstructions are placed at regular intervals along the brake in such a way so as to ensure that the impact of the sphere on the obstruction does not cause significant damage. There are exit openings at the side of the pipe at 1m intervals that allow spheres to exit the brake at that position.

Figure 11 shows a pictorial view of the brake and also depicts the process of filling as described below.

When the tank is empty, the spheres run all the way through the brake. The pebble bed height gradually increases until it reaches the bottom of the brake. When the spheres cannot exit at the bottom, they start to build up inside the brake until it reaches the first side opening. The next spheres then hits the last sphere in the pillar, and bounces out at the opening. This goes on until the pebble bed height is again at the opening level. The tank is thus filled from the bottom, with minimum increments of 1m. The side openings alternate between left and right in order to load the tank more evenly.

When the tank is emptied, the spheres roll out at the bottom. Full scale tests have shown that only in very rare circumstances where two halve spheres lie next to an opening is there a possibility for a blockage. This blockage does not prevent the spheres outside the brake from being unloaded. If a blockage does occur, it can be removed by a special prodding tool via the TUD after the tank has been unloaded. However, the probability of a blockage is so low that the special tool is currently not part of the standard maintenance equipment.

The SFT has one brake, while the UFT and GRT has three brakes, one for each loading line. It is attached with gussets to the centre tube, and is placed in between the bottom collection tubes as viewed from above. The brake is not physically attached at the top dish end, rather it aligns loosely with the sphere inlet nozzle at the top.

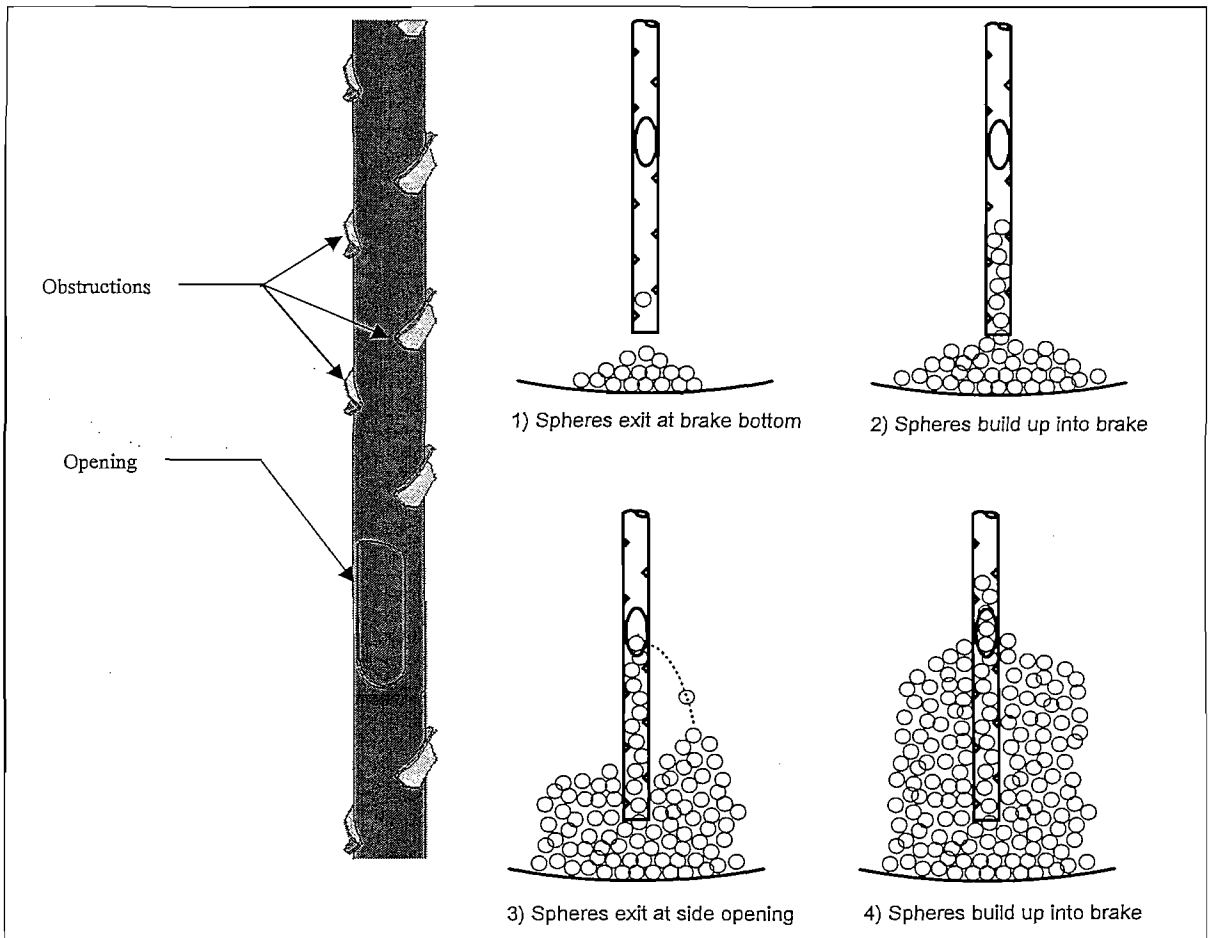

Figure 11: Pictorial view of a section of the mechanical brake along with the functioning of it.

The mechanical brake is a crucial component of the storage tank. The concept of the brake originated in the basic design of the 268MW reactor design. At that stage only a 1/10th scale test was performed using plastic spheres. Because of the difference in impact properties of the spheres, the brake did not function as reliably as required. Also, there was a risk that the stationary sphere at the opening will be pulverised when about 30000 spheres hit it on the same point.

For this reason a representative length of a full scale brake was made and tested with actual graphite spheres. This full scale test showed a much higher reliability, and also indicated that the stationary sphere is not hit on one point only, but rather rotates around the whole time. The damage to the spheres is also considered comparable to that of other FHSS process elements.

Another full scale test will be conducted in a helium environment. The test will be done for significantly more iterations in order to obtain a representative statistical distribution.

3.5 SPHERE UNLOADING PIPE

This pipe conveys the spheres from the bottom of the tank to the top. It is a standard ribbed sphere pipe as used in the rest of the FHSS. The pipe is welded to the outlet of the TUD Interface, and is then fastened to the vessel all the way to the top. The fastening is such as to allow for thermal expansion. Similar to the mechanical brake, some tanks have three unloading pipes, and others only one.

3.6 TEMPERATURE SENSOR ACCESS

The storage tank is fitted with three temperature sensor access tubes – one on the centre tube, one on an outer tube and one on the shell of the tank. A flexible temperature sensor can be inserted into the tube to measure the temperature at different heights. The temperature measurements will be used to obtain an accurate fill level, as well as to monitor the fuel temperature distribution in the tank.

4. SCALE MODEL TESTS

Two 1/6th scale models of the SFT was built and tested. The purpose of the tests was to verify the packing density inside the tank, as well as the sphere flow properties and if any spheres remain behind after unloading. The second model was built due to the standardisation of the tank geometries (see Chapter 4).

The conclusion of the tests was that no sphere blockage was noticed, and a packing factor of 0.60 was achieved. This result confirmed the value used for all volumetric sizing calculations. The value was obtained from reference [30].

Two 1/6th scale models of the UFT were also built and tested, with the same purpose as for the SFT, except that the sphere flow was also investigated on a preliminary basis. The sphere flow is of some importance, since it describes how the sphere distribution inside the tank will change as it is returned to the reactor. Although not a requirement of the UFT, it would be advantageous if minimal sphere shuffling occurred during the re-fuel mode.

Unfortunately, it was found that the spheres at the centre of the tank move significantly faster than the outer spheres. This results in negative cone shape at the top, and causes the volume to invert about two times before all the spheres were out.

The first model quickly showed a flaw in the design of the bottom tubes. The tubes were

spaced incorrectly and caused severe blockages (see Figure 12). A design change was done and the new UFT geometry was tested with great success.

Figure 12: Blockage at the bottom due to incorrect pipe placement.

5. CONCLUSION

The final containment barrier for radioactivity in the storage system is a storage tank made according to pressure vessel standards. This result in a much higher containment than what is theoretically required, since only the graphite dust contains significant contamination.

The storage tanks all have the same geometric design and main components. The pressure vessel part is an ASME VIII cylindrical vessel, with a number of cooling tubes running from the top to the bottom. The ring support at the top allows for free air movement, and also eliminates the buckling of the vessel.

Exact geometry and scale tests have been performed on the mechanical brake and pressure vessel to investigate the sphere flow and reliability. All the tests showed that the current design is suitable for storing fuel spheres.

Chapter 6 : New Tank Unloading Device

1. INTRODUCTION

The Tank Unloading Device (TUD) plays a cardinal role in the ability of the SSS to remove spheres from one tank and transfer it to another tank, back to the reactor or to a transport cask for final disposal. The device has had various concept configurations during the evolution of the SSS. These concepts often had a big impact on the sphere pipe layout and process design of the tank outlets. The details of the various concepts will not be described here, only their shortcomings will be illustrated.

The development of a device that complied with all requirements and assisted in simplifying the sphere pipe layout called for innovative ideas and several experimentation. The following paragraphs will present the requirements of the TUD, and describe the various tests and conclusions that were made in order to arrive at a feasible design solution.

2. REQUIREMENTS OF THE TUD

At the beginning of the project, the requirements of the TUD have not been formally documented. They were always deducted from performance requirements of the higher level system, and the current process layout. The following list could be seen as the design drivers for the TUD and formed the basis for the development of a new TUD concept.

a. A minimum discharge rate was always implied, and varied as the performance requirements of the FHSS changed. However, all the previous concepts had the ability to easily meet the discharge requirement.

b. The 400MW power upgrade required that the TUD should be able to discharge spheres into three lines. This was possible with a previous concept. However, it is also required that the contents of a storage tank be discharged into only one line (for example during decommissioning). It was not possible with the previous concept to simply block two of the three lines and unload from only one line, thus a complex system of valve blocks were required below the tanks to collect the spheres from three lines into one.

c. The requirement for pneumatic conveying of the spheres in the FHSS is that there may be only one sphere at a time in a lifting line. This requirement implies that the TUD should be able to discharge spheres at a controllable time interval. The alternative is a sphere buffer and indexer block below the tanks to control the time interval. All previous concepts did not have an explicit control over the discharge time interval.

d. There is an unwritten rule that there should be a sphere counter at the exit of each valve block to verify that the sphere has indeed exited from the block. This rule also applies to the TUD. However, with the previous concepts it was not possible to have a sphere counter in the TUD, but only in the sphere pipe a distance away from the TUD. This means that a blockage between the TUD and the counter will only be known when the sphere pipe is filled with spheres up to the TUD, and the TUD gets blocked.

Removing such an obstruction will be very difficult, as the FHSS maintenance equipment is designed to remove only 2-6 spheres from a blockage.

e. The maintenance philosophy of the FHSS requires that the maintenance of the TUD be done with the same equipment as the rest of the FHSS. This implies that all maintenance intensive components of the TUD should have the same interface as that of the FHSS process valves (see Appendix A for a short description of the FHSS process valves and its maintenance).

f. The TUD may not break a significant amount of spheres if it gets stuck for some reason. A *significant amount* cannot be defined, only that it should be As Low As Reasonably Achievable. It is very important, though, that once a sphere has been broken, it should not prevent the TUD from unloading the rest of the tank, nor may it cause damage to the next sphere. Some concepts have a scissor action, which if a sphere is cut in halve, will result in cutting all successive spheres in half too.

3. PRINCIPLE FUNCTIONING

All TUD concepts are based upon the same principle functioning. The device essentially consists of a rotating head, and a housing. The head and the housing each have a hole the size of one sphere diameter plus tolerance. By rotating the head, spheres are picked up one by one from the bottom of the sphere volume, released into the housing hole and discharged into a sphere pipe.

For the concepts presented in this thesis, the rotating head had two holes on the side opposite from one another. The housing had three outlet holes located 120° from each other. The two holes in the rotating head present a doubling in the discharge rate.

The housing is located below the head and the rotating head blocks its hole, except at certain head rotation angles. As the head rotates, it picks up a single sphere in its hole. When the hole passes the exit point on the housing, the sphere falls out, and the next sphere drops into the hole of the head.

With the proper head rotation speed, one can ensure that the second sphere does not also fall through the exit hole on the housing. Figure 13 shows the sphere movement as the head rotates. Note that the second sphere just hits the housing. This implies that there is only a small speed range in which the second sphere will not also fall through. If the speed is too low, the second sphere will also fall through, and if it is too fast, the first sphere gets jammed since there is not sufficient time to drop through the hole (see Figure 14).

This jammed sphere can also occur with the second sphere if it does not fall fast enough to miss the edge. The range in which a sphere can be jammed is quite large due to the high friction coefficient. This high friction coefficient is due to the Helium environment that results in no lubrication molecules between the contacting surfaces [31]. The bare materials therefore touch and chemical bonds are created. For steel, this can result in a pure metal bond or cold welding [32]. The friction between two graphite spheres is in the range of 0.6 at room temperature [33].

The jamming of the sphere is the biggest problem, since it can easily be sheared in two due to the inertia of the rotating head. The primary focus of the tests was therefore to arise at a rotating head design that will eliminate or highly reduce the possibility of jamming a sphere.

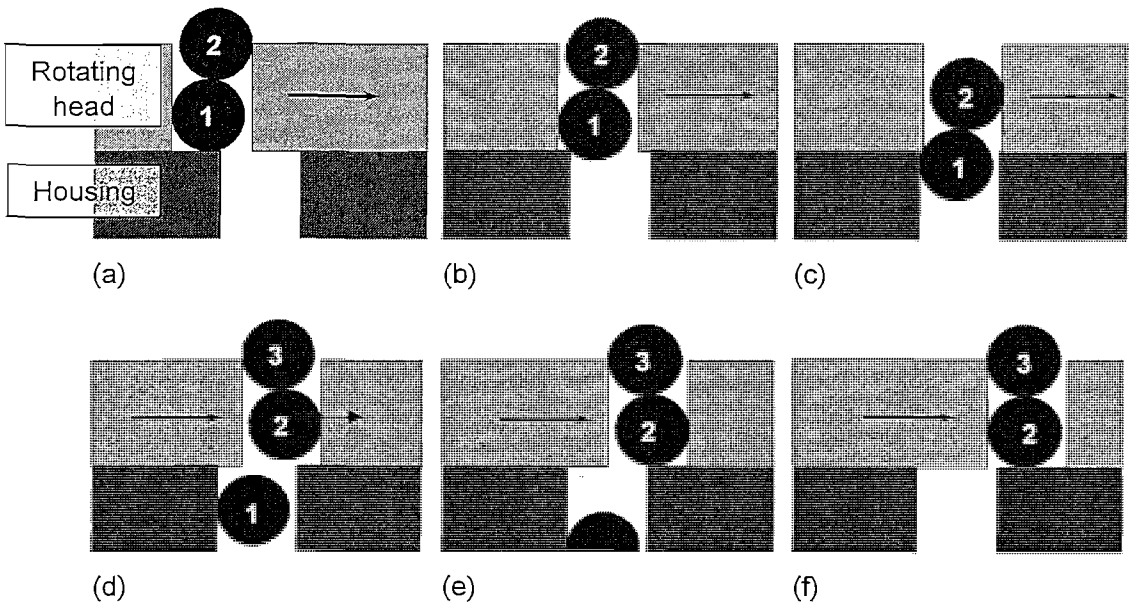

Figure 13: Sphere movement sequence (a)-(f) as the rotating head (top part) moving right past the housing exit point (lower part).

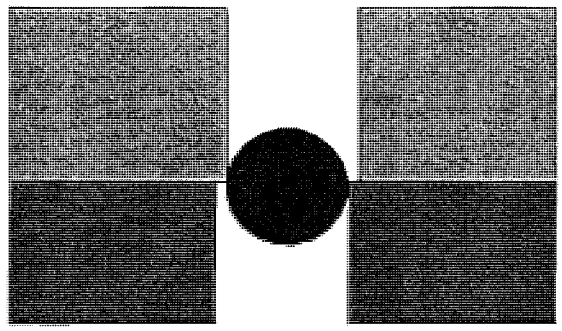

Figure 14: A sphere jammed between the rotating head and the housing exit hole.

4. ROTATING HEAD DEVELOPMENT TESTS

4.1 TEST SETUP

The tests were done on a 1/6th scale geometry of the storage tank bottom. 10mm Steatit spheres were used as they have a representative friction coefficient of approximately 0.5 in air [34]. Modifications to the test model were made as the concept changed. Eventually, a final concept TUD were manufactured and tested. The test stand is shown in Figure 15.

A wiper motor was used as the drive for the rotating head. It was powered by a variable voltage power supply. By changing the voltage, the rotation speed could be changed.

A light activated sphere sensor was located at the three exits of the housing. The signals from each sensor, as well as the voltage over the motor were recorded by an A/D card. The data was used to calculate the performance of the device.

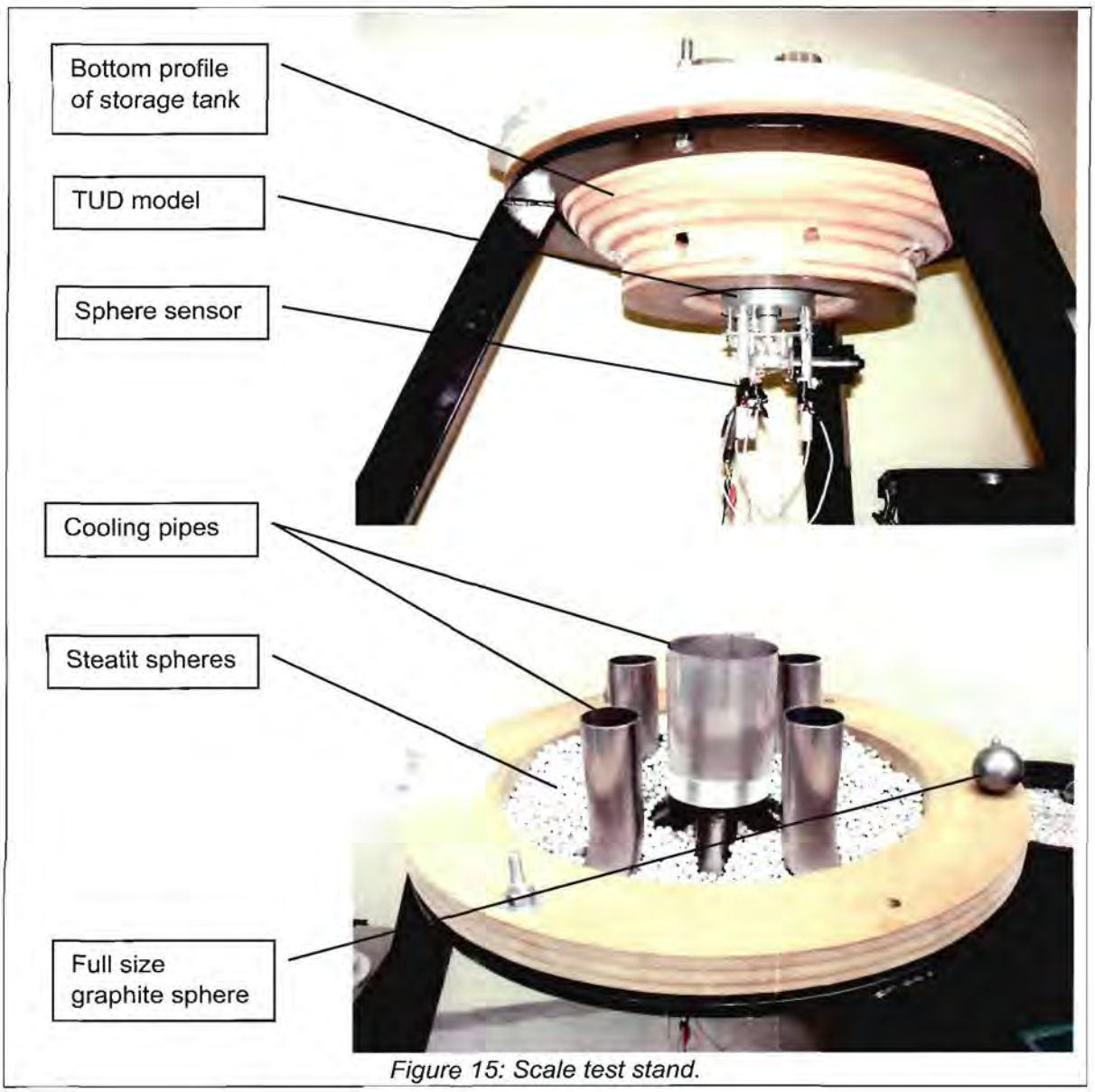

Figure 15: Scale test stand.

The bottom part of the tank was made from laminated hard-board, cut on an NC machine. The TUD itself was made from aluminium, and the cooling pipes of the tank from standard steel pipe.

4.2 TUD MOTOR CONTROL

When a sphere gets jammed in the TUD, the motor needs to be stopped, reversed for a small time fraction and then returned to the forward direction. This way the sphere can be released and the test can continue. This stop-reverse-forward action can be done manually for short-term tests, but for long-term tests a device is needed to automatically sense a blockage and stop-reverse-forward the motor.

The moment the motor stops, the counter emf of the motor falls away, resulting in an increase in motor current for a fixed voltage supply. If there is a small resistor in the wire to the motor, the change in voltage over the resistor can be used as a signal for an electronic device.

Alternatively, the power supply can be set to limit the current at a level just above normal operation. The moment the motor stops and the current increases, the limit is reached, resulting in a voltage drop at the power supply. This voltage drop is then the signal.

A number of attempts have been made to design an analogue circuit using relays and transistors to perform the sensing and motor control. None of these were successful. The devices were too sensitive to voltage changes, the relays latched and did not release, and the inductive pulses from the motor armature interfered with the electronics.

A programme was written using LabView [35] to control the motor from the A/D card. The power supply current limit was set very low and the voltage drop over the motor was used as the indication that there is a blockage. An analogue output signal was then sent to a relay that reversed the polarity over the motor. The signal was held for about 100 milliseconds. This resulted in the required stop-reverse-forward action of the TUD.

4.3 DATA COLLECTION AND POSTPROCESSING

Initially the voltage signal of each counter and the motor was sampled at a rate of 1000 samples per second. This rate is sufficient to ensure that at least 3 data samples are taken for the period where the sphere passes the sensor. The data was streamed to disk, and processed afterwards. Figure 16 shows what the sampled data looks like.

The first step in the data processing was to identify the time when a sphere has passed the sensor. This was done by monitoring the volt signal. The moment the volt is above 4V, the time is recorded. Similarly, the time was recorded when the motor voltage changed polarity. This would indicate a reverse of the motor. The time interval between successive spheres was calculated. This time interval will indicate whether a sphere was skipped ("dry-run"), or if the second sphere has followed the first ("double sphere"). The resultant data then looked like Figure 17.

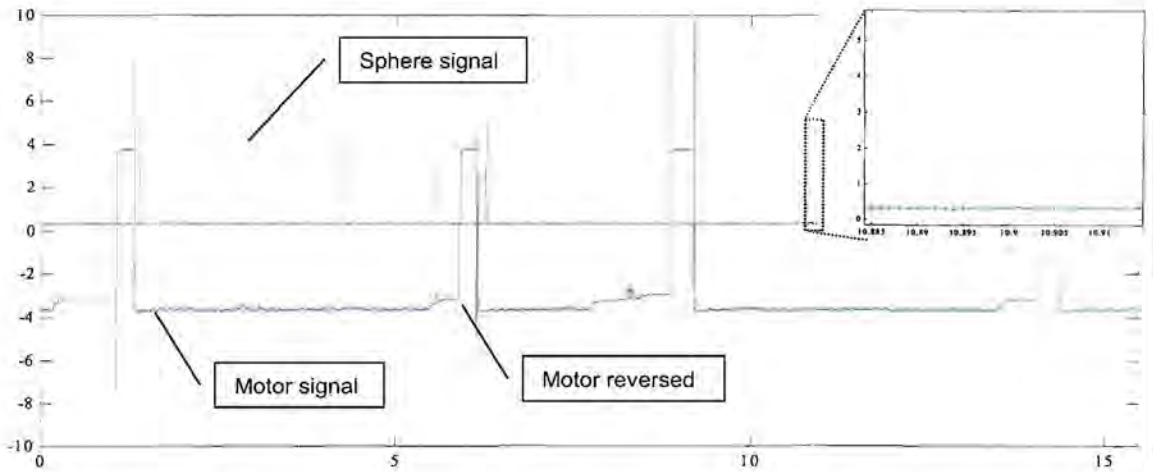

Figure 16: Sampled data showing the motor signal and sphere sensor signals.

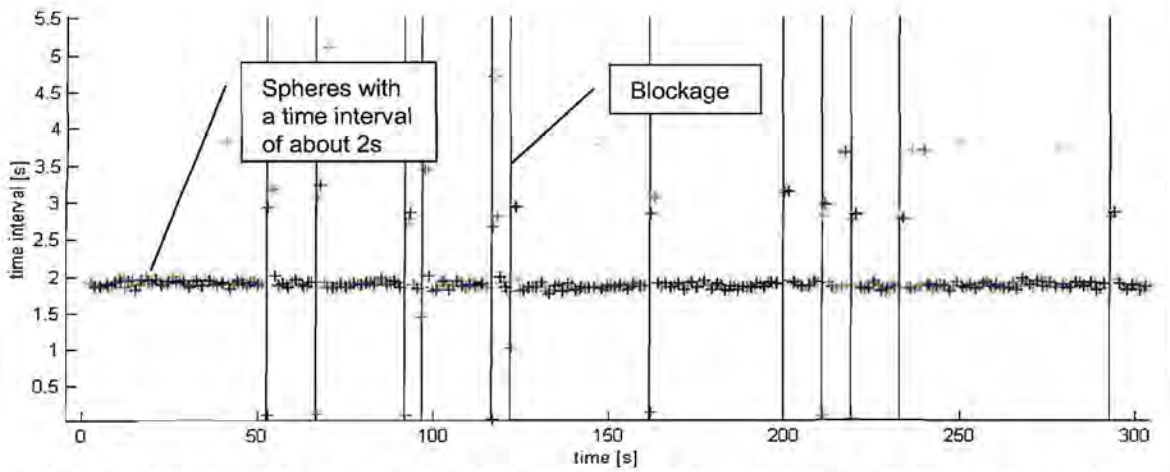

Figure 17: Processed data showing the time interval between successive spheres and the time of the blockages.

After the time intervals between spheres have been extracted, a histogram can be plotted of the time intervals. The histogram looks like Figure 18. From this histogram, a number of deductions can be made. Firstly, the large peak indicates the spheres that were discharged at the correct time interval. The peak resembles a normal distribution [36]. The number of spheres represented by the peak can be calculated by using a 3*sigma bandwidth. The mean of the normal distribution depicts the time interval between correctly-loaded successive spheres (for Figure 18, this is 1.84s). If there is a dry-run, the time interval will be around the 2*mean range. This can be seen as the small cluster around 3.6s on the figure. The cluster close to zero represents double spheres, i.e. the second sphere has followed the first sphere. This often coincides with a blockage, since the reverse action sometimes causes the second sphere to also pass through. The cluster between 1.8s and 3.6s resembles the delayed spheres during a blockage.

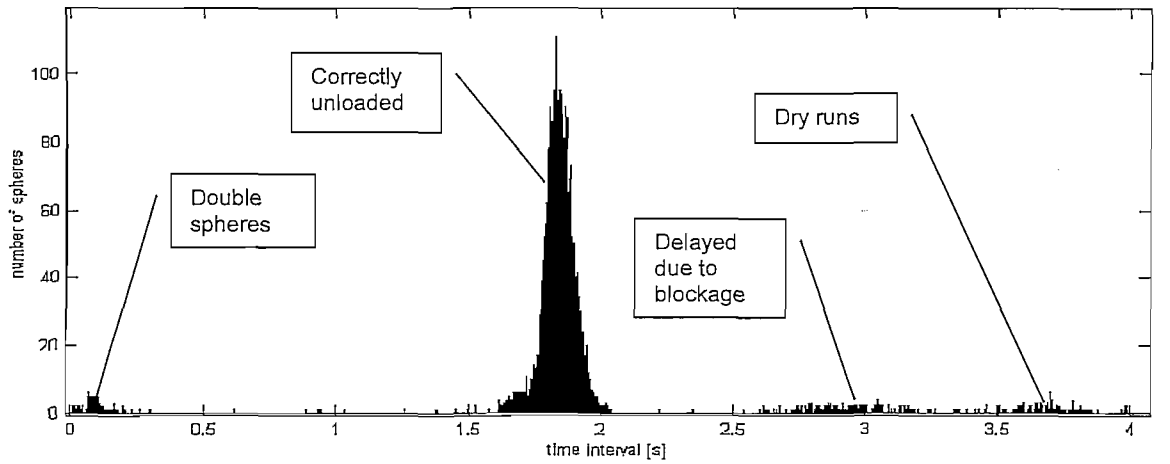

Figure 18: Histogram of time intervals showing the correctly loaded spheres, dry-runs and double spheres.

With the data calculated from the histogram, a number of ratios are calculated in order to compare different tests and concepts with each other. The ratios are:

Correct unloading: The number of spheres in the 3*sigma range around the mean time interval divided by the total number of spheres. This ratio represents the reliability of the device to discharge all the spheres at the same time interval. The ideal is 100%, however, blockages and dry-runs will reduce this number. The 3*sigma range was chosen to account for the variation in motor velocity and voltage supply.

Blockage per rotation: The total number of blockages divided by the total number of head rotations. This ratio represents the frequency of blockages. This ratio has an inverse relation to the correct unloading, i.e. the more blockages per rotation there are, the lower the correct unloading will be. Ideally this value should be 0%. The results can also be expressed as blockages per total number of spheres. For a TUD with two holes in the rotator and three in the housing, the blockages per total spheres is six times less than the blockage per rotation, since six spheres are discharged per rotation. This ratio is a better indication of the probability that a sphere may be damaged.

Double spheres per blockage: The number of spheres with a time interval less than ½ mean interval divided by the total number of blockages. This ratio indicates how many spheres are discharged during a stop-reverse-forward action. A value of 100% means there are always two spheres discharged in succession. A value less than 100% means that sometimes the second sphere does not follow the first, and more than 100% means that the third sphere also passed through. Ideally this value should be 0%, and might be accomplished if the time between reverse and forward is controlled as a function of rotation speed.

Dry runs per rotation : The number of spheres around the 2*mean interval range divided by the total number of rotations. This ratio is a measure of whether the first sphere is always replaced by a second. A value above 0% indicates that the hole in the rotating head sometimes stays empty for a full revolution. Ideally this should be 0%.

4.4 SCALABILITY OF THE RESULTS

A dimensional analysis on the discharge characteristics of the TUD has been done. The following Buckingham Pi [37] groups were identified:

$$\Pi_1 = \frac{d}{D} \qquad \Pi_2 = \frac{f}{\omega} \qquad \Pi_3 = \frac{d \cdot f^2}{g}$$

$d \equiv$ "Sphere diameter" [m]

$D \equiv$ "Rotating head hole PCD" [m]

$f \equiv$ "Discharge frequency" [1/s]

$\omega \equiv$ "Rotating head angular velocity" [1/s]

$g \equiv$ "Gravitational accelleration" [m/s^2]

If the scale model is $1/6^{th}$ of the full scale, Π_3 can be used to calculate the relation between the model discharge rate and the full scale rate:

$$f_{full} = \frac{f_{model}}{\sqrt{6}} \approx \frac{f_{model}}{2.5}$$

For example: If the model discharges spheres at 3s per sphere, the full scale model will discharge spheres at:

$$\left(\frac{\frac{1}{3}}{\sqrt{6}} \right)^{-1} = 7.348 \text{ s per sphere}$$

4.5 INITIAL CONCEPT

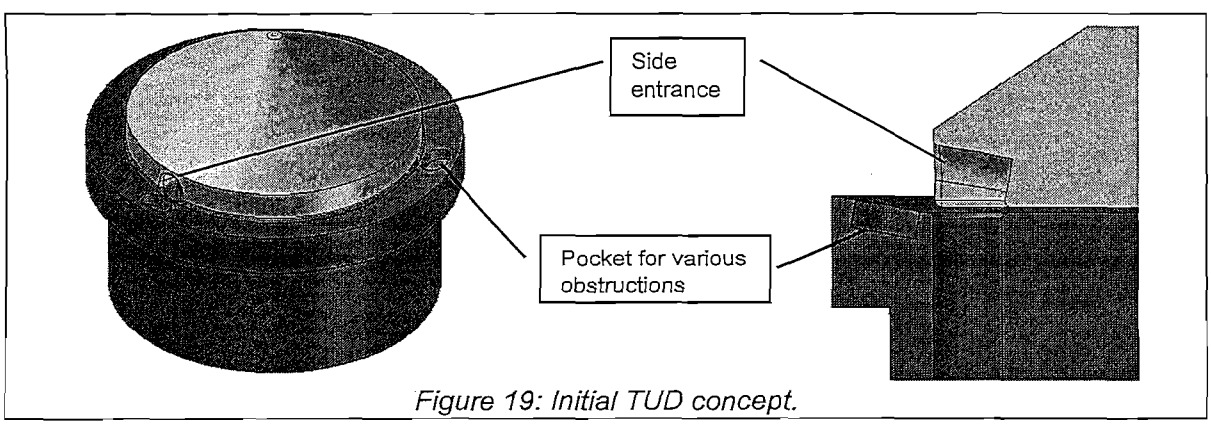

Figure 19: Initial TUD concept.

The initial concept is shown in Figure 19. It had a side entrance on the rotating head, instead of the top entrance as shown schematically in Figure 13. It was believed that this side entrance would reduce the possibility of the second sphere from following the first sphere. As an additional measure, it was contemplated to add a minor obstruction right in front of the

exit hole on the housing. This could help in preventing the second sphere from following the first sphere.

In order to vary the geometry of the obstruction, a pocket was machined out of the housing. Body filler was used to shape different obstruction geometries. They ranged from small pockets, small protrusions and even large barriers in front of the hole. The results of the different obstruction geometries are presented in the table below.

Table 2: Effect of obstruction geometries

Obstruction type	Results
Small pocket	No effect.
Small protrusion	Sometimes a sphere gets jammed between the protrusion and the rotating head.
Large barrier plate	The spheres get jammed the moment the hole moves behind the barrier plate.

To conclude, the additional obstruction in front of the exit hole either caused a blockage, or had no effect on preventing the second sphere from following the first sphere.

4.6 MODIFIED INLET HOLE

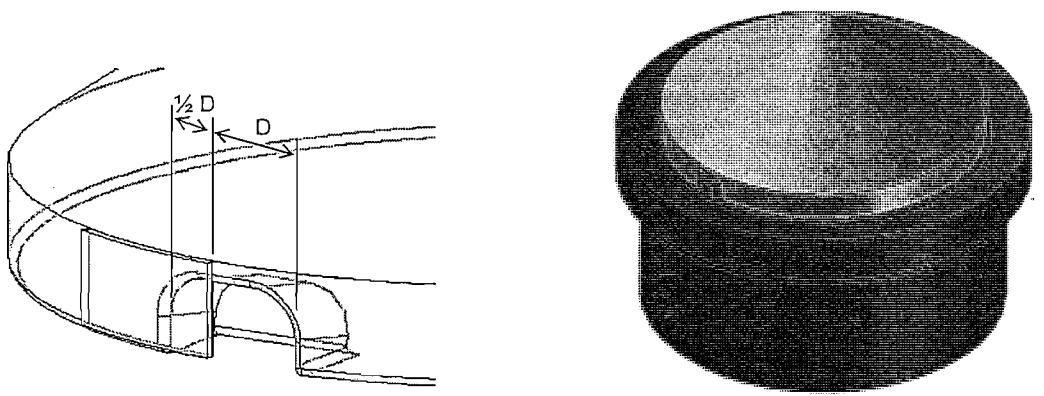

Figure 20: Modified inlet hole.

A modification was made to the hole in the rotating head, which prevents the second sphere from falling through above a certain speed. The hole is shown in Figure 20. The hole consists of an entry gap of one sphere diameter, but the gap then opens to 1.5D. The first sphere lies in this additional 0.5D recess, with the second sphere at the entrance. As the rotating head moves past the exit hole, the first sphere drops through as normal. The second sphere starts to roll in, but now the gap of the exit hole is already behind the entrance. Thus the second sphere cannot fall into the exit hole. Figure 21 shows how this modified inlet works.

There is a minimum speed above which the second sphere will not follow the first sphere. The maximum speed is limited by the first sphere dropping into the hole. If the speed is too high, the first sphere gets caught by the rotating head as it drops down. Within this speed range, it can be guaranteed that the second sphere will not follow the first, hence no blockage. However, if the hole is empty when it approaches the exit (called a dry run), and a sphere then drops in, there is the chance that it may still be jammed. The new inlet thus works well provided there is always a second sphere to replace the first one.

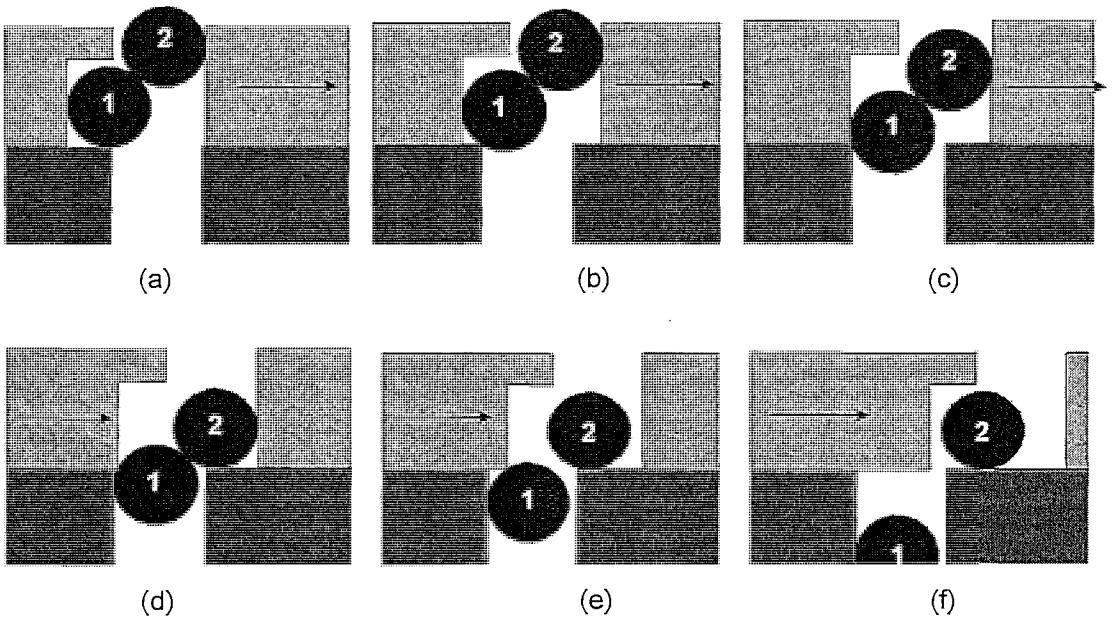

Figure 21: Illustration of the modified inlet hole functioning showing that the second sphere does not fall into the exit hole (a) to (f).

4.7 VERTICAL INLET

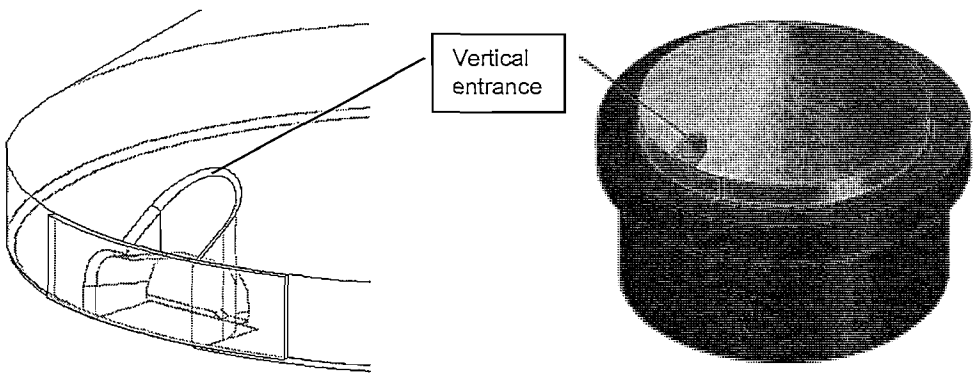

Figure 22: Modified TUD inlet to a vertical orientation.

In an attempt to limit the number of "dry runs", the inlet orientation was changed from sideways to vertical as shown in Figure 22. This worked well, but the blockages still occurred too frequently implying that there are still too many "dry runs".

4.8 RECESSED HEAD AND BI-DIRECTIONAL HOLE

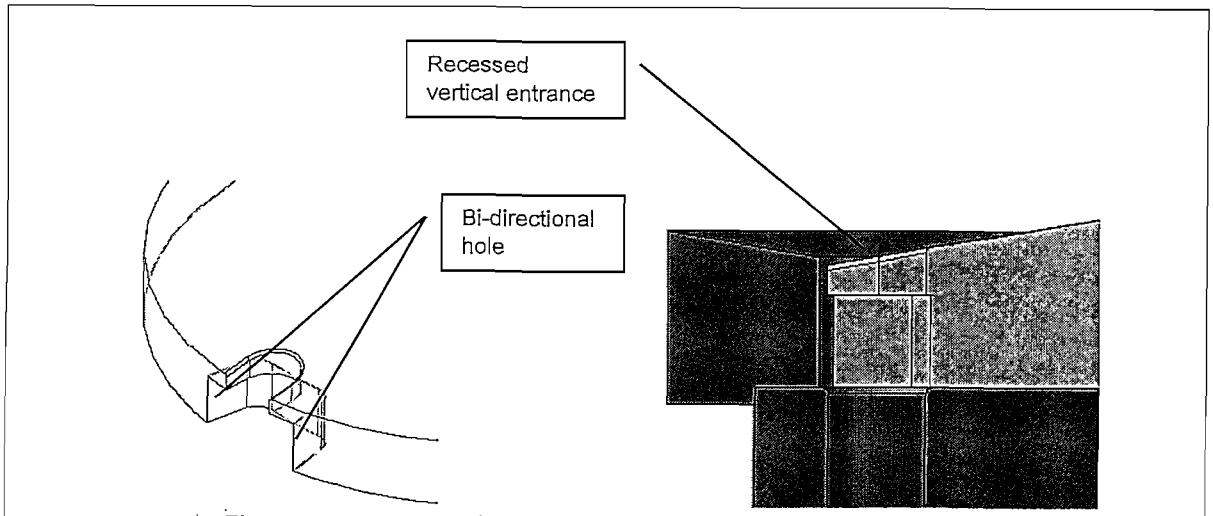

Figure 23: Recessed vertical entrance with bi-directional hole.

A new TUD model was built, based upon the results of the first one. The rotating head was recessed in order to have the lowest point of the device at the hole (note that the TUD in Figure 22 will not be able to remove all the spheres). Also the cut-out in the hole was made in both directions in order to make the device bi-directional. This was done to eliminate the reverse-forward action when a sphere gets jammed. Instead of returning in the same direction, the motor could run in the reverse direction until the next blockage.

It was soon realised that the bi-directional hole is not beneficial. This is because it is now possible for the first sphere to lie in the forward recess. The second sphere can now easily follow the first and cause a blockage. Figure 24 shows how the second sphere can follow the first.

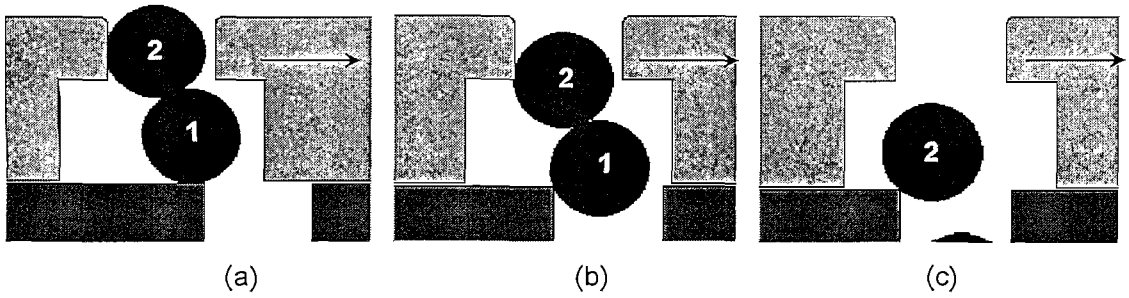

Figure 24: Second sphere following the first in a bi-directional hole (a) to (c).

When the device was run in one direction only, it blocked a minimum of 6.2% per rotation at a speed of 33rpm. At this speed, it had 2.5% dry runs per rotation (see Figure 26). This indicates that the second sphere does not immediately replace the first, causing the blockages. The reason for the dry runs is that the sphere directly above the hole is held in place by the spheres adjacent to it, as shown in Figure 25.

If the normal vector makes an angle less than $\theta = atan(\mu)$ with the horizontal, the sphere may be held in place. A friction coefficient of 0.6, results in an angle of 30°. If the friction coefficient is not that high, this phenomena would not be so pronounced.

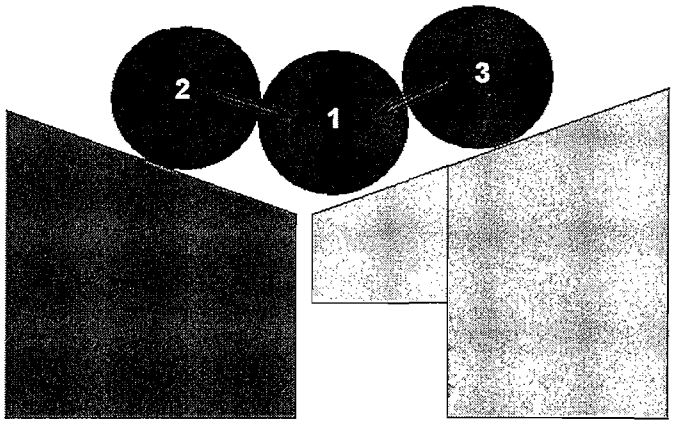

Figure 25: Sphere 1 is held in place by spheres 2 and 3, thus preventing it from entering the hole in the rotating head.

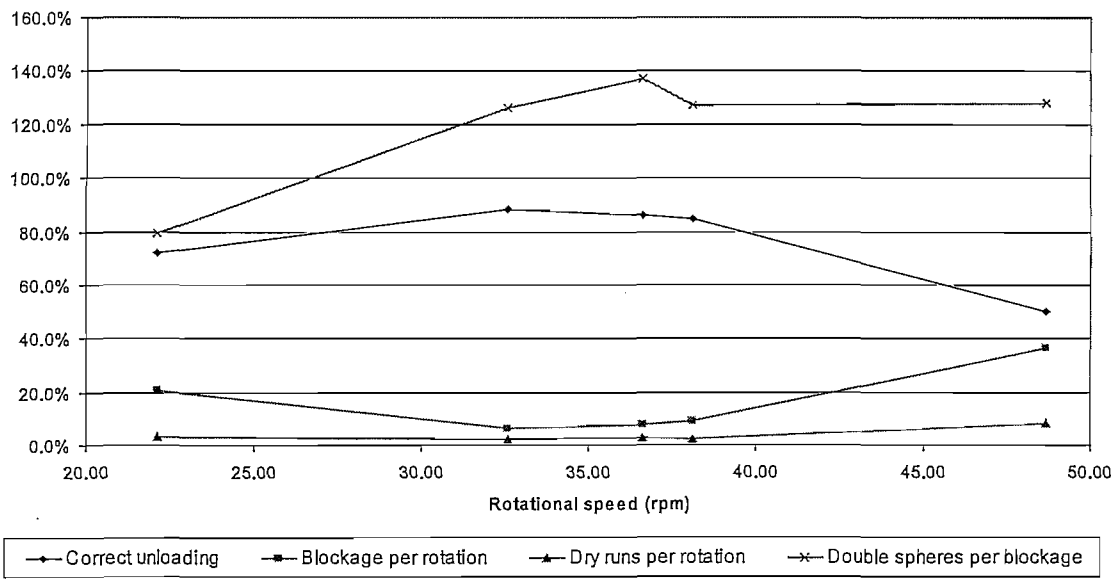

Figure 26: Results of tests for the concept with a modified inlet hole (bi-directional rotation not shown).

4.9 RECESSED ROTATING HEAD

To solve the problem of the previous concept, the inlet to the rotating head was recessed a full sphere diameter downward (as shown in Figure 27). This ensures that any normal force on sphere 1 is more than 30°. This effectively forces the sphere downward the moment the hole goes past. Because the head rotates continuously, it is not possible to form a static arc between spheres 2 and 3.

This modified model was tested and resulted in zero dry runs. The device was very sensitive to speed, which meant that there is a small range in which it works reliably.

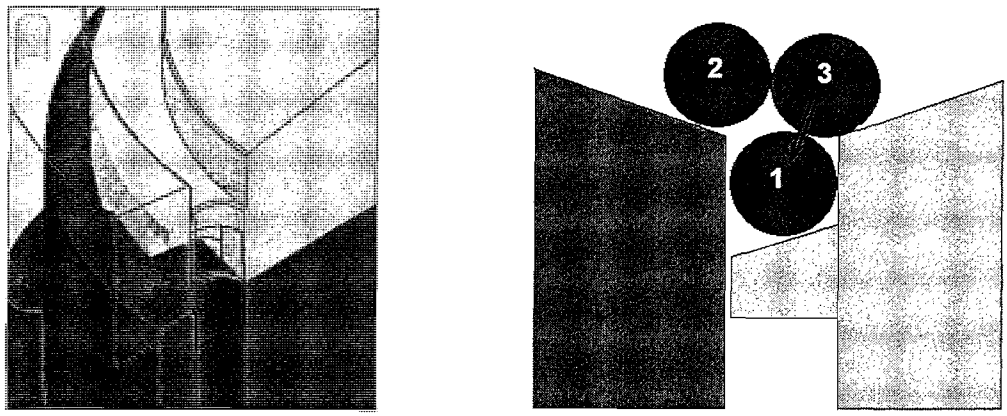

Figure 27: Recessed rotating head.

4.10 ADDITIONAL HOLE CUT-OUT

The small speed range of the previous concept is caused by the first sphere being caught by the rotating head as it drops down. To increase the speed range, an additional cut-out was made to the hole on the rotating head (see Figure 28). This cut-out is just smaller than ½D. This ensures that the sphere cannot jam in the corner of the cut-out. Figure 29 shows how the cut-out improves the speed of the device.

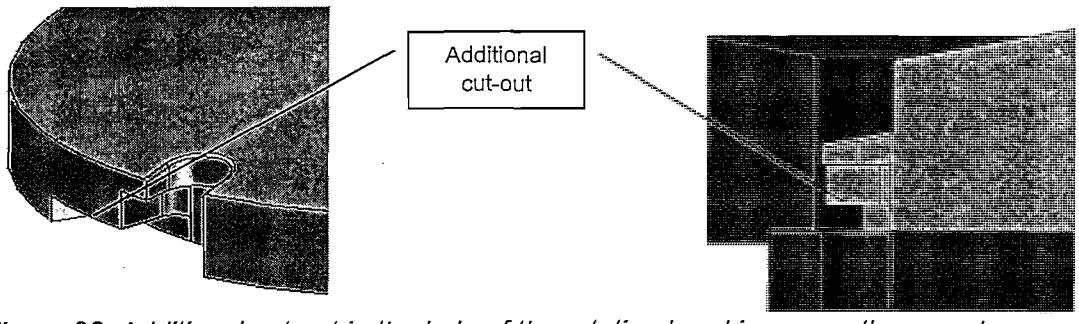

Figure 28: Additional cut-out in the hole of the rotating head improves the speed range.

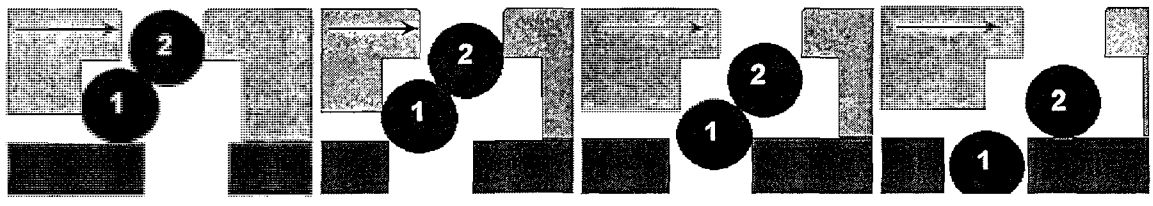

Figure 29: The extra cut-out prevents the first sphere from being caught by the rotating head at higher speeds (a) to (d).

With the modified hole, the device blocked on average 0.4% per revolution (or les than 0.1% per sphere) over a speed range from 29rpm to 42rpm. At a speed of 46rpm, it blocked only

2.5% per revolution (see Figure 30). At speeds higher than that, the first sphere moves too fast horizontally, and thus does not fall down into the hole.

The final design for the TUD is therefore based upon this concept. The minimum length of the additional cut-out still needs to be determined.

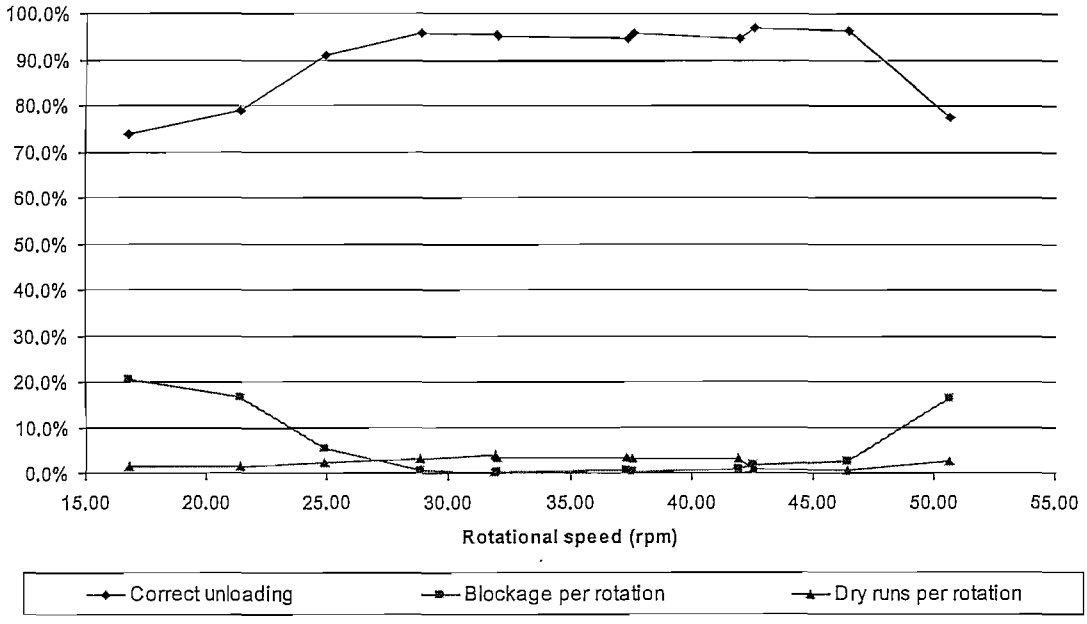

Figure 30: Results of the device with an additional cut-out in the hole.

5. SCALED PERFORMANCE FOR THE FULL SIZE TUD

The final concept TUD works reliably in a speed range from 29rpm to 42rpm. This relates to a full size TUD running between 11.6rpm to 16.8rpm. The minimum reliable time interval between spheres was 1.43s, and the maximum 2.08s. This relates to a full size range from 3.57s to 5.2s per sphere. It should be noted that the test model had two holes at 180° apart in the rotating head. This means that the discharge rate can be halved by simply removing one hole. The resultant full size range would then be from 7.14s to 10.4s.

More tests should be performed to see whether the range could be further enlarged, and to obtain more reliable performance figures.

6. SPHERE COUNTING AND CONVEYING

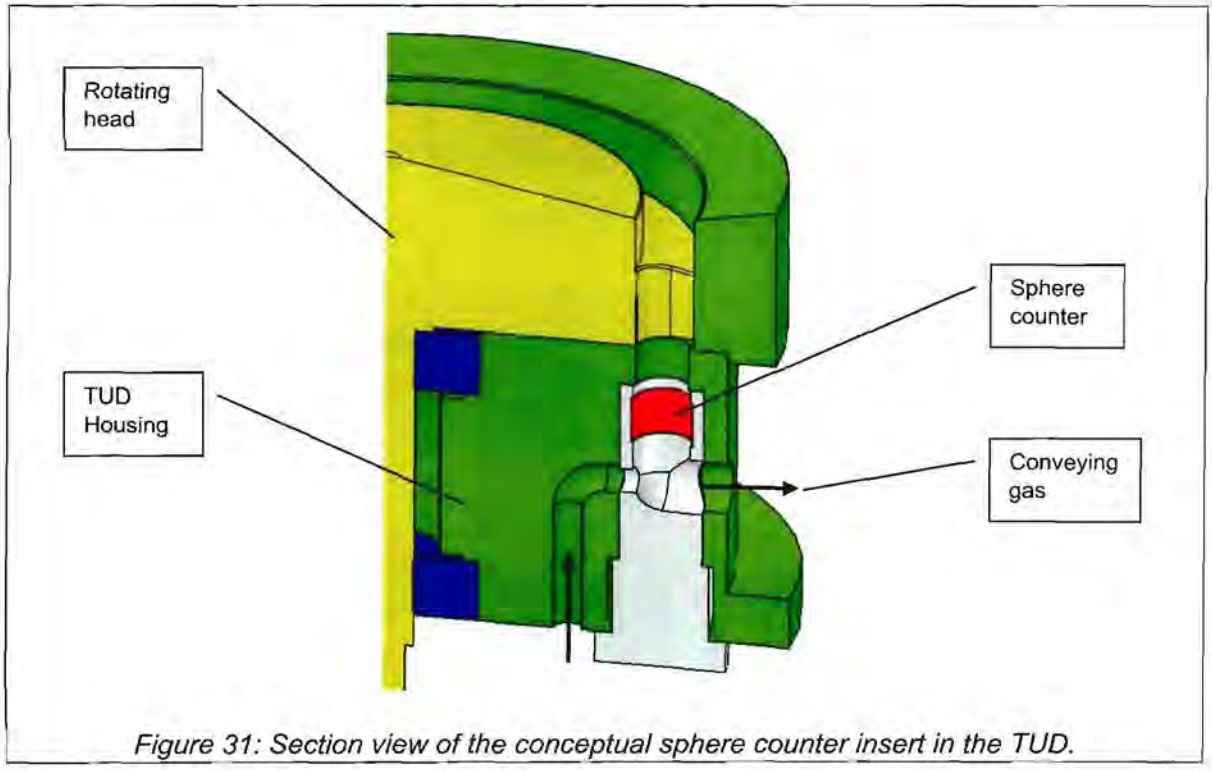

Figure 31: Section view of the conceptual sphere counter insert in the TUD.

In order to count the sphere immediately after it has left the rotating head, a special sphere counter insert is needed in line with the exit hole in the housing. This insert can be extracted from below like a standard valve block insert. The ceramic insert and coil part of an inline sphere counter can be used. Just after the counter, the sphere should be diverted 90° in order to exit the TUD at the side. High velocity gas (air or helium) is fed in from one side to transport the sphere. The lowest point of the unloading pipe is thus in the TUD. This way it is ensured that if the conveying fails, the sphere will roll down and come to rest inside the counter insert. From there it can be removed using standard valve block maintenance equipment.

7. ONE OR THREE LINE DISCHARGE FUNCTIONALITY

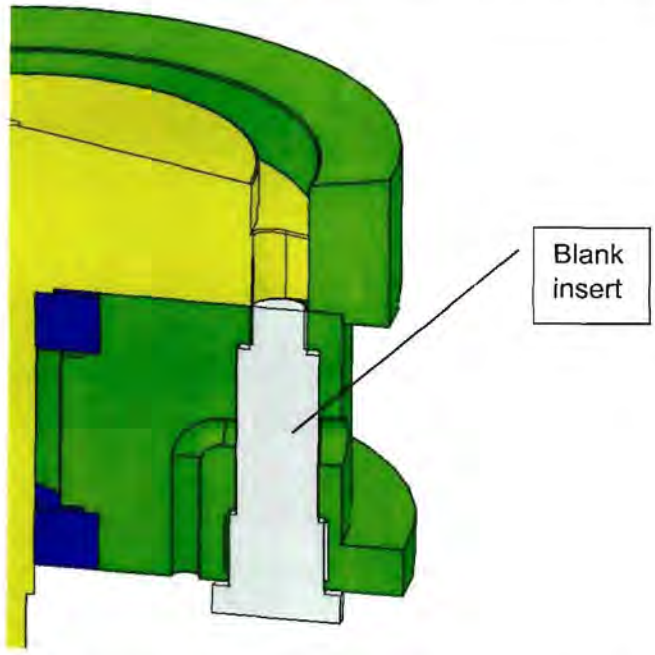

Figure 32: Blank insert replaces the counter insert to prevent sphere discharge at the specific exit hole.

As discussed in paragraph 2, the TUD should be able to discharge spheres in one line or in three lines. To prevent sphere discharge in a specific line, the counter insert can be replaced by a blank insert. This insert extends up to the top of the housing, thereby completely closing the outlet hole.

8. FINAL DESIGN

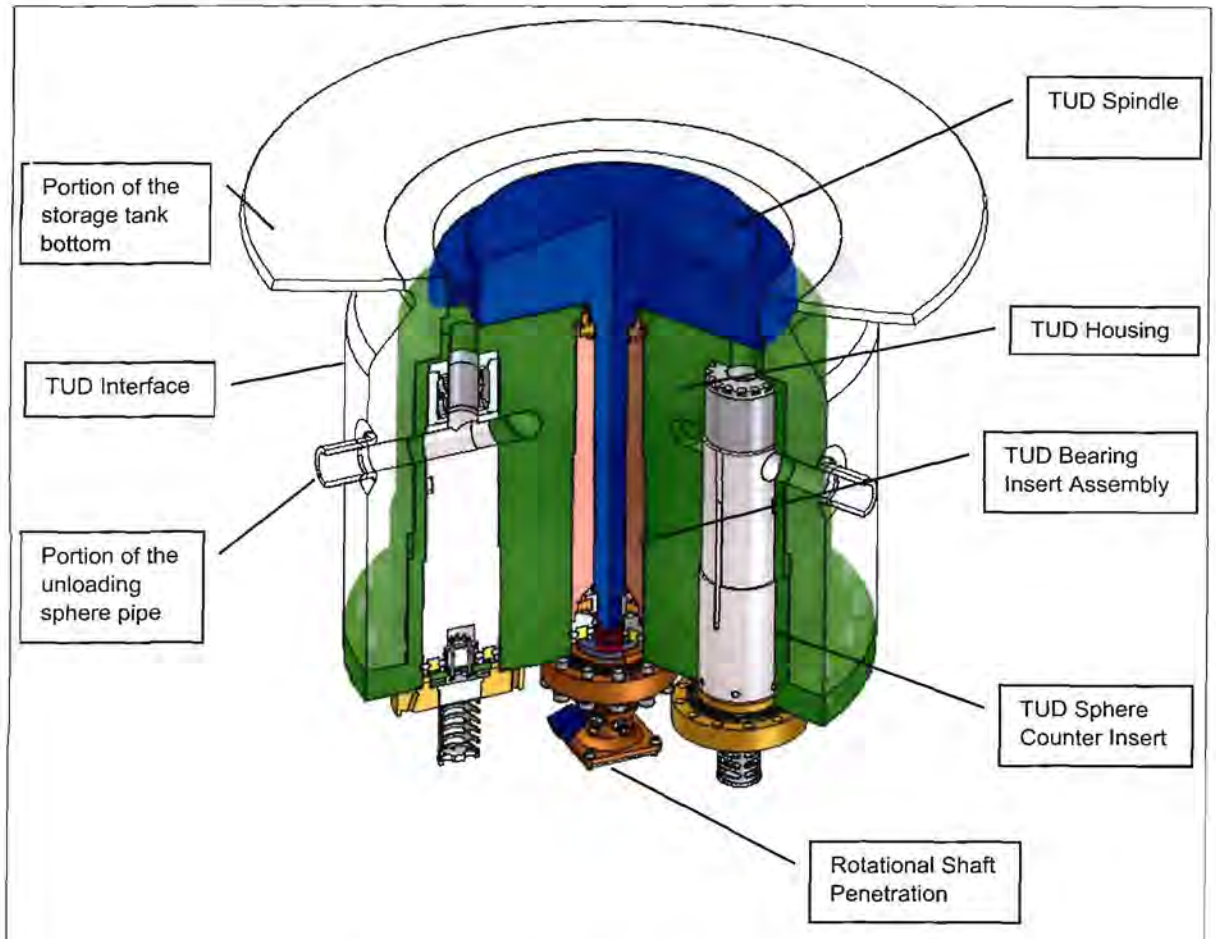

Figure 33: Layout of the full size TUD.

The final design of the TUD consists of the following main components:

TUD Housing: This forms the backbone of the TUD. It is a metal forging with penetrations machined into it for the interface with the other components.

TUD Spindle: This is the rotating head of the TUD containing the specially designed inlet hole. The spindle, along with the housing has to be installed before a tank will receive spheres, and cannot be removed afterwards.

TUD Bearing Insert Assembly: This insert contains the bearings needed when the spindle is being rotated. When installing this insert, the spindle is lifted a few millimetres up from the housing. The spindle therefore rotates without touching any metal component. Installation and removal of the bearing insert follows the same principle as that of other FHSS process valves.

TUD Sphere Counter Insert: This insert contains the sphere sensing equipment as well as a special insert body that diverts the spheres and allows for pneumatic conveying.

TUD Blank Insert: This insert is used to replace the TUD Sphere Counter Insert when that specific sphere line needs to be blocked.

specific sphere line needs to be blocked.

Rotational Shaft Penetration: This is a standard component also used on other FHSS valve blocks. It allows the rotating shaft of the spindle to penetrate the pressure boundary without leakage.

TUD Interface: The TUD housing fits into a special flange welded to the pressure vessel of the storage tank. This flange is called the TUD Interface and has a double seal surface.

Only the housing, spindle and blank plugs are installed before the tank receives spheres. When it is required to unload the tank, one or all three blank plugs are removed and replaced with counter inserts. The bearing insert, shaft penetration and motor are also installed. When the tank is empty, the components can be removed and installed in the next tank for unloading. This way the total cost of equipment can be reduced, and also the life of the components can be extended as they are installed only when required.

9. CONCLUSION

A new TUD concept has been developed that fulfils all the requirements. This has been achieved through numerous tests and experiments on a scale model. The result is a rotator with an intricate inlet hole geometry. The new design reduces the possibility of a blockages to less than 0.1% per sphere.

The final design makes use of modular inserts and enables the operator to minimise the total cost of the component by installing equipment only when needed.

The design fits in with the current storage tank design and detail design of the device can now be done.

Chapter 7 : Criticality Design

1. REQUIREMENT

For purpose of nuclear safety, the stored fuel spheres must be sub-critical at all times with a margin of 5%, resulting in a maximum allowable multiplication factor of $k_{eff} < 0.95$ [7]. The phrase "at all times" implies that the most conservative measures should be taken in calculating criticality. Also, the means to attain sub-criticality should be passive, and extremely reliable [5][6]. This negates the concepts of controllable absorber rods, or absorber fluids that could leak out.

Criticality analyses are done for optimum water moderation, and at the highest physical possible packing density of 0.64 (note, not the theoretical maximum [30]). The next conservative value to be used is to assume that the contents of the storage tank is fresh fuel. Taking all of the above factors into account, one ends up with a fuel volume that can never reach criticality, even in an event of sabotage.

The fresh fuel requirement is however over-conservative, resulting in a very expensive storage tank. In order to reduce the cost and complexity of the storage tank, credit is taken for the fact that the spheres do have a certain burn-up. Taking burn-up credit is an acceptable technique in spent fuel storage systems, and receives a lot of attention throughout the world [38].

Any storage tank should be able to contain the following sphere compositions:

a. Spent fuel at an average burn-up of 92 GWd/tu;

b. Used fuel – this is the full contents of a neutronically sound core;

c. A "dud" core or portion thereof – these are spheres that have a poor mechanical composition, but not a higher reactivity than an average core; and

d. Low enriched fuel – used for start-up purposes; it could be fresh or spent.

2. CRITICALITY

In a nuclear reactor, fissile material is split into fragments by neutrons. On average, 2.5 new neutrons are released in the fission reaction, along with a high amount of energy, which is converted to thermal power. The produced neutrons collide with other fissile material, and a chain reaction is formed [13]. Each step in the chain reaction is called a generation.

In order for a neutron to split an atom into fragments, it needs to collide with the atom at a certain kinetic energy level. The neutrons coming directly from the fission reaction are normally too fast, and have to be decelerated (or moderated) to the thermal kinetic energy range. To moderate fast neutrons into thermal neutrons, they are allowed to collide with non-fissile material that absorbs some of the kinetic energy. Water and graphite are very good neutron moderator materials.

Criticality is a term used to describe the sustainability of a nuclear fission chain reaction. It is expressed in an effective multiplication factor denoted as k_{eff}. This is the ratio of the number of fissions in one generation to the preceding generation's fissions. It can also be seen as the ratio of free neutrons after a generation to before the generation.

For $k_{eff} < 1.0$ there is not enough neutrons to keep on splitting fissile material, and the nuclear chain reaction will stop. The mass of fissile material is then called sub-critical. However, a $k_{eff} > 1.0$ results in a reaction which can accelerate at an extremely high rate (an atom bomb is super-critical). Nuclear reactors are operated at $k_{eff} = 1.0$.

The criticality of a volume of nuclear fuel is controlled by controlling the number of free neutrons. This can be done by either absorbing excessive neutrons, by letting them escape from the fissile mass, or by reducing the amount of fissile material in the volume. The reactor control rods are used to absorb the neutrons. They often contain Cadmium or Boron as the primary neutron absorbing material.

The geometry of the volume can be designed such to allow sufficient neutron escape from it. For any nuclear fuel, there is an infinitely long cylindrical geometry that will be sub-critical without any additional measures. The more fissile material there is inside the fuel, the smaller the sub-critical cylinder diameter needs to be. Similar geometries exist for an infinitely long flat plate of fuel, a cube and a sphere. If a fuel tank's diameter is larger than the infinite sub-critical diameter, absorber material is needed inside the tank to keep the fuel volume sub-critical. The smaller the infinite sub-critical cylinder diameter is, the more neutron absorber is required for a fixed tank diameter.

3. BURN-UP CREDIT

Burn-up is a term used to describe the amount of energy that has been released by the fuel element. An alternative term is the exposure of the fuel, as it relates to the amount of material that has been exposed to the fission reaction. Initially, only a small portion of the original mass of the fuel sphere participates in the fission reaction (about 10% of the 9g Uranium in a 200g sphere). Later on, some "fertile" material is transformed to fissile material*. The higher the exposure, the smaller the amount of fissile material left to participate in the fission reaction, which, in turn, will reduce the overall criticality of the fuel volume.

The implication of this is that if one knows that the fuel has a certain minimum burn-up, the calculated criticality of the fuel will be much lower than if one assumes it is all fresh fuel. As was explained in the previous paragraph, there is a cylinder diameter for which the fuel will be sub-critical without any absorbing material. Figure 34 shows the effect that burn-up credit has on the diameter of a sub-critical cylinder. The exponential increase in the diameter for an increase in burn-up credit shows the advantage one can get from taking credit for the fact that the fuel has a certain minimum burn-up.

The challenge in taking burn-up credit is to prove that the fuel has indeed undergone a certain minimum burn-up. This is quite difficult for water reactors, since the burn-up is usually deducted from the neutron flux history of the reactor rather than being directly measured. Also, the burn-up of a water reactor fuel element is not homogeneous and special care needs to be taken when mixing spent fuel in the storage system [38].

For the PBMR, each sphere is directly measured. The contents of a spent fuel tank, and the core are therefore well known. The PBMR equilibrium core contains a mixture of fresh, spent and used fuel spheres. This mixture is distributed evenly throughout the core, making it possible to describe the core contents in terms of an average burn-up of about 48GWd/tu.

There is a possibility that the burn-up measurement device performs incorrectly, resulting in fresh fuel being discharged rather than spent fuel. However, it takes about 3000 spheres, or 3 fresh fuel canisters to form a critical spherical mass. To discharge this amount of fresh fuel

* Breeder reactors make use of the conversion of fertile material to fissile material. These reactors were traditionally used to manufacture weapons-grade plutonium.

requires 6 days of incorrect operation. Such an error can be detected well in advance by the reactor power level monitors, or by the built-in verification of the measurement device.

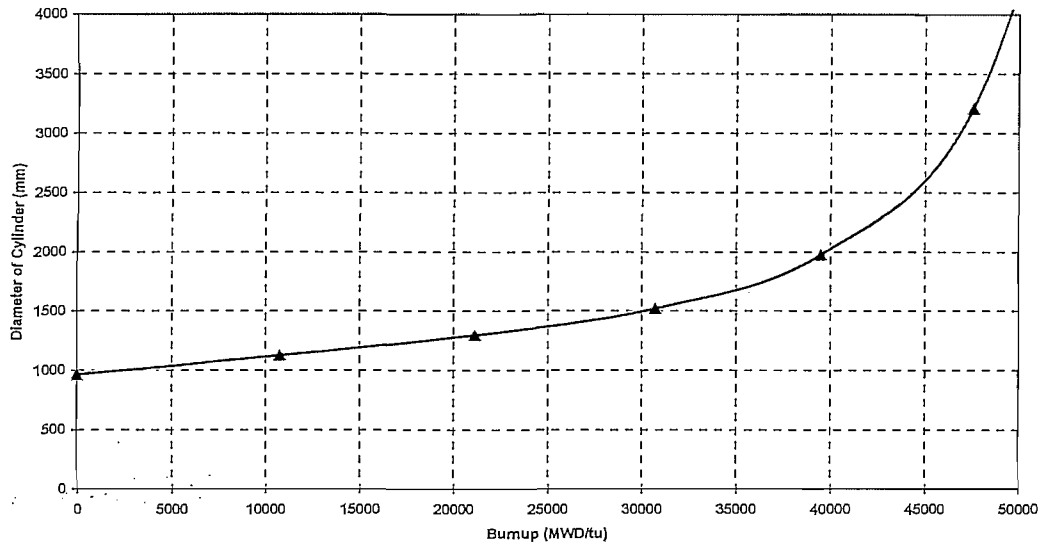

Figure 34: Diameter of an infinitely long cylinder, which will be sub-critical at a certain burn-up.

Another possibility to get only fresh fuel into a storage tank is by deliberately loading it into the tank from the fresh fuel loading station. This is an action of deliberate sabotage. It is the responsibility of the operator to ensure, by means of proper security measures, that the operations of the plant do not fall into malicious hands.

Based upon the above arguments, it is therefore considered appropriate to design the storage tanks for an average burn-up instead of fresh fuel. This burn-up credit simplifies the design significantly, and also reduces the cost of the storage tank. The burn-up credit value for all tanks is set at 40GWd/tu, which is 20% below the average burn-up of the core.

4. OPTIMUM WATER MODERATION

The reactor core is designed to have optimum moderation. This is done by the large graphite blocks around the fuel, and the graphite centre column. The blocks also act as a neutron reflector to reduce the amount of neutrons that do escape from the core. Any water ingress into the core will over-moderate the fuel volume, thus reducing the reactor criticality. However, in the storage tanks, there is no graphite reflector. The fuel volume is thus under-moderated. Water (or steam) inside a storage tank could significantly increase the reactivity of the stored volume, depending upon the water density.

It is for this reason that storage tank criticality analyses are done for optimum water moderation conditions. The optimum water density depends mainly upon the fuel composition. The tank geometry and the resulting amount of steel in the tank also play a minor role. It is therefore needed to perform a range of criticality analyses for different water densities between the spheres for each tank geometry contemplated.

In an attempt to reduce the criticality of the storage tanks, the probability of water ingress into the tank was investigated. The results showed that water moderation among the spheres has a significant effect on the overall criticality. The k_{eff} ranged from well below 1 for zero water to above 1 for optimum moderation conditions with fresh fuel and a certain tank geometry (see Figure 35).

The probability of water entering a storage tank is extremely low. This is because there is no water source in the FHSS, and the storage tanks are (except for the one being loaded) all sealed off. The only way for significant amounts of water to enter the tank is if the tank is ruptured, and the building flooded. However, the verdict was that the nuclear license for the demo module would be based upon deterministic values, and not probabilistic analyses. This negates all arguments about the possibility of a tank being filled with water, hence optimum water moderation is to be considered in the criticality design.

The issue of optimum water moderation might be raised again for the licensing of the commercial plants if needed.

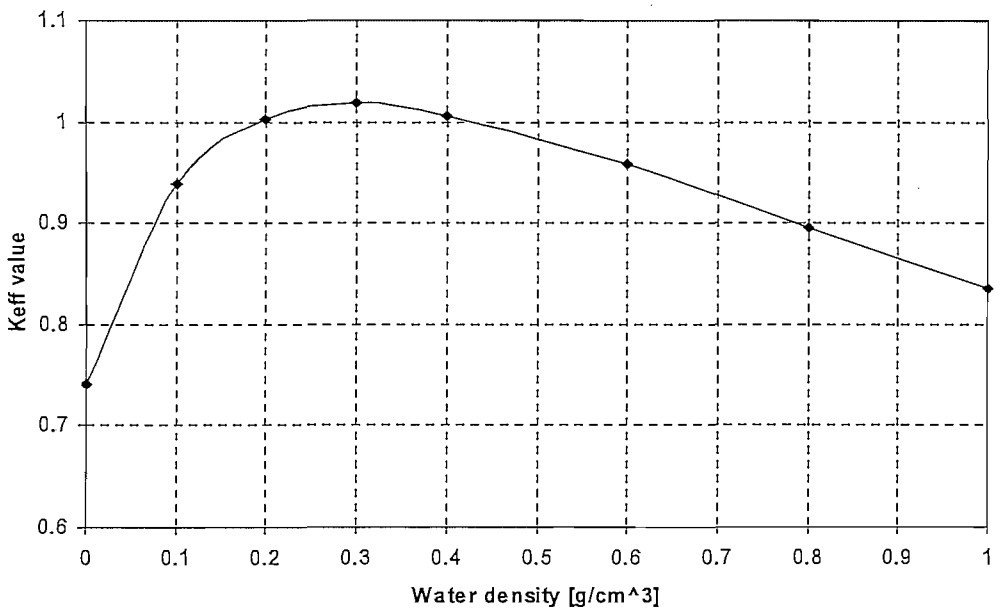

Figure 35: Effect of water moderation on criticality [39].

5. ABSORBER ROD ARRANGEMENT ALGORITHM

The initial tank concept had a large amount of neutron absorber rods inside (see Figure 6). The spacing of these absorber rods is very important: they should be placed such that the volume of fuel between adjacent rods is approximately the same. It is as if each rod has its own range of influence, and if there is a large volume without a rod, the volume does not "feel" the adjacent rods, and may become critical.

An algorithm was developed to calculate the position of each absorber rod for a certain number of rods such that the volumes in-between are more or less the same. The algorithm does this by assuming that each rod generates an opposing force when another rod is in its vicinity, similar to magnets of the same polarity.

Assume there is a 2D plane with a fixed amount of randomly placed rods. The position of rod **i** is defined as the vector $\mathbf{P}_i$ with coordinates $\mathbf{x}_i$ and $\mathbf{y}_i$. The distance vector from rod **i** to rod **j** is then:

$$d_{i,j} = P_i - P_j \qquad \{1\}$$

Let the force acting on rod **i** from rod **j** be inverse proportional to the distance between them. The direction of the vector $\mathbf{d}_{i,j}$ will determine the direction of the force. The resultant force acting on rod **i** is the vector sum of all the individual forces:

$$F_i = \sum_j \frac{Fmax}{\left(|d_{i,j}|\right)^n} \cdot \left(\frac{d_{i,j}}{|d_{i,j}|}\right) \quad \{2\}$$

The constants **Fmax** and **n** are chosen arbitrarily such that the algorithm is stable and converges within reasonable time.

Once the forces on each rod is determined, it is assumed that each rod will move in the direction of the force, and at a velocity similar in relative magnitude to the force. The new position of the rod after a small time increment Δt can then be calculated as follows:

$$\left(P_i\right)_{t+\Delta t} = \left(P_i\right)_t + F_i \cdot \Delta t \quad \{3\}$$

Equations 1 to 3 are iterated until the position of all rods between successive time steps converges to within a certain tolerance. If a rod moves out of the boundary, it is simply pulled back along its path such that it stays within the boundary.

Once convergence is reached, the sizes of empty volumes are calculated. This is done by calculating three-point and four-point circles between adjacent rods. The diameters of all circles should be approximately the same for a homogeneously spaced volume. Once a homogenous solution has been found, the geometry can be used to perform a criticality analysis.

Figure 36 shows the result of a cylindrical boundary of diameter 3000mm with 27 absorber rods inside. Sub-figure (a) shows the initial random position of the rods (blue circles) and their migration path (green dots) to its final position (red circles). One can clearly see how the rods end up in three concentric circles. Sub-figure (b) shows the rod final positions along with the minimum and maximum internal circles. From sub-figure (c) one can see that the circle diameters range from 740mm to 860mm, and sub-figure (d) contains a contour plot of the cell diameters. This arrangement is fairly homogeneous.

The algorithm can be used for any 2D geometry needed. One could also fix certain rods at a position and find the optimal spacing around them. This is particularly useful if there are some fixed internals in the storage containers. The algorithm assumes that all absorber rods have the same range of influence, however, it may be necessary to increase some rod diameters to obtain a better arrangement. The bigger range of influence can then be adjusted by increasing the **Fmax** constant in the force equation 2 for the specific rod. The relative magnitude of the **Fmax** values should be determined from a number of criticality analyses.

Unfortunately this algorithm has not been used to eventually determine the optimum rod spacing, as it was decided to rather use a sub-critical tank geometry than absorber rods. The option of sub-critical geometries is described in the next section.

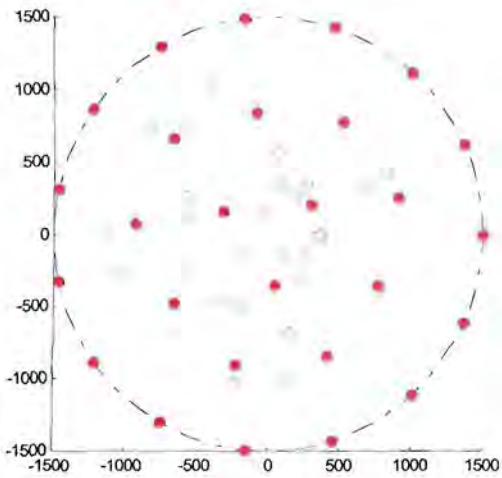

(a) Rod migration (green lines) from initial random position (blue circles) to final position (red circles).

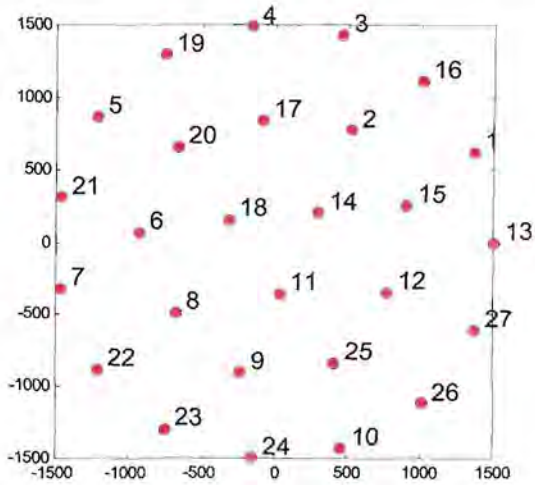

(b) Final rod position with minimum and maximum internal circles shown.

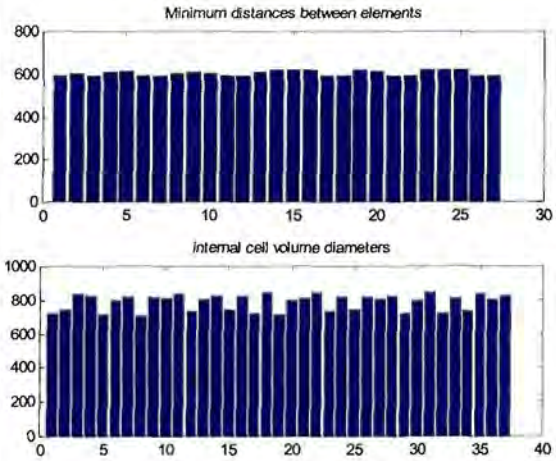

(c) Rod minimum distances and internal cell diameters.

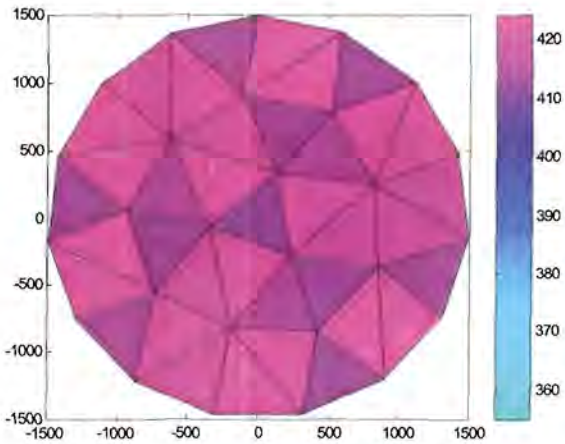

(d) Contour plot of cell diameters.

Figure 36: Results from the absorber rod position algorithm.

6. SUB-CRITICAL GEOMETRIES

The traditional way to achieve a sub-critical fuel volume is to add absorber material between the fuel. This is how the 268MW baseline spent fuel tanks were designed. The absorber material is often very expensive and ensuring that it does not degrade with time (or melt in the case of Cadmium) is a problem. During the value engineering exercise (see Chapter 4) it was realised that a sub-critical volume can be established by means of a geometry made from steel only.

This resulted in the design of the storage tanks with large diameter tubes running between the fuel. The diameter, position and number of tubes define the sub-critical geometry. The steel wall of the tube reduces the neutron coupling through the voids of the tubes. No additional absorber material is added to the tubes.

There is a large variety of tank geometries for which sub-criticality can be achieved. The final choice is a compromise between proper heat distribution, sphere flow and manufacturability. For the storage tank, it happened that the resulting geometry is far more sub-critical than required, due to the thermal design of the tank. As a result the storage tanks have a k_{eff}=0.85 for fuel with 40GWd/tu burn-up [40]. The final tank geometry with tubes sizes and position is shown in Figure 37.

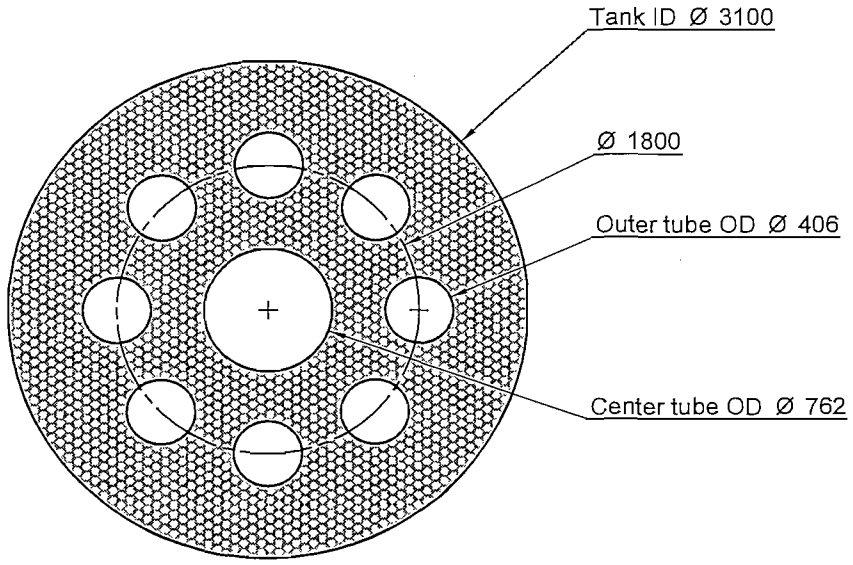

Figure 37: Storage tank cross sectional geometry.

7. A QUALITATIVE METHOD TO DETERMINE THE TANK CRITICALITY FOR DIFFERENT FUEL ENRICHMENTS

Many nuclear reactors are designed to operate with one fuel type, but are later on required to use other fuel types as well. This is mostly due to improvements to the fuel technology and attempts to increase the reactor's overall efficiency. The PBMR is no different. The demonstration plant is designed to initially contain fuel with a 9.6% enrichment. The spent fuel will have a target burn-up of 92GWd/tu. However, plans are to increase the fuel enrichment to 12.9% and the burn-up to 133GWd/tu.

The question is: will the storage fuel tanks still be able to keep the higher enriched fuel sub-critical? Answering this will require a number of criticality analyses. However, it is possible to make an analogy between the tank design and the reactor design, and their ability to keep the fuel critical or sub-critical. To do this, one needs to look at the reactivity potential (**Rp**) of the fuel mass in the reactor and in the tanks. The **Rp** is defined in this thesis as the potential of a mass of fuel to result in criticality (k_{eff}=1) if placed in a certain geometry and moderation. The units and absolute value of the reactivity potential has no meaning, only the relative difference between two scenarios.

From Figure 34, one could see that the infinite sub-critical diameter is somewhat proportional to the power of the burn-up **B** of the fuel. It can also be deducted that an increase in burn-up for a certain fixed diameter will result in a decrease in criticality, or reactivity potential. The **Rp** is thus inversely proportional to the power of the burn-up, i.e.:

$$Rp \frac{1}{\alpha} B^n \quad \{4\}$$

Another important parameter that influences the reactivity potential is the fuel enrichment **U**. If one assumes there is a fairly linear relationship between the criticality and fuel enrichment, the **Rp** is then proportional to the enrichment, giving:

$$Rp \ \alpha \ \ U \quad \{5\}$$

Equations 4 and 5 can be combined into one equality, by introducing a proportional constant **C**. However, since the absolute value of **Rp** has no direct meaning, the constant can be included into the value of **Rp**.

$$Rp = C \cdot \frac{U}{B^n} = \frac{U}{B^n} \quad \{6\}$$

Lastly, a relationship is needed between the average burn-up in the core **Ba**, and the target burn-up of the spent fuel **Bs**. This too can be assumed to be fairly linear, giving:

$$Ba = C \cdot Bs \quad \{7\}$$

The low enriched fuel has a spent fuel target burn-up of 92GWd/tu, and an average core burn-up of 48GWd/tu, which gives **C**=0.522. For the 12.9% enriched fuel at 133GWd/tu spent fuel burn-up, the reactor average burn-up would then be 69GWd/tu. Because of the linear relation between spent fuel and average burn-up, equation 6 can be used for average burn-up values.

In order for the demo reactor to be able to control the criticality for both the low enriched and high enriched fuel, the reactivity potential of the two fuel volumes should be the same, thus:

$$Rp_{low} = Rp_{high}$$

thus $$\frac{U_{low}}{B_{low}^{\ n}} = \frac{U_{high}}{B_{high}^{\ n}}$$

solving for n gives $$n = \frac{\log\left(\frac{U_{high}}{U_{low}}\right)}{\log\left(\frac{B_{high}}{B_{low}}\right)} = \frac{\log\left(\frac{12.9}{9.6}\right)}{\log\left(\frac{69}{48}\right)} \quad \{8\}$$

$$n = 0.814$$

The reactivity potential for fuel in the reactor can now be calculated as **Rp**=0.411. Previous criticality calculations showed that a storage tank filled with low enriched fuel at an average burn-up of 20GWd/tu results in k_{eff}=0.95. By using the exponent **n** determined above, the reactivity potential of the fuel in the tank is then 0.838. This means that the storage tank can store any fuel that has a reactivity potential less than 0.838. The contents of an equilibrium core has an **Rp**=0.411, hence it will be sub-critical in the storage tank.

One can now calculate the average burn-up of high enriched fuel in the storage tank that would result in criticality of k_{eff}=0.95 (thus having the same reactivity potential of 0.838):

$$B = \left(\frac{U}{Rp}\right)^{\frac{1}{n}} = \left(\frac{12.9}{0.838}\right)^{\frac{1}{0.814}} = 28.751 \quad GWd/tu$$

The result is well below the average core burn-up for the same enrichment (69GWd/tu), meaning that even if the fuel enrichment is increased, the contents of the reactor will be sub-critical in the storage tanks.

The method described above is only a qualitative way to show that the storage tank will be sub-critical for the low and high-enriched fuel envisaged. One can also extrapolate the conclusions to say that it will also be sub-critical for higher and lower fuel enrichments. This is because as long as the reactor design stays the same, the fuel inside should have the same reactivity potential. If the storage tanks can hold a higher reactivity potential, it will be sub-critical when the full contents of the core is transferred into the tank, no matter what the core contents consists of.

One very important fact to remember during the licensing of the storage tanks, is that the burn-up credit should be adjusted based upon the reactor average burn-up. If, for example, the burn-up credit was set at 20GWd/tu for both fuel enrichments, the calculations will show that the tank is not sub-critical for the high-enriched fuel. However, the average burn-up of the core has in fact increased, hence the burn-up credit for the tank can be increased. By setting the burn-up credit at a percentage below the average core burn-up, the spent fuel burn-up credit value will be adjusted accordingly.

8. CONCLUSION

The storage tanks will be sub-critical with k_{eff} = 0.85 taking optimum water moderation and 40GWd/tu burn-up credit into account. The fuel is kept sub-critical by means of the tank geometry and internal cooling tubes. There is no special absorbing material in the tank, only the steel thickness is required.

The algorithm developed to calculate optimum absorber rod spacing could be a useful tool for other storage tank applications. Unfortunately, it was not used in the final criticality design of the storage tanks.

The qualitative criticality method should eventually be tested with detailed criticality analyses, but with a burn-up credit margin of 20%, and the fact that the tanks have a k_{eff}=0.85, the chances that the tanks may not be sub-critical at higher enrichments are very low.

Chapter 8 : Corrosion Design

1. INTRODUCTION

The nuclear requirement for protection of the fuel integrity implies corrosion protection of the fuel sphere itself. This is simply done by keeping the fuel in an inert helium environment for the full period of storage. The corrosion problem is now transferred to the helium boundary, i.e. the storage tank. If the storage tank is corroded during its life, the helium environment may be lost, and corrosion of the fuel sphere may occur.

The corrosion design of the storage tanks was probably the most challenging of all the requirements. This is because the storage tanks need to last for a total period of 80 years. This is more than most other engineered structures, except perhaps for civil designs.

The problem is not in finding an 80 year solution, but in finding a cost-effective solution for 80 years, this includes the maintenance required over the life. Cost together with maintenance were therefore the primary drivers when evaluating the concepts. As a result, a specific process was followed to arrive at a suitable corrosion design, not only for the storage tanks, but also for all the SSS components exposed to a corrosive environment.

2. CORROSION DESIGN PROCESS

The design process followed in determining the most feasible corrosion solution is depicted in Figure 38. One starts off with a concept design, requirements and the environment. Based upon the concept, maintenance can be easy and components can be replaced, or maintenance can be extremely difficult.

An easily maintainable component's corrosion design is essentially a cost optimisation between material selection, coatings and a maintenance plan. If maintenance is not feasible, one needs to investigate the guaranteed service life of materials and/or coatings. If there are candidate materials, which can last the full service life without maintenance, the most cost-effective one is chosen.

On the other hand, if no service life solution can be found, one investigates options to change or control the environment. If no solution is found, one needs to revisit the requirements (reduced service life), and/or the concept (increased maintainability). If an environment change is feasible, one redefines the environment, and go through the process again. The most cost effective material is then chosen based upon the changed environment.

The paragraphs below contain the arguments in support of the storage tank corrosion protection design.

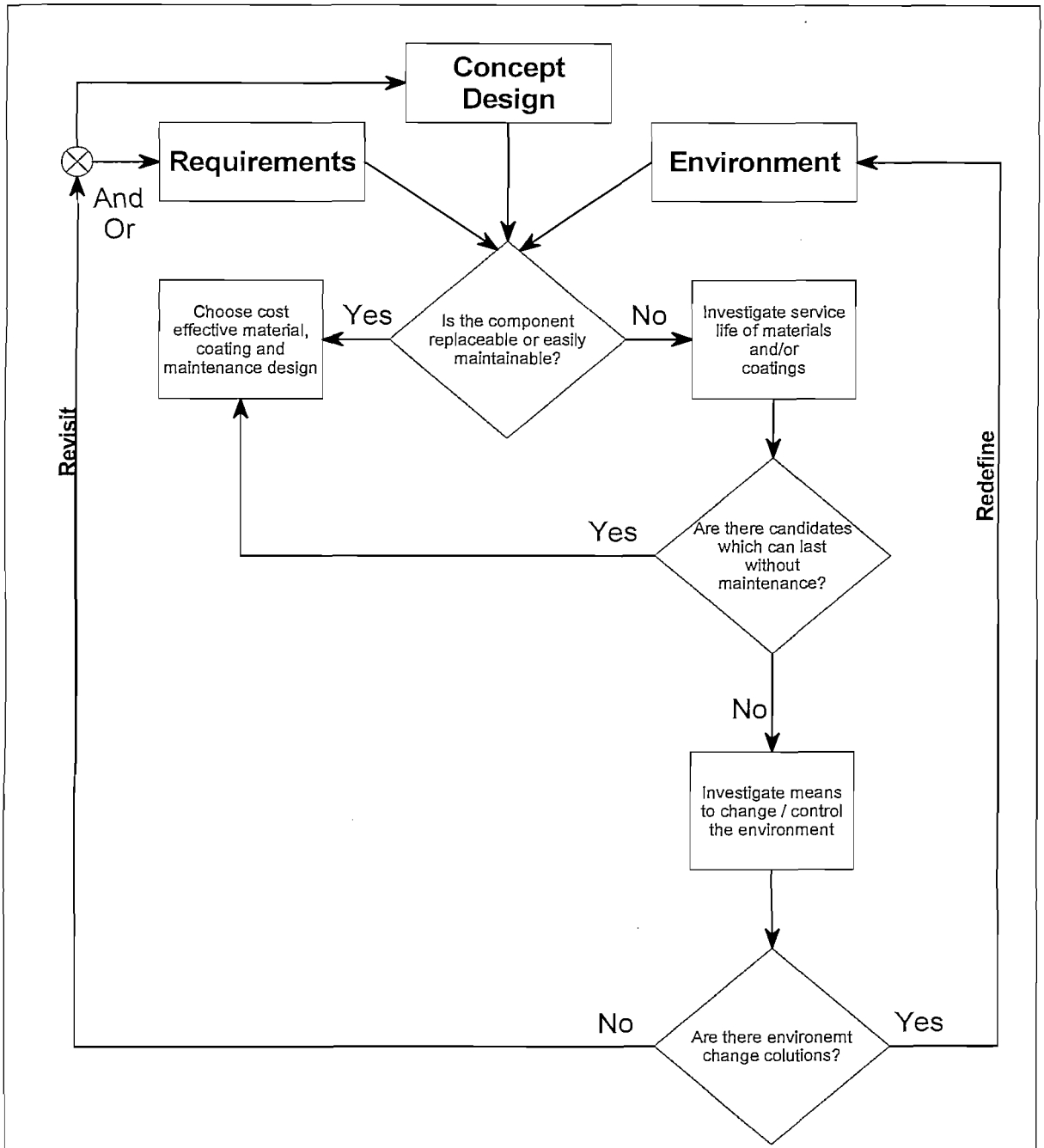

Figure 38: Corrosion design process decision diagram.

3. SERVICE LIFE AND ENVIRONMENT

Because the spent fuel will be stored for an additional 40 years after plant operation, the storage tanks need to last for a total of 80 years plus an additional 5 years before installation. This places a very high demand upon the design and material choice of the tanks.

To complicate matters, the environment where the PBMR demo module will be built (Koeberg, Western Cape), is one of the most corrosive coastal environments in the world [41]. In order to achieve passive cooling of the tanks (a goal of nuclear safety), they have to be directly exposed to this environment.

Because of the radiation of the stored fuel, it is not possible to gain access to the tank whilst it contains fuel. Remote maintenance on the tank is the only option, or the tank needs to be emptied. This complexity in the maintenance is because the tank is a thin-walled structure, with the radiation shielding performed by the building. Other dry storage containers used in the world have a very thick wall between the fuel and the cooling air. This wall performs the radiation shielding, but in return, significantly reduces the amount of heat allowed inside the container. The cost of such containers is also extremely high.

It is not only the pressure vessel of the storage tank which needs to last 80+ years, but also all other components which are not accessible for maintenance or replacement due to the radiation.

4. RADIOLYSIS

An additional complication over and above the coastal environment is the effect of radiolysis. This is the process where air is ionised into free radicals in the presence of gamma radiation. These radicals can then combine with other molecules in the air to form potentially corrosive or hazardous substances. There is a very large spectrum of radiolysis products which could form [42], but the one of most concern is the formation of nitric acid [43]. Figure 39 shows the chemical process involved.

The significance of nitric acid formation is that corrosion rates on carbon steels can increase by three times or more [44]. An investigation was done to quantify the radiolysis build-up of nitric acid and other products in the cooling air. The work was still in progress at the time of compiling this thesis, hence it cannot be said if there is a significant amount of radiolysis present or not. The assumption was that radiolysis is a problem that must be included in the corrosion design, until proven otherwise.

An important aspect to note in the chemical equation of nitric acid formation is that it can only be formed in the presence of moisture. A very dry environment thus has a low acid yield, even at high NO_2 concentrations. Unfortunately, the air needs to be extremely dry, since it takes only one water molecule to produce two acid molecules.

Another radiolysis product that could potentially increase the corrosion rates is ozone (O_3). Ozone is a highly reactive oxidant, and has been shown to cause significant corrosion [44]. A radiolysis test is planned to determine the ozone generation and to quantify its effect on the corrosion rates of the tank material.

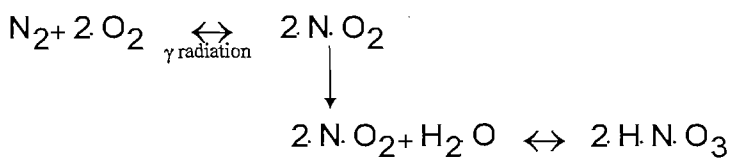

Figure 39: A chemical process involved when air is ionised by radiation to form nitric acid.

5. TANK MATERIAL OPTIONS

A thorough survey of the materials currently allowed by the ASME Boiler and Pressure Vessel code has been done in order to locate a cost-effective candidate that could last for the design life of 80 years. The findings are reported in a separate engineering report [45] of which the following paragraphs are a short summary.

Stainless steel: Stainless steel has proven itself over the years as a highly corrosion resistant material. Especially for nitric acid chemical plants, stainless steel is the material of choice. It is therefore not strange that the initial material choice for the tanks was stainless steel.

However, all stainless steels are susceptible to stress corrosion cracking (SCC) in the presence of chlorides. Although this was known for a long time, it was only recognised in the last few years that stainless steel in a chloride-containing environment is a poor material choice. This is because SCC is a material failure which is very difficult to detect at an early stage and it affects the most critical regions of the structure such as welds, load bearing corners and even residual stress regions originating from the manufacturing process. To make things worse, SCC is like a cancer, and the only way to stop it is to remove all traces thereof. This can result in extended down times, difficult machining techniques or even complete component replacement.

If the storage tanks were made from stainless steel, the formation of SCC will occur unnoticed until it is virtually too late because of the complexity to inspect each and every weld on the tank. A solution may be to physically remove all chlorides from the air-stream. This requires an active cleaning system that operates for the full 80 years. It also negates the possibility of passive cooling. Also the chlorides do not only originate from the air, but can be released by the concrete, they could come from an electrical fire somewhere, or even from flooding of the cavity.

Generally, stainless steel components cost twice as much as a carbon steel components.

Based upon the above arguments, stainless steel for the tank material is not regarded as an option.

Duplex steel: This type of steel can be called in layman's terms a "very sophisticated stainless steel". The biggest advantage of duplex steels is that it is significantly less susceptible to SCC. However, being a type of stainless steel, SCC cannot be excluded over an 80-year period. It is also a fairly new material with limited experience in the field.

Duplex steels are about two times more expensive than stainless steels, and the manufacturing is significantly more complex.

Duplex steel was seen as the final resort if no other more cost-effective solution could be found.

Other non-ferritic materials: Because the storage tanks are pressure vessels, the range of allowable non-ferritic materials is limited. Aluminium experiences inter granular corrosion, which is similar to SCC. Pure copper proved itself a viable material because of the preserved quality of artefacts from the copper age. However, pure copper does not have very good mechanical properties, and designing a pressure vessel from copper could be very expensive.

Carbon steel: Carbon steel is extensively used in the pressure vessel industry. It is not susceptible to SCC, and exhibits a measurable corrosion rate. Corrosion of carbon steel can be halted once it has started by using inhibiting chemicals or simply by removing the corrosive elements in the air. Carbon steel is about half the cost of stainless steel, but with comparative mechanical properties. A vessel made from carbon steel will probably cost the

least of all materials.

The big disadvantage of carbon steel is that it cannot last for 80 years in a marine environment, especially if there are radiolysis products present. Simply adding material for corrosion is not necessarily the solution. Pit corrosion can progress much faster than surface corrosion, and the additional material can quickly result in a tank cost similar to a stainless steel or even a duplex steel tank.

The only way that carbon steel may last for 80 years is that it is either protected against the environment with coatings or something similar, or the corrosive environment is eliminated.

6. COATINGS OR PROTECTIVE LAYERS

Coatings such as paint are the traditional way to protect a carbon steel component from corrosion. Essentially, the coatings prevent the corrosive elements from getting into contact with the steel. A small penetration through the coating barrier exposes the metal beneath. A microclimate is formed, and significant corrosion can develop. It is therefore paramount that coatings be inspected and repaired on a frequent basis. The gamma radiation of the fuel inside the tank also degrades all organic coatings. It is thus necessary to use inorganic coatings such as Siloxane.

An alternative to paint-type coatings is to plate the steel surface with a cathodic protecting material. Typical materials is zinc, cadmium, nickel etc. These protective layers can be applied using galvanizing, metal spraying or electrolytic deposition. Platings generally have a longer life than coatings, and are not affected by gamma radiation. However, they can be degraded by the radiolysis acid products.

The conclusion of the value engineering (reference [23]) was that a combination of zinc plating and Siloxane coating be used for the tank. However, even with the best application techniques available, the coating system can only be guaranteed for 20 years. This means that after 20 years, the coating on some tanks may need some repair. In order to repair the coatings, it will be necessary to move the contents of the tank to another tank before access to the tank can be attained. For this reason, the GRT was designed to be of the same geometry as that of an SFT in order to act as a swop tank when all the SFTs are filled.

As the design progressed, it became evident that it would be extremely difficult to repair or even completely re-coat the tank in the confined space available around the tank. Ensuring the coating does not get damaged during installation will also be very difficult.

It is also not preferable to move the spheres from one tank to another during the last 40 years of storage. Once they are in the tank, they should stay there until decommissioning. The residual radiation inside the tank, after the tank was emptied, may also present a maintenance problem.

In retrospect, it can be said that coatings is probably not the best solution.

Another option is to clad the tank with a corrosion resistant material. As was indicated previously, pure copper exhibits a very high corrosion resistance. It is thus an option to clad the complete tank with copper. However, copper cladded steel is not easily available, and cladding the support and other weld regions could be very costly.

Copper cladding was not studied in detail due to a lack of such applications in the industry. It would require significant market research and some process developments before a choice can be made for or against copper cladding.

7. THE MECHANISM OF STEEL CORROSION

In order to reduce or eliminate corrosion on steel, one needs to understand the mechanism involved. Only then will it be possible to remove the corrosive elements from the air. This section aims to give the reader a quick overview of the process. It should however be remembered that corrosion has many forms, and can be an extremely complex chemical phenomenon. This is therefore by no means a comprehensive description of corrosion, but rather addresses the primary mechanisms involved, specifically for carbon steel.

The primary mechanism in the process of atmospheric carbon steel corrosion at room temperature is an electrochemical reaction [46]. This involves ion exchange between the metal and another chemical substance. For ion exchange to occur, one needs an electrolyte, or an ion transport medium. By eliminating the electrolyte, the electrochemical reaction stops (similar to what happens to a lead-acid battery when it dries out).

Ions move the best in an aqueous medium such as water or acid. Therefore, to prevent corrosion in air, one needs to remove all the moisture. It is well known in literature that the corrosion rate of carbon steel in air can be reduced by reducing the relative humidity. Some researchers report that there is a minimum humidity below which corrosion is negligible [45]. This however, is affected by the various impurities in the air, as well as the initial oxide or corrosion layer on the metal.

For moisture to precipitate onto the metal, the temperature of the metal must be below the dew point of the air [47] (see the psychrometric chart in Figure 40). Since the air cools the tank, the tank will always have the same or higher temperature than the air. Hence, by increasing the air temperature, one also increases the tank temperature to a point higher than the dew point. Also, for the same moisture content, a higher temperature results in a lower relative humidity. That is why the relative humidity is the parameter to use rather than the specific moisture content of the air.

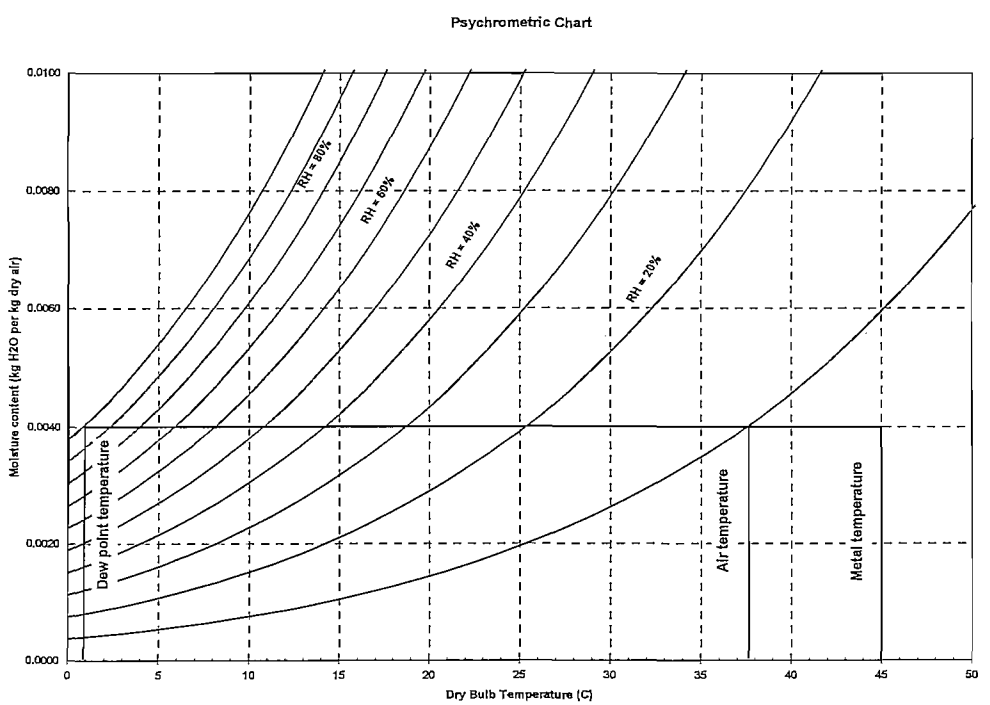

Figure 40: Psychrometric chart of air, showing the difference between the dew point, air and metal temperature for a specific moisture content.

The only way for moisture to get in contact with the metal if it does not precipitate is through molecule or droplet collisions. Generally, the lower the relative humidity, the smaller are the water droplets [48] and the smaller the collisions that occur with the metal. At very low humidity levels, the moisture is in a gaseous form, thus further reducing the possibility of precipitation on the steel for substrate temperatures above the dew point.

The hygroscopic nature of the layer on the surface of the steel can accumulate moisture in its crystalline structure, hence enhancing the corrosion. This is why the initial substrate layer is important in corrosion studies.

Although the primary mechanism for carbon steel corrosion is an electrochemical reaction requiring an electrolyte, some chemical reactions occur without the need for an electrolyte. This is governed by the number of reactive molecules colliding with the metal. A good example of such corrosion occurs between iron and ozone. The amount of radiolysis products and their direct chemical interaction with carbon steel is not sufficiently known, and forms part of the ongoing corrosion study programme.

The radiolysis products can also react with water molecules in the air to form acids. The dew point of the acid is often higher than that of water [49], meaning there is a higher possibility that the acid may precipitate on the steel and act as the electrolyte. To counter this effect, the moisture content of the air, as well as the concentration of radiolysis products should be reduced.

All metals have the tendency to corrode, even stainless steel or aluminium. The difference is that some metals exhibit a corrosion layer that is very stable and inert to the corrosive elements in the air. Although the metal has corroded, it is covered by a protective layer that retards diffusion of ionic species through the layer, hence preventing any further corrosion. The high chromium content of stainless steel is primarily responsible for its corrosion resistance due to the formation of a Cr_2O_3 surface layer [46].

8. ENVIRONMENT CONTROL

Since no viable solution could be found with materials or coatings, the focus was shifted to controlling the environment. This way one addresses the problem (corrosive elements) rather than the cause (corrosion). There exists an IEEE specification, [50] which defines a G1 environment for which "...corrosion is not a factor in determining equipment reliability". However, this specification is extremely tight, and is also more applicable to electronics.

In order to establish the minimum requirements for a corrosion free environment, a corrosion test facility was built. This facility and the test results are discussed in more detail in section 12. The main focus of the test was to establish a minimum air composition specification to prevent corrosion on carbon steel. The first step was to determine the minimum relative humidity, as well as to quantify the effect of radiolysis induced NOx gas in the air. Future tests will investigate the cumulative effect of other corrosive elements also found at Koeberg.

Controlling the environment requires that the cooling air be passed through an air-conditioner. This is an active system, which does not allow for passive cooling. Instead of designing a fully redundant safety-related active cooling system, it was proposed to that there be an automatic bypass of the active cooling so that passive cooling can take over during a failure. If the tank is made from carbon steel, the small amount of corrosion that may take place can be stopped once the active conditioned air is back in operation. However, a tank made from stainless steel could develop SCC during the bypass period, which cannot be stopped afterwards.

9. CLOSED LOOP CONDITIONED AIR

From thermal calculations it was determined that a cooling mass flow of about 3kg/s is required for each SFT. To condition this amount of air to a very high purity and dry condition on a continuous basis will be extremely expensive and would require a very large conditioning system. The alternative is to cool the tank in a closed loop circulation. This closed loop air only needs to be conditioned once, and then be maintained at that purity level.

To remove the absorbed heat from the closed loop, a heat exchanger is now required. Again, no passive cooling can exist through the heat exchanger, and it is therefore necessary to bypass it during a failure. Once the active components are repaired, the closed loop can be re-established. By simply diverting a small portion of the air on a continuous basis through an air-conditioning device, the air can be purified within a couple of days. The operating cost of such a purification system is significantly less than an open loop system.

The storage tank cooling design is therefore based upon the above arguments. The tank will be made from carbon steel without coatings or additional corrosion allowances. It will be cooled by air in a closed loop, which is conditioned to such an extent so as to minimise corrosion of the steel.

The only unknown factor in the corrosion protection is the effect of the trapped radiolysis process in the closed loop. The corrosion study aims to quantify this effect, and establish limit concentrations. The conditioning system should then be designed to control the concentration inside the closed loop by means of active removal or simply gradual air exchange.

10. CORROSION CONTROL OF THE EXTERNAL SIDE

By choosing the environment control route, the corrosion problem was essentially moved from the tank to a more maintainable area, which is the external side of the heat exchangers. This side will be subjected to the harsh coastal environment, but without the radiolysis products.

By following the design process depicted in Figure 38, it is clear that the final material choice is based upon a cost optimisation study since all the components can be placed at a highly accessible area. One needs to consider the cost of using very expensive long-life materials, or perhaps low cost materials with a coating, which needs frequent maintenance. This study will be done during detail design. PBMR has developed a set of guidelines for the corrosion protection design of maintainable components [51], which will also be used in the detail design.

11. CORROSION MONITORING

It is accepted that corrosion of the tank cannot be eliminated completely. The aim is therefore to establish an environment in which corrosion will be minimal. Because of the likely presence of some corrosion, a monitoring programme will be put in place. This programme will entail visual inspections of the tank surface at a regular basis. If significant corrosion is found, it will be inspected in detail through remote sampling, thickness measurements or other analysis techniques. It is also envisaged to place material coupons at different regions where the most severe corrosion is expected. These coupons can then be extracted and analysed in a laboratory.

Based upon the results of the corrosion inspection, a predicted life of the tank can be made. It is also possible to upgrade the air-conditioning device in order to improve the air quality if needed.

The first tank shall serve as the benchmark in the sense that inspections will be performed on a fairly regular basis (typically once every month). As the time progresses, and more information is gathered, the inspection could be reduced to once or twice a year.

Also, corrosion tests are planned to be performed at the Koeberg site, using the air-conditioning device of the final design. These tests will start 3-4 years before installation of any tank, and will run continuously for the operation of the plant. It will therefore serve as a head start for corrosion before it would occur on the tanks.

12. CORROSION EXPERIMENTS

The closed loop design is intended to curb the corrosion of the tanks, but there is an unknown factor namely radiolysis which needs to be addressed.

A corrosion test chamber was built at the CSIR in which humidity, air temperature and NOx concentrations can be varied (see Figure 41 and Figure 42). A number of candidate materials were placed inside this chamber, and the corrosion over time was measured. This corrosion test is seen as an ongoing process.

The test is described in more detail in reference [52] along with some preliminary results. Figure 43 shows the measurement of mass increase of various metal samples. The test was performed for different air compositions by varying the humidity, temperature and NOx concentration. Because of the relative short exposure time (100 days), the results can only be seen as preliminary.

The most important result so far is that it seems that carbon steel with about 2% Chrome has a better corrosion resistance than pure carbon steel. This is due to a more stable corrosion layer forming on the surface. This prompted the choice of tank material to a steel with a nominal composition of 2.25% Chromium and 1% Molybdenum. This is a fairly standard material used in ASME pressure vessel applications, and therefore does not cost significantly more than normal carbon steel.

Another conclusion that could be made is that corrosion on carbon steels does not occur at a very low humidity, even at high NOx concentrations. This resulted in a 10% relative humidity specification for the air-conditioning device.

Currently, only carbon steel, stainless steel and duplex steels were tested. It is also envisaged to test steels containing special coatings. Future tests will include other corrosive elements found at Koeberg, such as chlorides and sulphates.

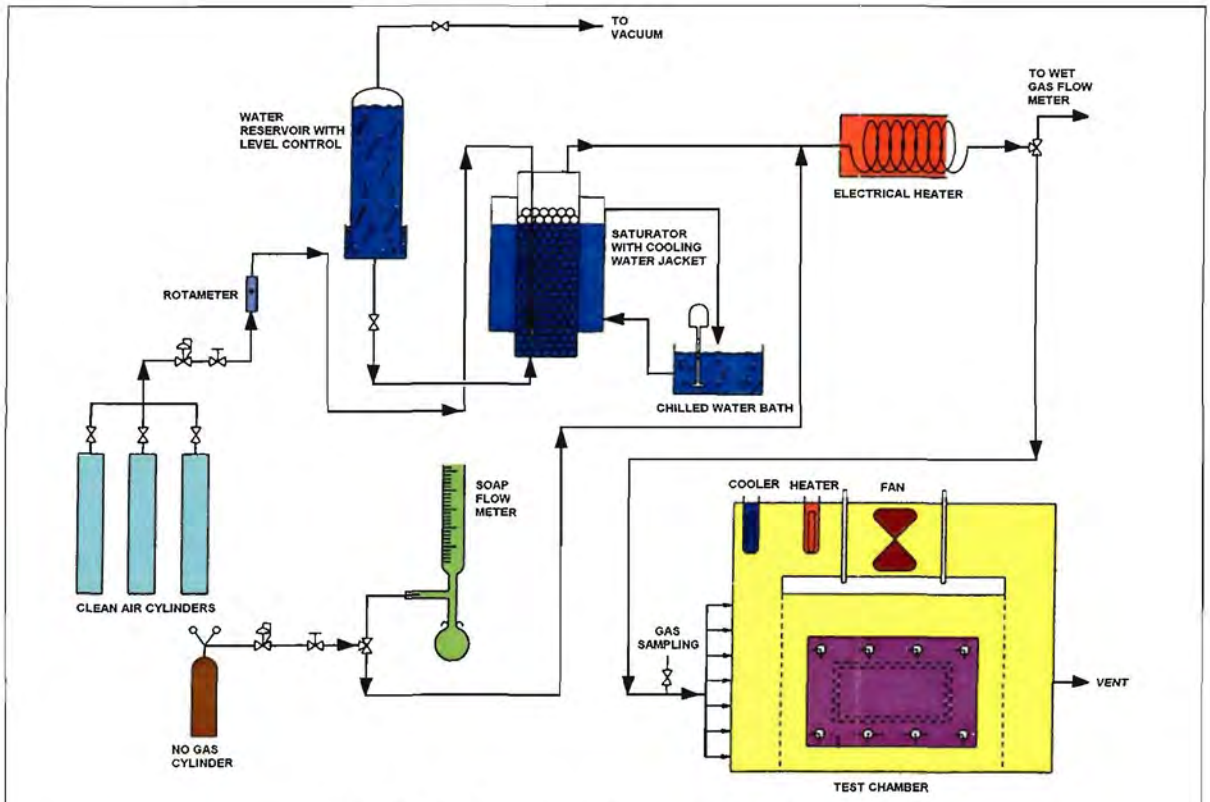

Figure 41: Corrosion test schematic diagram.

Figure 42: Photo of the corrosion test setup at the CSIR.

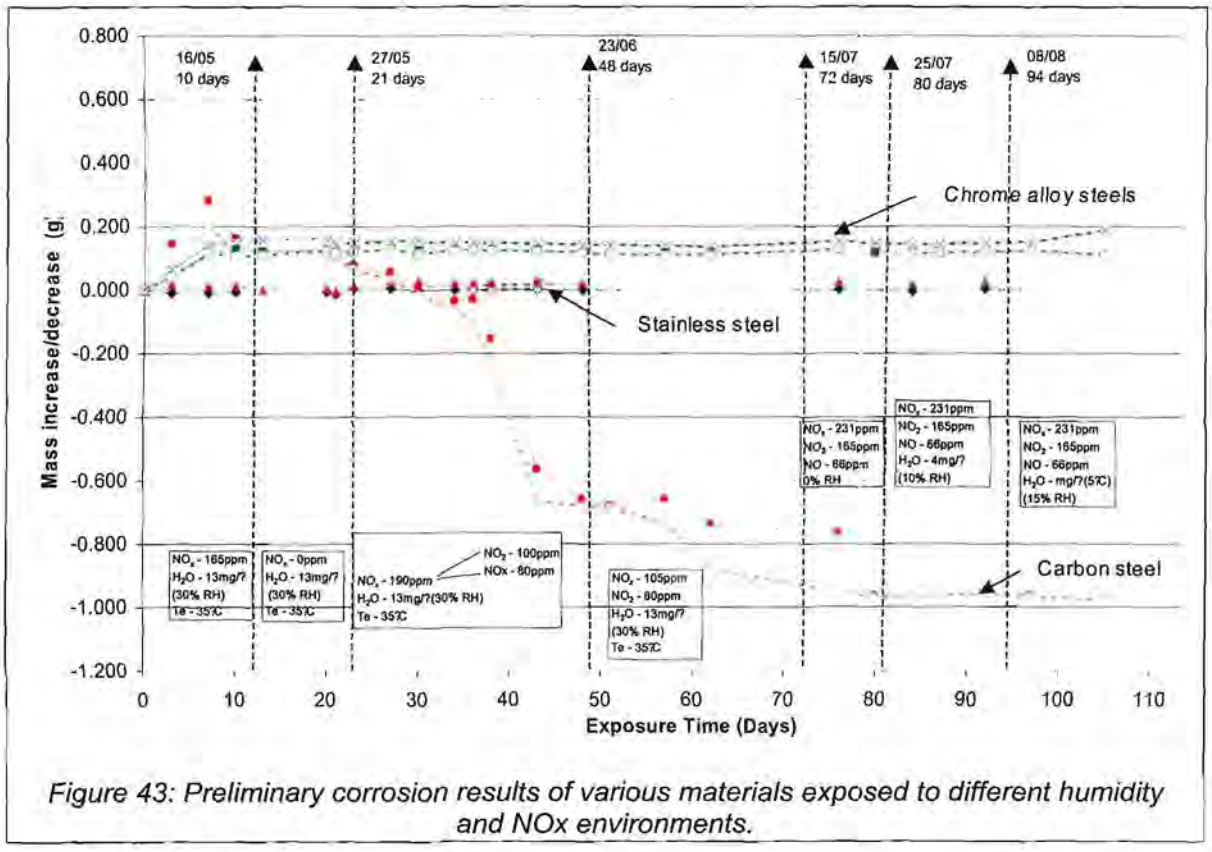

Figure 43: Preliminary corrosion results of various materials exposed to different humidity and NOx environments.

13. CONCLUSION

The corrosion design of the storage tanks was driven by cost and maintainability. Because it is not possible to access the tank when it contains fuel, remote maintenance will be the only option. Alternatively, a material should be used that can last the full 80-year operating life.

After a thorough study, it was concluded that there is no cost-effective material or coating that will last 80 years maintenance free. The alternative is to remove the corrosive elements from the cooling air. Because the primary mechanism in corrosion requires an electrolyte, it was decided to cool the tanks with dry air. Corrosion studies were performed that indicated a minimum of 10% relative humidity for the air, and a 2% Chromium content for the steel is required to minimize the corrosion.

The most cost-effective solution to cool the tanks with dry air is to keep the air in a closed loop. The cooling system requires a heat exchanger to transfer the heat from the closed loop to the outside air. The resultant is an active cooling system. In the event of an active cooling failure, the system is automatically bypassed to allow passive cooling.

Chapter 9 : Storage Tank Heat Removal

1. INTRODUCTION

The safe and reliable removal of the decay heat from the spheres formed a large part of the work done for this study. As a result, this chapter and the next are dedicated to the description of the cooling design. Initially the focus was on the heat removal from the tank to the cooling air. Various analyses and studies were performed in this regard, and are described in this chapter. The next chapter builds upon the conclusions of this chapter, along with the corrosion design conclusions to develop an integrated cooling design.

2. TEMPERATURE LIMITS, INPUTS AND GOALS

The starting point of any analysis is the inputs and the limits to be reached. For the tank heat removal, some limits were goals rather than actual requirements, and originated from the ALARA principle.

The graphite surrounding the fuel kernels can sustain temperatures well above 1600°C [24], but this is in the absence of oxygen. At temperatures above 400°C, the graphite will react with oxygen in an exothermic reaction. For this reason, the fuel temperature limit is set at 400°C although the tank is filled with Helium. Only after a beyond design base accident where large openings at the top and bottom of the tank occurs can oxygen enter the tank. This means that during abnormal conditions when the tank is still intact, the fuel temperature may be allowed to exceed 400°C.

Because of some uncertainties and approximations in the analyses, a goal temperature of 350°C was set. This does not mean that the limit is lowered to 400°C, rather, it gives one a margin in which temperature changes can be accommodated during detail analyses without needing to redesign the tanks.

The ASME III limit for most low alloy carbon steels (such as what is planned for the tank material) is 371°C [53]. The design goal of 350°C is thus still 21°C below the material limit. It should also be remembered that the hottest fuel region is a distance from any steel surface. Therefore, the steel is generally 20°C cooler than the hottest fuel. This results in a margin of 40°C or more for the steel surfaces.

The design code for the storage tank is in fact ASME VIII, and not ASME III. For this code section, the material limit for low alloy carbon steel varies between 454°C and 649°C [53]. However, the structural strength of most low alloy carbon steels starts to drop rapidly at 450°C. It would therefore be allowable to exceed 450°C on some materials, but then the structural strength and creep properties will determine the actual temperature limit.

The concrete temperature may not be higher than 65°C for long periods of time [54], and often resulted in being the limiting value of the cooling design. This problem was solved with the introduction of a thermal shield around the tank. The shield is mounted around the tank but a distance away from it. This creates a gap between the tank and the shield for the cooling to flow through. As a result, virtually no heat is radiated to the surroundings of the tank. All concrete temperatures are then not more than 5°C above the inlet temperature. It

may be that for low fill levels, thermal radiation from the bottom of the tank could still overheat the concrete floor. To eliminate this, the concrete can be insulated with a low thermal emissivity material. CFD analyses are still required to verify the need for this.

An air inlet temperature of 35°C was used as the maximum ambient temperature. For short durations lasting less than a day, 45°C is specified [7]. Proper analyses will be done during detail design to evaluate the effect of short duration large temperature variations. For closed loop active cooling analyses, an inlet temperature of 40°C was used to account for the temperature difference between the internal and external side of the heat exchanger. Passive cooling analyses make use of 35°C as it is an open loop cooling.

Table 3: Thermal limits imposed on the design

Location of peak temperature	Limit
Fuel sphere	• 400°C (to prevent oxygen corrosion)
Tank structure (shell or tube) ASME III ASME VIII	 • Carbon steel: 370°C • Carbon steel: 450°C
Concrete	• 65°C for continuous temperatures • <100°C for localised areas • 175°C over a short time-span

3. A NEW METHOD FOR THERMAL ANALYSES OF THE TANK

3.1 THE DIFFERENCE BETWEEN FEA AND CFD

Finite Element Analysis (FEA) is a technique in which any arbitrary geometry is divided into a finite number of small parts or elements that approximates the original geometry. The types of elements that can be used range from 1D (beam) to 2D (plates) to 3D (brick) elements. For each of these element types the governing equations of state can be defined. This could be stress equations, heat equations, magnetic equations, or any other type of physical law [55].

FEA software allows one to divide the geometry into applicable elements, and to assign loads and material properties to each element. The FEA software then compiles a matrix of all the equations in terms of the unknowns. This is then solved using different matrix solve algorithms. A post processor allows one to view the results of the solved problem graphically.

The simplest form of an FEA is a static linear analysis. In such an analysis, everything is constant over time, and everything behaves in a linear fashion. For non-linear analyses, the solver performs a number of iterations until convergence is reached. For most problems, the solution converges within 20 iterations. To perform transient analyses, the analysis is done in small time steps. The solution for each time increment is then calculated.

IST Nuclear uses Strand 7 [56] to perform scoping FEA work. Strand 7 is a general purpose FEA package capable of solving stress and strain problems, as well as heat conduction analyses for the mechanical and civil environment. It has a transient non-linear solver that

allows one to analyse a large range of real problems. It also has the functionality that loads can be applied as a function of position. This is a great advantage for the purpose of the storage tanks, since the heat and thermal properties varies significantly along the tank height.

The limitation of most FEA software is its rule of continuity. In other words, for one element to influence another, they should always be in contact, or linked to each other. This is valid for any solid type of problem. However, once you have a moving fluid as part of the problem, continuity cannot be maintained.

For this reason, Computational Fluid Dynamic software was developed. CFD is very similar in approach to FEA, except that it allows one to define moving fluids. Also, with the introduction of a moving fluid, the equations of state become substantially more complex. Solving a problem using CFD is therefore an iterative process instead of simple matrix simplification. Iterations of 2000 or more before convergence is reached is not uncommon.

To perform transient analyses, time is again divided into small increments. However, fluids such as air have a very small response period, and this causes the time increments to be very small, even though the solid mass changes very slowly. Techniques have been developed to increase the transient analysis speed, but it can still take a number of days to solve a few minutes of transient response. The CFD software PBMR uses is Star CD [57] and Fluent [58].

The technique described in this chapter was developed to solve thermal-fluid problems using FEA in order to speed up the time to reach a solution.

3.2 APPLICATION OF EMPIRICAL OR ANALYTICAL EQUATIONS

Before the days of fast computers and user-friendly CFD software, thermal flow problems were defined in empirical or analytical equations. The range and situation for which an equation is valid are always reported. These equations have been tested and proven on actual problems, and sometimes give more accurate results than CFD if used in its applicable range.

Many practical designs can be simplified or approximated with a combination of analytical equations. This allows the designer to perform scoping and sensitivity calculations in a fraction of the time it would take CFD analysis.

The cooling of the storage tanks can be approximated using equations for forced and mixed convection inside a duct. Because no heat should reach the concrete, the concrete need not be included in the thermal analysis of the tank. The flow of air inside the tubes is of importance as well as the flow of air around the tank. The tank is surrounded by a thermal shield that channels the flow in longitudinal ducts alongside the tank. It can therefore also be approximated as heated pipe elements. The details of the thermal shield is described later in Chapter 10 section 3.

3.3 THE FEA MODEL

A 3D FEA model is defined for the sphere volume only. A 45° section is needed due to the tank's symmetry. The heat generated per volume at a certain position is then applied as a heat load to the model. On the exposed surfaces, an applicable convection coefficient and ambient temperature is specified. The effective thermal conductivity of the spheres is applied as a non-linear material property to the solid volume.

This allows one to calculate the temperature distribution inside the tank. The steel's

participation on the heat transfer as compared to the spheres is negligible, and therefore need not be modelled.

It is also possible to calculate the fuel temperatures using a 2D cross section of the fuel volume. This technique assumes there is no heat flux in the axial direction, which is often the case at a section through the hottest portion of the fuel. Defining and solving a 2D model is 10 to 100 times faster than the 3D equivalent. Also, the 2D model can be used to study the effect of geometry changes without needing to calculate the exact temperature.

3.4 FUEL VOLUME DEFINITION

3.4.1 Thermal conductivity

The heat transfer among the spheres inside the tank is a complex mixture of radiation, conduction and local cell convection. This is represented by an effective thermal conductivity parameter. The conductivity is strongly dependant upon temperature, hence the FEA model needs to make use of non-linear material properties to define the conductivity. The actual value of the conductivity is a function of the fuel irradiation and other material properties. Several empirical and analytical correlations are available for use. As a rule, the data as used for the PBMR reactor analysis is used. Figure 44 shows the effective conductivity as reported by the Zenher-Schlunder model [59].

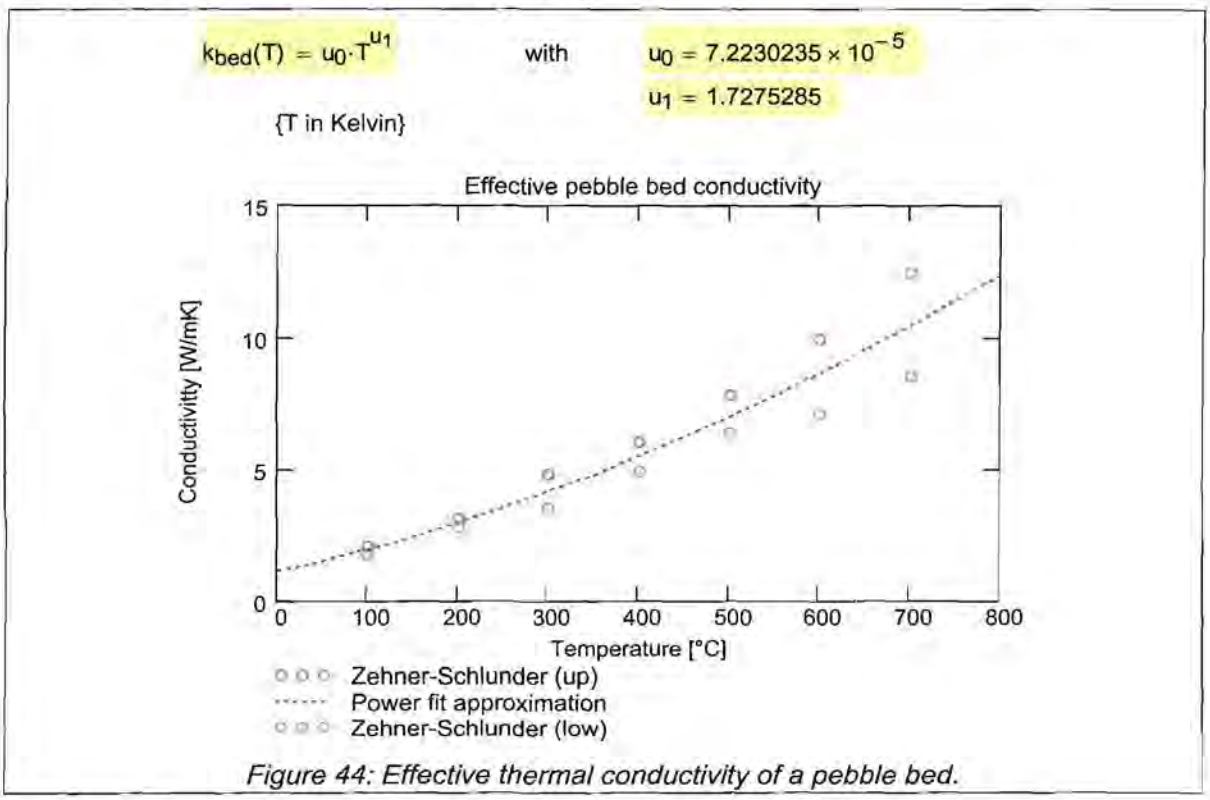

Figure 44: Effective thermal conductivity of a pebble bed.

3.4.2 Heat load

The pebble bed is represented by a solid volume, but only about 60% of this volume is occupied by spheres due to the packing factor. The heat load per sphere is obtained from the reactor core neutronics calculations done by PBMR, and is given as a function of time (refer to Appendix D). It is necessary to adjust the heat generated per sphere with the packing factor of the pebble bed to determine the FEA heat density. The same technique is

used for the CFD analysis. Because of the change in decay age of the spheres inside the tanks, the heat density is a function of position inside the tank. Equation 9 gives the heat density for the FEA volume at a certain height:

$$Q'''(z) = \frac{Q(z)}{V_s} \cdot PF \qquad \{9\}$$

with : $Q'''(z) \equiv$ "Heat density at height z" [W/m^3]

$Q(z) \equiv$ "Heat generated per sphere at height z" [W]

$PF \equiv$ "Pebble bed packing factor" [ ]

$V_s \equiv$ "Volume of a single sphere" [m^3]

3.4.3 Material density and specific heat

$$\rho \cdot C \cdot \frac{\partial}{\partial t} T = k \nabla^2 T + Q''' \qquad \{10\}$$

Equation 10 (taken from reference [60]) gives the general heat equation for a medium with internal heat generation and constant thermal conductivity. The density (ρ) and specific heat (**C**) only applies to the time derivative of the temperature. This means that for steady state analyses ($\partial T/\partial t=0$), the density and specific heat is not required.

For transient analyses however, the correct density and specific heat should be applied. Either the density or the specific heat value should be multiplied with the pebble bed packing factor (**PF**) to achieve the correct thermal response characteristics of the solid volume.

3.5 HEAT TRANSFER DEFINITION

3.5.1 Convection coefficient

To obtain the applicable convection coefficient and ambient temperature, empirical equations for the heat transfer inside a duct is used. The flow channels of the thermal shield can be expressed using a hydraulic diameter [60].

The literature is full of empirical equations for the heat transfer inside a duct. The equations are for various flow scenarios such as forced flow, buoyancy driven flow, mixed flow, constant heat load, constant wall temperature, local convection, average convection, entrance effects, uniform flow, laminar or turbulent flow etc. [61]-[66]. The choice of equation is very dependant upon the expected flow inside the pipes.

The Reynolds number for the flow inside the tube is more than 2300 for all mass flows analysed. The flow is therefore turbulent [67]. Also, due to the high heat load, the heat transfer is a mixture of forced and natural convection. This is an especially difficult regime and many researchers have tried to derive applicable correlations. A preliminary study has been done to choose the most suitable convection coefficient correlation. This study is given in Appendix B.

It should be noted that it is assumed that the flow is axi-symmetric. This is true for most of the cooling tubes, but not at the entrance of the tubes or the thermal shield channels. The

error made by this assumption needs to be quantified but is not expected to affect the overall results significantly. Another important aspect to remember when deciding which correlation to use, is that the convection coefficient (or more often described as the dimensionless Nusselt number), should be local values. Many correlations are average values, valid only when the inlet and outlet conditions are required. These equations cannot be used to calculate local effects.

3.5.2 Mass flow

One of the most important input parameters needed to calculate the convection coefficient is the mean flow velocity. The total mass passing through the tank can be defined as an input to the problem at hand. To determine the mass flow through each duct or pipe, the flow pressure drop through each duct is calculated. This should be equal for each duct. The flow velocity per duct can thus be calculated. The buoyancy effect of the air is assumed to be the same for each duct, therefore it need not be included in the equations.

The flow losses at the connection between the centre tube and small collection tubes are also taken into account.

The following equations 11 to 15 are solved numerically to obtain the mass flow per tube:

Outer tubes (p1) friction loss :

$$\Delta P = \frac{f_{Dp1}}{2 \cdot D_{p1}} \cdot \rho \cdot v_{p1}^{2} \cdot L_{p1} \qquad \{11\}$$

Channel around tank (ch) friction loss :

$$\Delta P = \frac{f_{ch}}{2 \cdot D_{ch}} \cdot \rho \cdot v_{ch}^{2} \cdot L_{ch} \qquad \{12\}$$

Center tube friction loss :

$$\Delta P = \left(\frac{f_{Dp2}}{2 \cdot D_{p2}} \cdot \rho \cdot v_{p2}^{2} \cdot L_{p2} \right) + \left(\frac{f_{Dp3}}{2 \cdot D_{p3}} \cdot \rho \cdot v_{p3}^{2} \cdot L_{p3} \right) + \frac{K_{loss}}{2} \cdot \rho \cdot v_{p3}^{2} \qquad \{13\}$$

{ centre tube} { collection tube} { transition }

$N_X \equiv$ "Number of tubes of type x" {14}

{15}

with : $f_X \equiv$ "D'Arcy tube friction loss factor"
$D_X \equiv$ "Diameter of tube x"
$v_X \equiv$ "Mean air velocity in tube x"
$L_X \equiv$ "Length of tube x"
$A_X \equiv$ "Cross sectional area of tube x"
$N_X \equiv$ "Number of tubes of type x"

p1 ≡ "Outer tube"
p2 ≡ "Centre tube"
p3 ≡ "Collection tube"
ch ≡ "Channel around the tank"

3.5.3 Air temperature

The FEA model requires a convection coefficient value and an associated ambient temperature. The bulk air temperature inside the tubes can be estimated by assuming a certain heat flux per height into the air.

Previous CFD analyses showed that the heat flux per unit height is more or less the same through all heat transfer surfaces. The heat is thus distributed evenly along the tubes and tank wall for a given height. The heat flux per unit length can then be calculated by:

$$Q' = \frac{Q'''(z) \cdot A_{tank} \cdot P_{pipe}}{P_{cool}} \quad \{16\}$$

with : Q' ≡ "Heat per unit length at position z" [W/m]

$Q'''(z)$ ≡ "Heat density of vuel volume at specific height z" [W/m^3]

A_{tank} ≡ "Cross sectional area of the fuel at height z" [m^2]

P_{cool} ≡ "Total heat transfer perimeter of all cooled surfaces" [m]

P_{pipe} ≡ "Heat transfer perimeter of the specific pipe" [m]

The local bulk air temperature can now be calculated by dividing the heated part of the tube into small increments. The increase in temperature from one increment to the next can be calculated by the following equation:

$$Tg_{i+1} = Tg_i + \frac{Q'_i \cdot \Delta z}{m' \cdot Cp} \quad \{17\}$$

with : Tg_i ≡ "Temperature of the gas (air) at increment i" [K]

Q'_i ≡ "Heat per unit length at increment i" [W/m]

Δz ≡ "Height increment" [m]

m' ≡ "Tube mass flow" [kg/s]

Cp ≡ "Specific heat of air at constant pressure" [J/kg*K]

The actual heat flux per pipe as calculated by the FEA analysis should be checked to see if the initial assumption is still valid. If needed, a second iteration should be done with corrected heat flux values. Although the heat flux at the top is not only axially to the pipes (because of heat loss through the upper surface), the error made should not affect the overall accuracy of the results.

3.5.4 Heat transfer from the upper surface

From CFD analyses, it was evident that a significant portion of heat flows through the upper surface of the pebble bed [68]. This heat is transferred with internal convection of the helium inside the tank and thermal radiation to the surrounding tank wall. From the tank wall, it is then removed through convection by the cooling air and radiation to the surrounding structures.

This process of heat transfer cannot be calculated by Strand 7 because of the intermediate fluid (helium) and the thermal radiation to another solid (tank wall). Convection or radiation can only be expressed in terms of a constant ambient or receiving temperature. Some other

software can solve solid-to-solid radiation, but the convection portion is still a fixed input.

In order to properly include the upper surface cooling, an effective convection coefficient was calculated such that it will have the same cooling effect as-if the actual process took place. This involves compiling the balance equations of heat from the surface to the tank wall, and from the tank wall to the ambient air. The equations are given below:

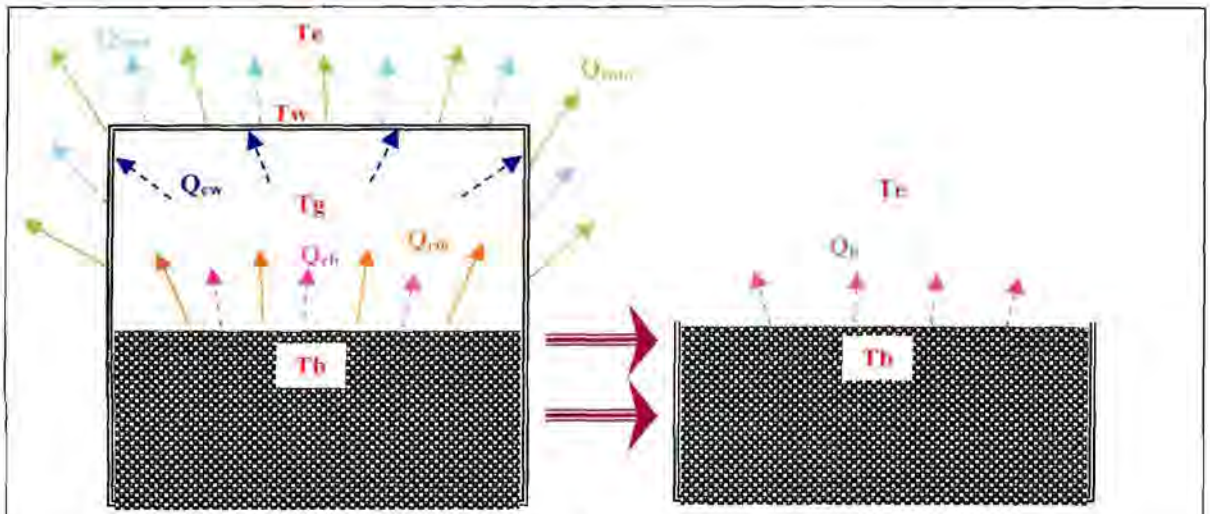

Figure 45: Converting from tank wall to effective convection.

Bed surface convection : $Q_{cb} = h_{cb} \cdot A_b \cdot (T_b - T_g)$ {18}

Bed surface radiation : $Q_{rin} = \sigma \cdot \varepsilon_{in} \cdot A_b \cdot (T_b^4 - T_w^4)$ {19}

Inner wall convection : $Q_{cw} = h_{cw} \cdot A_w \cdot (T_g - T_w)$ {20}

Outer wall convection : $Q_{cout} = h_{ce} \cdot A_w \cdot (T_w - T_e)$ {21}

Outer wall radiation : $Q_{rout} = \sigma \cdot \varepsilon_w \cdot A_w \cdot (T_w^4 - T_e^4)$ {22}

Effective convection : $Q_b = h_{eff} \cdot A_b \cdot (T_b - T_e)$ {23}

Heat balance equations : $Q_b = Q_{rin} + Q_{cb}$ {24}

$Q_{cb} = Q_{cw}$ {25}

$Q_b = Q_{rout} + Q_{cout}$ {26}

In these equations, it is assumed that the upper surface is at a constant temperature, as well as the ambient air and outer radiation surfaces. By choosing the bed and ambient temperature, the equations 24 to 26 can be solved for Tg, Tw, and h_{eff}. A graph of effective convection versus bed temperature can thus be compiled for a given gas temperature. This relation can be input into Strand7 for the upper surface convection coefficient.

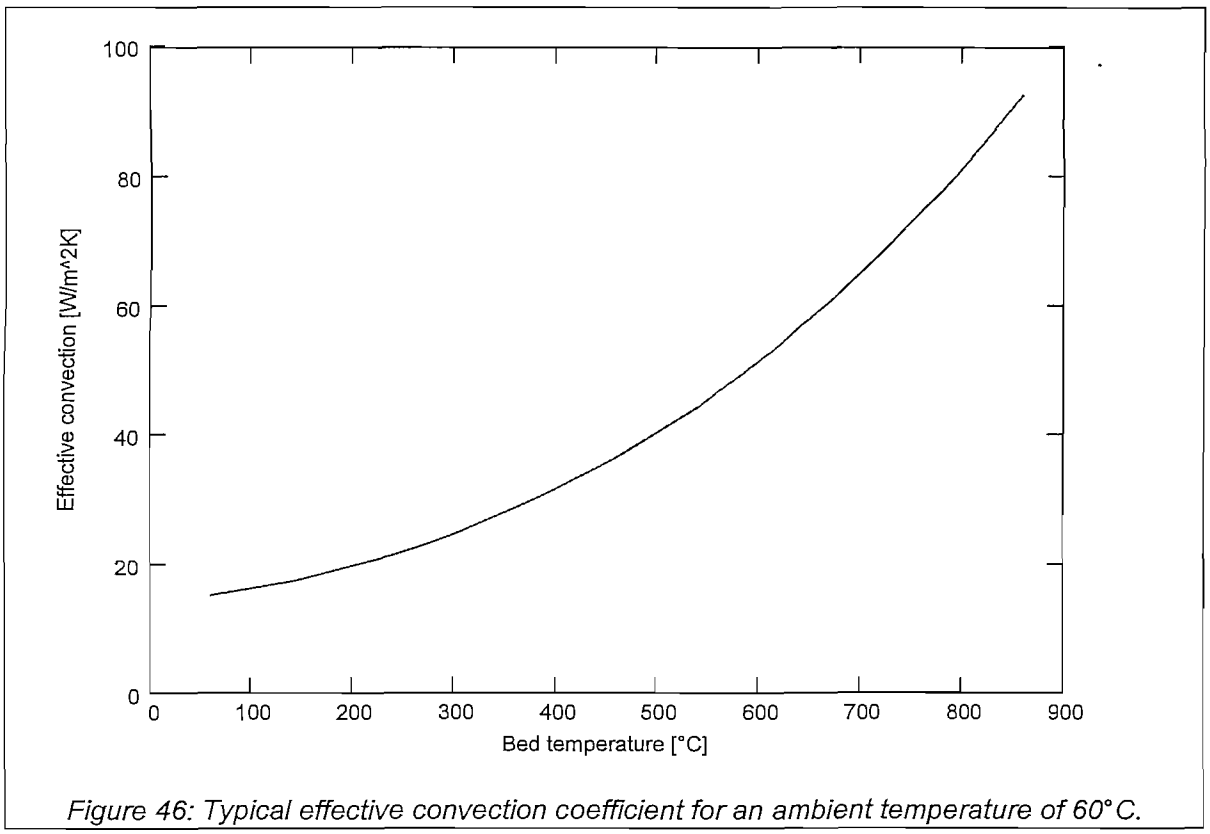

Figure 46: Typical effective convection coefficient for an ambient temperature of 60° C.

3.6 CALIBRATION OF THE FEA MODEL

It often happens that some property (such as loss coefficients or local flow velocities) needs to be chosen using an estimated guess. This guess can be calibrated using CFD analyses. This was the case at the bottom of the tank where there is a mixture of inverted natural convection and forced convection. Also, the flow velocities used to calculate the convection inside the tank to determine the effective upper surface convection were estimated from CFD results. However, these conditions are fairly constant for different analyses, and are also not the dominant heat transfer properties. The flow loss coefficients for the individual pipes were also extracted from CFD.

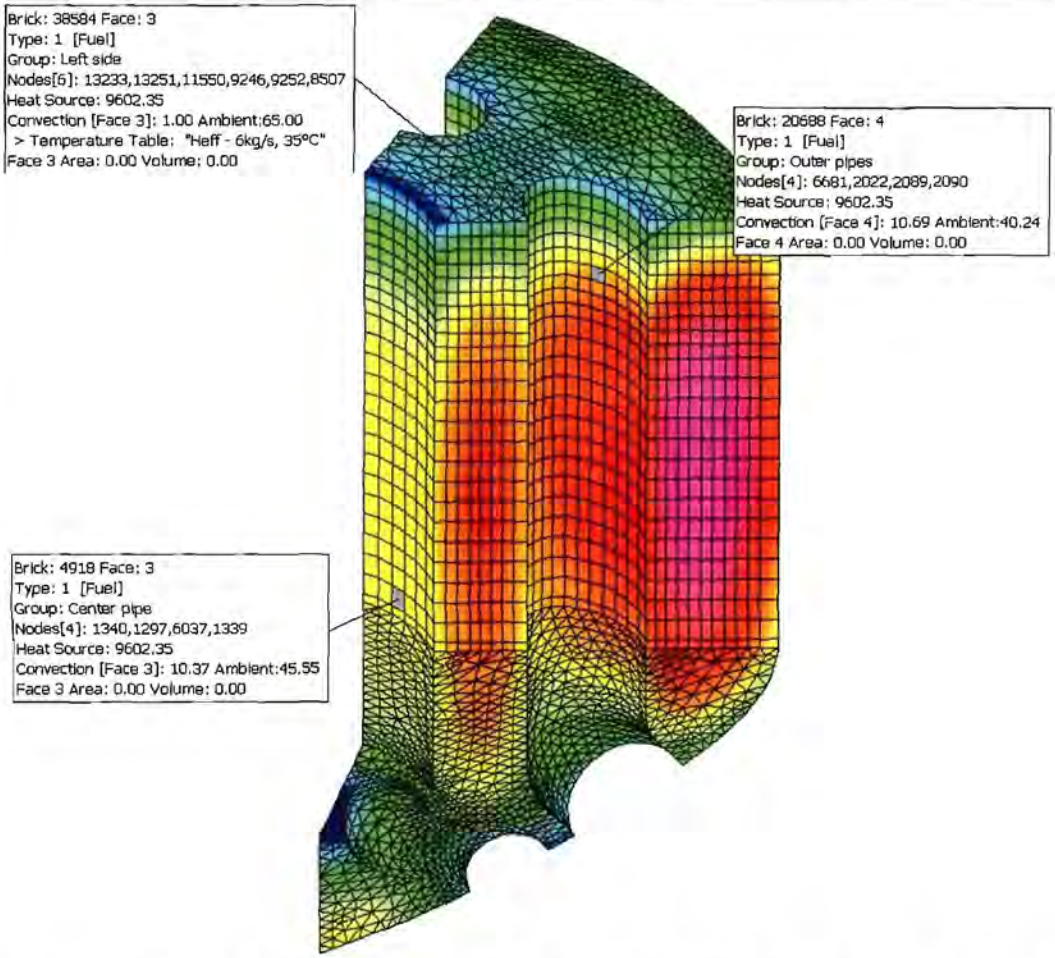

Figure 47 : Strand7 45° model of a 20% filled storage tank with heat load and convection applied.

3.7 COMPARISON WITH CFD ANALYSES

A substantial amount of FEA analyses were performed, and compared with available CFD results. Various geometries, heat loads and cooling flows were used. The algorithm used to calculate the convection coefficients and temperatures used as input to the FEA model is given in Appendix G.

Figure 48 shows a comparison between the FEA and CFD analysis of the UFT. The maximum temperature is shown, as this is the most significant result of the analysis. The maximum difference is 10%, at the 5% fill level analysis. This difference can be expected as the bottom part of the tank plays a bigger role in the heat transfer at this low fill level, but the FEA analysis does not have proper convection correlations for this region. An estimated general value was used. The minimum difference is 1%, and is found between 25% to 50% fill level. This is very useful as the hottest fuel is found around this fill level. In all cases however, the FEA method slightly over-estimates the temperature, hence the analysis produces more conservative results.

Figure 49 to Figure 52 show temperature contour plot comparisons of various results. There is a remarkable resemblance in the temperature result, especially at the maximum fuel temperature. The difference in the low temperatures can be attributed to local flow effects, as well as some internal convection inside the tank. In general, the difference in maximum temperature was found to be within 5% of the CFD results.

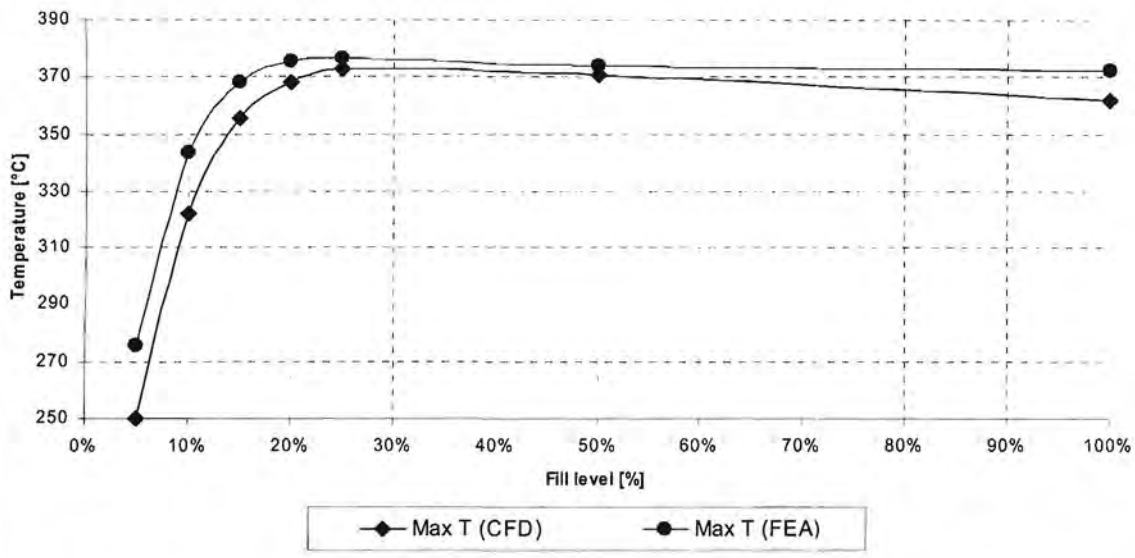

Figure 48: Maximum fuel temperature results comparison between the FEA method and CFD [69] for the UFT at approximately 5.7kg/s cooling flow.

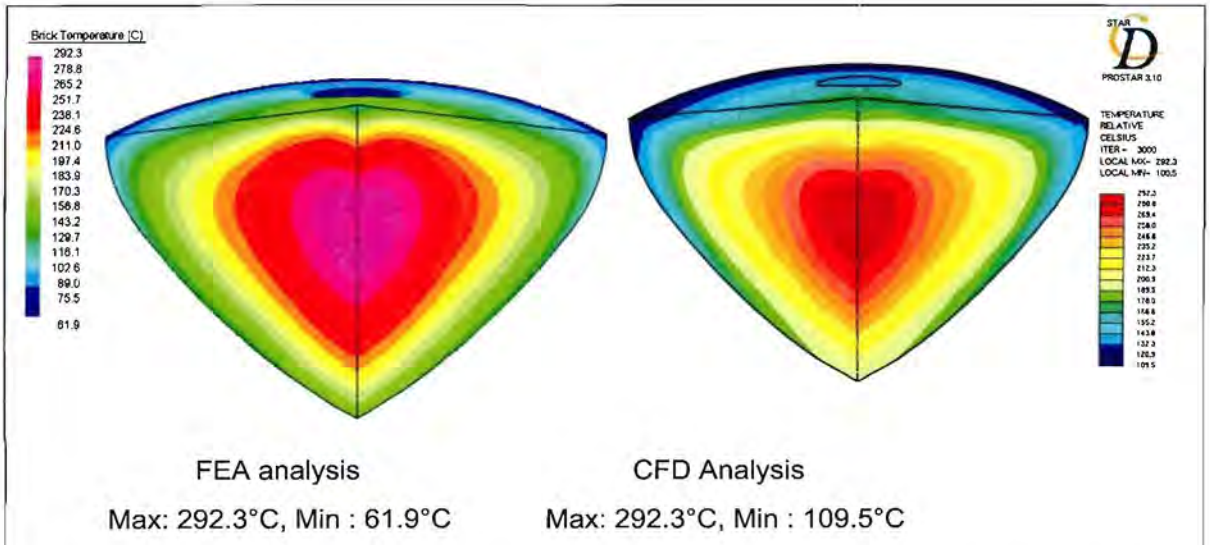

Figure 49: Comparison between FEA and CFD [70] analysis of an old SFT geometry at 5% fill level.

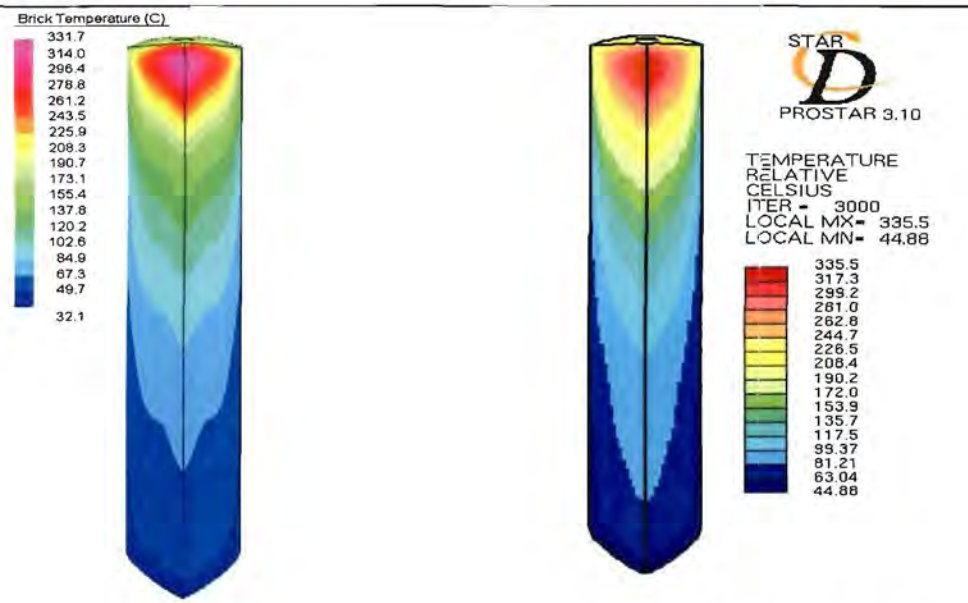

FEA analysis

Max: 331.7°C, Min: 32.1°C

CFD Analysis

Max: 335.5°C, Min: 44.88°C

Figure 50: Comparison between FEA and CFD [70] analysis of an old SFT geometry at 100% fill level.

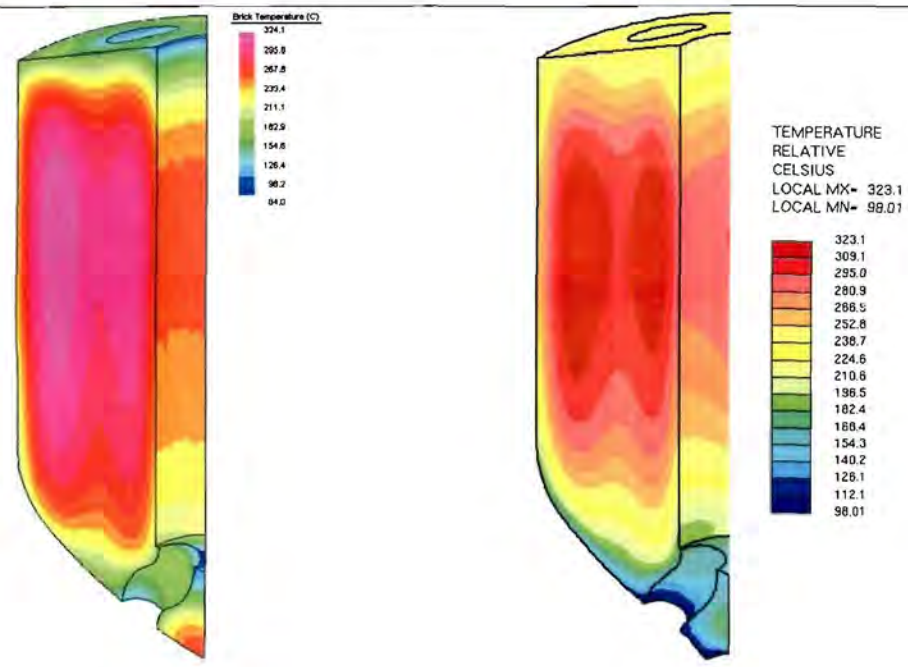

FEA analysis

Max: 324.1°C, Min: 84.0°C

CFD Analysis

Max: 323.1°C, Min: 98.0°C

Figure 51: Comparison between FEA and CFD [71] analysis of an old UFT geometry at 20% fill level.

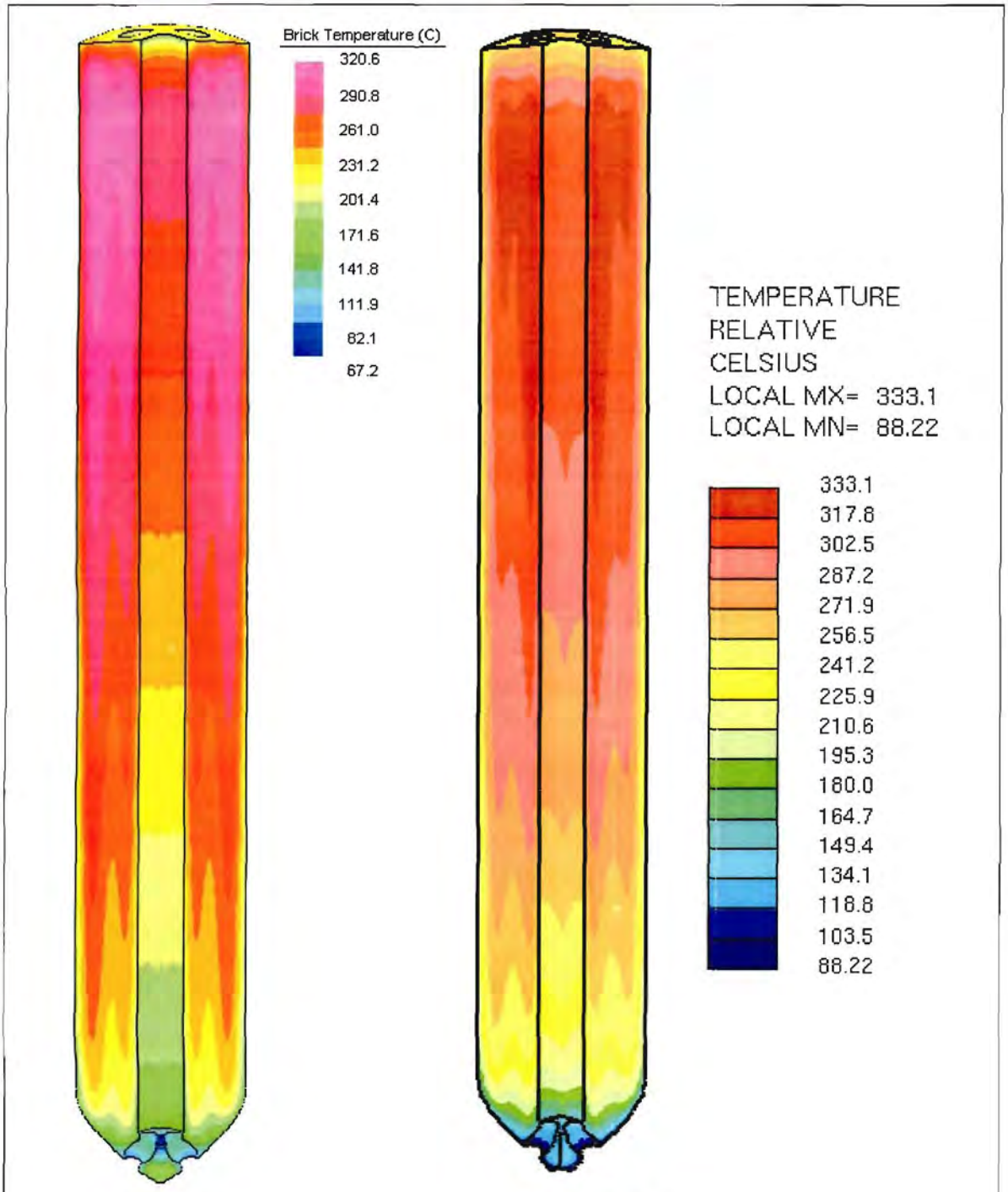

Figure 52: Comparison between FEA and CFD [71] analysis of an old UFT geometry at 100% fill level.

4. SPENT FUEL TANK ANALYSIS

4.1 DECAY HEAT LOAD

Spent fuel is added to the tank at a rate of 340 to 484 spheres per day. The rate depends upon the actual power consumption and reactor power level. For conservatism, the maximum value of 484 spheres per day was used for all the analyses. At this rate, it will take about 3 years to fill a tank. Based upon a postulated power profile over the life of the plant, it will take about 3.5 years to fill a tank. This was used as the default time to fill a tank, although the decay heat was calculated based upon a rate of 484 spheres per day.

The decay heat per spent fuel sphere starts at 1.2W when it enters the tank, and drops down to below 0.6W after 2 months (see Appendix D). This implies that by the time the tank is full, a large portion of the spheres produces virtually no heat. The heat generated inside the tank therefore varies significantly along the height of the tank.

In order to accurately determine the age (or time of decay) of a sphere at a certain height, the cross section area of the fuel volume at different levels is needed. This can be determined using a 3D CAD model of the fuel volume. The following equation is then used to calculate the decay age.

$$t(z) = \frac{1}{V'} \cdot \int_0^z Ac(z)\, dz \qquad V' = \frac{Ns}{V_s \cdot 24 \cdot 3600} \cdot PF \qquad \{27\}$$

with : $Ac(z) \equiv$ "Tank cross section at height z" [m^2]

$V' \equiv$ "The rate of volume increase" [m^3/s]

$Ns \equiv$ "Number of spheres per day" [1/day]

$V_s \equiv$ "Sphere volume" [m^3]

$PF \equiv$ "Sphere bed packing density" [unitless]

It is assumed that all the spheres are of the same decay age at a certain height. Once the decay age is known, the heat per volume can be calculated from the sphere decay heat curve. The fact that the spheres do not occupy all of the volume of the tank is accounted for by a packing factor.

$$Q'''(z) = \frac{Q_{decay}(t(z))}{V_s} \cdot PF \qquad \{28\}$$

with : $Q_{decay}(t) \equiv$ "The decay heat of a single sphere after t seconds"

The decay heat curve is probably the most significant of all inputs. Any change in fuel decay heat or loading rate should be carefully analysed to verify the validity of previous analyses. Appendix E contains the algorithm used to calculate the heat load profiles shown in Figure 53. One can clearly see that most of the heat is being generated at the top portion of the tank. One can therefore expect the hottest fuel to be in this region. Also note how the high-density region moves upward as the tank is filled.

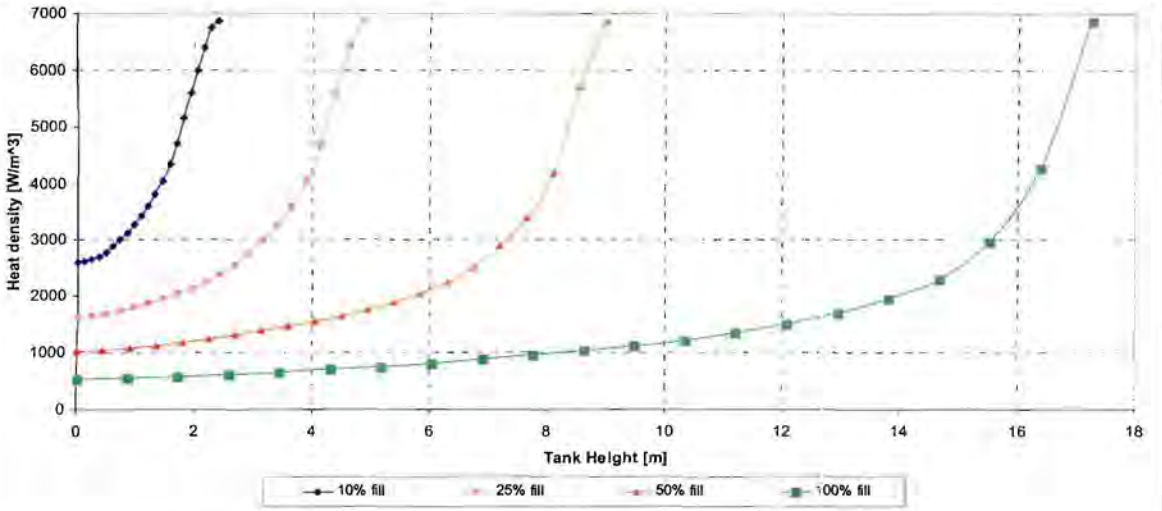

Figure 53: Typical heat density profiles of the SFT at various fill levels.

The total decay heat load can be calculated by integrating the heat load profile over the length of the tank, and incorporating the change in fuel volume cross section. The result is presented in Figure 54. The total heat increases dramatically at low fill levels, and then more gradually at higher fill levels. This is because the high-density region is first formed at the low fill level, and then moves upward. The slower increase at higher fill levels is caused by the gradual contribution of the "older" fuel in the tank. One can expect a similar characteristic from the fuel temperature as the tank is filled.

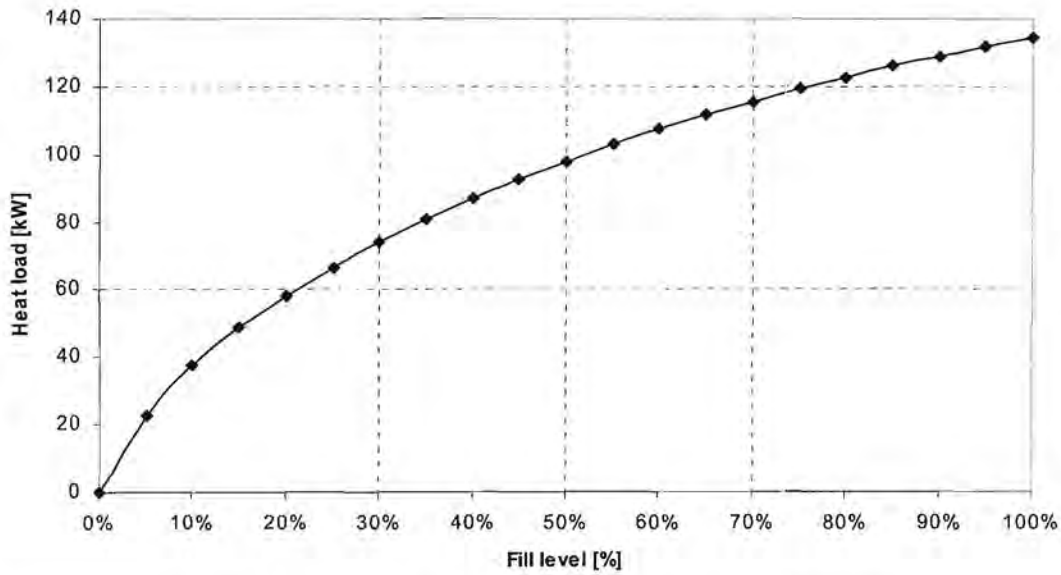

Figure 54: SFT total decay heat load for different fill levels.

4.2 TANK GEOMETRY SENSITIVITY ANALYSIS

The effect of the radial position (PCD) of the outer cooling tubes was investigated using a 2D plate FEA model. Initially, the tank had four outer tubes. The model resembled a section through the hottest expected region where heat flows only in a radial direction. The decay heat at this region is about 4kW/m^3 with an outer convection coefficient of about 9W/m^{2}K. Figure 55 shows the effect of increasing the PCD from 1500mm to 1800mm.

Although the temperature distribution varies between the different configurations, the maximum fuel temperature only differs with 13°C. It can thus be concluded that the positions of the outer tubes may be driven by other factors such as manufacturability or sphere flow rather than temperature.

A PCD of 1800 was chosen because this gives sufficient room for the bottom region where the centre tube splits into four smaller tubes. Later changes to the UFT caused the SFT design to have eight tubes at a PCD of 1800mm.

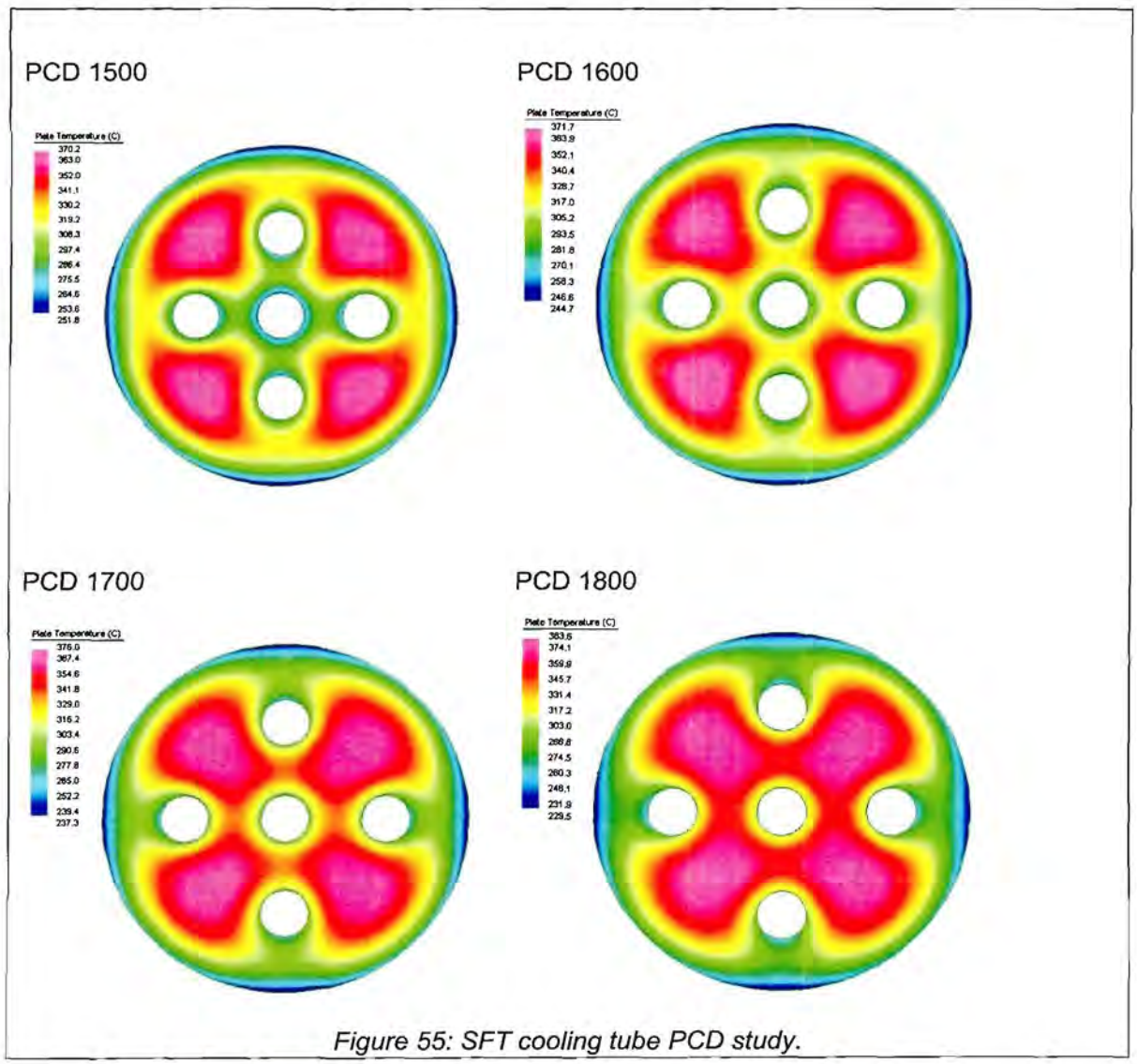

Figure 55: SFT cooling tube PCD study.

4.3 COOLING FLOW SENSITIVITY ANALYSIS

The effect of cooling mass flow was investigated for the 100% fill level case. The results are given in Figure 56. It can be seen that a cooling mass flow of 1.7kg/s or more is necessary in order to keep the temperatures below 350°C. It is also evident that by increasing the flow significantly more than 4kg/s, will not result in a similar drop in temperature. This is due to the thermal conductivity of the pebble bed that drops as one reduces the temperature; also the equation for the heat transfer coefficient has an inverse parabolic shape with respect to flow velocity (see Appendix B).

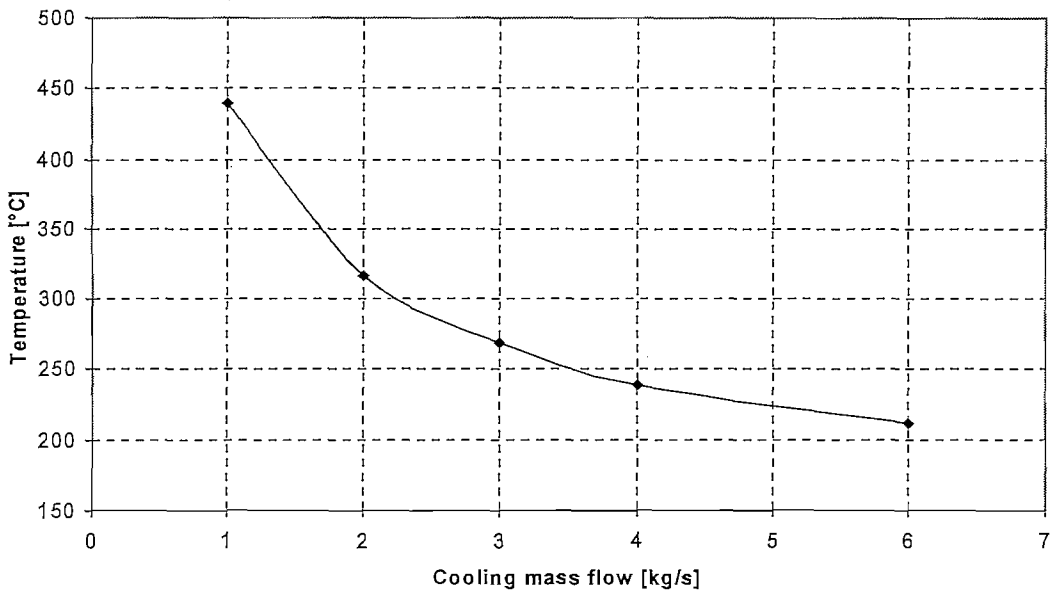

Figure 56: Maximum temperatures for different cooling flows of a 100% filled SFT, inlet 40°C.

4.4 ACTIVE COOLING ANALYSIS DURING TANK FILLING

A number of 3D thermal analyses were performed with the final tank design using the FEA method. The cooling flow was set at 3kg/s as it was found that a similar mass flow is achieved during passive cooling. The inlet temperature was set at 5°C higher than ambient to account for the difference caused by the heat exchanger (see Chapter 10 for a discussion of the heat exchanger and passive cooling).

Table 4: Primary parameters used for the SFT active cooling analyses

Parameter	Value
Tank geometry	As shown in Figure 37.
Tank loading	484 spheres per day, total of 530 000 spheres
Cooling	3 kg/s at 40°C inlet temperature

A 45° section of the tank was analysed. This is necessary to capture the symmetry properties of the bottom region of the tank. However, the majority of the tank has 22.5° symmetry. The hottest part of the fuel is also found between two outer cooling pipes. To show the hot spot, the results are given with one half of the top section hidden.

Figure 57 shows the maximum fuel temperature for the different fill levels, while Figure 58 and Figure 59 show the corresponding 3D temperature distribution. One can see that the maximum temperature follows a similar pattern as the total decay heat, i.e. it rises sharply at the beginning and then more gradually at higher fill levels. A hot spot is also very clear in the temperature distributions. This hot spot is about 1 metre below the top of the pebble bed, and moves upward as the tank is being filled. The temperature scale of the figures is shown in a histogram form to indicate the relative amount of fuel that is at a certain temperature. From this, it can be seen that there is only a small portion of the fuel at temperatures above 200°C, especially for high fill levels.

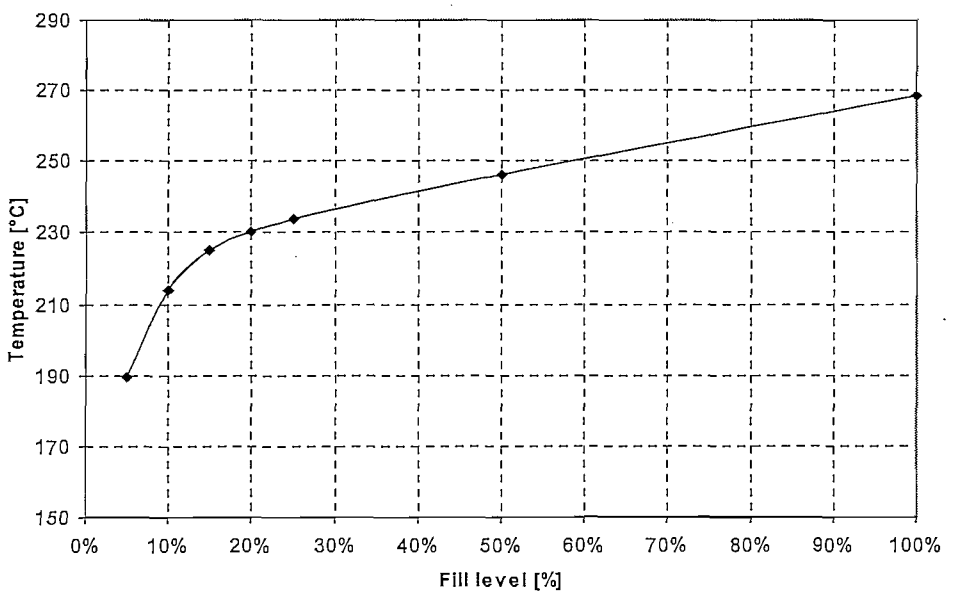

Figure 57: Maximum fuel temperature in the SFT for different fill levels.

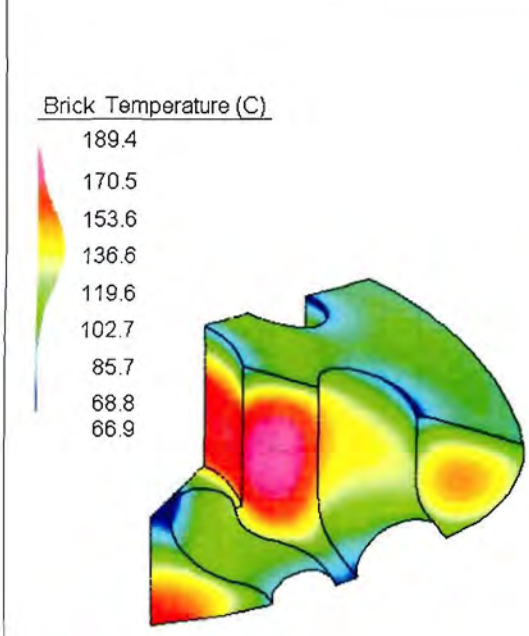

5% fill

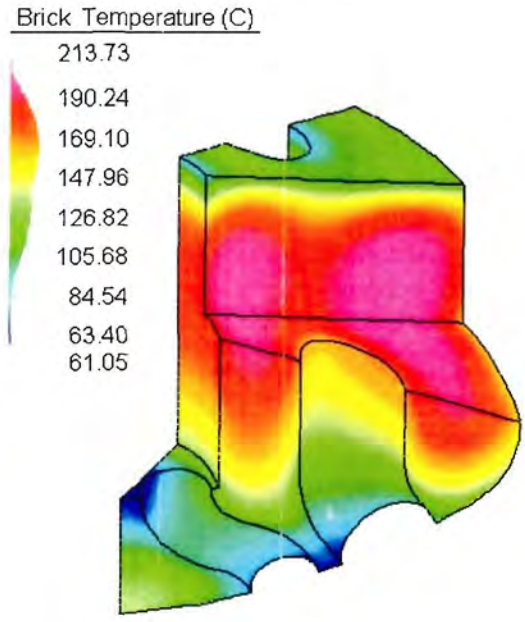

10% fill

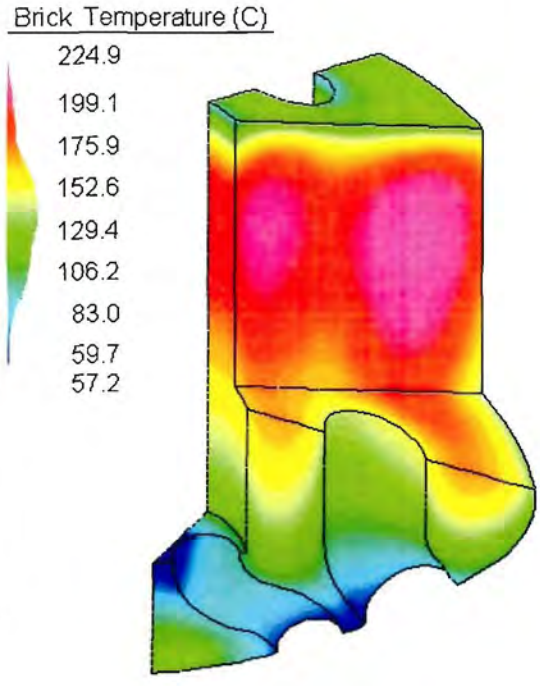

15% fill

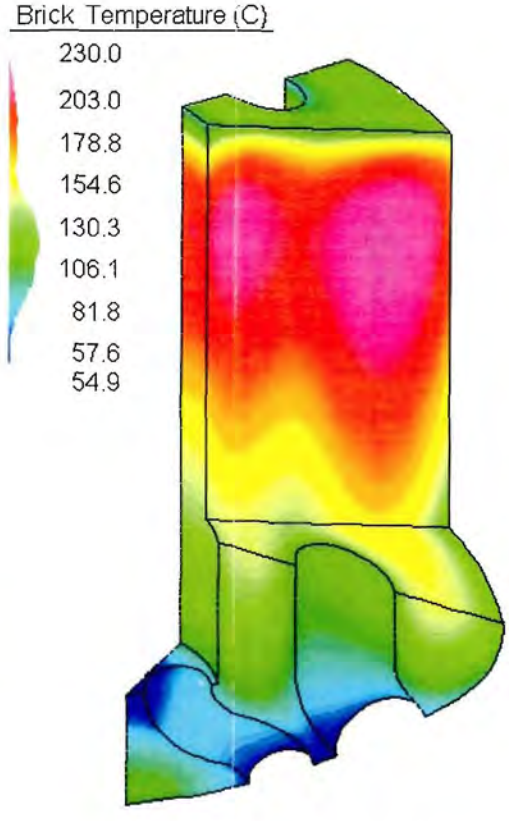

20% fill

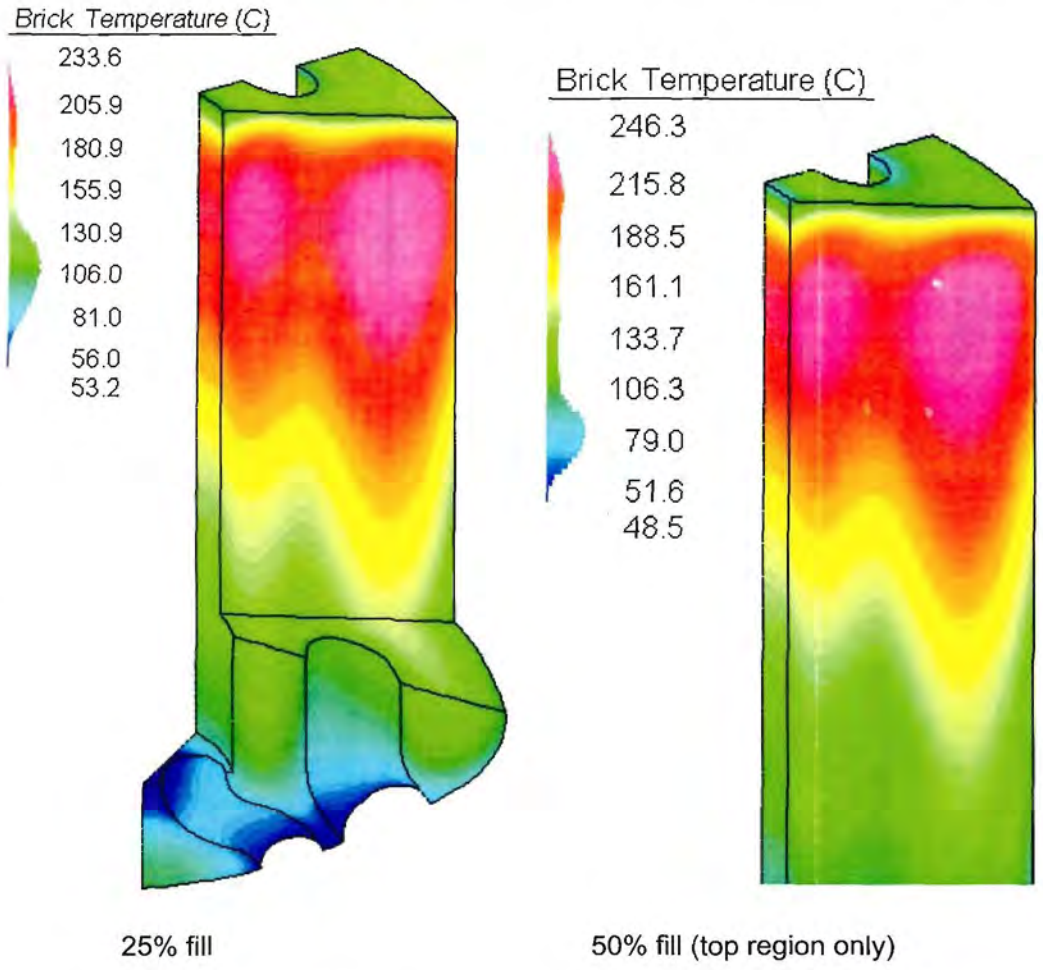

Figure 58: SFT temperature distributions for different fill levels.

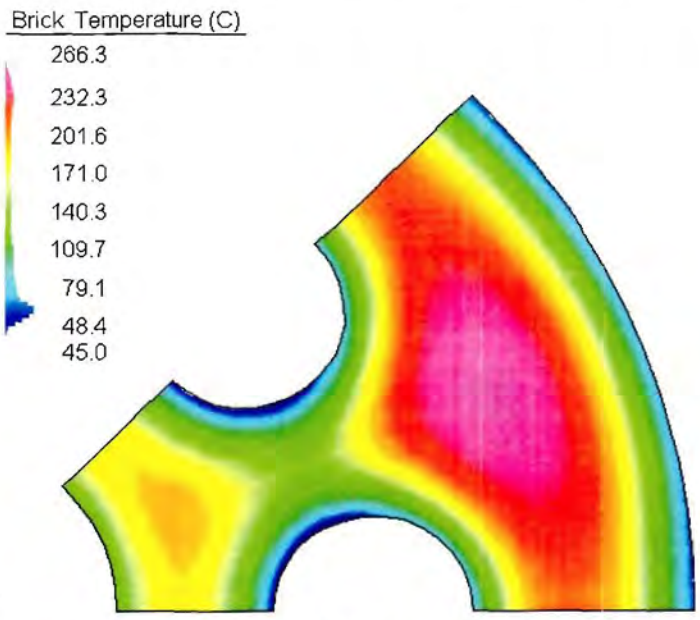

Figure 59: Cross-section through the hottest region of the SFT at 100% fill level.

4.5 TANK COOL DOWN TEMPERATURES

After the first tank has been filled, it will be stored for 80 years before decommissioning. The temperatures inside the tank as the spheres decay were calculated for different decay times. A cooling mass flow of 3kg/s were used up to 3.3 years decay, after which 1.5kg/s was used. This is because the heat load is 25% of the original amount after 3.3 years, allowing one to reduce the cooling mass flow.

Figure 60 presents the maximum fuel temperature for the cases analysed along with the total decay heat. There is a good relation to the drop in maximum temperature with the drop in decay heat. After 80 years of decay, the maximum fuel temperature is less than 50°C, and only about 5kW of heat is being generated by the 530 000 spheres.

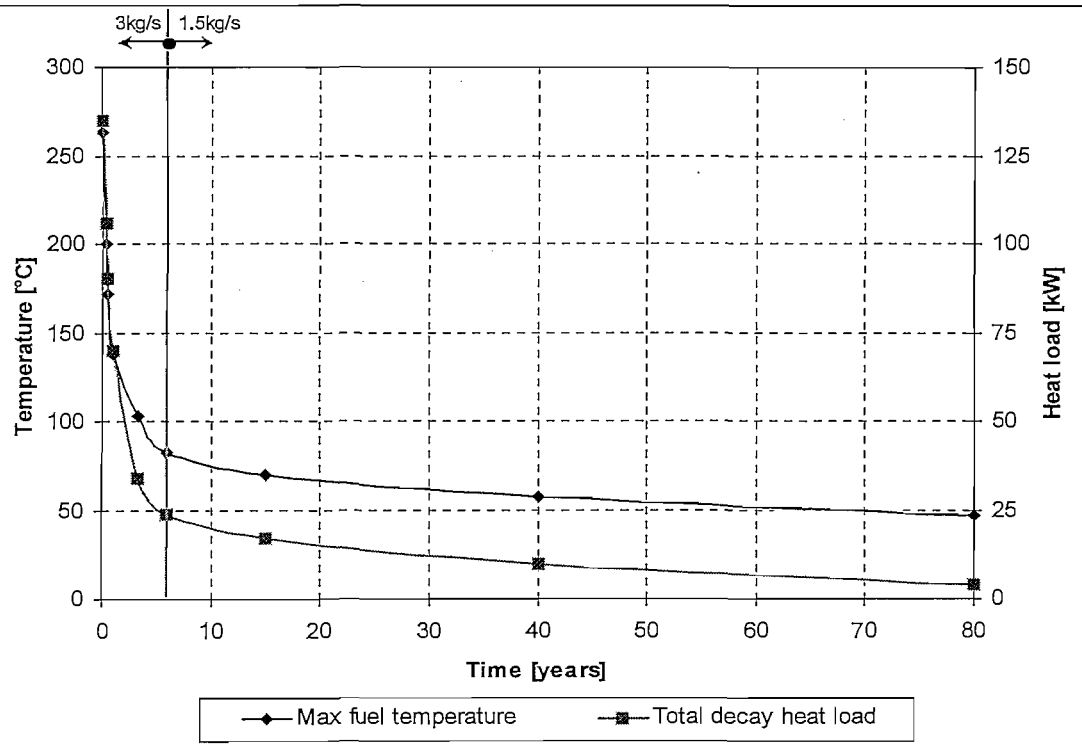

Figure 60: Maximum fuel temperature and total heat load vs. decay time for a 100% filled SFT.

4.6 TRANSIENT ANALYSIS DURING LOSS OF COOLING

Transient analyses were done to investigate what happens to the tank when all cooling is lost and passive cooling cannot be initiated. The analyses were done for 100% fill level using the FEA method described previously. The analysis was started at equilibrium temperature, but with all convection coefficients set to zero. It is as if the tank has been covered by a 100% insulating blanket. In practise, the cooling air will circulate around the tank and transfer some of the heat to the surrounding structures. The result from this analysis is therefore more conservative and it can be expected that the temperature increase will be slower in reality.

The theoretical maximum rate at which the temperature increases can be calculated from the following equation:

$$\frac{\partial}{\partial t} T_{max} = \frac{Q'''}{\rho \cdot C} \qquad \{29\}$$

with : $t \equiv$ "Time"

$T_{max} \equiv$ "Maximum temperature"

$Q''' \equiv$ "Decay heat density"

$\rho \equiv$ "Material density"

$C \equiv$ "Specific heat"

If the specific heat and material density stay constant, the rate of temperature increase is proportional to the decay heat density. The actual specific heat increases slowly with increase of temperature, and this reduces the slope as the temperatures increase with time.

The moment cooling is lost from the tank the hottest spot is about 1m below the pebble bed surface. However, the heat density there is only 4kW/m^3 as opposed to the top layer that generates about 7kW/m^3. Therefore, the top layer's temperature increases faster than the initial hot spot. The hot spot therefore slowly moves upward until it is at the top layer. Figure 61 shows the temperature increase of selected points on the fuel volume. One can see how the hot spot moves upward in the successive images of Figure 62.

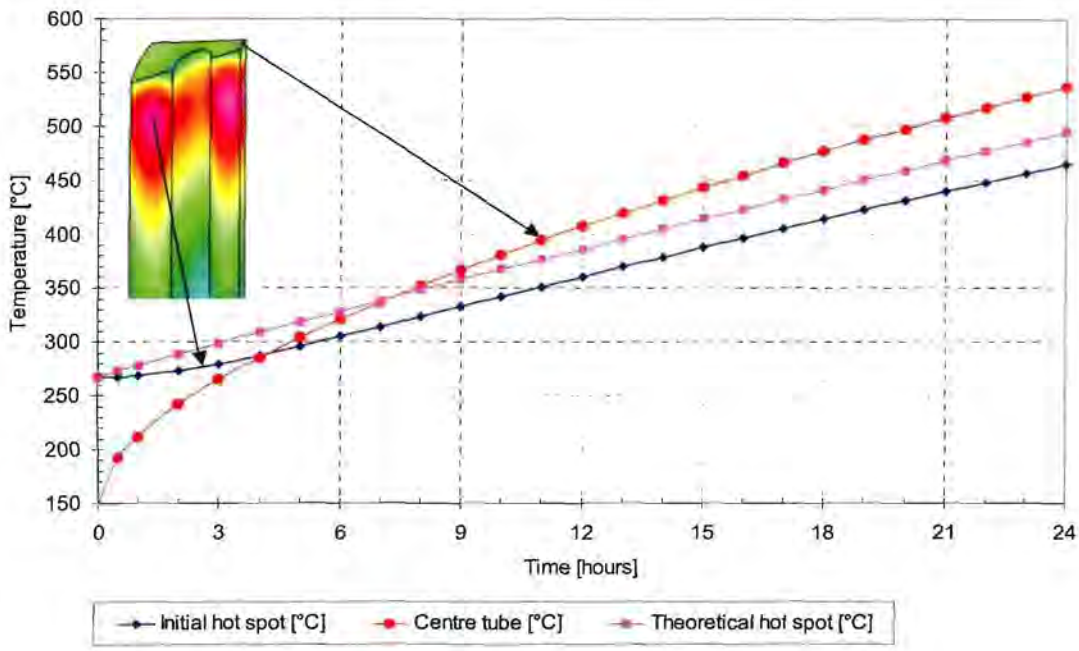

Figure 61: 100% filled SFT transient thermal response during a LOC, initial cooling flow of 3kg/s, 40°C inlet.

Equation 29 is valid only when the fuel sphere that generates the heat absorbs all of the heat. If some of the heat conducts to nearby spheres, the rate of temperature increase of the specific sphere will be lower. This is evident in the transient temperature plot given in Figure 61. The theoretical temperature of the hot spot is shown with the actual result. Eventually the temperature slope stabilizes to that of the theoretical value, but there is an initial delay due to heat conduction.

During a loss of cooling event, the fuel temperatures may be allowed to exceed 400°C, provided that the helium remains inside the tank, i.e. the spheres are not exposed to oxygen. The time before any action needs to be taken (called retention time) is thus determined by the maximum allowable temperature of the tank. This may be either 450°C if the mechanical properties of the tank are taken as constant, or 650°C if the loss of mechanical strength is included in the analysis of the tank. As a conservative measure, 450°C is taken as the cut-off temperature.

The transient results show that the centre tube reaches a temperature of 450°C after 15.6 hours for the 100% fill level. This means that one has about 15 hours to initiate the passive cooling or restore the active cooling before the temperatures could exceed the tank material limit.

The time it takes for a region to reach the maximum allowable temperature depends upon the rate of temperature increase as well as its initial temperature. It is not possible to control the rate of temperature increase because it is a function of the decay heat and sphere properties. The only parameter that can be controlled is the initial temperature. This can be achieved by increasing the forced cooling flow to lower the tank temperatures.

The retention time for different fill levels are shown in Figure 63. From this one can see that the minimum retention time is for the 100% filled case. This is because the initial temperature is the highest. The maximum decay heat density is the same for all fill levels, as it corresponds to the most recently loaded spent fuel spheres. As a result, all fill levels change temperature at the same rate. In the actual case, if convection is taken into account, it may be that a lower fill level has the lowest retention time. This is because the low fill levels have less heat to drive the buoyancy re-circulation flow. In either case, the retention will not be less than what is predicted using the FEA model.

Figure 64 shows the thermal response of the SFT caused by a sudden change in cooling flow and inlet temperature. This case is typically what would happen if one cooling unit fails (the integrated cooling design described in the next chapter has two cooling units delivering the required active cooling flow). It can be seen that the maximum fuel temperature stabilizes to just above 350°C after 48 hours. This is still within the tank and fuel limits, hence it will not be needed to switch to passive cooling if only one cooling unit fails.

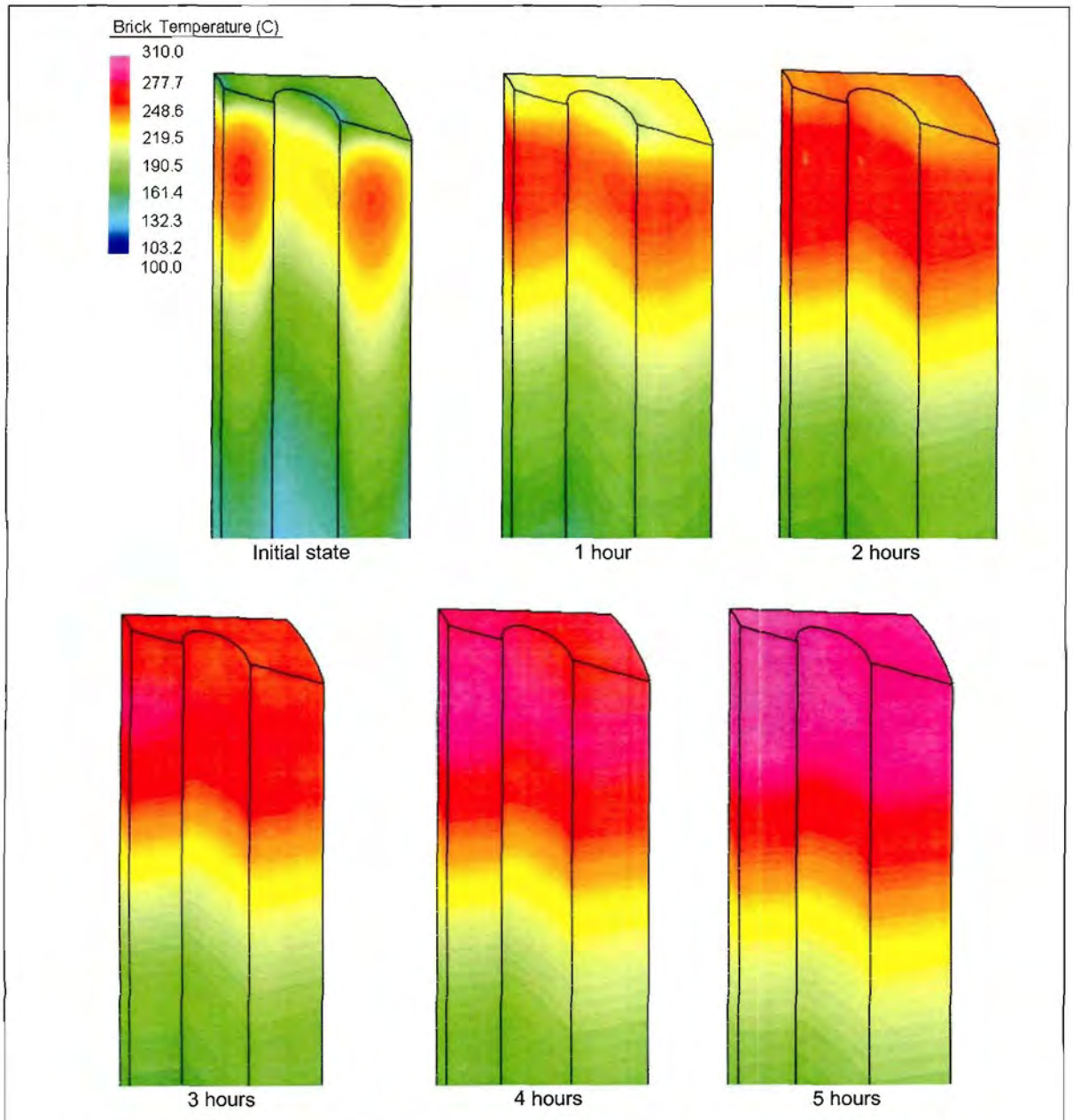

Figure 62: 100% filled SFT temperature distribution during a LOC event, initial cooling flow of 3kg/s, 40°C inlet.

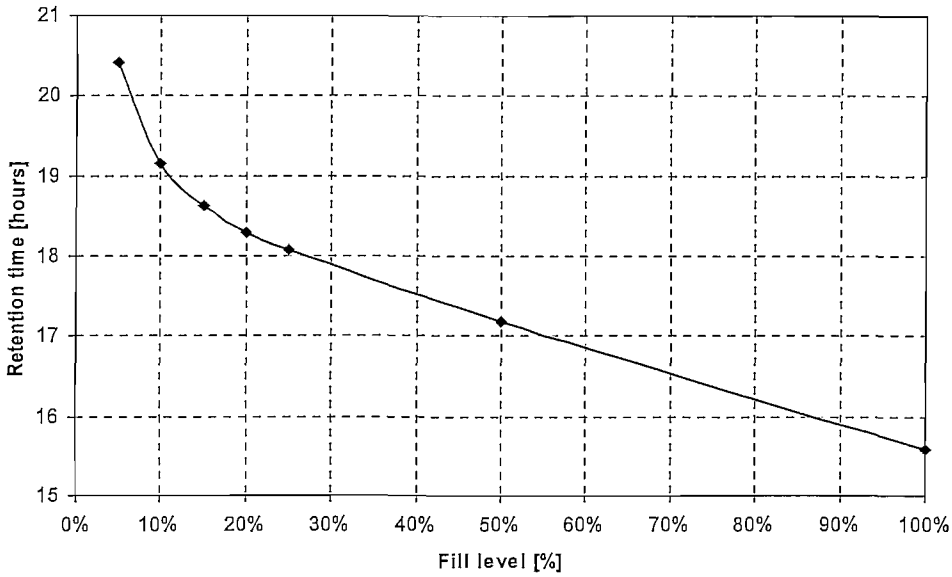

Figure 63: SFT retention times for a LOC event at different fill levels.

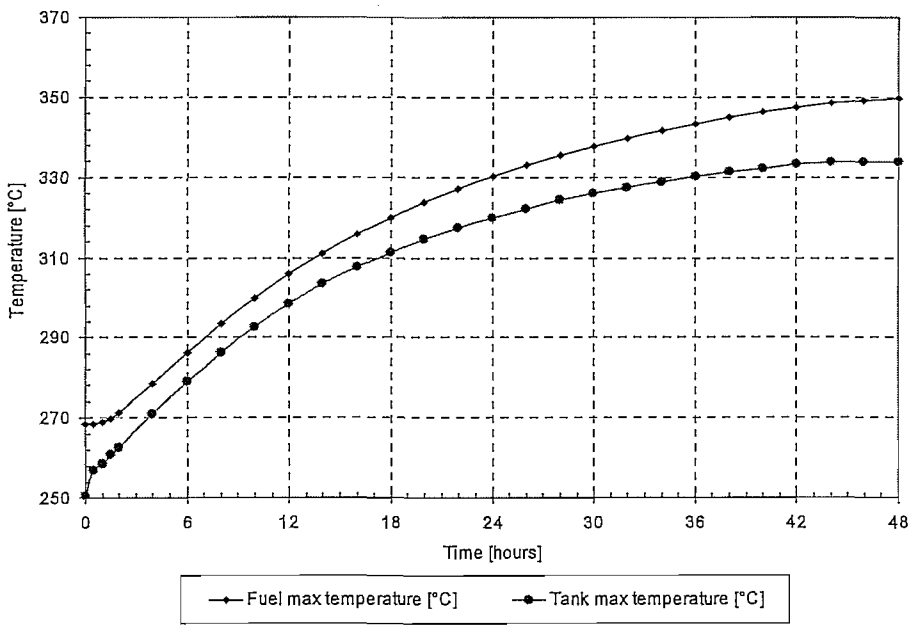

Figure 64: Thermal response of 100% filled SFT during transient from 3kg/s 40°C cooling to 1.5kg/s 45°C.

All the transient results given so far are for a tank that has just been filled (the top layer of spheres haven't decayed much yet). For a tank that has decayed for a few years, the rate of temperature increase can be estimated using equation 29 given before. Figure 65 shows the rate of temperature increase as a function of decay time for different initial temperatures. This graph can be used to calculate the conservative retention time for a tank that has decayed for a while. For example, after one year, the temperature increases by 4°C/hr for an initial temperature of 200°C. It will therefore take 62.5 hours for the fuel to reach 450°C, and even longer before the tank reaches 450°C.

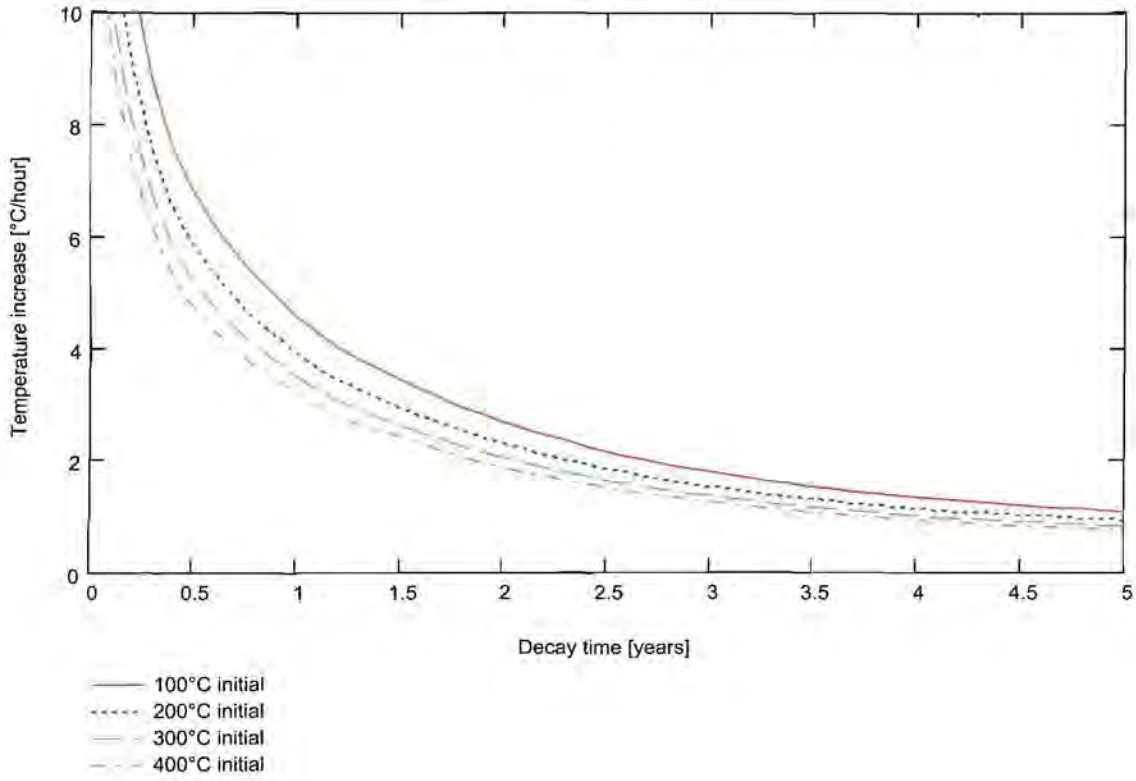

Figure 65: Rate of temperature increase of spent fuel at an initial temperature and decay age.

5. USED FUEL TANK ANALYSIS

5.1 DECAY HEAT LOAD

The Used Fuel Tank (UFT) is utilised to store the contents of the reactor core for the duration of core maintenance. The decay age of each sphere is the time since the core has been shut down. In other words, all spheres inside the UFT generate the same average decay heat. This is reflected as a constant heat per unit volume throughout the tank height as opposed to a varying heat load along the height for an SFT.

Because it takes a number of days to unload the reactor, the heat load changes as the tank is being filled. There are two parameters that govern the heat inside the tank for a specific fill level: the time delay before unloading starts, and the time to completely unload the core.

Figure 66 shows the impact of the delay time on the heat density in the tank for a constant unloading time. It can be seen that the heat density increases dramatically at low fill levels as the delay time is decreased. However, at high fill levels, the heat density approaches the same value. The significance of this effect is that the heat density is the dominant factor governing the maximum temperature. This will be illustrated in more detail in paragraph 5.3.

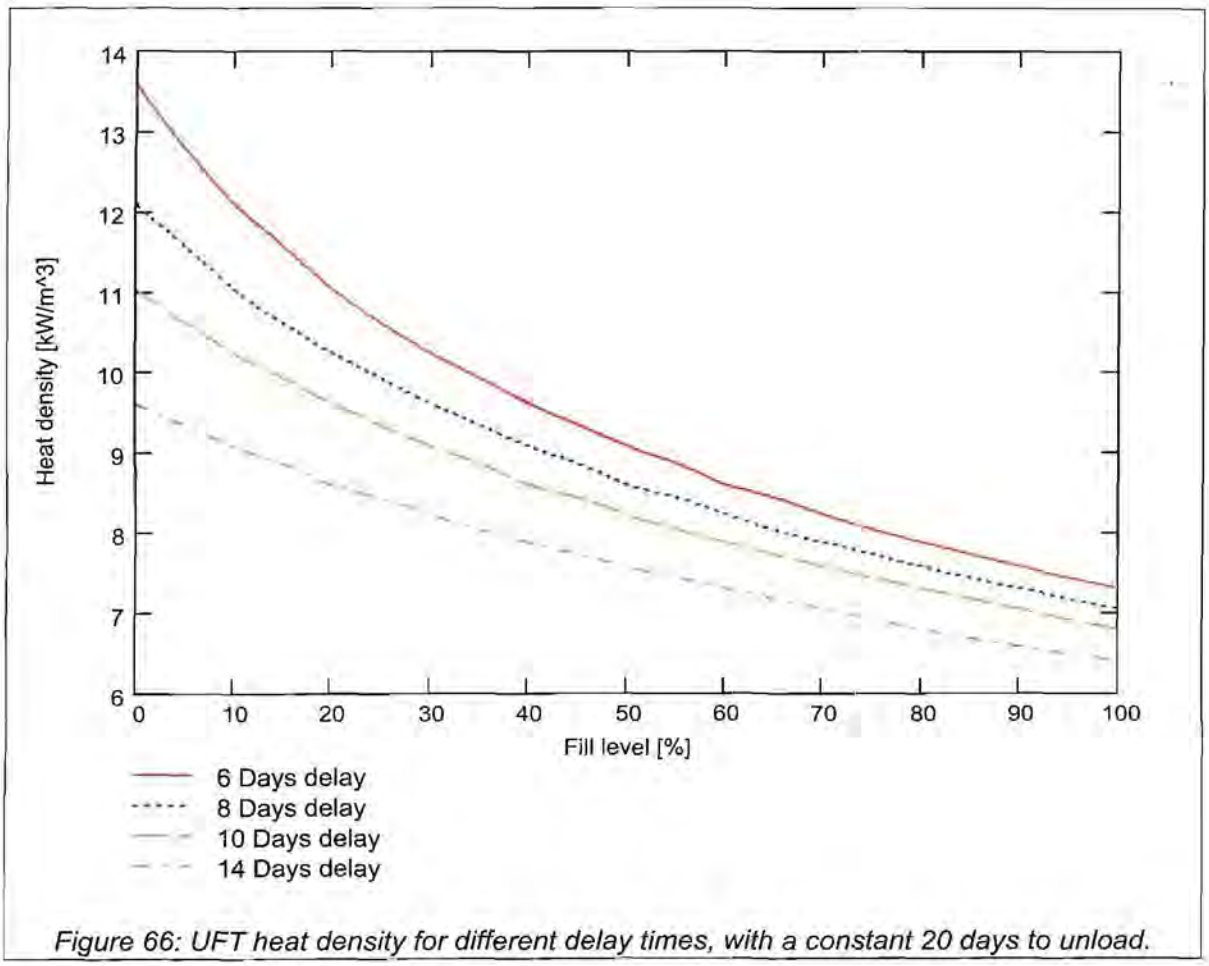

Figure 66: UFT heat density for different delay times, with a constant 20 days to unload.

Figure 67 shows the impact on the total heat load of the tank for different unload times at a constant delay time. It is clear that the longer it takes to unload, the lower is the total heat load. This has an impact on the cooling air maximum temperature and required cooling flow. Appendix F contains the algorithm used to calculate the heat load profiles of the UFT.

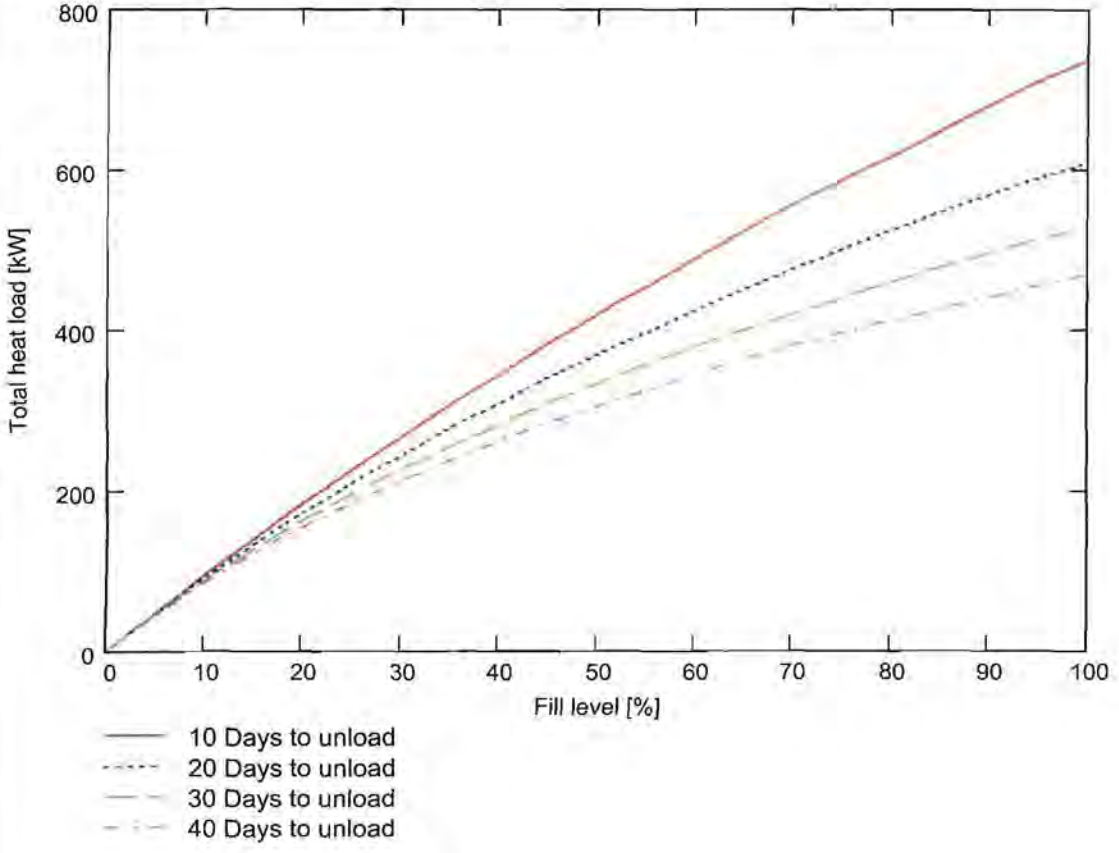

Figure 67: Total heat load for different unloading times, with a constant 10 days delay time.

5.2 TANK GEOMETRY SENSITIVITY ANALYSIS AND STANDARDIZATION

For criticality purposes, the storage tank only needs four outer tubes and one centre tube, all with a diameter of 400mm such as the old SFT geometry. However, the goal was to standardize all the tanks to the same geometric design. With the higher heat load inside a UFT relative to the SFT, it was necessary to increase the number and size of the cooling tubes.

A number of 2D analyses were performed to determine the optimum geometry. The geometries were chosen such that it allows for proper sphere flow, as well as to accommodate the total volume of spheres. The tank diameter was also varied between 2.85 and 3.1m. A constant heat load of 10kW/m^3 was used, as this roughly resembles the heat load of the hottest fill level at a point where only radial heat flux occurs.

From the analyses, it was found that a 2.9m diameter tank with 8 tubes of 400mm diameter spaced at a pitch circle of 1800mm, and a 700mm centre tube is the optimum. This geometry can just hold the number of spheres required.

After a manufacturability exercise, the outer tubes were increased to 406mm (16inches) outer diameter, and the inner tube to 762mm (30inches). These sizes are consistent with standard available tube sections. The increase in tube diameter required an increase in tank diameter. Since the tank diameter is already close to that of the SFT, it was decided to make it also 3.1m.

The last step in the standardization was to add the extra four cooling tubes to the SFT, and increase the centre tube diameter. The result is a storage tank design that can hold 530 000 spheres of any origin, being spent or used fuel. Also the criticality of the stored fuel has dropped to 0.85, which is well below the 0.95 requirement (refer to Chapter 7 for a discussion on the criticality design).

5.3 LOADING RATE SENSITIVITY ANALYSIS

As was indicated in paragraph 5.1, the rate at which the tank is filled plays a major role on the maximum fuel temperature. To determine the optimum filling conditions, a range of thermal analyses were done. The cooling flow was kept constant, while the delay time and time to unload were varied. The maximum temperature results are given in Figure 68 and Figure 69.

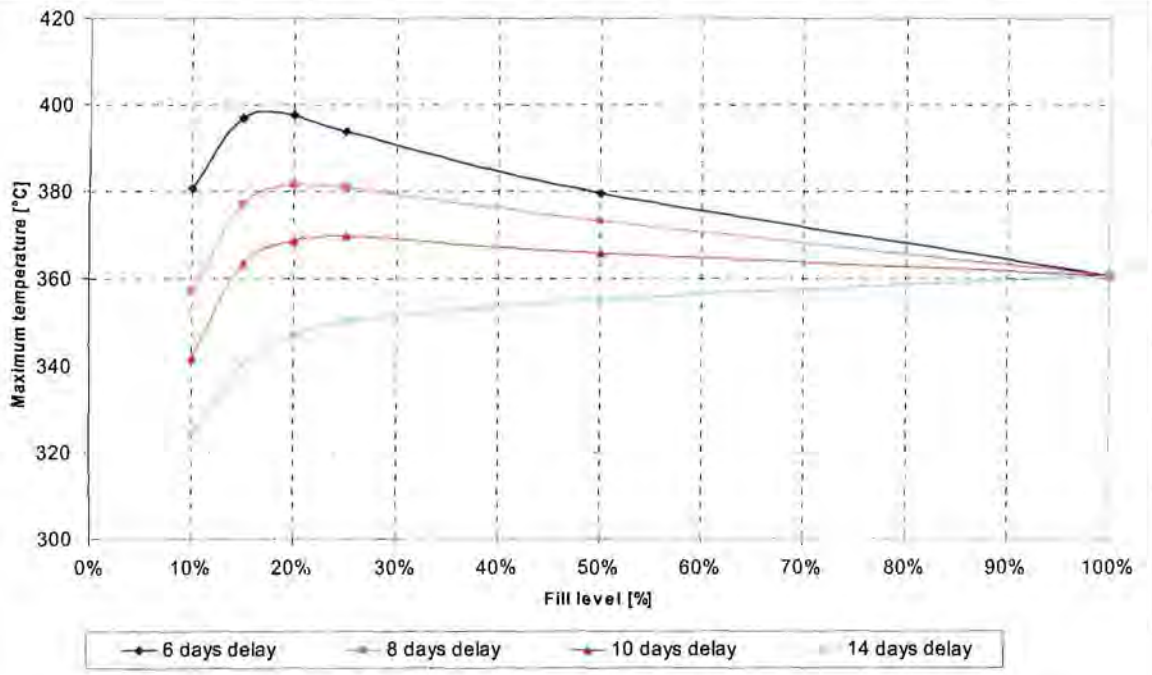

Figure 68: Maximum fuel temperature for different delay times with a constant total time (delay + unload time) of 30 days, 6kg/s cooling flow.

From Figure 68 it can be seen that there is a fill level at which the temperatures are the highest. This point is called the critical point and lies between 15% and 25% fill height. At this point the total heat transfer surfaces are in balance with the total heat to be removed. Below and above the critical point, the heat is less than the capacity of the exposed surfaces. This critical point is more pronounced as the delay time decreases and almost vanishes at long delay times.

The significance of the critical point is two-fold: Firstly, if one knows there exists a critical point, this would be the only fill level to analyse in detail. Secondly, one should aim to keep the variation in temperature as moderate as possible as the tank is being filled. However, there is not unlimited time to wait before unloading starts. The optimum delay time is therefore between 10 to 12 days.

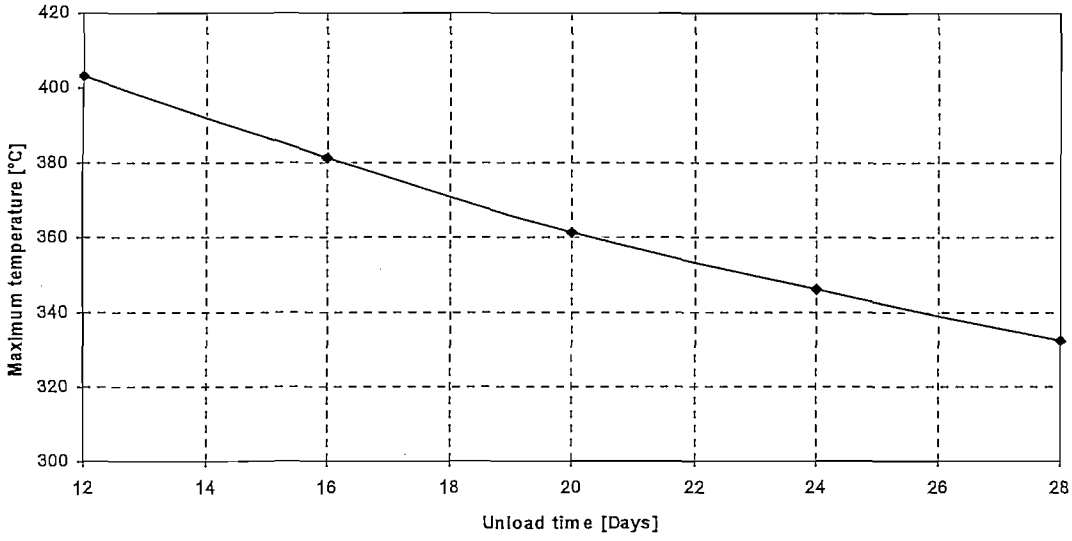

Figure 69: Maximum temperature for different unload times with a delay time of 10 days, 6kg/s cooling flow.

Figure 69 shows an expected result, i.e. the longer the time from reactor shutdown to UFT completely full, the lower the maximum temperature will be. This can also be seen from inspecting the total heat load in Figure 67. Again, there is not unlimited time to unload the core. To keep the maximum temperature below 350°C, an unload time of 24 days is required. However, other factors such as allowable down-time may dominate this value.

For all subsequent thermal calculations, the total time was taken as 30 days, with a delay time of 10 days and 20 days to unload. This is seen as a moderate condition.

5.4 COOLING FLOW SENSITIVITY ANALYSIS

The effect of cooling flow was investigated for different fill levels with the 10 days delay, 20 days unload scenario described above. The results are given in Figure 70. The analyses were done only for the 20% fill level case, as this is the critical point.

From the results it can be seen that a cooling mass flow of 7kg/s or more is necessary in order to keep the temperatures below 350°C. The same trend that was seen for the SFT is seen here, which is that a higher mass flow rate does not relate to an equivalent drop in temperature.

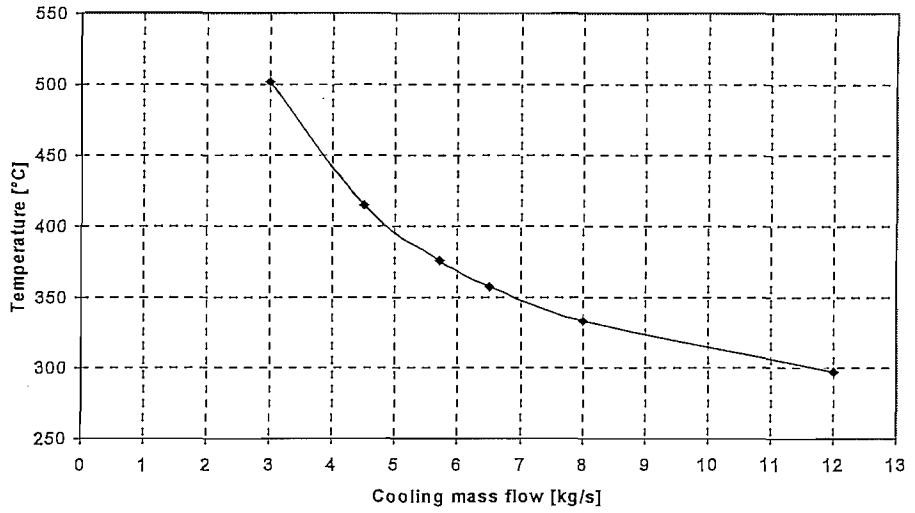

Figure 70: Maximum temperatures for different cooling flows of a 20% filled UFT, inlet 35°C.

5.5 HOT SPOT AND 2D APPROXIMATION

The height of the hottest region in the tank was measured for different fill levels. It can be seen from Figure 71 that the hottest spot is about 2m below the top of the bed surface for fill levels above 40%. The hottest spot also resembles the position where heat predominantly flows in a radial direction. In such a case, the temperature distribution can be calculated by analysing a 2D cross section of the fuel volume at the specific height.

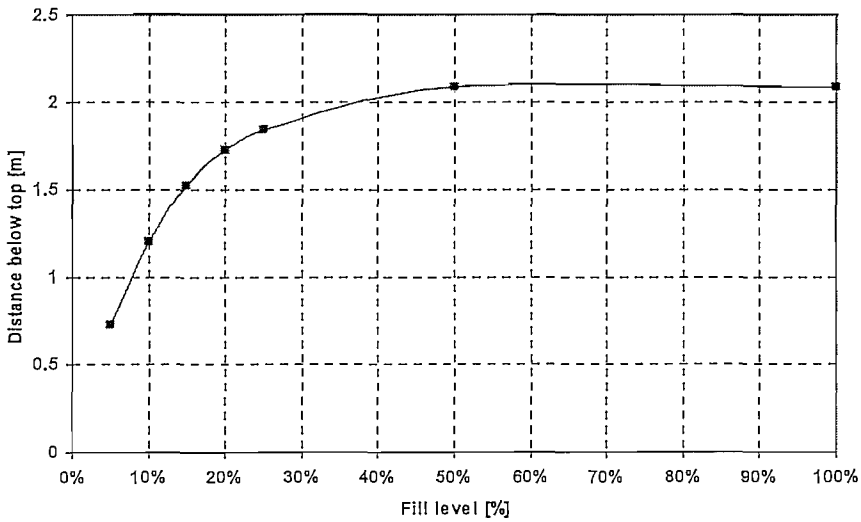

Figure 71: Distance of the hot spot below the bed's upper surface.

In order to verify the validity of the 2D approximation, analyses have been done for the different fill levels at 6kg/s cooling flow. The results are depicted in Figure 72. At fill levels below 25%, the 2D results deviate significantly from the 3D results. This is an indication that the assumption of pure radial heat flux is not valid for these fill levels. Above 25% fill level, the difference is less than 1%.

It can thus be concluded that if the fill level is above 25%, one can use the 2D approximation to obtain maximum fuel temperatures.

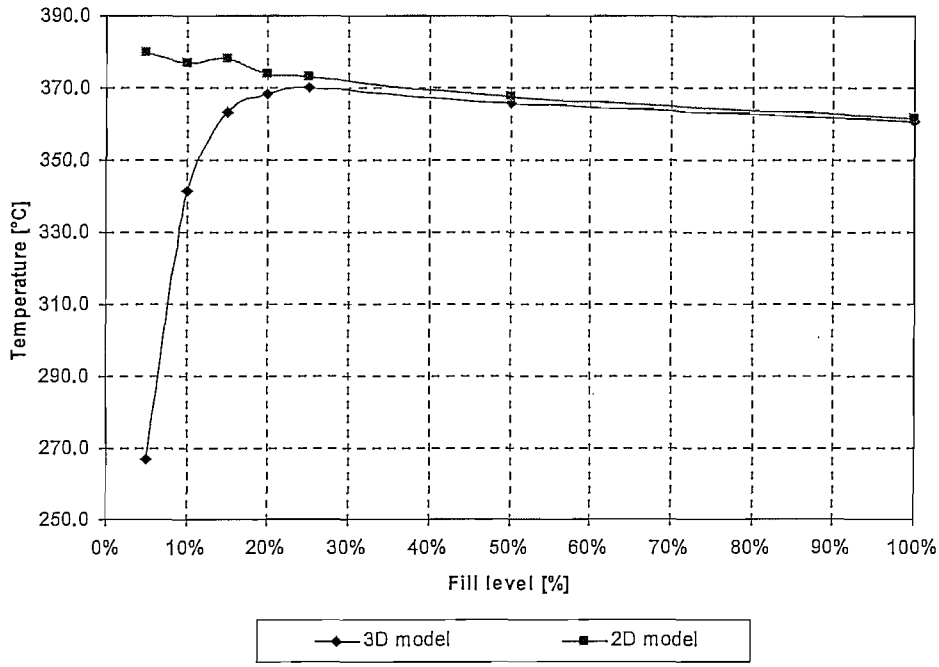

Figure 72: Comparison of 3D model versus 2D model for 6kg/s cooling flow.

5.6 ACTIVE COOLING ANALYSES DURING TANK FILLING

A number of 3D thermal analyses were performed with the final tank design. The design is summarized below.

Table 5: Primary parameters used for the UFT active cooling analyses

Parameter	Value
Tank geometry	As shown in Figure 37.
Tank loading	10 Days wait and 20 days de-fuel, 500 000 spheres
Cooling	7 kg/s at 35°C inlet temperature

The exact same FEA model of the SFT analyses was used. Figure 73 shows the maximum fuel temperature for the different fill levels, while Figure 74 and Figure 75 show the corresponding 3D temperature distribution.

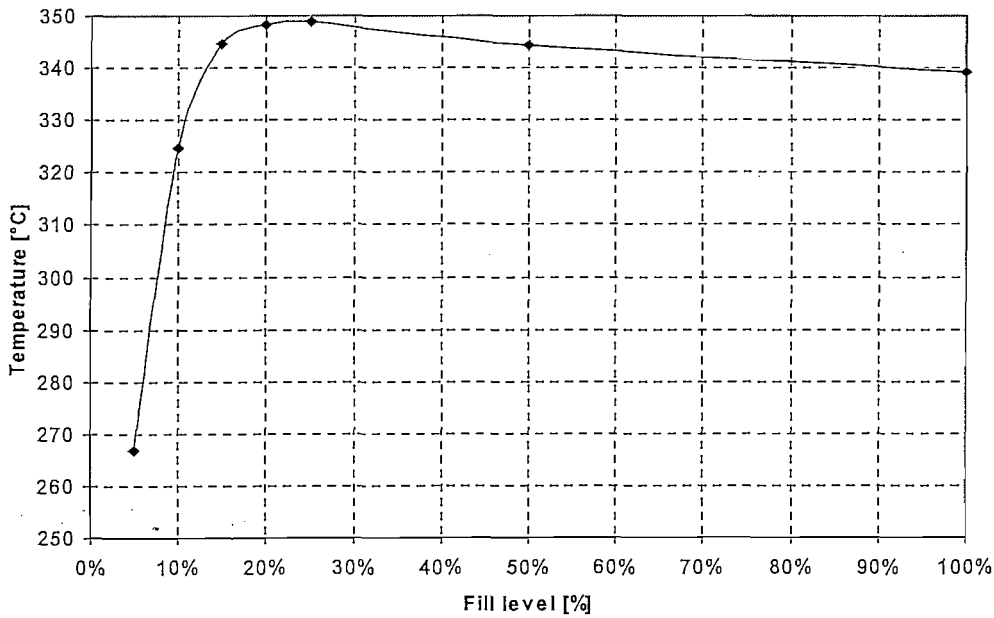

Figure 73: Maximum fuel temperatures of the final UFT design and cooling flow.

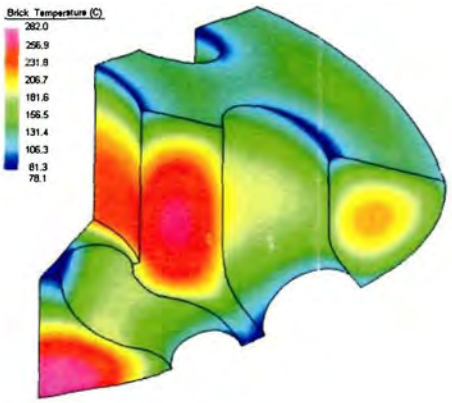

5% fill

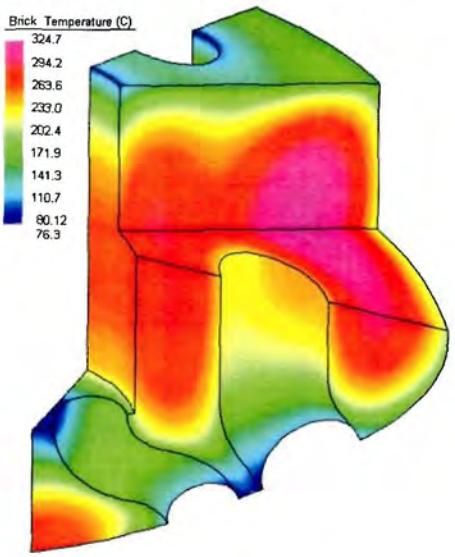

10% fill

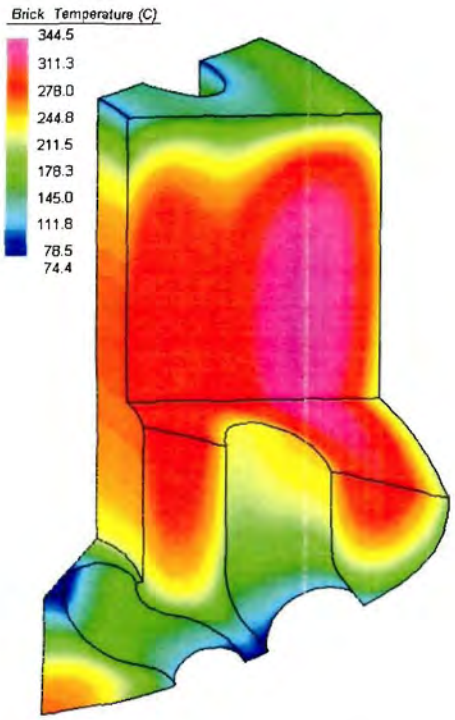

15% fill

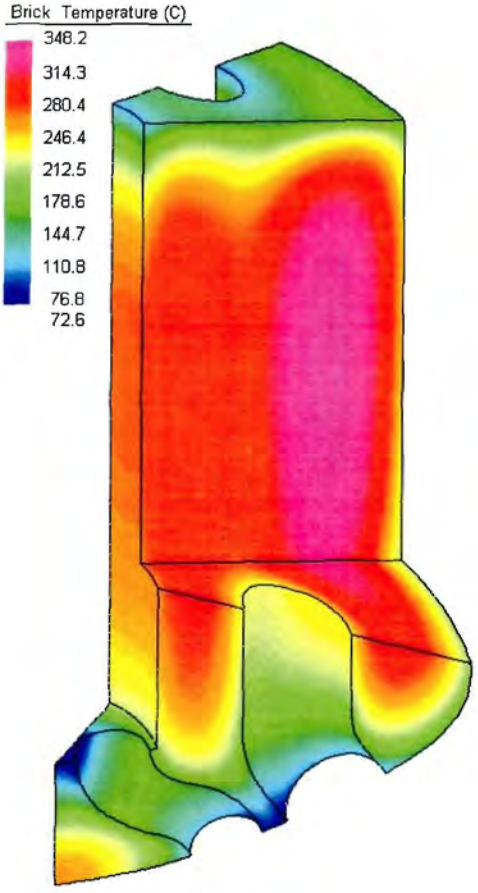

20% fill

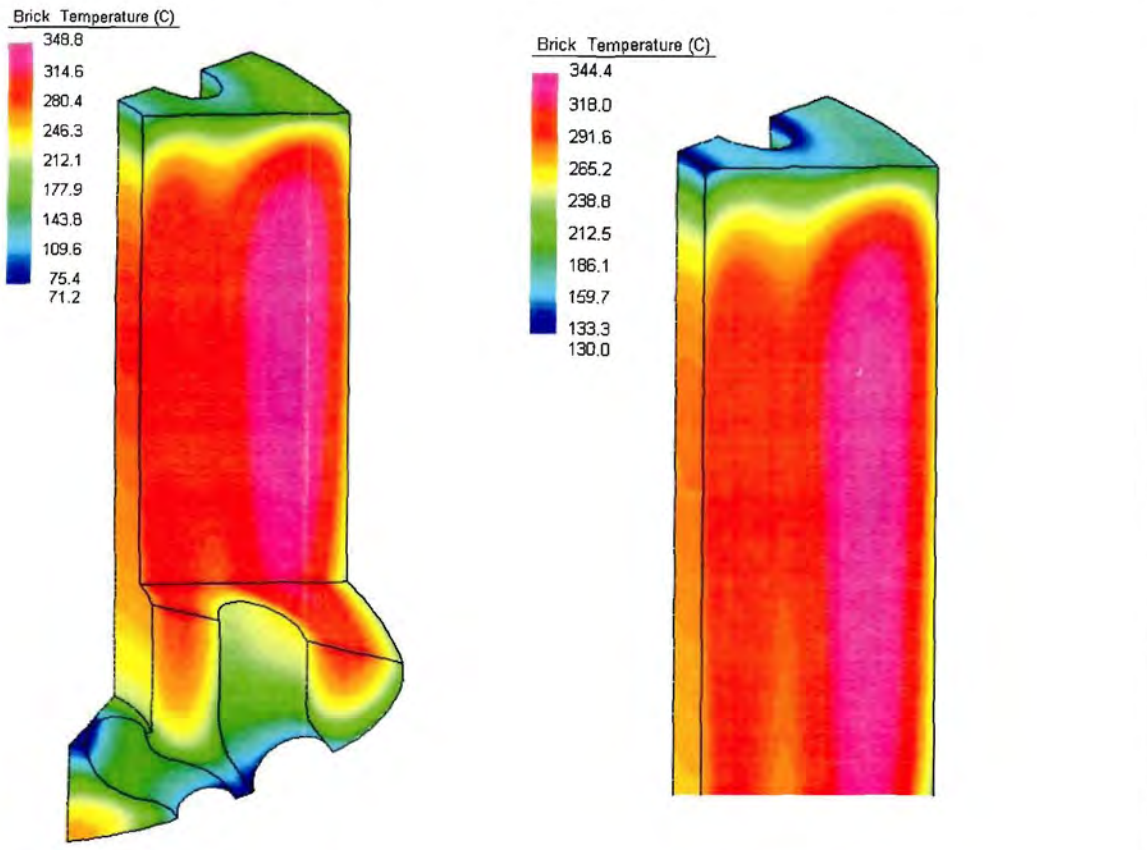

Figure 74: UFT temperature distribution for different fill levels, 6kg/s cooling flow.

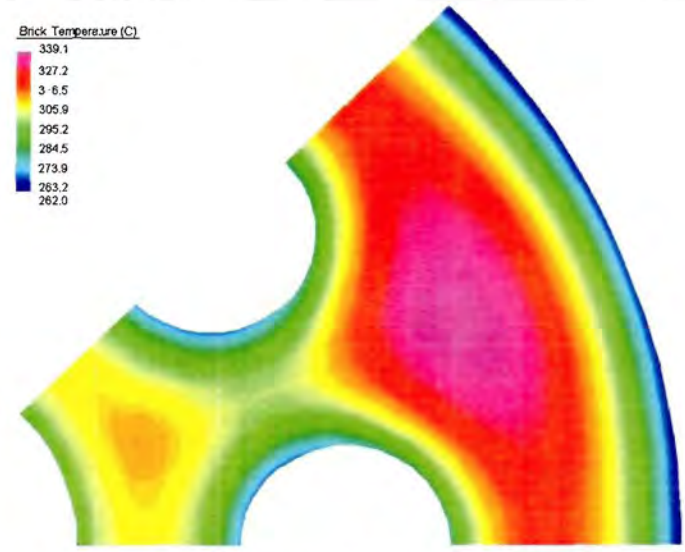

Figure 75: Cross section through hottest region, 100% fill level.

5.7 TANK COOL DOWN TEMPERATURES

Once the UFT is filled, the spheres will stay inside the tank until maintenance on the core has been completed. This maintenance can take two months or more. The moment maintenance is complete, the core will be re-fuelled from the UFT and the plant will be brought back into operation. The temperature of the fuel once re-refuelling starts should be below 250°C to ensure that it does not exceed the operating temperature of other FHSS components.

Figure 76 illustrates how the maximum fuel temperature decreases with time. A constant cooling flow of 7kg/s was used for the analysis. It can be seen that the UFT can be unloaded in less than two months after being completely filled without exceeding the FHSS temperature limits.

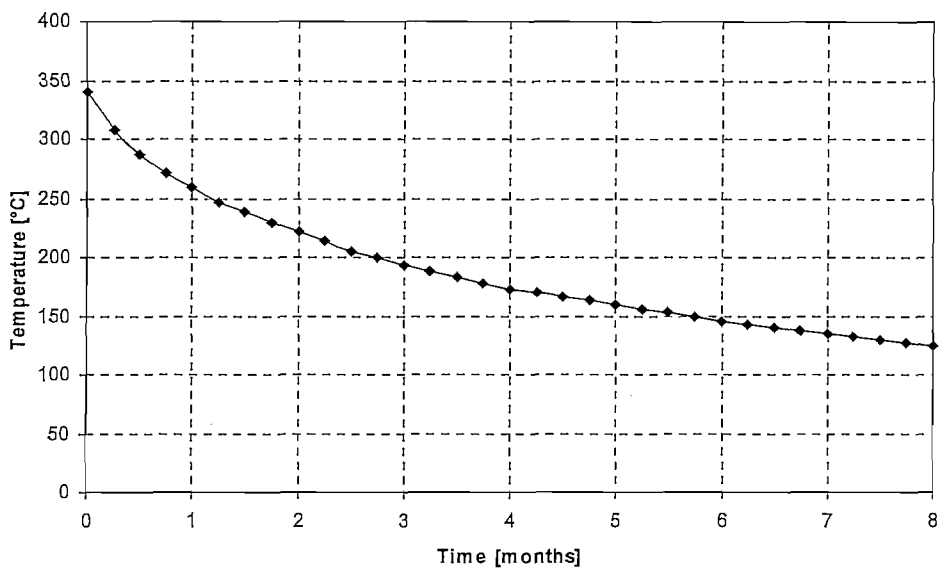

Figure 76: Maximum fuel temperature versus the time after the tank is filled.

5.8 TRANSIENT ANALYSIS DURING LOSS OF COOLING

The transient response of the UFT at the critical fill level of 20% has been analysed during a loss of cooling event in the same manner as for the SFT. The temperature increase follows the same characteristics as for a SFT, except that the hot spot does not move upwards. The temperature rather spreads evenly over the total volume. This is because of the constant heat density throughout the tank.

In Figure 77 it can be seen that the temperature increases at an average rate of 20 °C/hour. This corresponds well with the theoretical rate shown in Figure 78. After 6.2 hours, the temperature of the tank reaches 450°C, which is twice as fast as for the SFT case. The transient temperatures follow a linear increase after 4 hours. This is an indication that not much heat is conducted through the volume. The temperature distribution for a number of time steps is given in Figure 79.

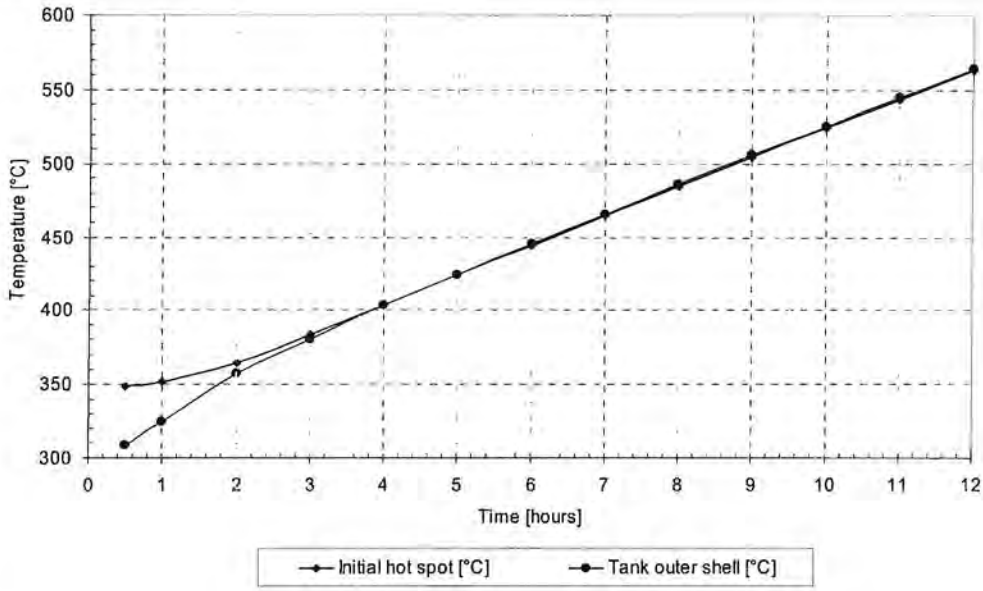

Figure 77: 20% UFT transient temperatures during a LOC, initial cooling flow of 7 kg/s.

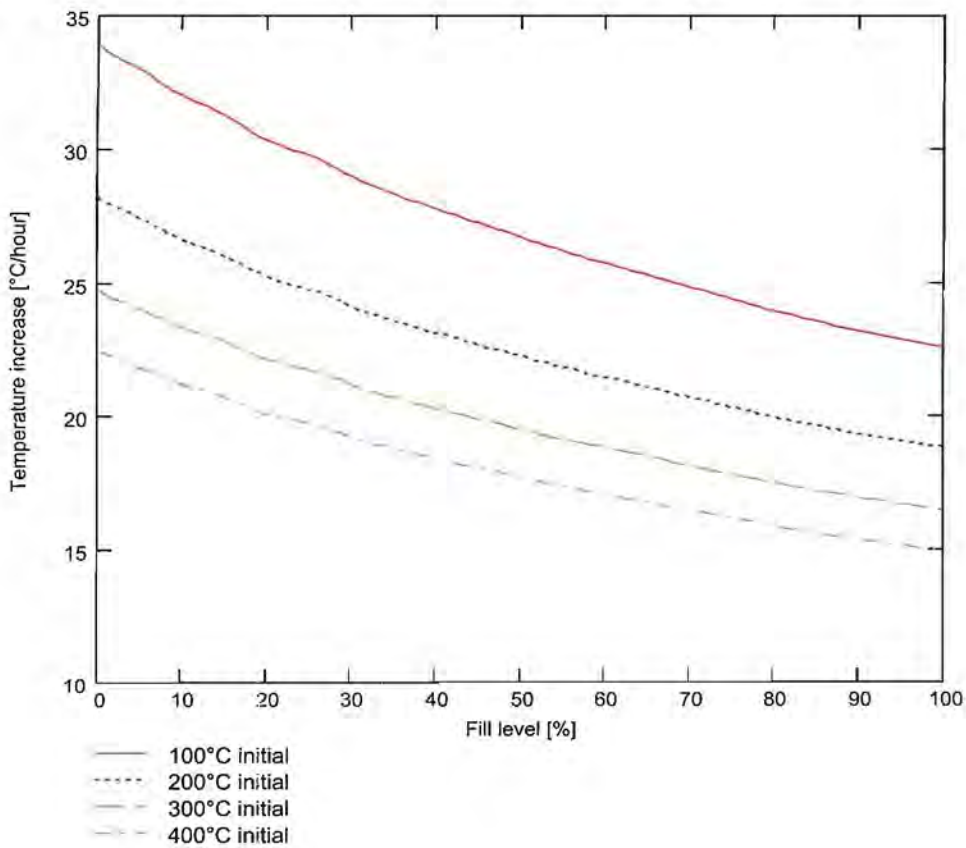

Figure 78: Theoretical rate of temperature increase versus fill level for different initial temperatures based upon 10 days delay, 20 days unload scenario.

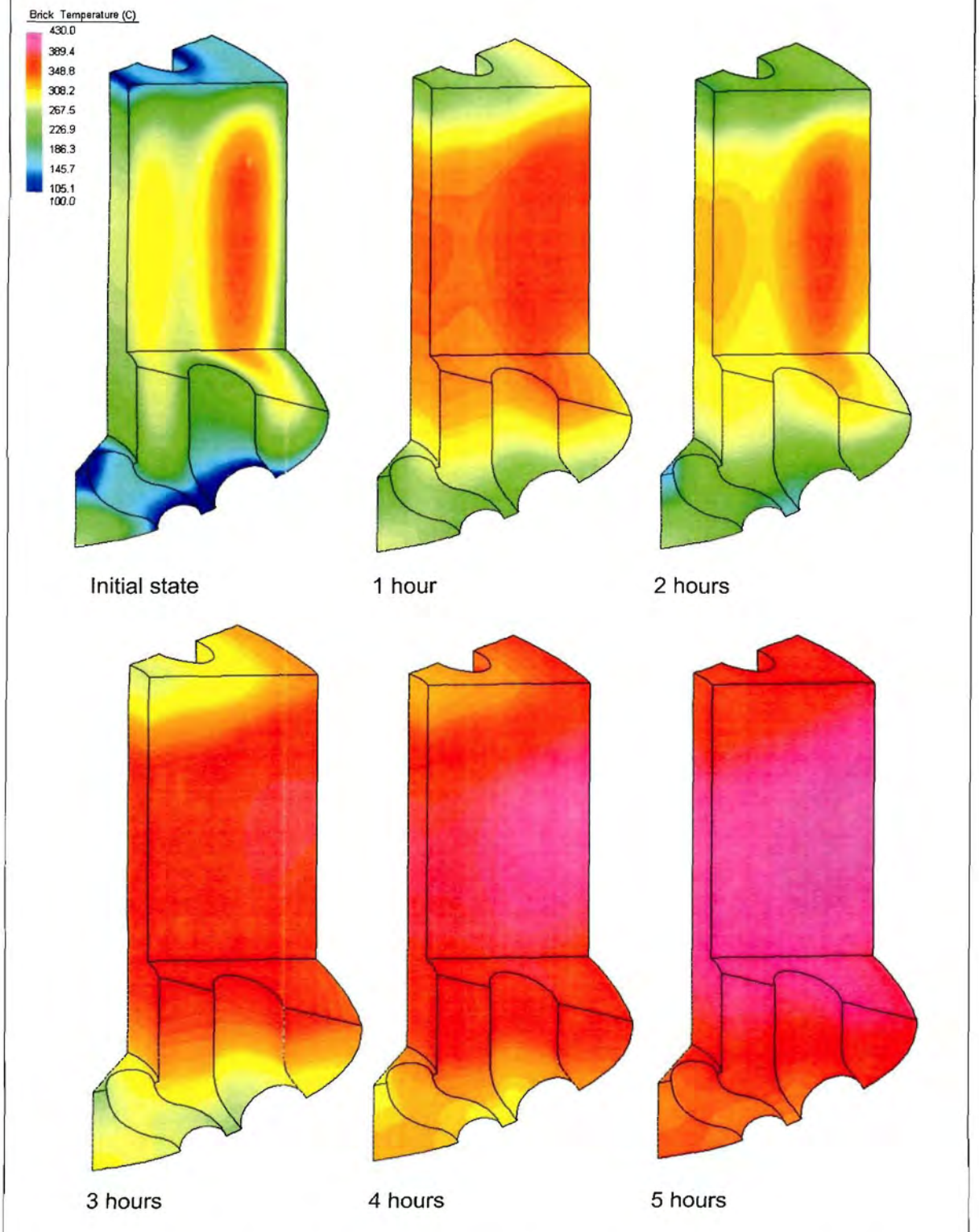

Figure 79: 20% filled UFT temperature distribution during a LOC event, 6kg/s initial cooling flow.

Transient analyses were also performed for the full range of fill levels. The time it took the tank to reach 450°C was determined for each case. This gives the minimum retention time at a certain fill level. The results are presented in Figure 80. It is clear from the figure that the 20% fill level case is indeed the most critical point, as it has the lowest retention time. The heat density is quite high, but the mass of fuel to absorb the heat is small. Also, the 20% fill level is the hottest scenario during active cooling.

Figure 81 shows the transient of a 20% filled tank when the cooling suddenly drops from 7kg/s to 3.5kg/s. This resembles a case where one of the two cooling units fails (see Chapter 10 for a description of the cooling units). During such a transient, the fuel reaches a temperature of 470°C after 48 hours, but the tank is still below 450°C. It can therefore be said that there is no immediate danger if such an event occurs.

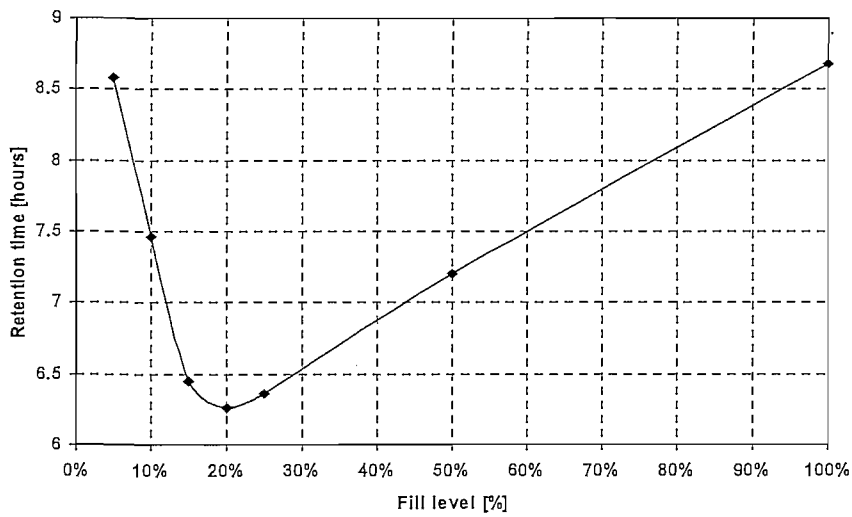

Figure 80: Retention time of the UFT for different fill levels.

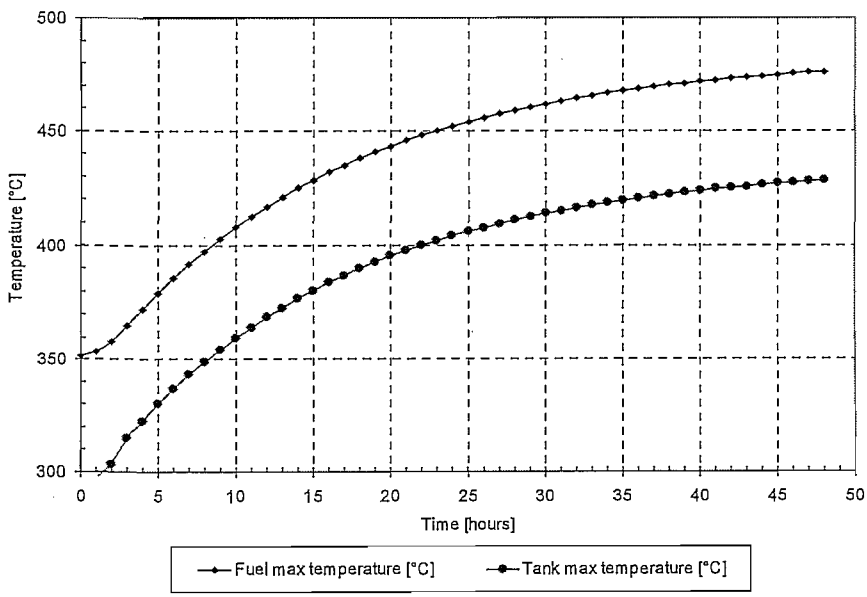

Figure 81: Thermal transient of a 20% filled UFT during a sudden change from 7kg/s to 3.5 kg/s cooling flow

6. TANK CONVECTION CHARACTERISATION

All the CFD analyses and especially the FEA technique rely on the assumption that the convection coefficients are correctly calculated. As was concluded in Appendix B, the flow regime inside the tubes is quite complex, and not much is known about the actual local heat transfer. For this reason, a full scale test is planned to measure the local heat transfer for actual expected heat scenarios. This will add a great deal to the confidence of the CFD analyses. Also, new characteristic curves can be defined for use in the FEA technique.

This section describes the details of such a planned test. The test setup has not been built yet at the time of the compilation of this thesis.

6.1 PURPOSE

The main purpose of this test is to accurately measure the heat transfer characteristics of the storage tanks. A further purpose of the tests is to investigate the effect of minor changes to the entrance and exit geometry of the cooling tubes in order to improve the flow characteristics. The test setup may also be used in future to quantify the effect of heat transfer augmentation devices inside the tubes.

The results of the test will be used as qualification for the thermal characteristics of the tank, hence the level of quality control and reliability of the results shall be very high.

6.2 GENERAL DESCRIPTION OF THE TEST

The tank convection test shall consist of three separate test setups. Each setup shall represent a specific heat transfer geometry of the tank. The test setups shall be of the exact geometry and heat input representations of the tank. The test setups shall all have heater element segments along the height, each capable of supplying a variable heat input. Accurate measurements of the flow and temperature are required at several radial and axial positions of each test setup.

The geometry of the three test setups should be taken from the detail drawings of the tank. Approximations to the geometry may be made provided that the flow characteristics are not influenced. The relative height of the inlets to the ground should also be correct.

It should be possible to induce a specific mass flow in the test section. A fan should be located at the outlet of the test so as not to influence the flow development at the entrance. It should be removed when passive flow measurements are done.

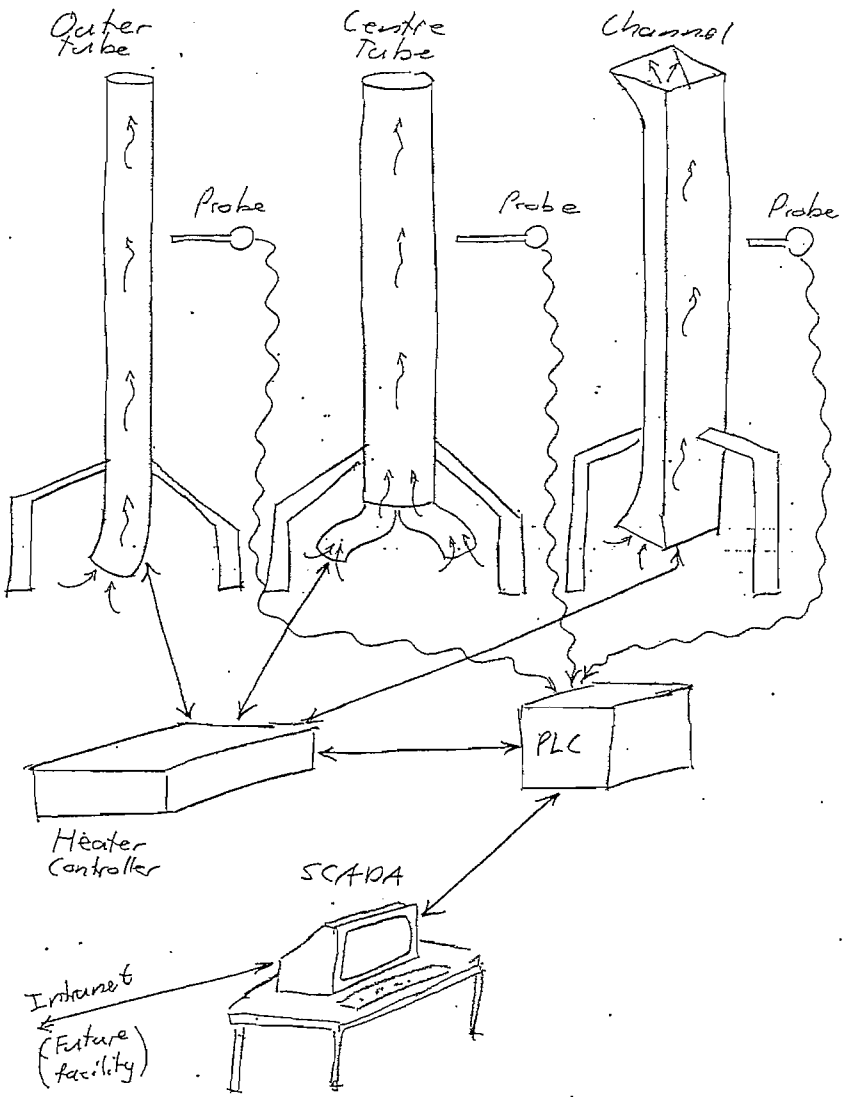

Figure 82: Schematic drawing of the test facility.

6.2.1 Fixed parameters

The following parameters shall be fixed for the individual test setups:

Geometry: The exact dimensions of the cooling pipes and thermal shield channel shall be used as defined in tank detail drawings. This includes the length, inlet and outlet section. The inlets and outlets are penetrations through a semi-ellipsoidal dish end. These penetrations can be approximated by conical sections with an outer diameter of at least two diameters of the test section.

Inlet height: The inlet of the test sections shall be correct relative to the floor as if it was part of the tank, given that the bottom of the tank is 1m above the ground.

Fluid: The working fluid shall be ambient atmospheric air.

6.2.2 Variable parameters

The following parameters shall be variable per test section for different test runs:

Heat flux profile: The heat flux profile along the test setups shall be variable to any profile required within the range that can be expected for the actual case. This is one of the primary variables to change for different test runs.

Total mass flow: The total air mass flow through the test section per run should be controllable when required. For passive flow tests, the mass flow will be a measured output.

6.2.3 Insignificant parameters

Atmospheric conditions: The atmospheric conditions shall be within the range as expected for the tanks. It is not required that any control be implemented to keep the conditions within the limits, rather, no tests should be done during adverse weather conditions.

Thermal expansion: It is not the intention of this test to verify the structural properties of the tank. Hence, the effect of thermal expansion and the related structural stresses are not important, however, the geometry of the expanded test section should not deviate significantly from the initial geometry. This can be ensured by making the tests from materials with nominally the same expansion coefficient as that of the tank design.

6.3 DETAIL TEST SPECIFICATIONS

6.3.1 Flow Measurement

It is required that the velocity and temperature distribution be accurately measured along the full length of each test section. The exact position and number of measurement increments should be chosen such that a representative distribution can be obtained. It should be noted that the flow inside the tubes is highly mixed turbulent convection, i.e. there is not the traditional parabolic flow profile. Rather, the highest velocities are found in close proximity to the heated wall (see Figure 83).

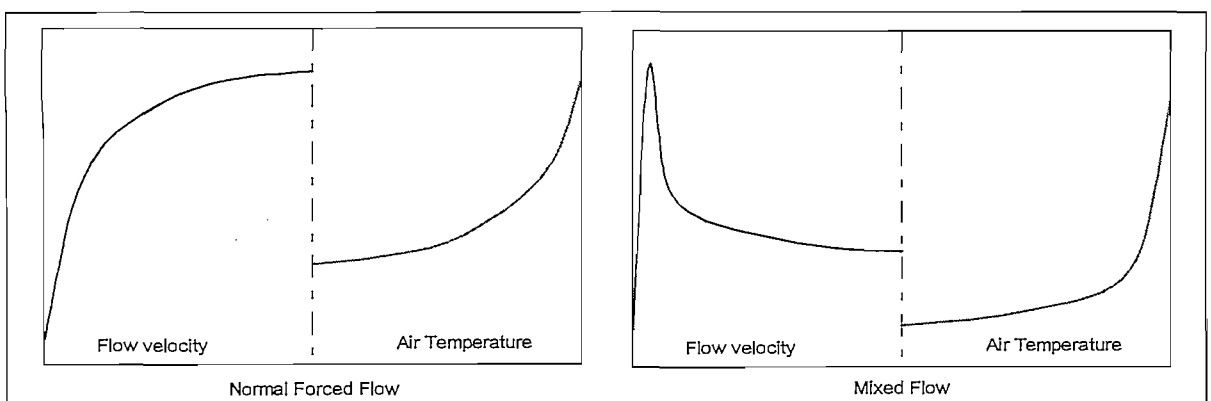

Figure 83: Difference between normal forced flow and mixed flow.

The velocity inside the tubes are predominantly vertical (axial), with insignificant radial flow. However, the velocity is not axi-symmetric, especially the centre tube with its complex flow at the bottom. Flow measurements should therefore not be done in only one plane, but in two or more planes in order to accurately measure the flow.

It is proposed that the temperature and flow velocities be measured by a specially developed measurement rake. This is to reduce the number of instrumentation required for the test, but still have an accurate control over the position of the measurements.

The rake may be in the form of a thin tube (so that it does not influence the flow significantly), fitted with sensors along its length (see Figure 84). This tube can be inserted via an access hole through the heater element into the flow region. The positions of the sensors should be such that they measure the wall temperature, local boundary conditions and a number of positions in the bulk flow. Three such rakes will be required, one for each test setup. The maximum flow velocity expected is 4m/s and the temperature is 250°C.

6.3.2 Centre tube test setup

The centre tube branches into four smaller tubes at the bottom. These branches should also be included in the setup. The complete setup, along with the bottom branches should be surrounded by heater elements. Measurement points are only required in one of the branches. The number and position needs to be determined by the test designer.

6.3.3 Outer tube test setup

The outer tube has a slight bend at the bottom before it penetrates the bottom dish end. This bend should also be included in the test setup. The setup should also be fitted with heater elements along the full length. Flow measurements are required along the full heated length, including the bottom bend region.

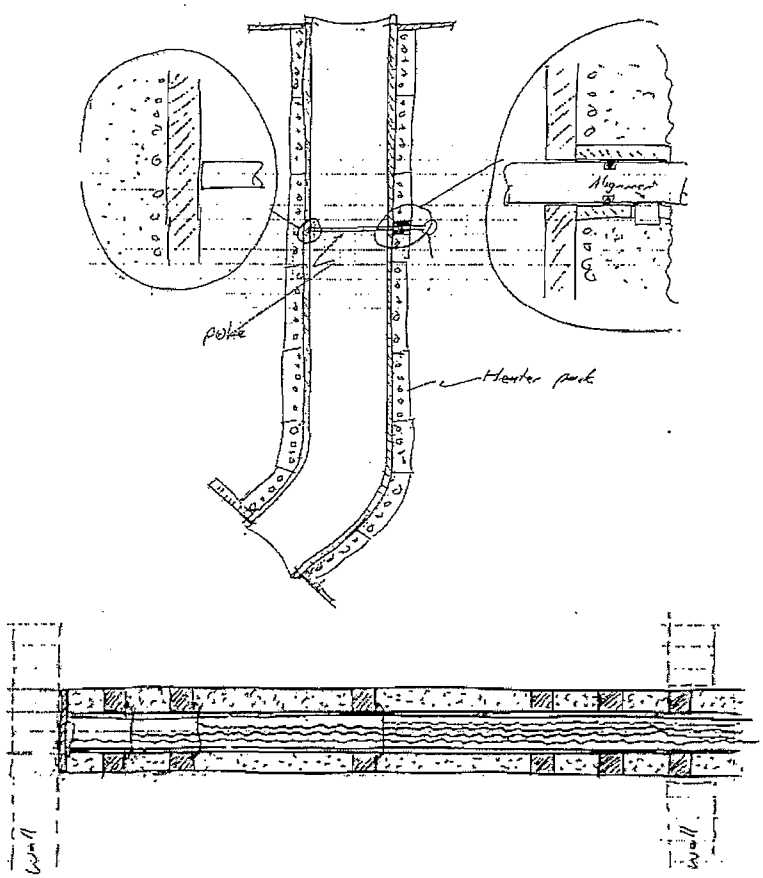

Figure 84: Conceptual illustration of the measurement rake.

6.3.4 Thermal shield test setup

This test setup is somewhat more complex, as it should represent the gap between the thermal shield and the tank. The test setup should represent a single flow duct of equivalent dimensions and the full height of the tank. The inlet and outlet has to follow the geometry of the tank dish ends. The test can be made rectangular although the actual geometry would be concave.

Heat input is only from the side of the tank surface. The sides where the braces are should be properly insulated so that thermal symmetry is achieved. The thermal shield itself should be made from the materials as indicated on the detail drawings and no additional insulation is required. This specific test should not be exposed to direct sunlight that could introduce an additional heat input from the shield side.

Flow and temperature measurements are required along the full length of the test.

6.3.5 Heater specification

Each test setup shall be fitted with a number of individual heater segments. These heater segments should supply a constant heat flux through the contact area with the test itself. The heaters should be independently adjustable from each other. Proper insulation material is required between the heaters to minimise axial conduction, and at the outside to minimise heat loss. A maximum of 3000W/m^2 is expected for the test.

6.3.6 Forced flow specification

A removable fan should be located at the outlet of each test setup. This fan should be able to force airflow at a certain rate through the setup. Due to the chimney effect, it may not be possible to reduce the flow to a certain amount with the fan alone. A set of flow baffles should be used to choke the flow then. The fan and baffles shall be removable when passive cooling tests are required. A maximum mass flow of 1.0kg/s is expected for the test.

6.3.7 Control and instrumentation

A PLC shall be used to control the tests and perform the data acquisition. A SCADA system shall be used for the interface between the test operator and the PLC. The software shall have a highly user-friendly interface with sufficient status output of the running test and control over the test conditions.

6.4 FUTURE MODIFICATIONS

Attempts may be made in the future to improve the flow and thermal characteristics of the tubes. This includes special inlet and outlet geometries, internal fins or vortex generators. The test setups of the centre and outer tube should therefore make provision for such modifications.

6.5 TEST PROCEDURE

The tests should be performed in dry stagnant air conditions. Sufficient provisions should be made so that the exhaust flow does not re-circulate and influence the inlet flow. The average atmospheric pressure, inlet temperature and relative humidity should be recorded for the duration of the test. These values should not change significantly during the duration of measurements.

A range of test conditions will be specified for each test setup. The conditions will generally be a certain heat load scenario and mass flow. All results should be reported for the steady state condition. This implies that sufficient time should be provided for all the temperatures to stabilise before any reading is taken.

7. CONCLUSIONS

7.1 THE FEA ANALYSIS METHOD

The use of non-linear FEA software in calculating the internal temperatures of a storage tank fuel volume is applicable and accurate. It enables fast analyses of different scenarios without the use of slower CFD techniques.

The most important factor in achieving acceptable results lies in the correct and accurate definition of the external heat loss conditions. The storage tanks can be defined in terms of known physical thermal processes (such as the pipe convection) that allow one to apply empirical and analytical correlations in order to calculate the external conditions. At some places, an equivalent condition needs to be derived (as for the upper convection) in order to capture some characteristics, which cannot be defined directly using FEA. Also, in some cases one needs to make an educated guess as to what the external conditions are. The guess can be "calibrated" using CFD results, however, the "calibration" should not play a major role in the overall heat transfer properties.

Because the only direct correlation between CFD and FEA is the way in which the heat conduction is calculated inside the pebble bed, the FEA can be seen as an independent technique. This boosts the confidence of the calculated performance of the tanks if the results obtained with the two techniques are in good agreement. The FEA technique can therefore be used to do semi-independent verification of CFD results. A fully independent verification is not possible since the technique requires some CFD results for calibration.

7.2 THE SPENT FUEL TANKS

It was found that a cooling flow of 1.7kg/s is sufficient to keep the SFT temperatures below limits at all circumstances, although 3kg/s of cooling flow was chosen due to passive cooling considerations. The hottest fuel region is approximately 1m below the pebble bed surface. The hottest steel area is at the centre tube, at a level of the hottest fuel temperatures. The hot spot moves gradually upward as the tank is filled, leaving the rest of the tank substantially cooler.

Once the tank has been filled, it takes about 3 years for the temperatures to fall below 100°C, with an eventual temperature of less than 50°C at the time of decommissioning.

It will take 15 hours or more before the steel temperature limit of 450°C is exceeded in the event of a loss of cooling. This retention time increases significantly as the duration of storage increases. The passive fallback cooling is therefore only necessary for the time the tank is filled, and probably 2-5 years thereafter.

7.3 THE USED FUEL TANK

The rate at which the UFT is loaded has a significant effect on the tank temperatures. In principle, the longer the delay before unloading to the UFT, and the longer the time to unload, the lower will the maximum temperatures be. However, for practical reasons the time is not unlimited. An optimum condition of 10 days wait and 20 days unload has been defined.

The geometry study made it possible to standardize to one tank geometry for the UFT and SFT. It also resulted in a more sub-critical design for the storage tanks.

For fill levels above 25% it is feasible to analyse only a 2D cross section of the hottest region. This has a significant impact on solution time and effort required to define the model, and allows for numerous sensitivity analyses to be done.

A cooling mass flow of 7kg/s is required to keep the fuel temperatures below 350°C. The thermal critical point for the UFT is around 20% fill level. At this point the heat density is very high, but there is not a lot of exposed surfaces to transfer the heat to the air. Also, this low fill level has significantly less total heat, which is needed to drive natural convection during passive cooling.

The tank temperature rises to 450°C after only 6 hours after a total loss of cooling. For this reason, special care should be taken in designing the passive fallback loop in order to achieve mass flows in the order of 7kg/s.

Due to the dramatic drop in decay heat over time, the fuel is below 250°C after 1.5 months of storage in the UFT. The used fuel can then be re-introduce into the core without the risk of exceeding the FHSS temperature limits.

Chapter 10: Integrated Storage Unit Design

1. INTRODUCTION

The previous chapter presented the thermal design and analyses of the storage tank alone. The result was fuel temperatures versus cooling mass flows. This chapter will address the issues of how to supply the required cooling flow to the tanks. It also incorporates the conclusions made for the corrosion design. The result is an integrated design presenting the total solution for the nuclear requirement of storage.

The concept of a storage unit, which is the combination all the functional components needed to perform the storage function, is introduced. This includes the storage tank, cooling units, ducting, shields etc. Three storage units are defined; namely a Spent Fuel Storage Unit (SFSU), a Used Fuel Storage Unit (UFSU) and a Graphite Storage Unit (GRSU). The name is derived from the type of tank inside the storage unit. However, as was mentioned in Chapter 5 for the storage tanks, the differentiation between a SFSU, UFSU and GRSU is merely for historic and process definition purposes. The physical design and functionality of all three storage units are the same, although they may be operated differently due to variations of the heat load in the tank.

2. STORAGE UNIT COOLING MODES

Each storage unit can operate in four cooling modes as shown in Figure 85. The modes are:

a) Closed Loop Active Cooling;

b) Open Loop Passive Cooling;

c) Open Loop Active Cooling; and

d) Closed Loop Conditioning.

The closed loop active cooling mode is the mode as concluded from the corrosion design study. During this mode the air that cools the tank is trapped in a closed loop and is continuously being conditioned to limit corrosion on the tank. This is the dominant cooling mode and will be used for the full 80-year period. A heat exchanger transfers the heat from the closed loop to an open air loop where the heat is then discharged to atmosphere. It is an active system, as fans are required to drive the two airstreams through the heat exchanger.

If the closed loop active cooling fails for some reason, the storage unit automatically switches over to the open loop passive cooling mode. In this mode all the major flow loss elements such as the heat exchanger and filters are bypassed, allowing external air to directly cool the tank via natural convection and the chimney effect. This mode can be seen as the first line of defence during abnormal conditions. It is therefore not a mode in which the storage unit will be operated for a prolonged period due to the corrosion exposure on the tank. Once repaired, the closed loop active cooling should be restored and the air purified again. However, this mode can be initiated at any time, and could be operated indefinitely if the corrosion rates and radiation effect on organic material in the air are found to be negligible.

When a storage tank is loaded with used fuel, the heat load is significantly higher than for spent fuel. This requires much larger heat exchangers, and higher cooling flows. However,

this operation is foreseen to happen only once during the plant operational life, and that is during the mid-life core refurbishment. The period is also about three months. Instead of over-designing all the storage units' heat exchangers for this singular event, it was decided not to cool a tank containing used fuel with a closed loop, but with an open loop. To reduce the corrosion, a filter is proposed at the inlets, which in turn, requires fans to supply the air. This results in an open loop active cooling mode. The corrosion will be more than for the closed loop mode, but it is felt to be acceptable when comparing 3 months to 80 years of exposure. Again, if the active components fail, the system should automatically fall back to the open loop passive cooling mode.

Because the tanks are loaded one at time, there are tanks that will be empty for almost 35 years before receiving spent fuel. These tanks still need to be protected from corrosion even though there is no heat load in the tank. For this the closed loop conditioning mode is used. Only the air conditioning device is operational, and no heat exchanger is installed.

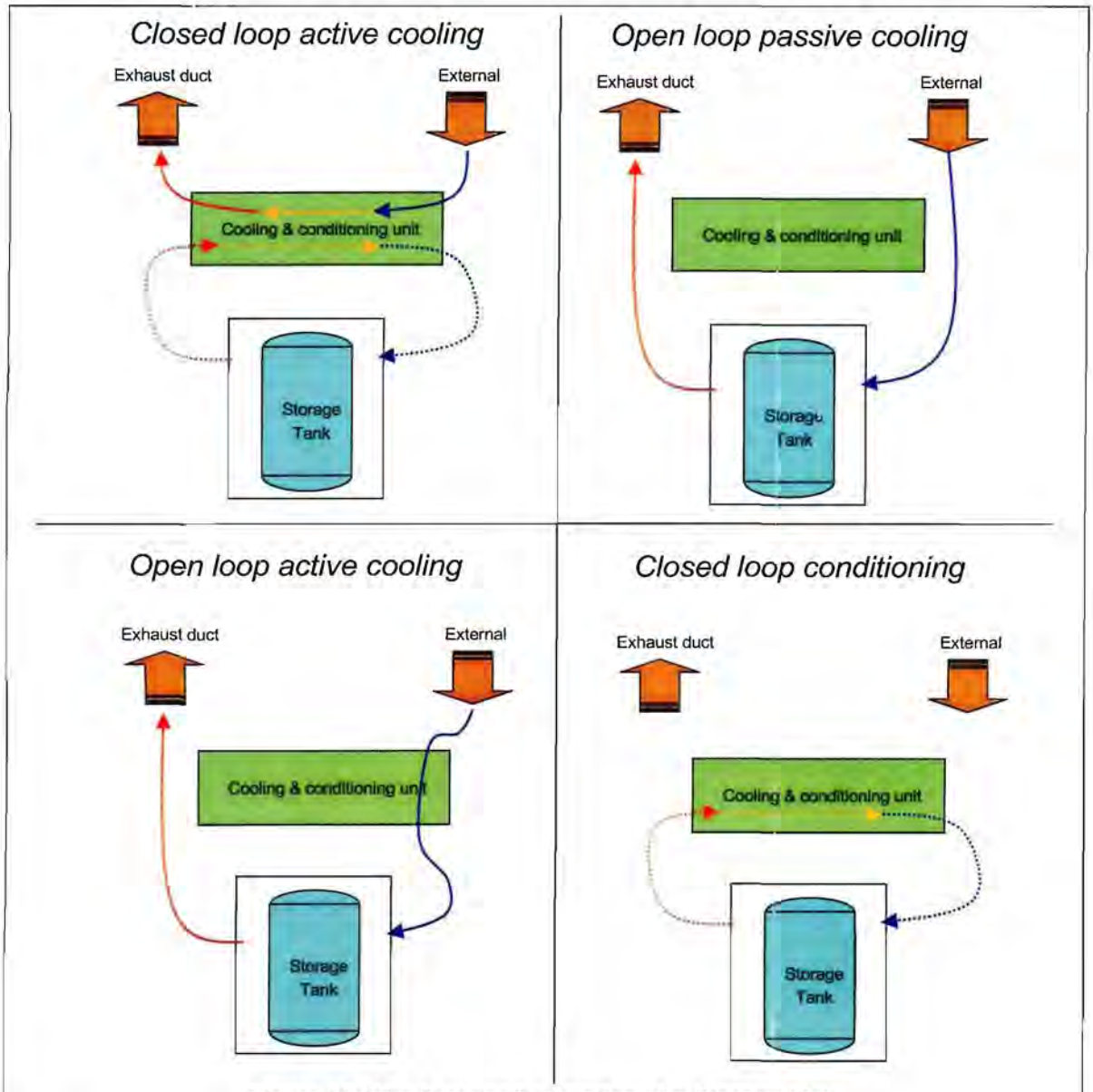

Figure 85: The four cooling modes of a Storage Unit.

3. STORAGE UNIT LAYOUT AND AIRFLOW

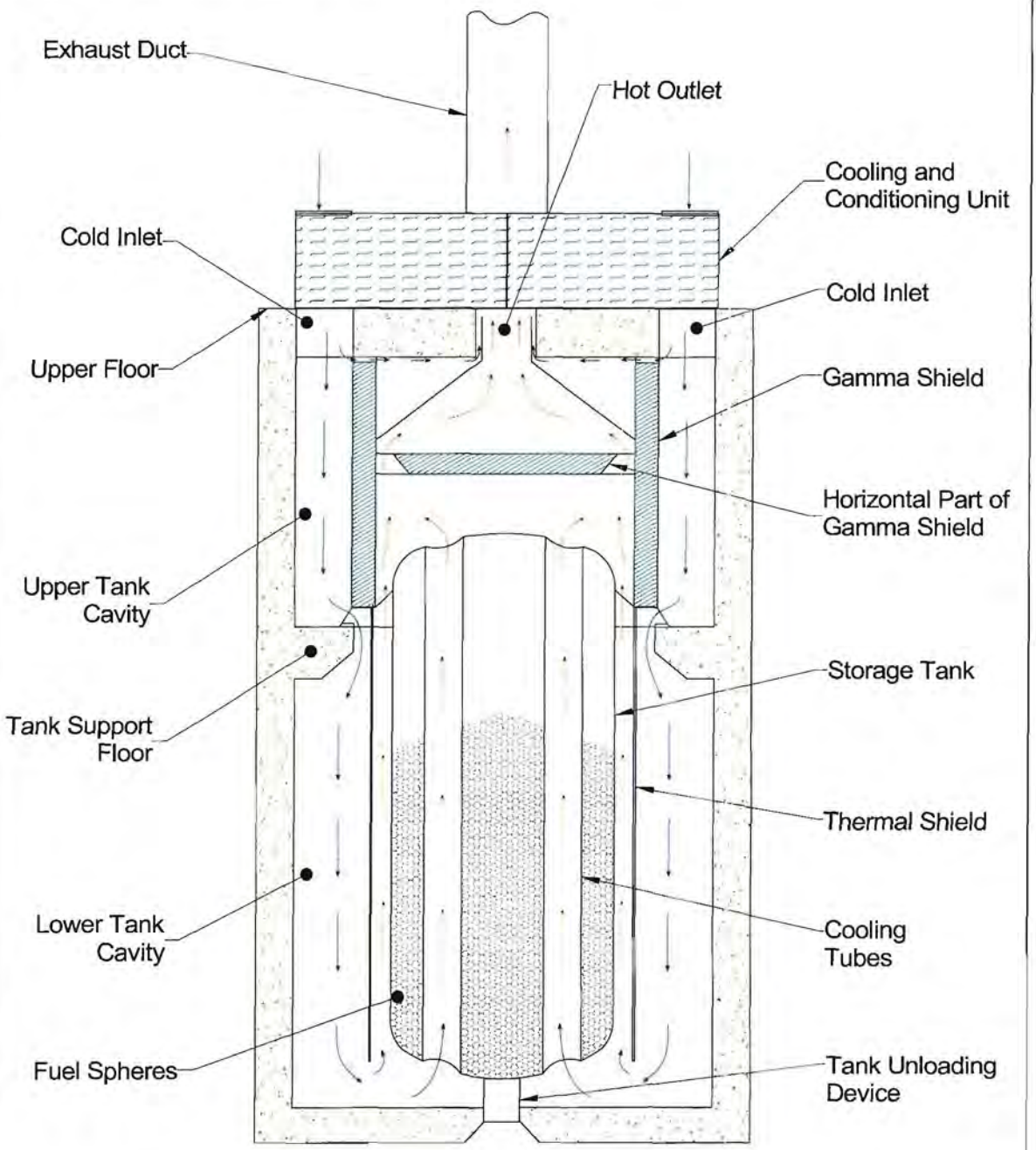

Figure 86: Schematic layout and airflow of a storage unit.

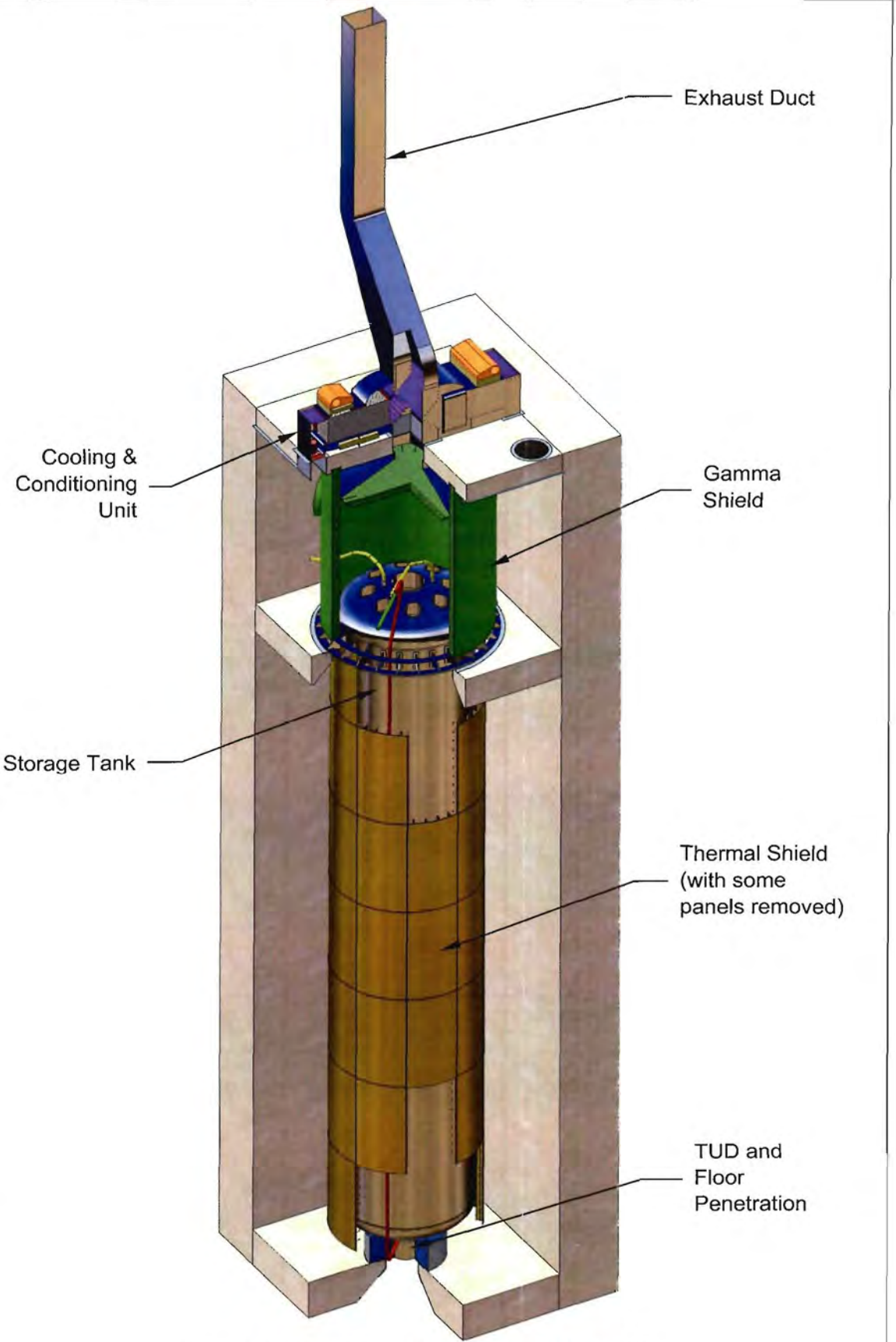

Figure 87: Pictorial view of a single Storage Unit.

A schematic diagram of a generic storage unit is presented in Figure 86. The primary components and their purposes will be described in the following paragraphs.

Storage Tank: The heart of the unit is the storage tank. This can either be an SFT, UFT or GRT. All other components of the storage unit are in support of the tank, either through cooling, structural support, maintenance etc. Refer to Chapter 5 for a detailed description of the storage tank.

Tank cubicle: The storage tank is located in a concrete cubicle. This cubicle is 5mx5m in plan cross section and has outer walls of 500mm. There is a split 19m above the bottom floor, which acts as the support floor for the storage tank. This split creates an upper and lower tank cavity. At the top is the upper floor, which has all the inlet and outlet penetrations for the cooling flow.

Tank Unloading Device: The TUD is used to remove the spheres from the tank when needed. The design is described in detail in Chapter 6. The TUD penetrates the bottom floor to enable maintenance of the device from below.

Thermal Shield: The Thermal Shield consists of 61 removable panels, 9 around the perimeter and 7 rows along the length of the tank. These panels are about the size of a door, and light enough for one person to handle. The panels are fixed all around the tank using special stand-offs.

The purpose of the shield is to provide a well-defined flow path for the cooling air, and it prevents thermal radiation to the concrete surroundings. The panels are a distance of 150mm from the tank, and contain longitudinal guide-vanes. When assembled, the shield creates rectangular flow channels on the outside of the tank.

Because the thermal shield is only needed when the tank contains fuel, it need not be installed on empty tanks. This is advantageous since one has the opportunity to do design upgrades without cost implications, and some of the initial capital cost can be postponed. It also simplifies the inspection of empty tanks.

Another motivation to postpone the shield installation is to ensure a high surface quality when needed. This is because the shield makes use of a low thermal emissivity (bright aluminium surface) to reduce thermal radiation. Corrosion increases the emissivity, and it would thus be difficult to ensure that the shield is in good condition after 35 years. A low emissivity is only required for the first 10 years of a storage tank containing fuel.

Gamma Shield Assembly: This is another crucial component of the storage unit. Its primary function is to provide gamma radiation shielding from the tank. It creates an accessible area around the upper region of the tank for maintenance and inspection. Additionally it separates the inlet from the outlet cooling flow.

The gamma shield consists of a cylindrical part, and a horizontal divider. It is a hollow steel structure, with shielding material inside. The type of shielding material is yet to be determined, but will be a cast-able material such as high-density concrete or small steel spheres. The shield rests on the ring support of the tank, and is laterally supported at the top. The horizontal divider has openings on the perimeter to allow airflow to pass through. Above the divider is flow ducting that channels the flow to the centre outlet opening.

Cooling & Conditioning Unit: The Cooling & Conditioning Unit (CCU) forms the heart of the cooling design of the tank. Each storage unit has two CCUs facing each other. The units are mounted on the top service floor. The CCU is described in detail in section 4.

Exhaust Duct: Each storage unit has a dedicated Exhaust Duct running from the CCUs to the top of the building. The duct channels the hot exhaust air out to the atmosphere and acts as a chimney during passive cooling mode. The final geometry of the duct will be determined after optimisation of the flow losses and pressure recovery at the outlet.

Figure 86 shows the airflow patterns around the tank and inside the cubicle. Cold air enters the cubicle from two positions at the top. The air distributes around the outside of the gamma shield, and then passes through the ring support of the tank. At the bottom of the cubicle the air distributes into the cooling tubes and in the channels formed by the thermal shield around the tank.

The decay heat is absorbed as the air moves up past the tank surface. At the top the air collects and flows around the horizontal part of the gamma shield before it exits at a single central outlet.

A small portion of the cold air leaks in between the gamma shield and the top service floor. This air moves between the gamma flow ducting and the floor in order to insulate the floor from the hot outlet gasses.

The cooling path described above is the same for all storage units, no matter what the heat load or cooling mode. In other words, the storage tank is not aware of the changes of cooling modes apart from a change in mass flow and air temperatures.

This is of particular importance for the passive cooling mode. The best way to achieve proper natural convection flow, is to have the flow "started" in a certain direction. Because there is no change in flow path during the transition from active cooling to passive cooling (from the viewpoint of the tank), all flow paths are well defined when passive cooling needs to take over.

4. COOLING & CONDITIONING UNIT

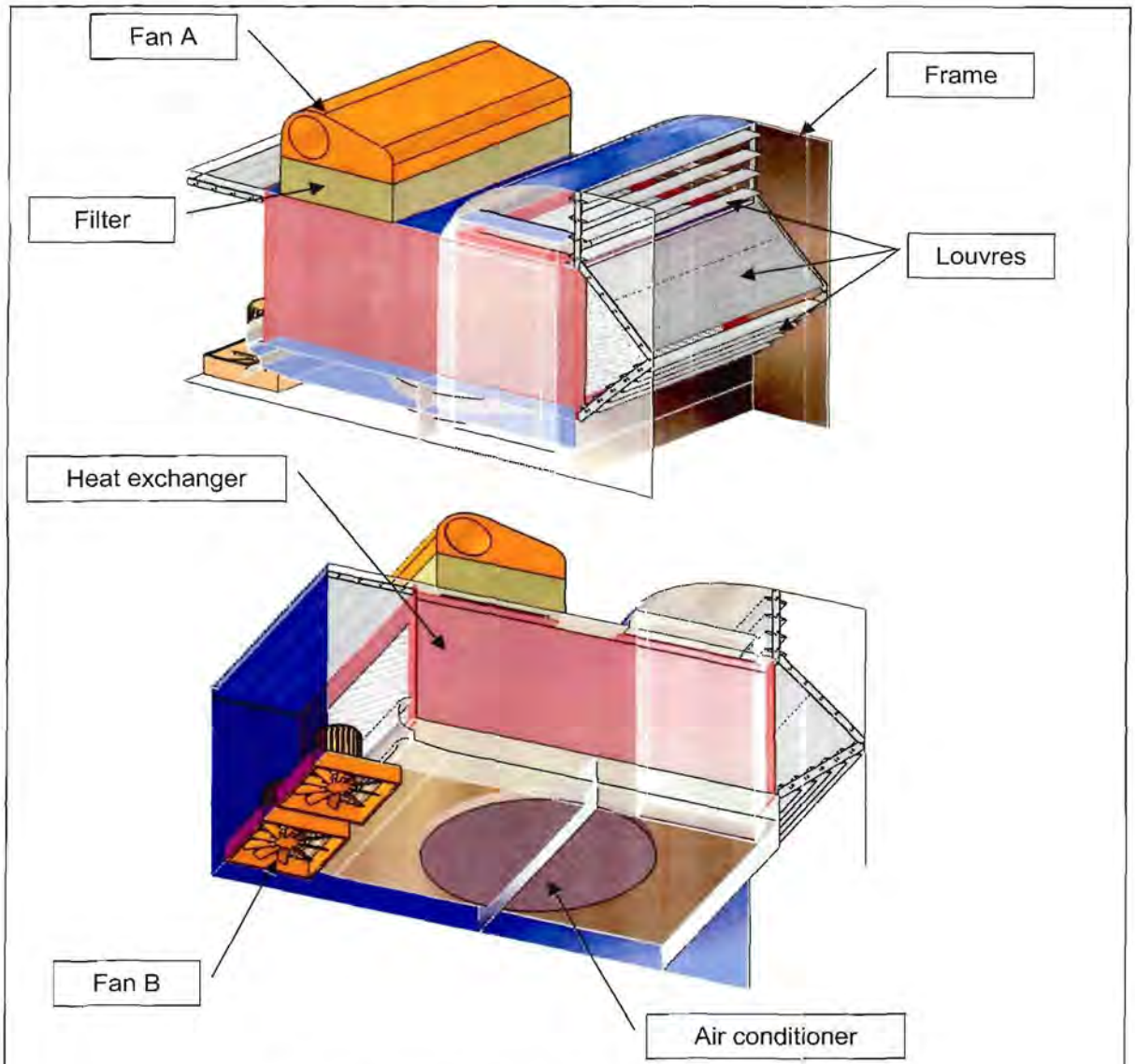

Figure 88: Cooling & Conditioning Unit physical layout.

Each storage unit has two identical Cooling & Conditioning Units (CCU) fitted to it. These CCUs perform all the cooling functions needed to keep the storage tank temperatures within limits. They also condition the air around the tank during the closed loop operation. All the components are interchangeable with other CCUs, and are designed for easy replacement. A CCU has a number of possible configurations in which it can perform certain functions.

The CCU consists of the following main components which are shown in Figure 88:

CCU frame: This item forms the assembly platform for all the other components. It contains all the necessary interfaces to allow for simple replacement of the other components. The frame is installed during plant construction and need not be removed to change the CCU configuration. The frame also acts as the platform for all external interfaces. It is a sheet metal construction made of a corrosion resistant metal, still to be finalized. All components fit like cartridges into the frame, and are fastened by the least complex but suitable mechanism – this could be a number of bolts, or even clamps. The interfaces all have seals to reduce

leakages between the different flow paths. The frame has an external insulation layer that keeps the surface temperature below 40°C even when hot air at 120°C circulates through it.

Louvres: There are four louvre sets per CCU. The louvres are fixed to the frame and need not be removed except for maintenance by replacement. The louvres control the flow path of the air. All louvres have a "normal operation" position, and they are kept in place by means of a magnetic lock. In the event of a power failure to both CCUs, the louvres will fall open to a "fallback" position in order to allow passive cooling to take place. The louvres must be reset manually after they have opened. The louvres can also be opened manually, or completely removed if the mechanism is stuck.

The louvre blades are all aerodynamically smooth to limit the flow losses when they are open. There are special seal surfaces on the blades that ensure a tight configuration when the louvre is closed.

Motorized fans: The fans are the most important active components of the CCU. Failure of the fans will imply a failure of the active cooling. The type of fan A is not fixed and depends upon flow characteristics and dimensional limitations, however, a centrifugal fan seems to be the most feasible. Two axial fans are envisaged for fan B due to size constraints and flow requirements. Because these fans are always in the flow path, they should have a minimal passive flow loss. If no suitable standard fan can be obtained which has low passive flow losses, it may be needed to design a special fan rotor of which the blades feather to zero angle of attack when the motor is not operational.

Because the fans are the only active components needed for cooling, they are designed to be replaceable within a few hours. For this reason, the rotor of the fans are all fixed to the motor, and not belt-driven.

Inlet filter: The inlet filter's function is to reduce the amount of particles and salts in the secondary side flow path, thereby limiting corrosion of the associated components (which are the secondary side of the heat exchanger, some regions of the frame and the exhaust duct). The filter type is not fixed, and shall be a compromise between cost, performance and maintainability. There is a differential pressure indicator across the filter, which is inspected frequently. If the pressure is above a certain limit (to be specified by the filter supplier), the filter will be replaced.

Heat exchanger: The heat exchanger is a crucial component of the CCU. It determines the CCU heat load capacity and drives the overall dimensions. It was the size of the heat exchanger that led to a design with two CCUs. This was to reduce the size of an individual heat exchanger. The resulting benefits were that the flow is more symmetric into the tank cubicle, and the active cooling is semi-redundant, meaning if one CCU fails, all the cooling is not lost.

The heat exchanger is a direct air-to-air plate heat exchanger, similar to what is used in industrial heat recovery systems [72][73]. It has an I-U counter flow configuration (refer to Figure 89). The heat transfer plates of the heat exchanger can be made from steel, aluminium or other special materials, also with additional corrosion protective coatings. The heat exchanger is modular in design, making it easy to replace and/or upgrade without affecting the connection interfaces. Depending upon the flow and temperatures, thermal heat transfer efficiencies of 90% can be achieved [74]. Because of its modular design, the heat exchangers are relatively cheap, and they can be handled using a fork-lift.

Each heat exchanger is required to transfer about 75kW of heat from the internal closed loop to the external air. This heat originates from the spent fuel. However, the heat load drops to about 35kW after 3 years from the time the tank was sealed. The heat exchanger can then be replaced by a lower cost unit that has fewer heat transfer plates.

The CCU can therefore contain either a High Load heat exchanger, or a Low Load heat

exchanger. When the high load heat exchanger is replaced by a low load one, the replaced component can be moved to the next storage unit's CCUs. This way, there are a maximum of 4 high load units required at any time during the SSS operational life. Refer to section 6 for a more detailed description on the sequencing of heat exchangers. Whether the heat exchanger is replaced or not, is a decision to be made by the operator.

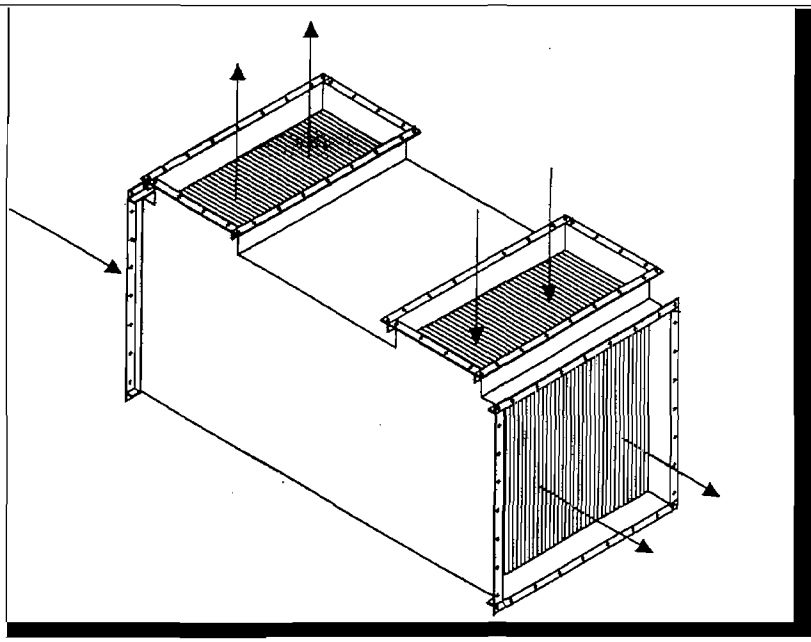

Figure 89: Illustration of the CCU Heat Exchanger (Courtesy Des Champs Technologies).

Air conditioner: The air conditioner's purpose is to condition the closed loop air to a specified purity and humidity level. It is modular in design to allow for future upgrades. Only a portion of the closed loop air passes through it. This is achieved by means of a flow scoop situated at the outlet of the heat exchanger.

The air conditioner will be sized to "clean" the closed loop air from a pessimistic Koeberg composition with 60% RH at 35°C [75], down to the required purity level within seven days. It will be able to maintain such purity levels in the closed loop, with all postulated leakages such as concrete diffusion and interface leakages taken into account.

The final purity level specification has not been finalized yet, as it is driven by the ongoing corrosion tests. However, preliminary indications showed that the relative humidity should be kept below 10% [52]. There is also the possibility that other gaseous elements such as NOx's need be removed. For this reason, it was decided to use a desiccant wheel dehumidifier as the primary component of the air conditioner.

A desiccant is a porous type of material that has a high affinity for water or other molecules. Desiccants work either by absorption (chemically) or adsorption (adhesion) in order to trap molecules [47], and it also filters the gas passing through it. Desiccants are often used in very dry air systems, and also to purify air in "clean rooms". To remove the trapped molecules from the desiccant material, it needs to be regenerated. One way to regenerate the material is to move the material from the cleaned air to a hot exhaust air. This is easily achieved if the desiccant is in the form of a rotating wheel. By rotating a portion of the wheel through the air stream to be conditioned, water is trapped in the material. The moisture-laden portion of the wheel then passes through the hotter regeneration airflow where the water is evaporated from the wheel. The regeneration flow transports the water to the

exhaust [76]. This moisture extraction is a continuous process, and relative humidity levels below 10% can easily be achieved.

There is a large range of desiccant materials available in the industry [77]. The choice of material is a based upon its specific characteristics and cost. Some materials can dry the air to extremely low humidity levels, but may be susceptible to clogging or chemical attack, while others may be more chemically inert.

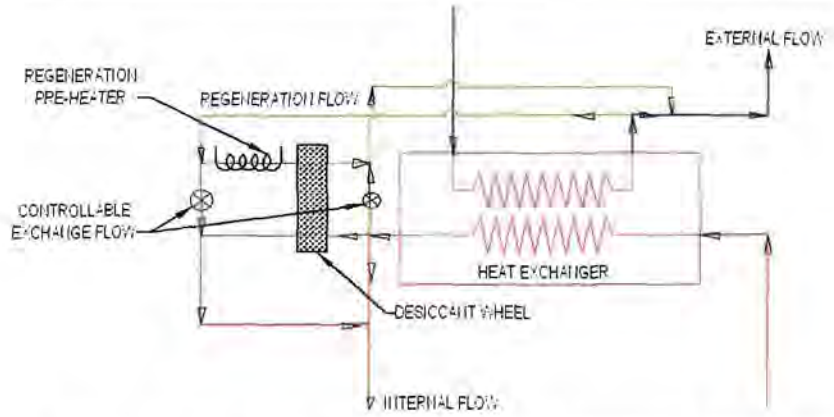

Figure 90: Flow diagram of the air conditioner using a desiccant wheel dehumidifier.

Figure 90 shows how a portion of the air from the internal side is diverted through the wheel, and then returned back to the main stream. The regeneration flow originates from the external side of the heat exchanger. Depending upon the temperature of the external flow, a pre-heater will be activated to lift the temperature to the desired regeneration level. The extraction and return openings for the flow is aerodynamically designed to prevent re-circulation from taking place.

What is also shown is a controllable air exchange flow path. This is a functionality that enables the air conditioner to gradually replace the contents of the internal flow with that of the external flow. The reason for this function is that there is the possibility that NOx elements, generated by the gamma radiolysis of the air, may accumulate inside the closed loop. To prevent the concentration from reaching health or corrosion limits, it may be necessary to gradually replace the air. The actual values of air replacement will be determined after a complete radiolysis and corrosion analysis.

The wheel also acts as a self-cleaning filter. The replacement frequency depends upon the actual environment in which the wheel operates, but the aim is not to replace it more than once every 10 years.

Barrier plate insert: This component replaces the heat exchanger. It fits exactly onto the interface of the heat exchanger and blocks all openings except for the two closest to the fans, thereby creating a flow path from Fan A to Fan B. This insert will be used during the open loop active cooling configuration (see section 5.4 for more details on the cooling flow).

Straight insert: This component acts in a similar manner as the barrier plate by replacing the heat exchanger, but different inlets are blocked. It channels a portion of the flow past the air conditioner in order to protect the empty tank from corrosion. It will be used during the closed loop conditioning mode.

5. CCU CONFIGURATIONS

Although the CCUs can function individually, they are designed to operate as a pair in order to achieve the required cooling mode of the storage unit. The following paragraphs describe the CCU configurations necessary for the various cooling modes. The CCUs are illustrated schematically, with the air conditioner shown in front of the heat exchanger rather than below as in the physical layout.

5.1 CLOSED LOOP ACTIVE COOLING

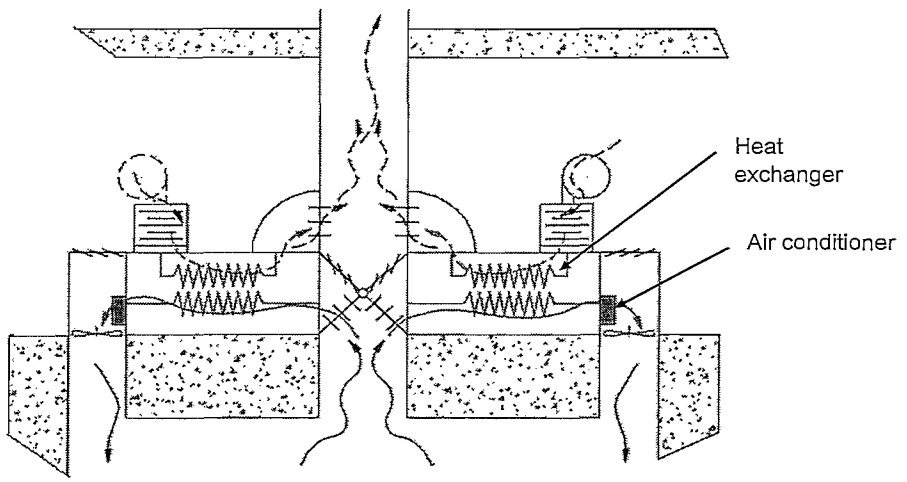

Figure 91: CCU configurations for the closed loop active cooling mode.

For the closed loop active cooling mode, both CCUs are fitted with a heat exchanger, fans and inlet filter. An air conditioner is also installed in one or both units, depending upon the capacity of the air conditioner (to be finalised during detail design). The louvres are positioned as shown in Figure 91.

The fans at the cubicle inlets circulate the closed loop air through the heat exchangers and then past the storage tank. A small portion (10%) of the internal flow is diverted through the air conditioner, and then returned to the main stream. On the external side, air is extracted from the room above the top floor and passes via a filter through the heat exchanger. The two hot airstreams from the external side collect into the exhaust duct and gets discharged to atmosphere.

Depending upon the heat load inside the tank, the heat exchanger could be a High or Low load unit. Refer to section 6 for a discussion on the various heat exchanger configurations.

5.2 CLOSED LOOP ACTIVE COOLING, ONE UNIT OUT OF SERVICE

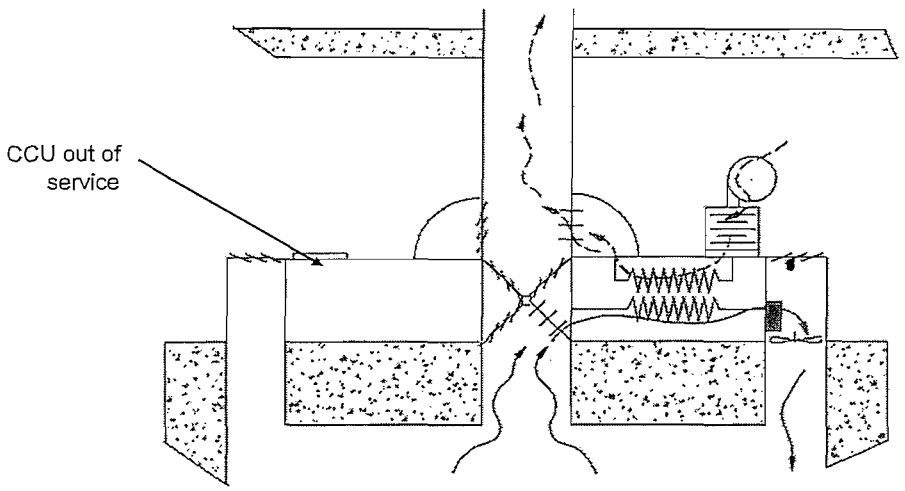

Figure 92: CCU configurations during closed loop active cooling, but with one unit out of service.

This cooling mode is a sub-set of the primary closed loop active cooling mode. In this case only one CCU is operational. This is achieved by means of positioning the louvres as shown in Figure 92.

In this mode, it is possible to perform maintenance on one unit, without completely cutting off the cooling flow. Also, when the heat load is significantly low, only one CCU is required to perform the cooling.

5.3 OPEN LOOP PASSIVE COOLING

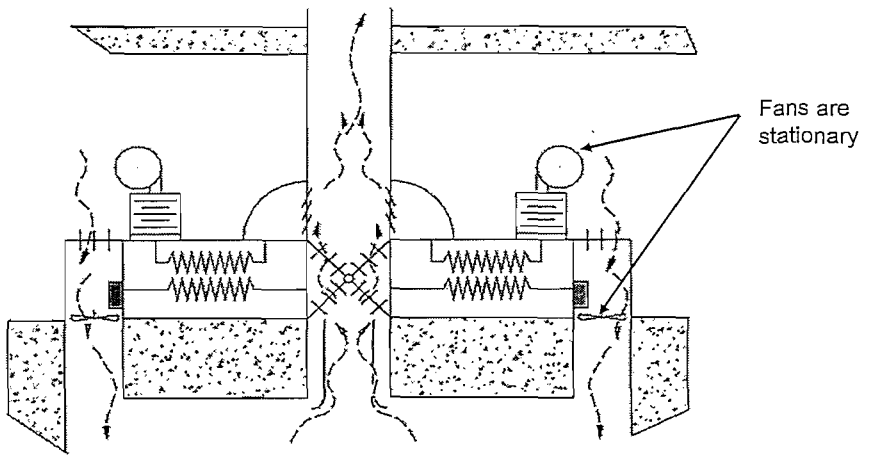

Figure 93: CCU configurations during open loop passive cooling mode.

The open loop passive cooling is achieved by changing the louvre positions as shown in Figure 93. This way the heat exchanger and the inlet filter is bypassed. The flow resistance is then low enough that sufficient air can be drawn into the cubicle by means of natural convection. In this mode, no corrosion control is performed, which implies that passive cooling should only last as long as it takes to restore the CCU operation.

5.4 OPEN LOOP ACTIVE COOLING

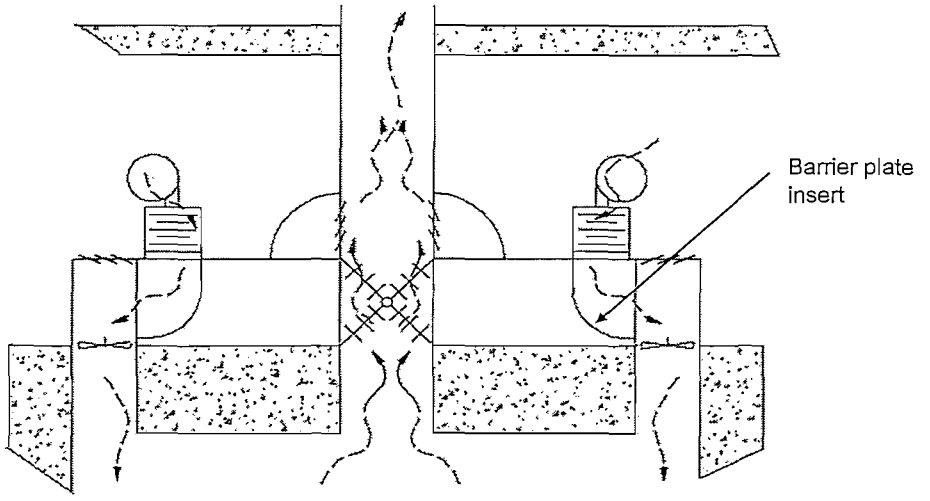

Figure 94: CCU configurations during open loop active cooling mode.

During the open loop active cooling mode, the heat exchangers are physically replaced by barrier plates, and the louvres are set in the positions shown in Figure 94.

During this mode, air is drawn from outside through the inlet filter and then goes straight into the tank cubicle. No air passes through the air conditioner, hence it need not be installed. The hot air moves directly into the exhaust duct and out to the outside. Corrosion protection is done by the filter only.

5.5 CLOSED LOOP CONDITIONING

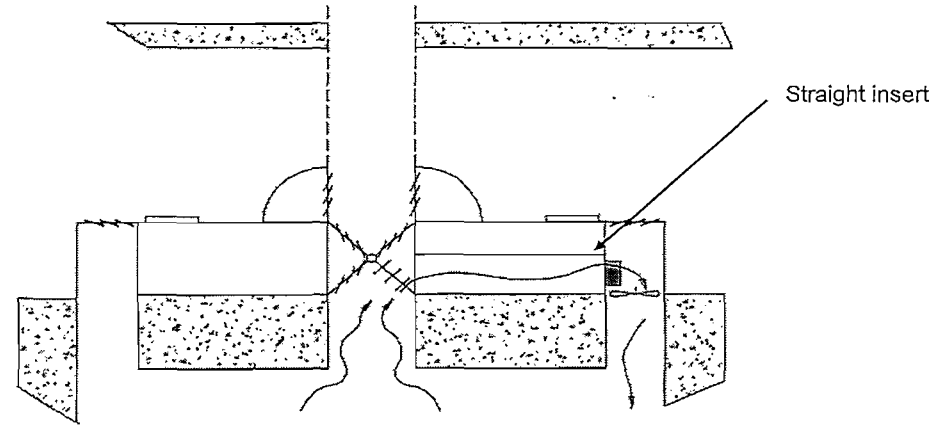

Figure 95: CCU configurations during closed loop conditioning mode.

For the closed loop conditioning mode, the heat exchangers are replaced by straight inserts which channels the flow through the air conditioner only. The air is thus circulated and kept at a specific purity and humidity level in order to prevent corrosion. Depending upon the capacity of the air conditioner, only one or both CCUs will be operational. What is not shown in Figure 95 is the regeneration airflow. This is a relatively small airflow and will be driven by a fan in the air conditioner itself. It may also be necessary to have a small heater in order to stabilise the temperature during day-night transients.

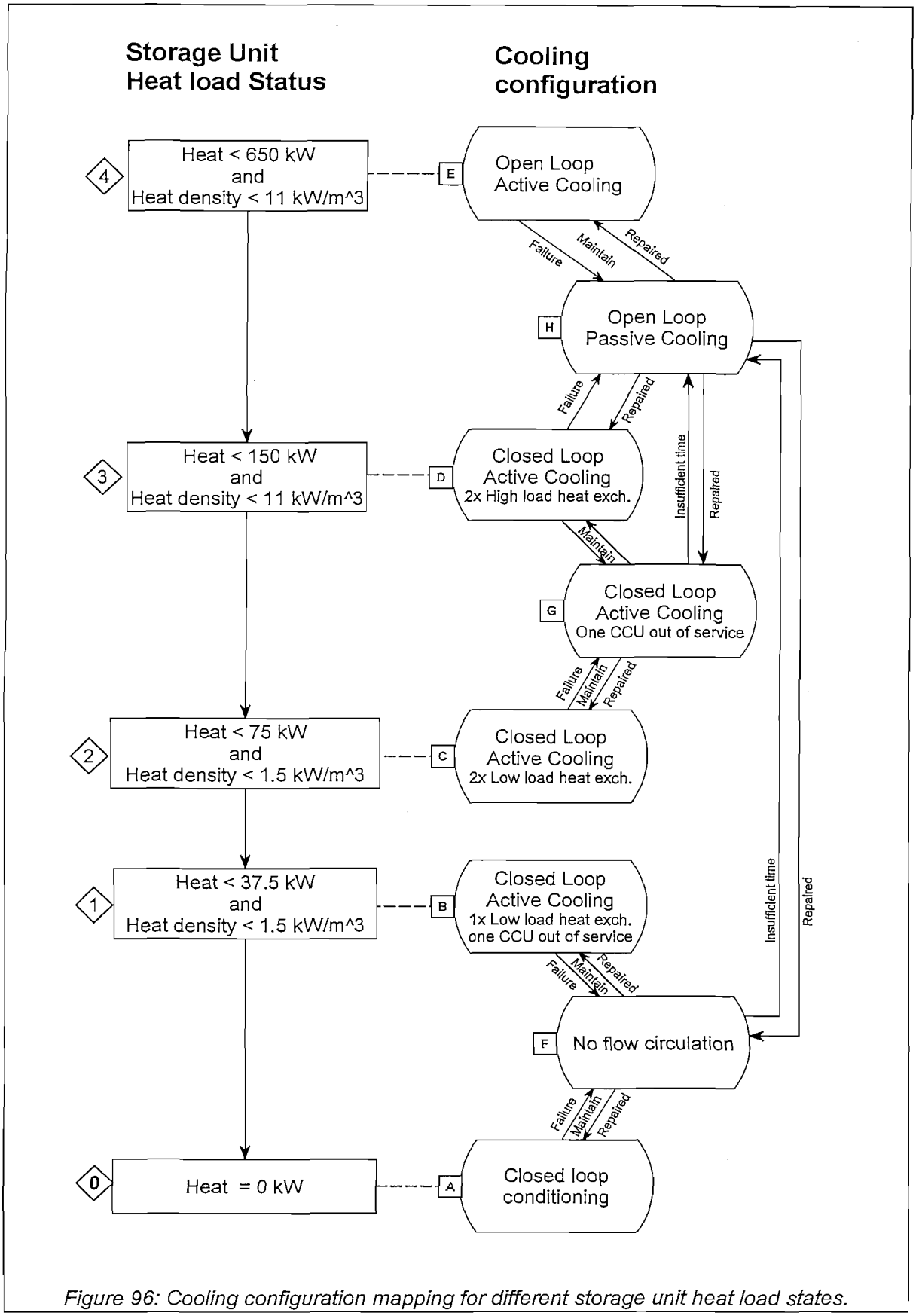

Figure 96: Cooling configuration mapping for different storage unit heat load states.

Figure 96 shows that the cooling configuration will be based upon the heat load state of the storage unit. The heat load state is driven by the type and decay age of the spheres contained in the storage tank. This was discussed in detail in Chapter 9.

The highest heat load that a storage unit can accommodate is 650kW. For heat loads above 150kW to 650kW, cooling is done in an open loop active mode. There is also a limiting heat density of 11kW/m^3. For heat loads of 150kW and lower, a closed loop active cooling mode is used. For the instances where the heat density inside the tank is higher than 1.5kW/m^3, the open loop passive cooling mode is seen as the first line of defence in the event of a total CCU failure. This does not mean that one could not revert to passive cooling during lower heat densities, only that it may not be necessary to do so because the thermal response is so low that one has several days before cooling needs to be re-established (one should remember that passive cooling introduces corrosive elements).

When the heat load has dropped to 75kW, the two high load heat exchangers can be exchanged by two low load units, which are less expensive. This does not mean one has to change to low load units, but it may be a way to reduce the total capital cost of the CCU over its operational life. When the heat has dropped to below 37.5kW, only one low load heat exchanger is needed to remove the heat. The other CCU can thus be taken out of service, and its components moved to another CCU if needed to further reduce the total cost.

At the stage where two CCUs are operational, maintenance can be performed on one of the units by simply taking it out of service, without having to revert to passive cooling. The time before any thermal limit is reached is sufficiently long that maintenance can be done. If for some reason the maintenance cannot be completed in time, one simply needs to revert to passive cooling.

When there is no heat to be removed, the closed loop conditioning mode will be active via which corrosion on the tank is controlled.

6. STORAGE UNIT COOLING SEQUENCE

6.1 SPENT FUEL STORAGE UNIT COOLING

The maximum heat load of a tank containing spent fuel is 140 kW (it then contains 530 000 spheres). This load drops by half in 1.1 years, and to a quarter after a further 2.2 years. After 40 years, the total heat load inside a tank is only 10 kW.

At day one of a tank being filled, it will be fitted with two high load heat exchangers (configuration D in Figure 96). This is because the heat density is about 7kW/m^3, even though the heat load reaches 75kW only after a year's loading. The high load heat exchangers will be in place for the 3.5 years it takes to fill the tank, and for another 1.1 years thereafter. At that stage the load has halved, and the two high load heat exchangers can be replaced with two low load heat exchangers (configuration C in Figure 96). After another 2.2 years, the load has halved again, and one of the low load heat exchangers can be removed (configuration B in Figure 96), while the last one stays there for the remainder of the storage period, which could be between 40 to 80 years.

Figure 97 shows how the arrangement of heat exchangers may be for the 10 SFSU's over the life of the plant. From the figure, it can be seen that there is a maximum of 4 high load heat exchangers required at any time. The low load heat exchangers are introduced one at a time from year 4.6 with a maximum of 11 low load heat exchangers required at any time. The service life of the heat exchangers is yet unknown, since part of the heat exchanger will

be exposed to the coastal environment and the material selection for the heat transfer plates still needs to be done. Table 6 shows the number of heat exchangers needed during the 80 years, based upon a certain service life.

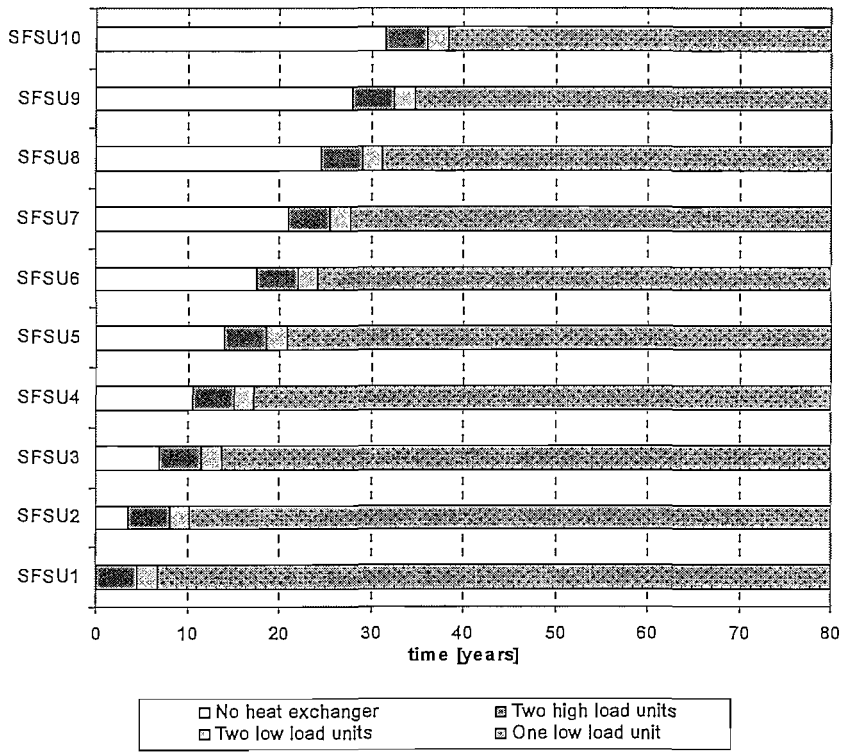

Figure 97 : Heat exchanger arrangement for each SFT over the storage life.

Table 6: Heat exchanger "consumption" scenarios.

Service life	High load units	Low load units
5 years	32	135
10 years	16	68
20 years	8	34

6.2 USED FUEL STORAGE UNIT COOLING

The only difference in terms of cooling between an SFSU and a UFSU is the maximum heat load. While the SFSU has a heat load of only 140kW, the UFSU has 640kW. This means that a UFSU is cooled in an active open loop manner (configuration E in Figure 96). As for the SFSU, if an active component fails, the CCU's louvres change position to allow passive cooling to take over (configuration H in Figure 96). The only difference is that the CCU has a barrier plate insert instead of the heat exchanger (compare Figure 94 with Figure 93).

When the UFSU contains the last core, it will start with an open loop active cooling mode until the heat has dropped to below 150kW. From there on, the cooling will follow the sequence as described for an SFSU.

6.3 GRAPHITE STORAGE UNIT COOLING

When the GRSU contains graphite, no heat is generated and the CCUs will be configured for closed loop conditioning mode. However, a GRSU is designed exactly like an UFSU, and can therefore follow the cooling scheme of an UFSU if it is loaded with used or spent fuel.

7. EXTERNAL AIR SUPPLY AND DISCHARGE

Outside atmospheric air is used for the external side of the storage unit cooling. The air has to enter the building from one side, and exit through another. This section discusses the issues around the air supply and discharge for cooling.

7.1 BUILDING INLETS

There are three large inlets at the rear wall of the building and two inlets located on each side of the building. The total capacity of all the inlets is 20kg/s airflow. These inlets open into the room where the CCUs are situated. Each CCU then draws the required flow from this room. This means there is no physical connection between the outside and the cooling unit inlets, rather the room acts as a large supply plenum for all the units. This arrangement makes the inlet to each unit more reliable, and also simplifies the layout because there are no inlet ducting required.

The flow resistance of the building inlets should be as low as possible in order for the passive cooling to work properly. There are thus no filters on the inlets, only de-misters to minimize moisture spray. The upper service floor is thus at atmospheric conditions and pressure.

To protect the inlets and cooling units from an external missile, a barrier wall is added to the building. Figure 98 shows what this barrier wall looks like.

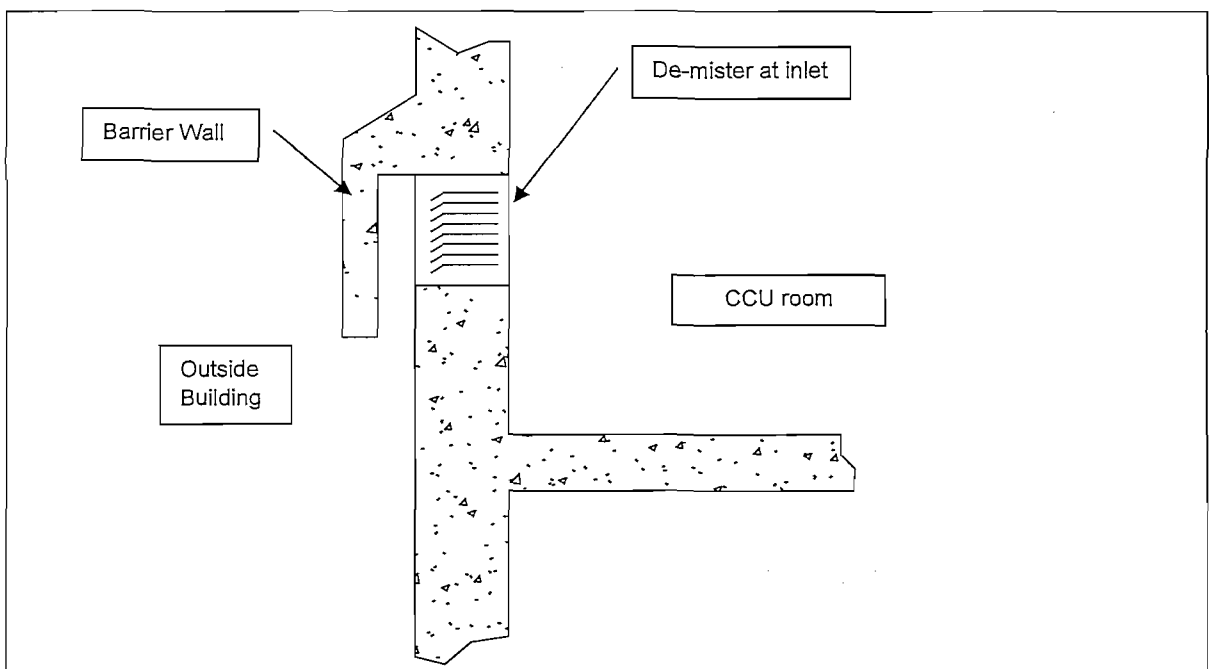

Figure 98: Building inlet with barrier wall.

7.2 EXHAUST AIR

The exhaust duct is designed to minimize flow and heat loss of the exhaust air. It is also optimized (to be completed during detail design) to enhance the passive cooling of the tank.

The outlet at the top of the building is protected such that it cannot be plugged accidentally. This is done by means of a common concrete outlet cavity for all of the ducts. Figure 99 shows an illustration of the outlet. The water trap wall prevents rain from entering the ducts. It is also expected that the proposed outlet geometry may cause external winds to generate a low pressure at the outlet, thus enhancing the passive cooling.

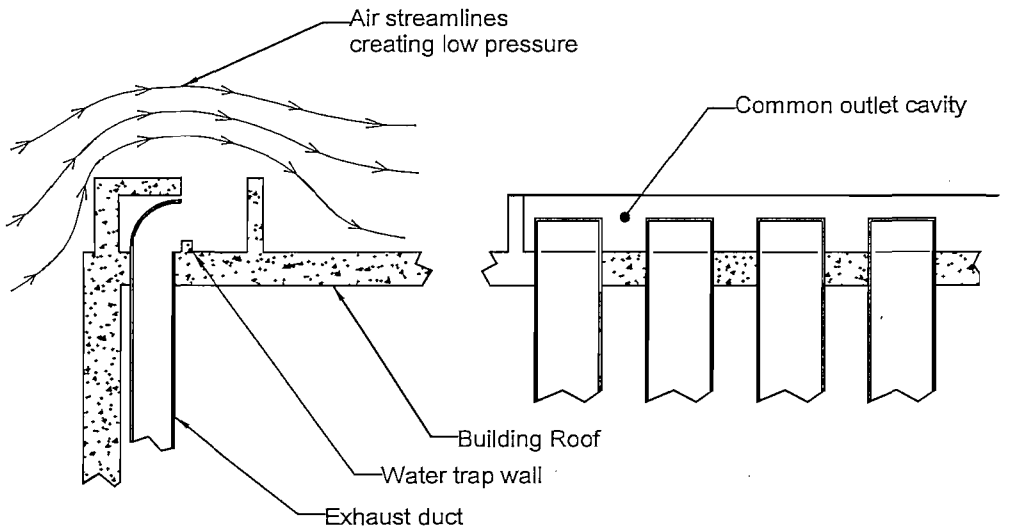

Figure 99: Exhaust duct outlet manifold.

7.3 EXTERNAL WIND EFFECTS

For reliable passive cooling, the building should be such that the pressure drop from the CCU room to the exhaust outlets is always positive for any external wind. In other words, if a negative pressure drop exists across the inlet to the outlet of a storage unit, the air may flow in the reverse direction through the storage unit, or reduce the mass flow during passive cooling.

A study was done using CFD analyses to determine the pressures at the inlets and outlets of the building for various wind velocities and directions. Changes were proposed to the building geometry such that the pressure at the outlet is always lower than at the inlet, i.e. a positive pressure drop. The results are given in reference [78].

Initially the analysis was performed by assuming no air movement inside the building. The result was a pressure distribution along the building inlets that was quite sensitive to the wind direction. This was caused by the flow separation around the building corner creating a low pressure at the inlets in the separation zone, and a high pressure at the inlets in the re-attachment zone. This can be seen in Figure 100.

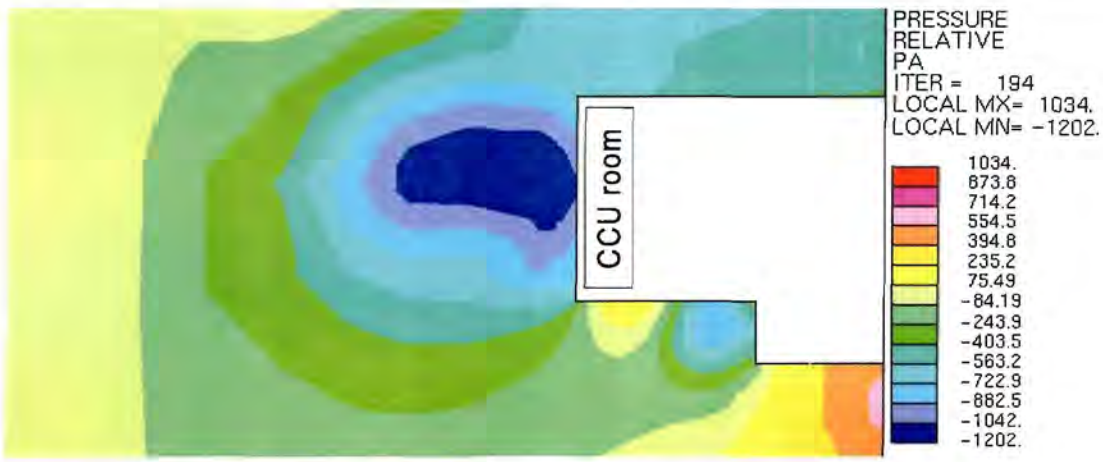

Figure 100: Pressure distribution with no flow coupling inside the building

A second analysis was done, and this time the CCU room was also modeled, and the outside air was allowed to flow into and out of the room. The result was a much more constant pressure distribution along the length of the CCU room. This is because the pressure in the separation zone was equalized by air flowing out of the room, and coming in from the re-attachment zone.

Initially there was only one inlet on either side of the building, and five at the back. It was realized that the openings on the side was too small to allow sufficient air to enter and that the two inlets at the back, closest to each corner do not contribute much to the flow. These two inlets were subsequently moved to the sides of the building, as shown in Figure 101. This resulted in a CCU room pressure that was constant for all wind directions and velocities.

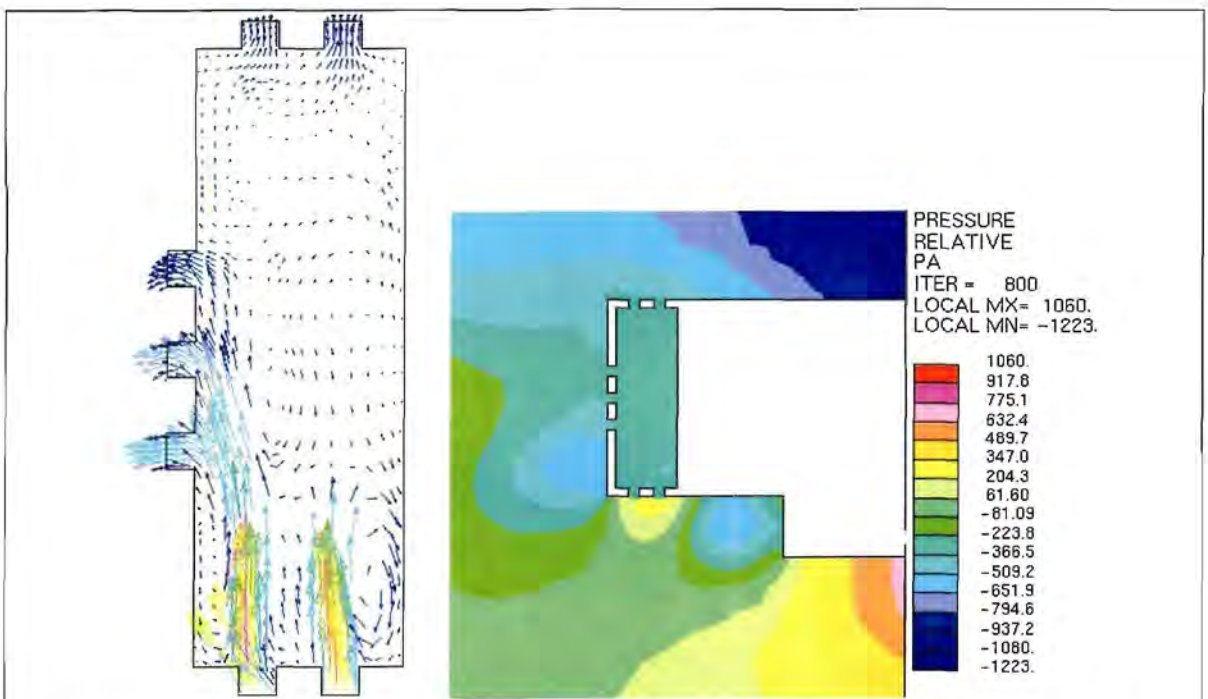

Figure 101: Airflow through the CCU room resulting in an even pressure distribution.

As was expected, the pressure at the exhaust outlet was always lower than the static pressure for all wind directions. No changes were therefore needed to the outlet geometry.

Figure 102 shows the final pressure drop from the inlet to outlet for a wind speed of 38m/s, for all eight wind directions investigated. It can be seen that the pressure drop never goes negative, meaning that the flow will always move in the correct direction.

It is proposed that a dimensionally similar model of the module building with inlets and outlets be tested in a wind tunnel to serve as a verification of the CFD analyses.

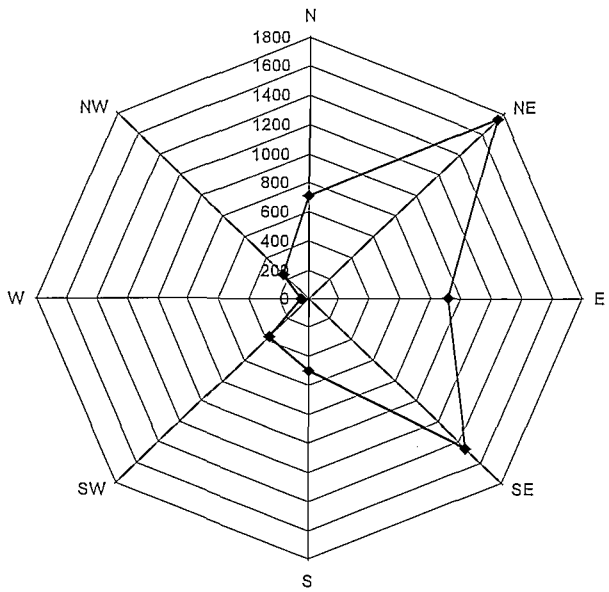

Figure 102 : Pressure drop [Pa] from the inlet to the outlet for various wind directions.

8. PASSIVE COOLING ANALYSIS

It was already established during the value engineering exercise (refer to Chapter 4) that the storage tanks have a very good passive cooling ability. This is due to the long vertical tubes inside the tank that act as heated chimneys. However, the tank does not stand open in the outside air, rather, it is built inside the storage unit. The effects of the other components and inlets of the storage unit may reduce the tank's passive cooling ability.

Passive cooling analysis can only be done using CFD, and also the complete storage unit geometry has to be analysed. The analysis is performed by initially solving the airflow for a specific given active cooling mass flow. This mass flow is chosen such that the pressure difference between the inlet and outlet of the geometry is almost zero. The forced mass boundary condition at the inlet is then changed to a fixed inlet pressure. A new solution is reached that resembles the passive cooling flow. If the initial mass flow was chosen too far away from the resulting passive flow, the solution may not converge. Therefore, passive cooling analysis requires significantly longer solve times and also some experimentation on the initial conditions required.

It was decided to analyse the complete storage unit from the top floor downward. The inlets and outlets in the top floor formed the CFD boundary. The effect of the exhaust duct, which acts as a long chimney, and the flow losses through the building inlets and CCUs were therefore not included. The strategy was to arrive at a storage unit layout around the tank that results in the required passive cooling mass flows. The exhaust duct design then only

has to assist in overcoming the extra flow losses through the building inlets and CCUs.

An optimization study has been done to reduce the total flow losses through the storage unit. The results are reported in reference [79]. It was possible to reduce the total losses by 50% as compared to the original geometry by increasing the gap through the ring support and the horizontal part of the gamma shield. The result is a storage unit that generates approximately the same mass flow during the passive cooling mode as during active cooling. Table 7 summarises the results.

Table 7. Passive cooling resuls from CFD analyses

Description	Heat load [kW]	Fuel temperature [°C]	Passive cooling [kg/s]
100% filled SFT	135	220	3.5
5% filled SFT	23	160	2.2
100% filled UFT	640	358	5.8
25% filled UFT	220	386	4.9

Because passive cooling analyses take so long using CFD, it is not feasible to calculate the passive cooling for a full range of storage tank heat loads. A technique was developed to analyse the passive cooling flow using pipe network analysis software. The cubicle and tank was approximated with a network of pipes and flow loss elements. The analyses were done using Flownex [80].

Figure 103 shows the pipe network overlaid on a diagram of the storage unit. Notice that the CCUs are also modelled. This allows one to calculate the actual mass flow for a given fan characteristic curve, heat exchanger properties and heat load in the tank. The portions of significant flow loss (such as the ring support and gamma shield) are modelled using flow loss elements. The loss coefficient is determined from CFD analyses for various flow and temperature scenarios. The tank and thermal shield is simulated as a number of parallel pipes. The pipes are divided into a heated and unheated part.

In order for the software to properly include the buoyancy effect, the height of each node is specified. Also, the inlet and outlet node is defined at the same height with a constant pressure boundary.

The results are mass flows and temperatures in each pipe element. No information is calculated for the tank and fuel temperatures, however, the active cooling analyses can be used to deduct the tank and fuel temperatures. This is because from the tank's point of view, only a known mass flow is required to determine the temperatures.

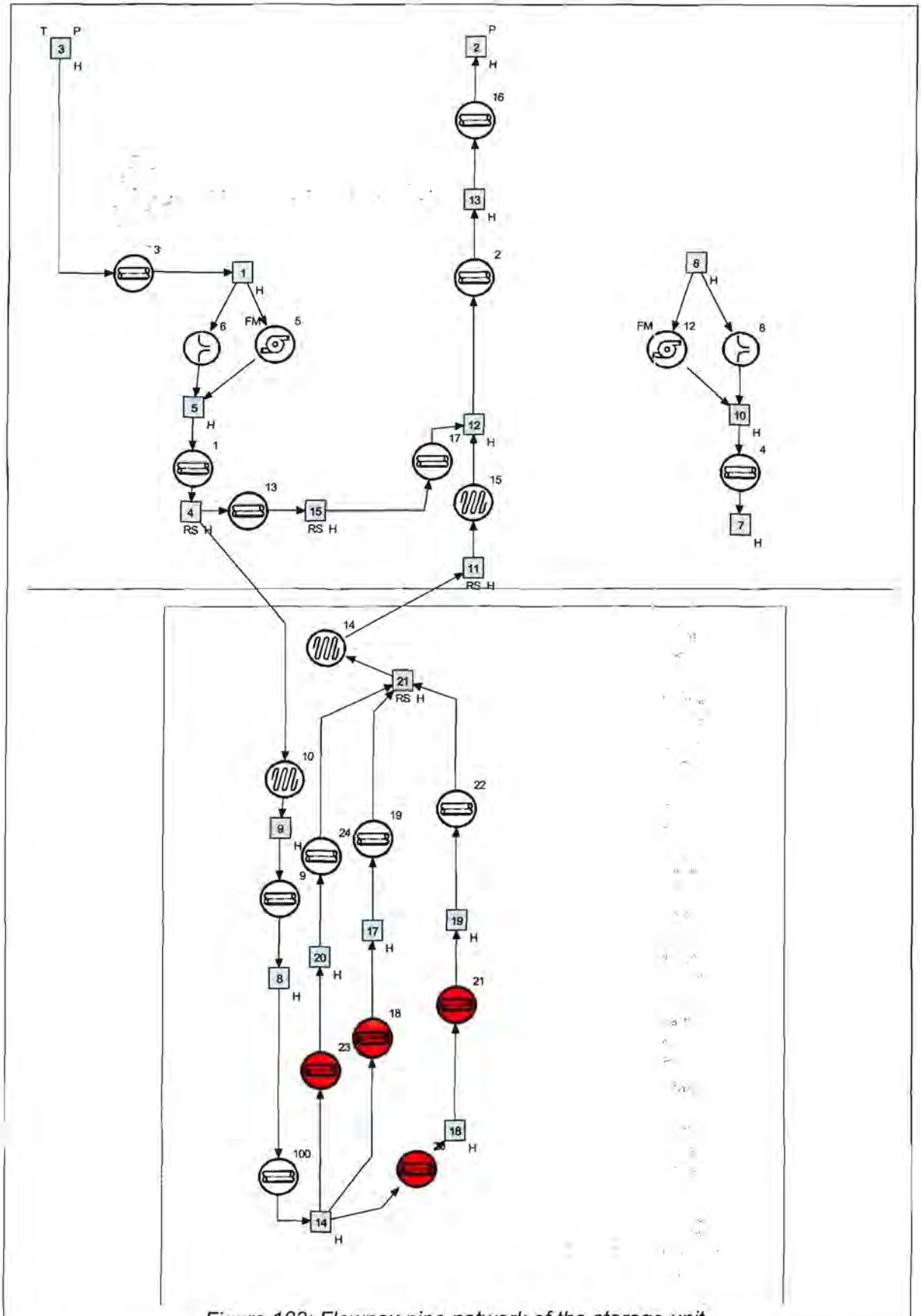

Figure 103: Flownex pipe network of the storage unit.

It is also possible to investigate flow transients given that the tank temperatures do not change significantly. A constant temperature input is then applied to the pipe elements, rather than a constant heat input. It was thus possible to investigate the effect of a sudden pressure increase at the chimney outlet, causing the flow to move in the opposite direction. Figure 104 shows the time history of the mass flows and temperature through the chimney and tank cooling pipes during such an event. Note that the colour plots at the bottom of the figure are post-processed data of the Flownex output. The post-processing was done using MatLab, and helped to visualise the flow direction and temperatures during the transient.

The absolute value of the mass flow and temperatures are for this case of less importance, as it depends upon the actual heat load inside the tank. What is noteworthy is the direction and relative magnitude of the mass flow. The flow is defined positive in the direction showed in Figure 86, hence a negative mass flow will indicate reversed flow.

The pressure increase causes the flow in the chimney to reverse and reach an equilibrium state after about 60 seconds. In this state, an important phenomenon is seen: the flow in the centre tube and outer tubes are upward, while in the channels of the thermal shield it flows downward. There is thus a re-circulation that occurs around the tank. This re-circulation was also seen from a transient CFD analysis of a completely blocked system. The re-circulation can be attributed to the strong chimney effect of the pipes.

After 120 seconds the outlet pressure was restored to the original pressure, equal to the inlet pressure. Again, within 60 seconds, a new equilibrium is reached, however, not the original passive cooling state. It seems that once a reverse equilibrium has been forced, the flow patterns will stay that way. This phenomenon is somewhat surprising, and CFD analyses are planned to confirm this.

In order to return the flow to its original directions, the inlet openings are closed for 120 seconds. During this time, hot air starts to build up in the gamma shield volume and chimney. Re-circulation around the tank still continues, but at much lower mass flows. When the openings are opened after the 120 seconds, there is enough buoyancy difference between the air in the gamma shield volume and the concrete cubicle so that the flow will start in the desired direction. The original passive cooling equilibrium is reached after 60 seconds.

The rate at which new equilibrium states are reached is very important. The fuel has a maximum temperature increase rate of about 25°C/hour (0.42°C/minute). This rate is so slow, that within the 60 seconds it takes the air to stabilize, the tank wall temperatures do not change. The constant wall temperature assumption during transients is therefore quite valid.

The technique to calculate the mass flow in and around a tank using the pipe network software Flownex allows one to analyse a large range of active, transient and passive cooling scenarios. By relating the results with tank and fuel results from 3D analyses, one can deduct the actual temperatures. It is also the only feasible way to introduce the flow characteristics of the CCU, since modelling a complete CCU with CFD is just too complex.

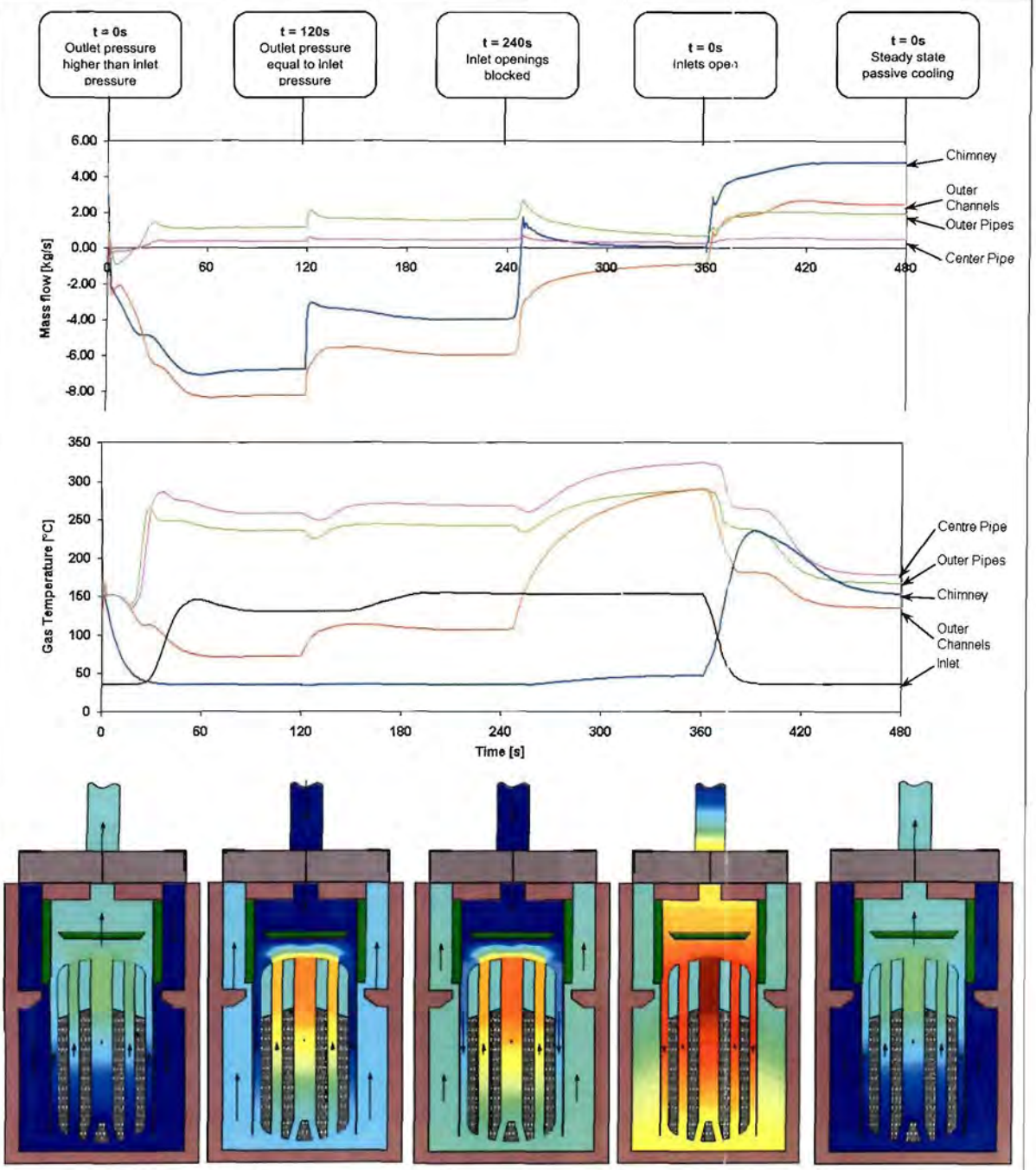

Figure 104: Transient results during passive cooling for the case where a reverse-flow is induced and then recovered by blocking the inlets.

9. PASSIVE COOLING DEMONSTRATOR

9.1 PURPOSE OF THE TEST

The purpose of this test setup was to demonstrate the principle functioning of the passive cooling of the storage units. The test was intended to demonstrate how passive cooling of the tanks would work. It was not intended to present any design information or verification of CFD analyses. Therefore, the test was not thermally or dimensionally similar. The only prerequisite was that it indicated the flow pattern correctly, and responded to transient conditions as expected for the storage tanks.

The following observations were possible:

a. The airflow direction in the tank cubicle and through the tubes. The detail flow pattern was of less importance, since it is dependant on flow velocities, corner radii and local re-circulation zones;

b. The relative effect of bigger or smaller flow restrictions in the flow path. The absolute value of temperatures and flow velocities was not important, only the relative temperature among various positions, or the change in temperature during a transient;

c. The relative effect of a chimney on the passive flow;

d. The ability to start natural convection and passive flow in the desired direction without the aid of fans at the inlets; and

e. The response of the cooling air after a forced reverse flow condition.

9.2 CONCEPTUAL LAYOUT

The test setup was intended to simulate the flow characteristics that exist inside the cubicle and the tank. To simplify the experiment, it was a two dimensional representation. Figure 105 shows a schematic drawing of the flow path in the tank cubicle, as well as for the test setup.

The fuel volume was represented by three rectangular heater elements placed a distance from each other. This created two flow channels between the heaters, which would act in the same manner as the cooling tubes of the tank. However, for the storage tank, there are three flow channels as shown. It was felt that by adding another heater to also have three flow channels would not change the results significantly.

The heater elements were heated along its full length, thus simulating a full tank. It was also possible to apply heat only at the bottom to simulate a tank at about 5% fill level.

The gamma shield and thermal shield were represented by a single "shield" running from the top to the bottom. The effect of the tank support is thus not included. This did not affect the results significantly. The horizontal part of the gamma shield was however present in the test model. It was possible to remove the horizontal part to see the effect on the flow.

An extension could be added to the outlet to simulate a chimney. The length, contraction ratio and exit geometry could be changed to indicate the effect.

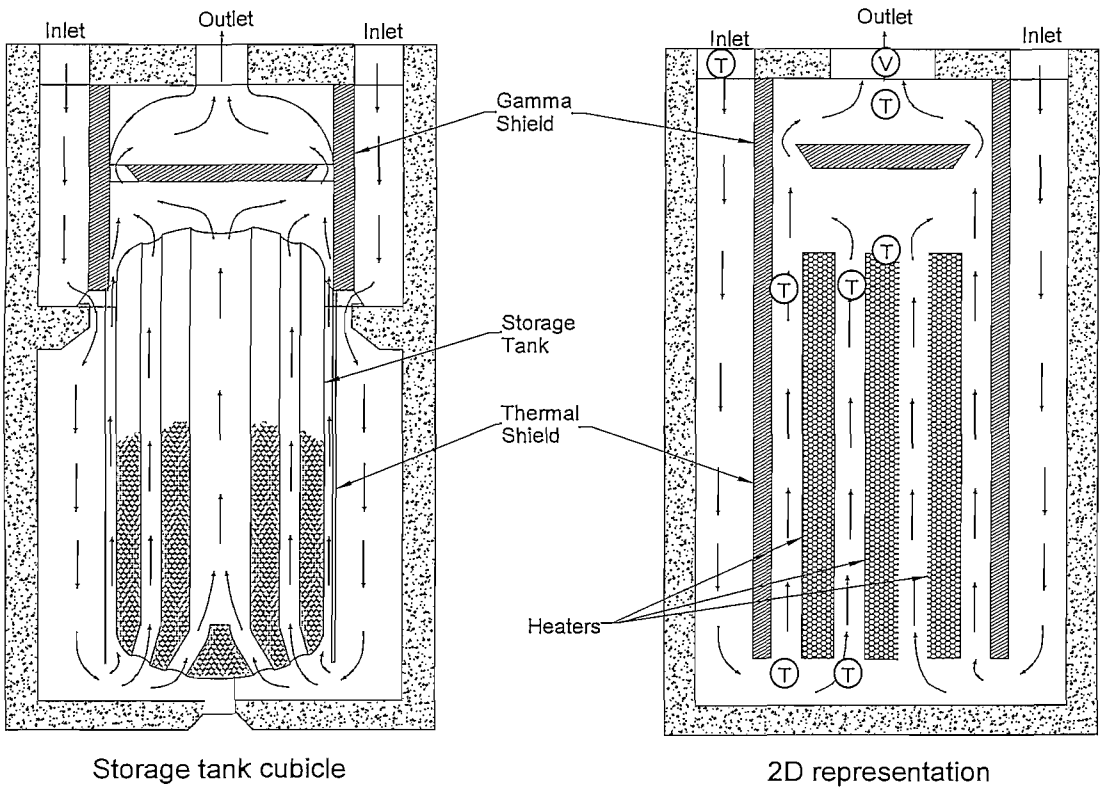

Figure 105: Schematic of the analogy between the storage tank cubicle and the 2D passive cooling demonstrator test setup.

The flow regime in the test was laminar as opposed to the turbulent flow expected for the tank. This implied that the heat transfer coefficients and flow losses were less than for the tank. However, only the resultant mass flow and temperatures were different, not the flow pattern.

In order to visualise the flow effects, temperature sensors were placed at various positions in the air stream as indicated in the figure. By looking at the relative temperatures, one could deduct the flow direction. Also, the rate at which the temperature changed gave an indicating to the transient response. The actual temperature value was thus of minimal importance. Additionally, smoke traces were injected at different positions to visualize the flow.

9.3 LAYOUT AND DIMENSIONS

The overall dimensions of the test setup were such that it would be a table-top experiment. With this in mind, the heater element length was chosen as 500mm, with a nominal cross section of 40mm x 40mm. The test setup was thus 40mm deep.

The closest approximation to a circular tube would then be a square, hence the gap between the heaters should also be 40mm. This gives a "cooling tube" aspect ratio of 500/40 = 20. The storage tank outer tubes have an aspect ratio of 18000/400 = 45. In general, the larger the aspect ratio of a fully heated chimney, the stronger is the chimney-effect. This means that the cooling tubes of the storage tanks will probably have a stronger chimney-effect than

for the test setup.

The gap between the heaters and the "shield" was chosen as half the gap of the flow channels, thus 20mm.

The total cross section of the two inlets of the tank cubicle is approximately $2m^2$. The total cross section of all the cooling tubes and gap of the thermal shield of the tank is approximately $3m^2$. This gives a ratio of 2:3. This ratio was also used for the test setup, resulting in an inlet width of 40mm for each inlet.

The outlet cross section should be the same as the two inlets together, thus it was made 80mm wide.

The rest of the dimensions were chosen such that the relative geometry looks in proportion. The dimensions of the test section are shown in Figure 106.

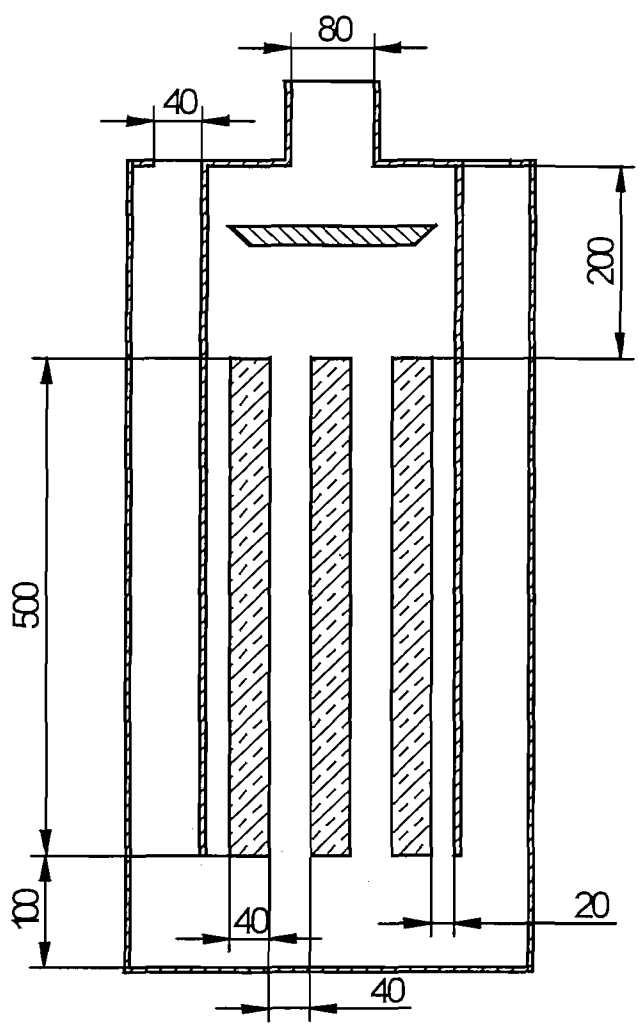

Figure 106: Basic dimensions of the test section.

Figure 107 shows a 3D representation of the complete test setup. Note that it was later decided that the test should have its own stand and will not be placed on a table. The test setup consisted of a mounting frame made from extruded aluminium square tubing. It formed the backbone of the setup. The heaters and "shield" were mounted on an asbestos

back plate. In the front was a transparent plate made from tempered glass, allowing the audience to see the heaters and airflow. Behind the back plate was a cover that hid all the electrical equipment and wiring of the test. Below the test was the control panel holding the power switch, temperature indicators, heater control and other instruments. The panel was tilted such that a person standing 2m from the test could clearly see the temperature displays.

At each inlet was a small ventilation fan used to simulate forced flow conditions. The fans were mounted on hinges so that they can be moved away from the inlet during passive flow simulations.

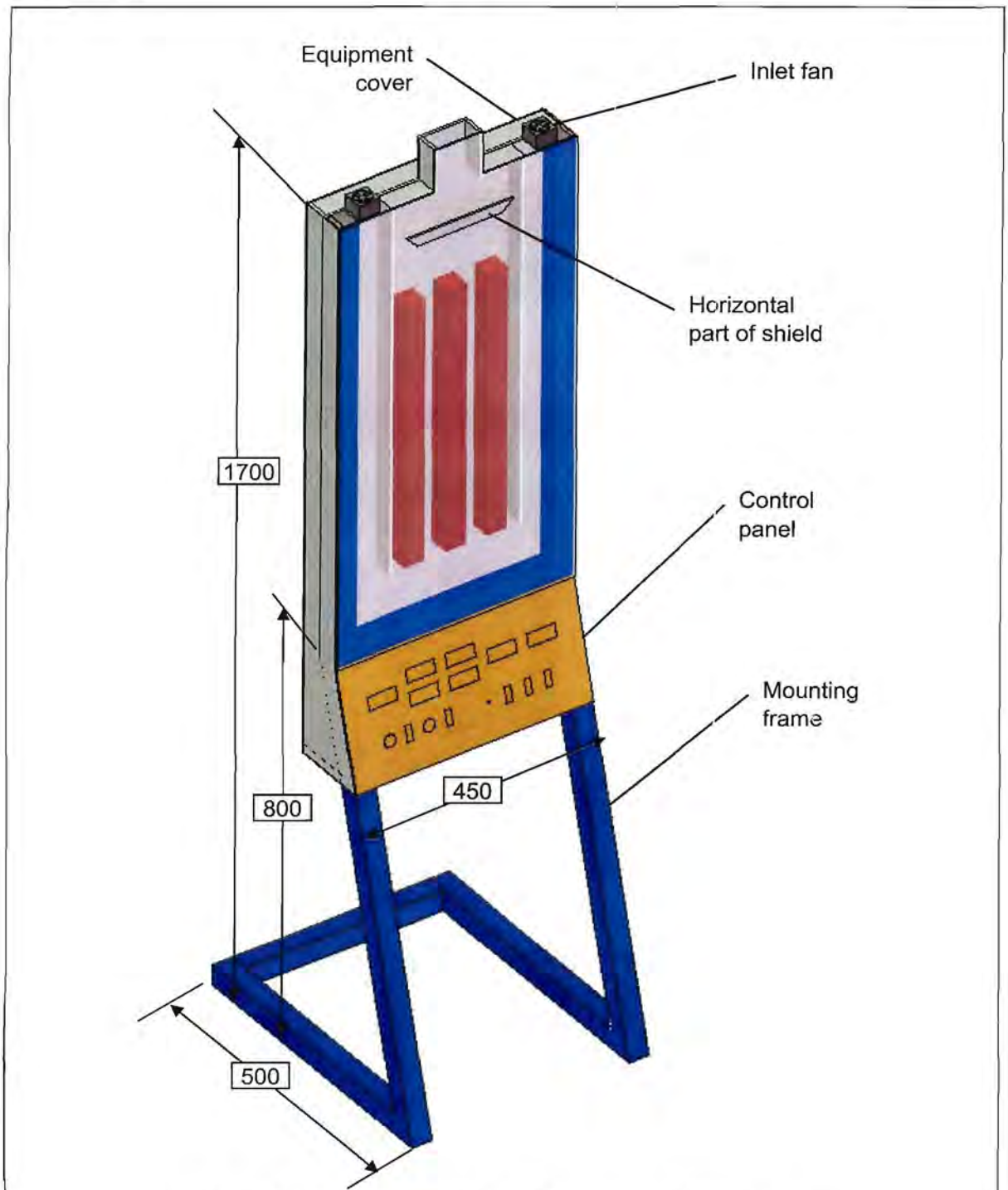

Figure 107: 3D representation of the complete test setup.

9.4 THERMAL DESIGN

A maximum temperature of 100°C was chosen for the heater surface. By using the dimensions as given in Figure 106 the heat rating of the heaters was calculated as follows:

The laminar local convection coefficient of a rectangular heated chimney is given by [81] as:

$$hc_z = \frac{Nu_z \cdot k}{z} \quad \text{with} \quad Nu_z = 0.556 \cdot Ra^{0.215} \quad \text{and} \quad Ra = \frac{g \cdot Q'' \cdot z^4 \cdot Pr}{T \cdot \nu^2 \cdot k} \qquad \{30\}$$

Q" is the heat flux per unit surface, and z is the height measured from the bottom.

The flow is assumed to be laminar, giving the friction loss factor of:

$$f = \frac{64}{Re} \quad \text{with} \quad Re = \frac{v \cdot D}{\nu} \quad \text{and} \quad D = \frac{4 \cdot B \cdot W}{2 \cdot (B + W)} \qquad \{31\}$$

B and W is the breadth and width of the flow cross section.

The buoyancy pressure caused by the heated air can be calculated for the gap between the heaters, the gap between the shield and heater, and for the chimney as follows:

$$Pboy_{gap} = \frac{1}{2} \cdot g \cdot (\rho_{in} - \rho_{air}(T_{out})) \cdot H_{heat} \quad \text{with} \quad T_{out} = \frac{Q_{heat}}{m \cdot Cp} + T_{in} \quad \text{and} \quad m = \rho_{in} \cdot v \cdot A_{gap} \qquad \{32\}$$

$$Pboy_{shield} = \frac{1}{2} \cdot g \cdot (\rho_{in} - \rho_{air}(T_{out})) \cdot H_{heat} \quad \text{with} \quad T_{out} = \frac{Q_{heat}}{2 \cdot m \cdot Cp} + T_{in} \quad \text{and} \quad m = \rho_{in} \cdot v \cdot A_{shield} \qquad \{33\}$$

$$Pboy_{chim} = (\rho_{in} + \rho_{air}(T_{out})) \cdot (H_{upper} + H_{chim}) \cdot g \quad \text{with} \quad T_{out} = \frac{N_{heat} \cdot Q_{heat}}{m_{tot} \cdot Cp} + T_{in} \qquad \{34\}$$

Note that the upper volume above the heaters is included in the chimney buoyancy equation.

The pressure loss due to flow friction can also be calculated for each flow region. A loss factor of 0.5 is taken for inlets, and 1.0 for outlets [67]. The total for a section with inlets and outlets is thus 1.5. The pressure loss due to the contraction from the upper region to the chimney is accounted for at the chimney loss. The hydraulic diameters of the various flow sections were used.

$$Ploss_{gap} = \frac{f}{2 \cdot D_{gap}} \cdot \rho_{in} \cdot v^2 \cdot H_{heat} + 1.5 \cdot \frac{\rho_{in} \cdot v^2}{2} \qquad \{35\}$$

$$Ploss_{shield} = \frac{f}{2 \cdot D_{shield}} \cdot \rho_{in} \cdot v^2 \cdot H_{heat} + 1.5 \cdot \frac{\rho_{in} \cdot v^2}{2} \qquad \{36\}$$

$$Ploss_{inlets} = 0.5 \cdot \frac{\rho_{in} \cdot v^2}{2} \qquad \{37\}$$

$$Ploss_{chim} = K_{contract} \cdot \frac{\rho_{out} \cdot v^2}{2} + \frac{f}{2 \cdot D_{chim}} \cdot \rho_{out} \cdot v^2 \cdot H_{chim} + \frac{\rho_{out} \cdot v^2}{2} \quad \{38\}$$

For passive flow, the inlet and outlet pressure is the same (if the height difference is negligibly small). This results in two pressure balance equations:

$$Pboy_{gap} - Ploss_{gap} = Pboy_{shield} - Ploss_{shield} \quad \{39\}$$

$$Pboy_{gap} + Pboy_{chim} = Ploss_{gap} + Ploss_{inlets} + Ploss_{chim} \quad \{40\}$$

By choosing a heat per element Q_{heat}, these equations can be solved simultaneously for the flow velocities in each segment. The results can then be substituted into the various equations to obtain the air and heater temperature at different positions.

In this way, the maximum heater wall temperature is found, and verified against the 100°C limit. For the case where there is no chimney and air enter at 20°C, a heat load of 15W per element results in a maximum heater temperature of 106°C. The air outlet temperature is then 45°C, and a flow velocity of 0.3m/s is generated in the gaps between the heaters.

Note that the analysis assumes that all the heat is absorbed by the air. In the actual test it was found that even with the insulation at the back and the glass front, a significant amount of heat was lost through these surfaces. It was thus necessary to increase the heater setting to achieve the desired heat input to the air.

9.5 HEATER ELEMENTS

The heaters consisted of 60W, 240V cylindrical incandescent lights, mounted inside a square aluminium tube. The light had a diameter of 30mm and was 490mm long. It fitted neatly into a standard aluminium square extrusion of 38x38mm.

The inside of the aluminium tube was painted by a heat resistant black paint, in order to improve the thermal absorption of the tube. An asbestos strip was located on the inside at the front face of the heater in order to insulate the front face from the heat. The asbestos also had an aluminium foil bonded to the side facing the light. Figure 108 shows the layout of the heater element.

For the low fill level heat input, 15W bed light units were used. They were mounted in the same manner just below the full-length heaters.

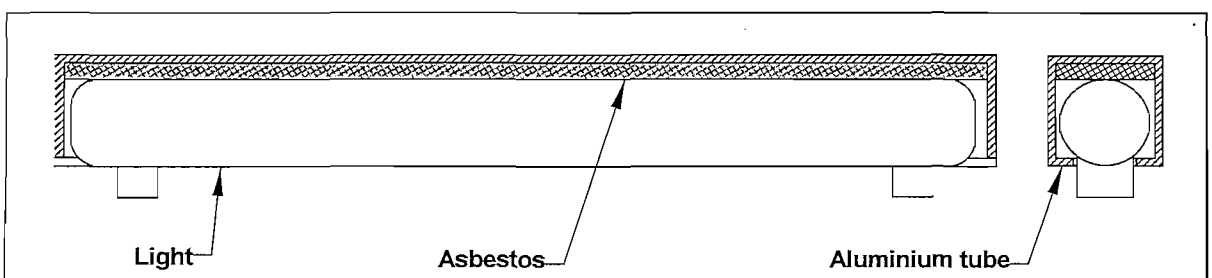

Figure 108: Layout of heater element.

9.6 TEMPERATURE SENSOR

Digital temperature sensor modules (sourced from RS catalogue # 650-728 [82]) were used. The sensor shows temperature at an accuracy of 0.1°C, with an update frequency of 1Hz and maximum displayed temperature of 70°C. Above 70°C, the display does not show any temperature, however, this does not mean that the probe failed at that temperature. It was felt that the probe could sustain temperatures up to 150°C since it is a normal bi-metal type probe.

The temperature probe was connected on extension wires and mounted inside the air stream. The temperature was measured at the seven positions as indicated in Figure 105. The measurement of the one heater element was only there to indicate the difference between the air and the heater, and did not show a reading in some scenarios.

The temperature modules had the facility to sound an alarm when a certain limit had been exceeded. This was used to warn the operator that the test may overheat.

9.7 FLOW VELOCITY SENSOR

A highly sensitive flow velocity probe was installed at the outlet as shown in Figure 105. The probe uses a hot-wire anemometer to indicate velocities with an accuracy of 0.01 m/s [83]. The instrument was used to give the audience a feel for the actual flow velocity. The display of the probe was mounted on the control panel.

9.8 INLET FANS

The inlet fans were standard 40x40mm 12V dc cooling fans used in electrical equipment. The fans were powered by a commercial 220Vac to 3-12Vdc power supply. A multi-station knob was used to select a setting from 3 to 12 V power for the fans in order to vary the fan speed.

9.9 SAFETY

The test was located in an office display area. For this reason, safety of the test was very strict.

Firstly, the power switch was a key operated type. This ensured that no unauthorised person could switch on the test.

The temperature sensors were set to sound an alarm when the air in the tube outlets reached 70°C. However, the test could sustain much higher temperatures without failure. A 150°C thermal fuse was mounted on each heater element to protect them from overheating. This was the final protection system. During a safety test it was not possible to reach the thermal fuse temperature setting, even after adding insulation to the front and the back of the test. It thus seems that the heat input from the heaters is less than the external losses, making the test passively safe.

All electrical equipment, the heaters and the frame were properly grounded to earth, and the unit had a maximum current fuse connected to the main power input. All wiring was properly insulated and hidden behind the equipment cover.

9.10 ELECTRICAL AND CONTROL PANEL DESIGN

Figure 109 shows the electrical wiring diagram of the test setup.

The maximum possible power consumption from the test is 3x60 = 180W (the fans' consumption are negligible). For a 240V source, this results in a maximum current of 0.75A. The limit for the fuse was thus chosen at 1A. The power light indicated that the switch is on, and that the fuse is working.

The dimmer switch was a commercial light dimmer. It had a capacity of 500W, and an off position. A two-way switch was used to alternate between the full-length heaters or the low fill level heaters.

Because the heaters are incandescent lights, they were used as pilot lights as well. A small hole was drilled in the aluminium tube on the front side allowing light to shine through. The intensity of the light would also be an indication of the power level of the heater.

The seven temperature indicating modules and the flow velocity probe are battery driven. They were automatically switched on when the power is turned on via a 240Vac relay.

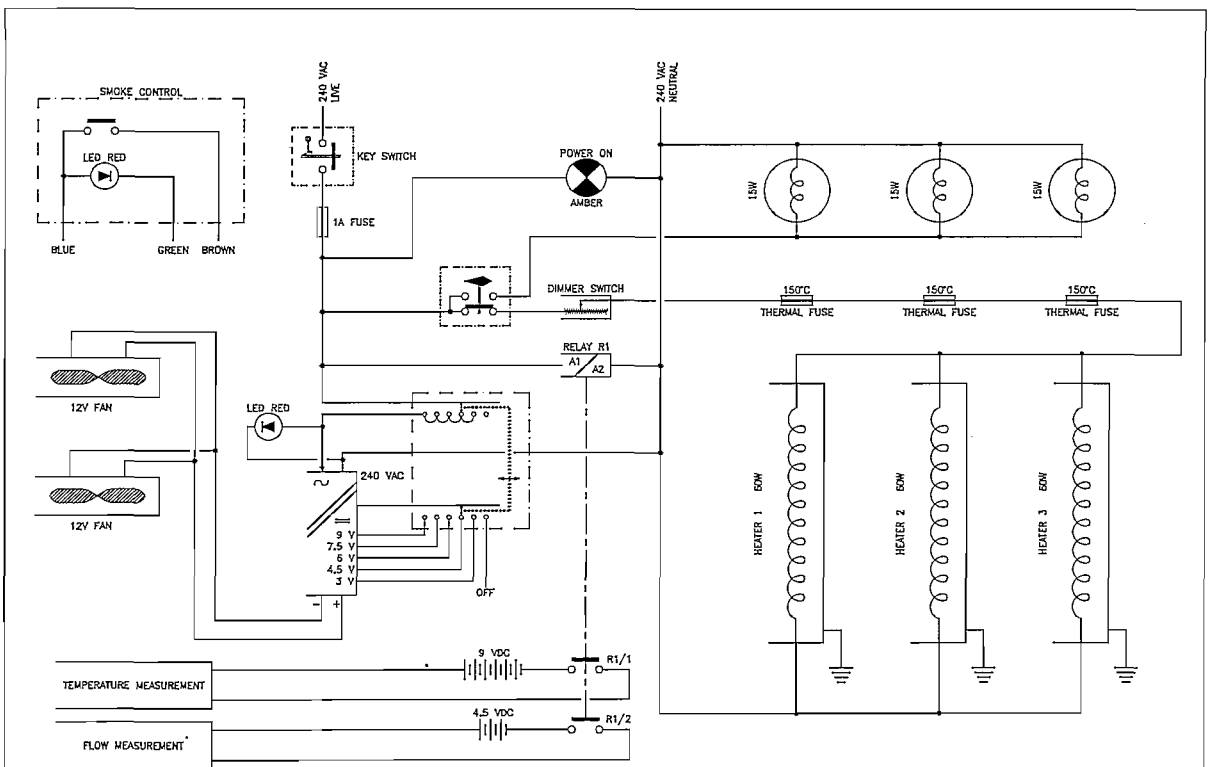

Figure 109: Wiring diagram of the test setup.

9.11 FLOW VISUALIZATION

The aim of the flow visualization was to indicate airflow streamlines showing the direction and pattern of the flow. This was achieved by means of smoke traces introduced at different points of the test setup. A commercial stage-smoke generator was used. It uses a glycerol-water mixture that is pumped through a very small heated nozzle. The result is a very dense white smoke. A pipe manifold was made to distribute the smoke to the various openings. Figure 110 shows a sequence of photos as the smoke is introduced in the air stream.

Figure 110: Sequence photos showing the smoke visualization.

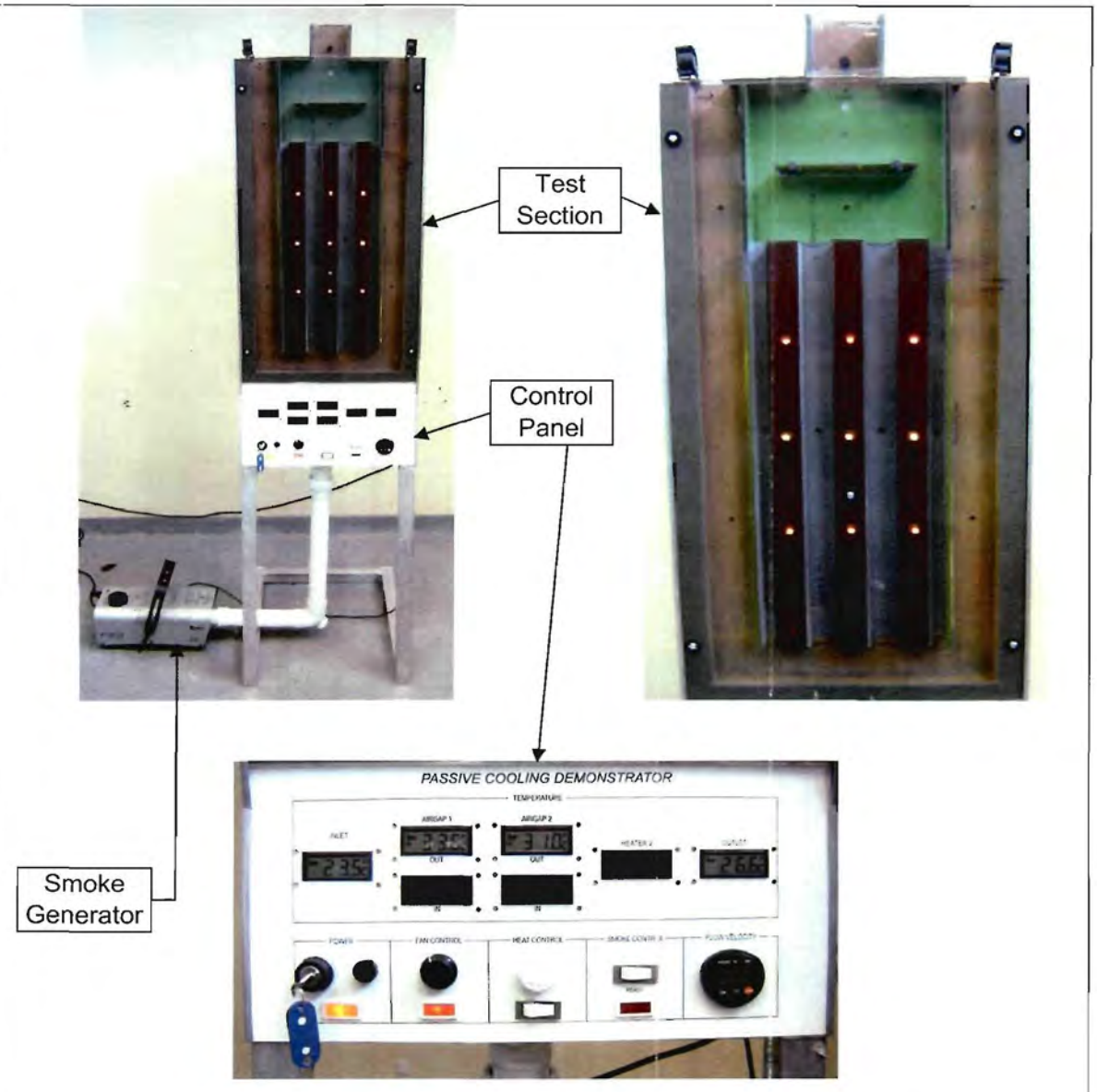

Figure 111: The completed passive cooling demonstrator setup.

9.12 TEST RESULTS AND CONCLUSIONS

The test setup was overall a great success. Figure 111 shows the complete test setup. The temperature probes clearly indicated the direction of airflow, as well as the effect of transients. With the heater at 70°C, the maximum air temperature reached 40°C with an inlet of 25°C. Flow velocities of about 0.3m/s was measured at the outlet during passive flow. This is quite a significant flow if one considers that there is only 15°C temperature difference that drives the buoyancy flow.

The smoke visualization was very useful to illustrate the effects of transients, for example, when the outlet was blocked one could see how the air stops and starts to form local circulation zones. During such a case, the air changes direction in the gap of the thermal shield, creating a circulation up through the inner tubes and down through the thermal shield gap. Another circulation zone is established in the gap between the shield and the "concrete" wall. Figure 112 illustrates what happens. The same phenomenon was seen in transient CFD analyses [84], and it demonstrates that when the outlet is blocked, the heat transfer path is naturally changed to the surrounding concrete structures. The result is a much slower rate of fuel temperature increase as was calculated for a totally insulated tank (see Chapter 9 paragraph 4.6). The moment the blockage at the outlet was removed, the flow started again in the desired direction. It took less than 3 seconds for all the smoke that remained in the test to be vented, i.e. the passive flow starts so quickly that within a few seconds it is back to equilibrium.

Another test was done where the flow was forced with the fans in the reverse direction through the test. This would represent an unfavourable pressure difference across the building. The flow was kept in reverse for sufficient time that the hottest part of the air was in the gap between the shield and the "concrete". One could argue that the flow should be able to sustain itself in that direction once the forced flow is removed, but on the contrary, the flow immediately stops when the fans are switched off and return in the "correct" direction. Again within a few seconds the passive flow is re-established. Hence, the stable reverse flow found with the Flownex analysis method could not be duplicated with this test. It may be because the Flownex model as yet do not incorporate the thermal interaction of the concrete during the reverse flow.

The test was also started from cold by switching on only the low fill level heaters. The passive cooling started on its own, and never did the air move in the incorrect direction. This is a clear demonstration that even at very low heat and fill levels, passive flow will start in the desired direction. Also, it is not necessary to "start" the flow using a fan, it can start on its own.

In conclusion, it can be said that the passive cooling demonstrator was highly successful. It proves all of the phenomena that was found from CFD analyses, and helped to convince sceptics of the reliability of the passive cooling design. The demonstrator is placed in the display area of IST Nuclear and has been shown to various local and international visitors.

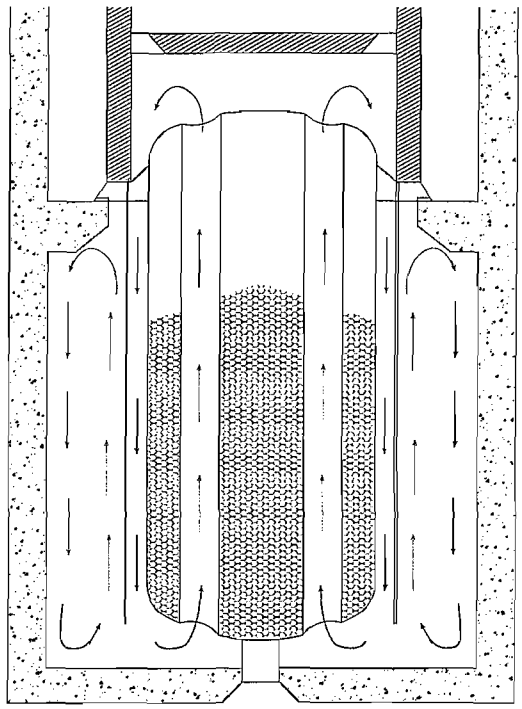

Figure 112: Flow re-circulation when the outlet is blocked.

10. STORAGE UNIT MICRO MODEL

The next step in qualifying the passive cooling is to build a complete storage unit. It is however not feasible to build a full scale test, since it will be 60m high and could cost more than what a storage unit in the demo plant would cost. In order to build a dimensionally similar model, one needs to have the Reynolds number and Grashof number similar. The problem lies with the Grashof number, as it contains a gravity term that is very difficult to scale. As a result, natural convection problems are not easily scalable.

The only option is to build a small representative model and scale the mathematics. If the mathematics (or CFD model) can predict the small model's characteristics correctly, it should be able to predict the larger model as well. One needs to be very careful in the design of the small model so that aspects such as flow transitions do not make the mathematics un-scalable to the full size.

A very important aspect to note is that one only requires a smaller model, not a scale model. The geometry need not be fully compatible with the actual case, rather, it should result in flow conditions similar to what is expected for the full scale.

The small scale test design will comprise of a tank geometry with heated tubes, a gamma shield and the chimney. The CCU is in this case of lesser importance since it is essentially bypassed during passive cooling. However, a device can be used to simulate forced flow conditions.

Several tests can be performed such as: started passive flow; non-started flow; blocked entrances; additional flow resistance; missing thermal shield panels etc. For all the tests performed, a CFD analyses should also be done and the results compared.

This test can also assist in design optimisation of some regions since it may be much faster to test an idea than to analyse it. Whether such a test will be built or not depends upon the available funds and need for further qualification.

11. CONCLUSION

A storage unit is defined that consists of the storage tank and all other components needed for the integrated cooling of the tank. The storage unit can be seen as an autonomous entity, performing all the nuclear requirements like cooling, sub-criticality etc. A storage unit can operate in four different cooling modes. The mode in which a storage unit operates depends upon the heat load inside the tank.

Each storage unit has two Cooling & Conditioning Units that performs all the cooling functions of the storage unit. It has a plate heat exchanger and bypass louvres to allow an automatic transition from active to passive mode. A CCU can be configured in a number of ways, depending upon the desired storage unit cooling mode. The CCU also conditions the air during closed loop operation with a desiccant wheel dehumidifier to minimise corrosion.

All storage units are located in the building. The inlets and outlets of the building have been designed to ensure that a favourable pressure gradient exists for all wind directions.

Because the CCUs are modular in design, the heat exchanger can be replaced or downgraded as the heat load decreases with time. The result is an optimal usage of heat exchangers over the life of the pant, as well as a reduction in total operational cost.

A new and faster method was developed to analyse the passive and transient flow of the storage unit using Flownex. This is the only feasible method to analyse the interaction of the fans and heat-exchanger with the storage tank. The method showed a stable reverse flow condition that needs to be confirmed with CFD analyses.

A two-dimensional demonstrator model has been built to prove the principles of passive cooling of the storage unit. The model was very successful and showed all the phenomena that was found using CFD analyses. As a result, it can be said with great confidence that passive cooling is a viable mode for all heat load conditions.

Chapter 11: Integrated Sphere Storage System

1. INTRODUCTION

The previous chapter introduced the concept of a storage unit. This unit fulfils all the storage related requirements. It is now time to integrate the storage unit into a complete system. At this level, the process design is performed and many of the functional requirements are met. It also includes aspects such as logistics, installation and maintenance. The result is an integrated yet modular Sphere Storage System.

2. SYSTEM HIERARCHY

The Sphere Storage System (SSS) is a sub-system of the Fuel Handling and Storage System (FHSS) and is configured to function autonomously from the FHSS or the rest of the plant. This results from the requirement to store the spent fuel for 40 years after plant operation.

Figure 113 shows a schematic diagram of the SSS. The SSS has a prominent interface via the sphere pipes with the Sphere Circulating System (SCS), which performs the core circulation and spent fuel discharge functions of the FHSS. The SSS is always available to receive spheres from the SCS, and then stores the spheres for the required duration.

Within the SSS, there are twelve storage units. These units perform the storage function and all the other nuclear safety requirements such as sub-criticality, heat removal etc. The type of storage unit depends upon the type of storage tank it contains. There are ten SFSU's normally storing spent fuel, one UFSU to store used fuel and one GRSU to store graphite spheres. The names of three storage units are historic and also for ease in the process description, as there are actually only two storage unit designs: A single line (SFSU) and a triple line (UFSU & GRSU) storage unit.

The storage units receive and return their contents via the SSS Sphere Piping from the SCS. Spheres can be redistributed from one storage unit to another by means of a movable Air Conveying Unit. Alternatively, if the FHSS is at 1MPa operating pressure (typically during plant maintenance) the spheres can also be returned to the SCS in Helium. The SSS Gas Piping is a group of all the other pipes not transporting spheres. It includes helium conveying gas lines, vacuum lines, and clean helium lines.

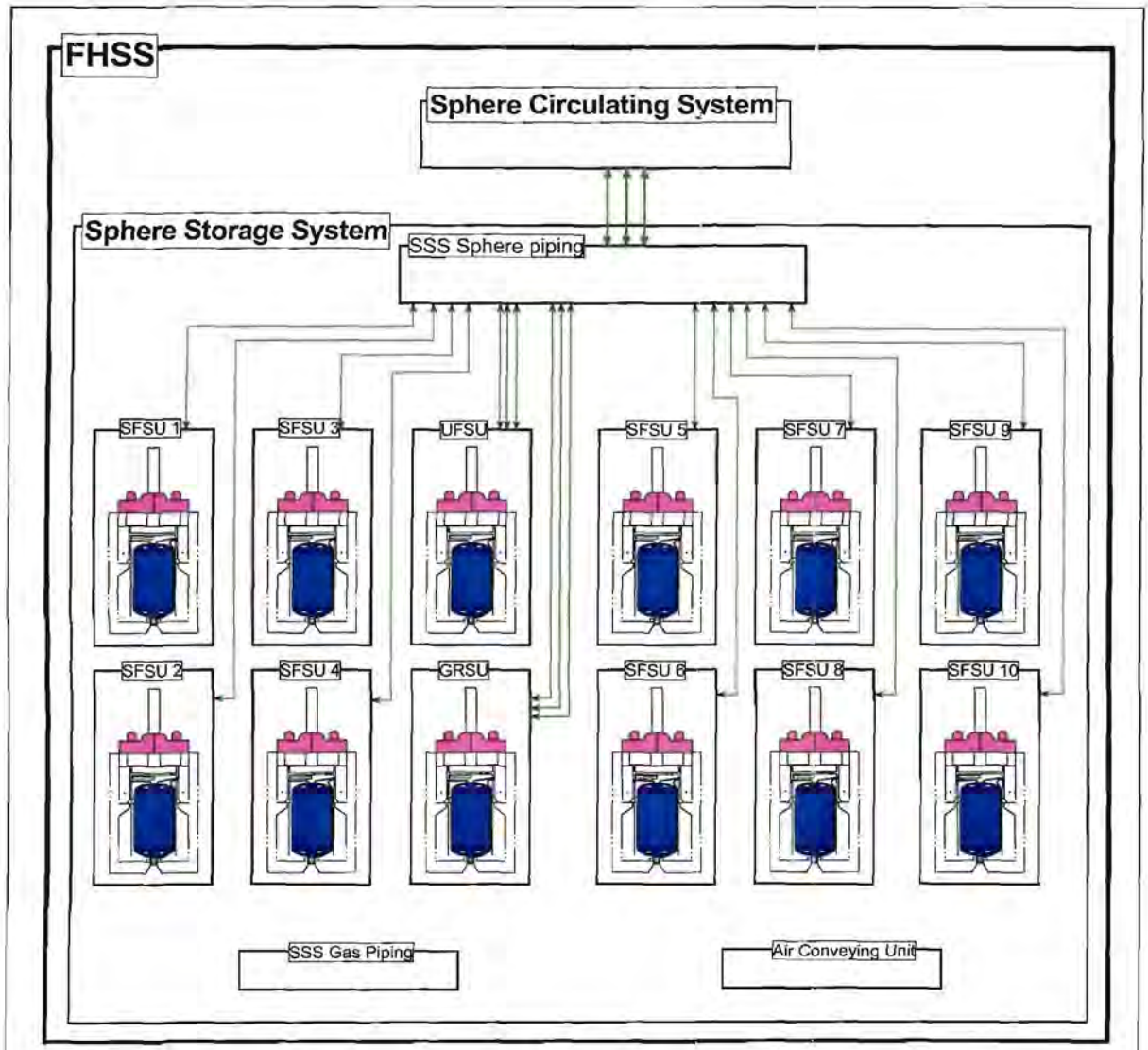

Figure 113: Sphere Storage System schematic diagram.

3. BUILDING AND SYSTEM LAYOUT

The SSS occupies the bottom rear portion of the module building. It extends from the basement of the building to two floors above ground level and it spans the total width of the building. The twelve exhaust ducts run along the rear wall of the building to the top. The ducts run on the inside of the wall, and passes through equipment rooms used for the plant HVAC and other services.

The SSS area is divided into four horizontal regions (see Figure 114 and Figure 115). At the bottom is the Lower Service Floor, then comes the Lower Tank Cavity, then the Upper Tank Cavity, and at the top is the Upper Service Floor (or also called the CCU room).

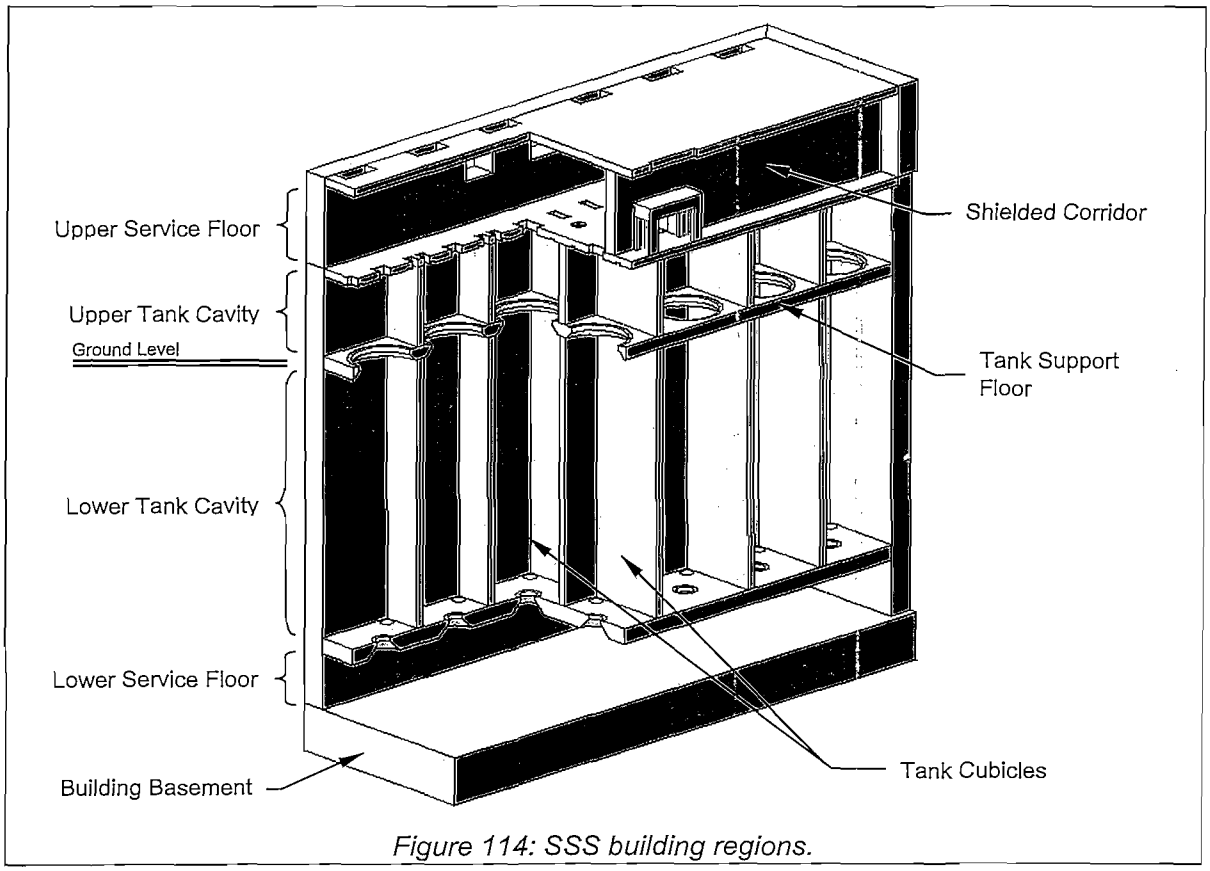

Figure 114: SSS building regions.

The Lower Service Floor area is void of any large stationary equipment. This area provides free access for maintenance to the Tank Unloading Devices on the Storage Tanks. The roof of this floor is sufficiently thick to perform radiation shielding from the tanks above.

The two tank cavities are divided by 500mm concrete walls into two rows of cubicles, containing six cubicles each, 5m x 5m in plan dimension. The two cubicles where the UFT & GRT are situated are more than 5m in one dimension. The tanks are situated on one side of these wider cubicles. This creates a gap between the CCU's at the top service floor through which maintenance equipment can move. The twelve storage tanks are supported and pass through the floor separating the upper and lower regions. This floor roughly lines up with the module building's ground level. It also serves as a radiation shield, making the top region accessible for inspection personnel.

The Upper Service Floor area contains the cooling equipment for all the tanks. It also has a shielded corridor on the one side. All the sphere distribution pipes are located inside this corridor. Controlled access is provided to this corridor via a central passageway to allow maintenance on the pipe connections.

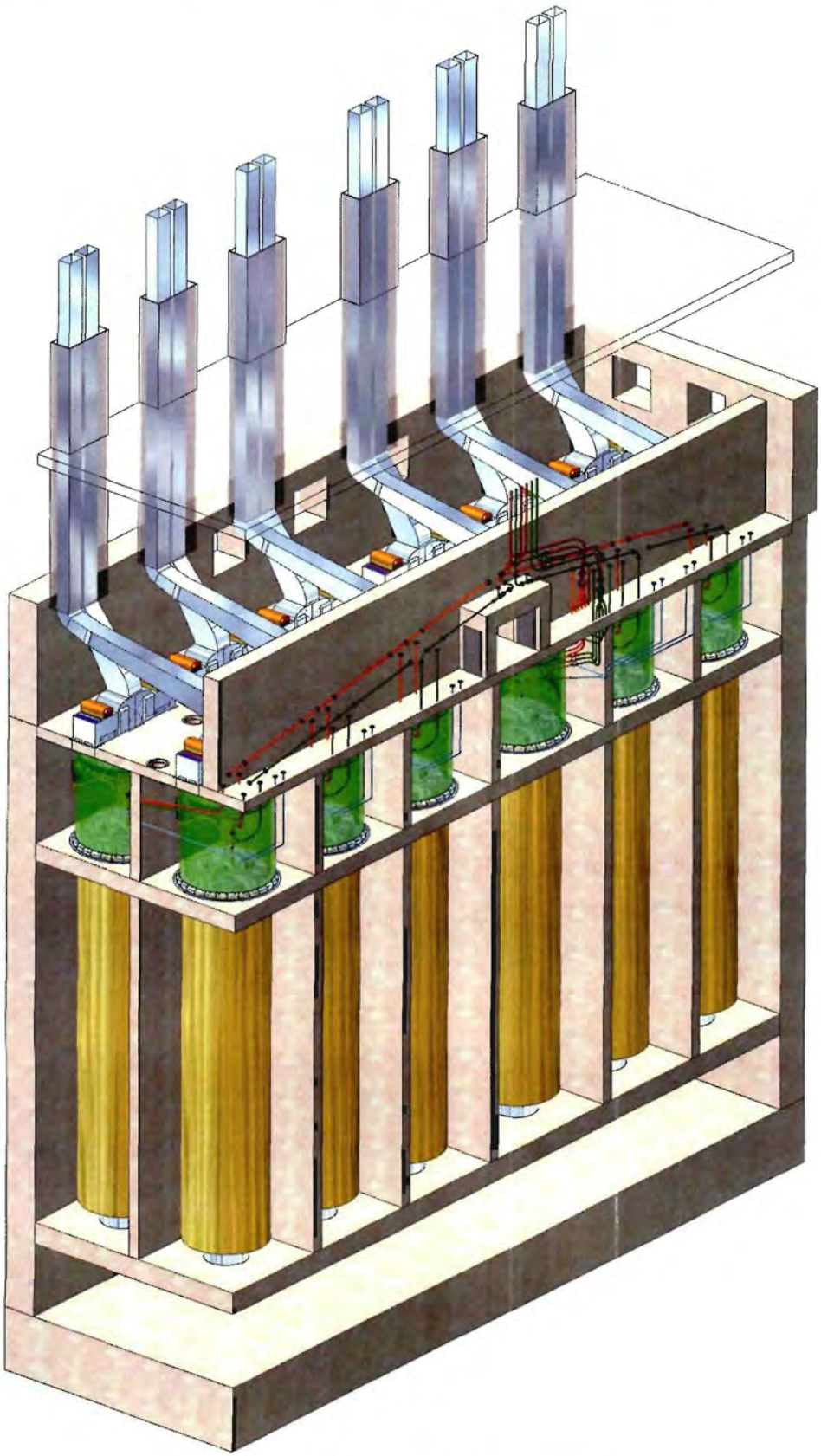

Figure 115: Pictorial view of the SSS.

4. NOVEL SPHERE PIPING DESIGN

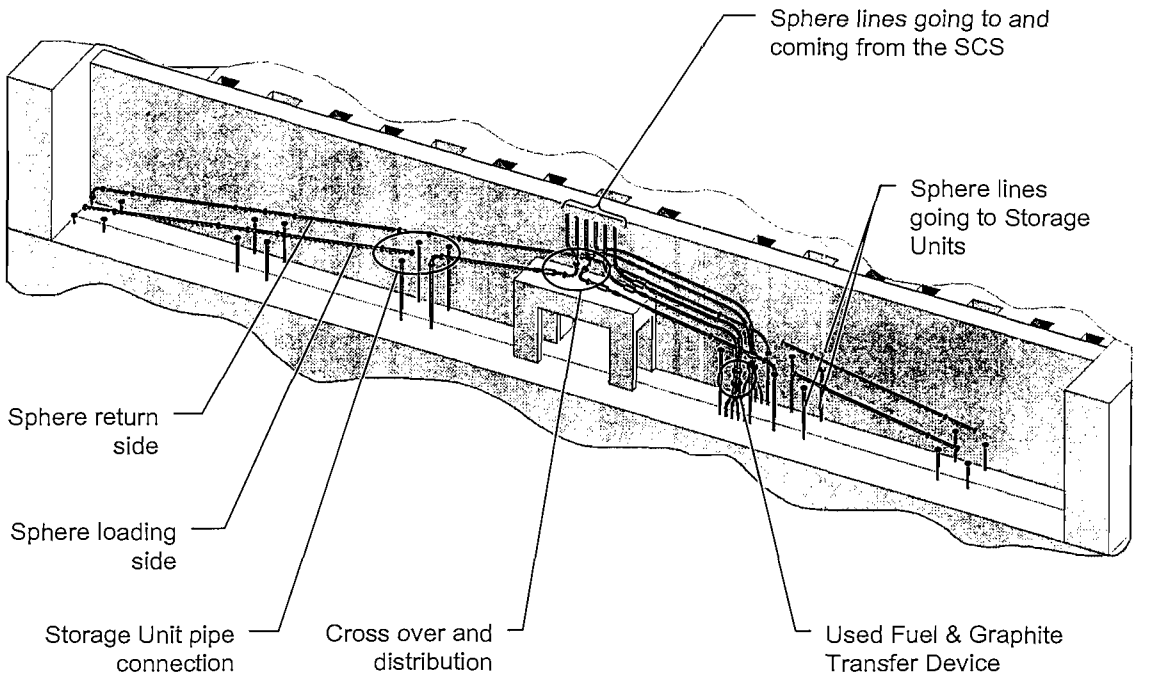

Figure 116: Physical layout of the SSS Sphere Piping.

The SSS Sphere Piping is a group of sphere pipes and connecting pieces that act in a similar manner as a railroad shunting-yard. The route for a sphere can be defined from the SCS to a Storage Tank by connecting and disconnecting different pipe sections. There are also routes between Storage Units, and return routes back to the SCS. Most of the components are situated in the Shielded Corridor at the Upper Service Floor. Once the route is defined, it is static while spheres are being transferred.

Refer to the Process Flow Diagram in Appendix H for the schematic layout of the SSS Sphere Piping. The SSS Sphere Piping is divided into two sides, a sphere loading side, and a sphere return side. In the centre, there is a cross over between the two sides. Spheres travel via gravity in the loading side, and pneumatically in the return side. Both the loading and return side pipes are at an incline of 10° with the horizontal. Most of the other sphere lines are also at 10°, but due to layout constraints, some of the return lines are less than 10°. This should not be a major problem, since the spheres are pneumatically conveyed in the return lines. The pipe is thus continuously cleaned from dust and debris. If the conveying fails, the spheres should roll easily down to the bottom of the tank where they can be extracted manually via the TUD.

Most of the bend radii on the loading side are 300mm in order to make the layout more compact. The smaller bend radius may introduce minor additional abrasion damage to the spheres, but it is not considered to present significant problems. It was however attempted to make the bend radii of the return side 650mm where possible because of the expected higher sphere velocities.

There is also a separate group of lines (defuel-refuel lines) that run directly to and from the UFSU and GRSU. These lines are in pairs, and together with the additional line from the loading or return side, the core defuel-refuel can be achieved with three sphere lines. There are transfer devices in the defuel-refuel lines that are manually changed in order to connect

to either a UFSU or a GRSU.

At the cross over region, there are inline sphere counters connected to each loading line, as well as to the return lines going back to the SCS. These counters indicate that a sphere has reached the half-way mark on its route. There are also pneumatic brake gas exit devices used to decelerate the spheres in the loading lines.

There is an electric wire attached to each pipe section. When a specific sphere route has been set up, the wires of the pipe sections are connected, creating a continuous path from the discharge point of the SCS to the receiving tank. By introducing a different voltage signal at the individual tanks, one can independently verify which tank is connected to which sphere pipe of the SCS.

The following paragraphs discuss the details of some specific regions in the SSS Sphere Piping.

4.1 CONNECTED AND DISCONNECTED STORAGE UNITS

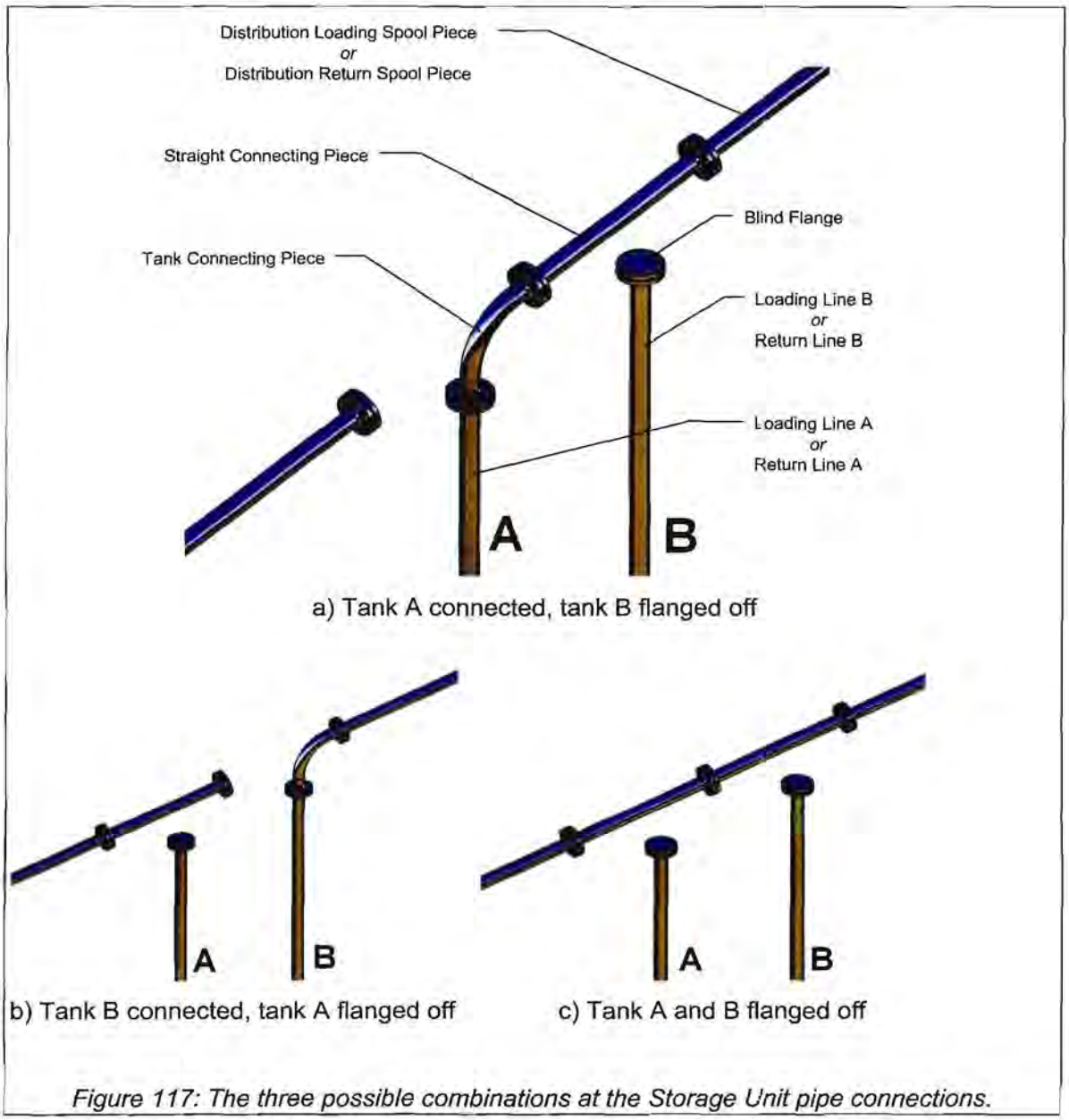

Figure 117: The three possible combinations at the Storage Unit pipe connections.

Figure 117 shows the details of a typical connection layout of the loading or return side. Both sides have the same configuration, and are connected in a similar fashion. For simplicity, only the loading side will be described. The descriptions below are valid for the return side by simply substituting the word "return" with all occurrences of the word "loading".

A loading side is made up of fixed and movable components. The first fixed component is the Distribution Loading Spool Piece. There are a number of these spool pieces mounted in line onto the wall.

Another fixed component is the sphere line going to the specific storage unit, called an SFT Loading Line X, where X denotes the number of the SFT it is connected to. There are also three GRT Loading Lines, and three UFT Loading Lines. The physical geometry of the Loading Lines differs from one another because of the different routing to the tank. See Figure 120 and Figure 121 for pictorial views of some loading lines.

The first movable component is a Blind Flange. This flange is connected to all pipe flanges that are not connected to any other sphere pipe. The Blind Flange is also used to blank the storage tanks off from any pressure source when the tanks are not in use.

Secondly, there are Straight Connecting Pieces. As the name implies, this is a straight sphere pipe with flanges at both ends. When the two adjacent storage units (A and B) are disconnected, two of these connecting pieces are used to complete the route to the next two units (refer to Figure 117c).

If storage unit B needs to receive spheres, a Tank Connecting Piece is used. This is a 300mm radius bent pipe section with flanges on both ends. If storage unit A needs to receive spheres, a Straight Connecting Piece is also needed (refer to Figure 117a&b).

All movable components stay within the Shielded Corridor, unless it requires replacement due to unforeseen damage. There are only two Tank Connecting Pieces that are moved around as the loading moves from one tank to the next.

4.2 CROSS OVER AND DISTRIBUTION

The cross over and distribution region is located in the centre of the SSS Sphere Piping. This divides the SSS Sphere Piping into a left and right side. Distribution Connecting Pieces are used to connect the different sides with each other.

The two configurations which will exist for the majority of the time are shown in Figure 118b&c. Spent fuel is discharged from the SCS to a SFSU by means of one of these configurations. The Distribution Connection Piece is orientated so as to link the correct loading side with the sphere line from the SCS.

Figure 118d shows a connection to redistribute the contents of a storage unit on the right side to a storage unit on the left. This is a typical configuration during the last 40 years storage period, when the SCS is not functioning any more. The same type of configuration will be used during decommissioning. There are four valid combinations of this type, including the one shown in the figure: left to left; left to right; right to left; and right to right.

Figure 118e shows that redistribution can also be done while loading from the SCS. Redistribution can be from any side, but only to the side not being loaded from the SCS.

The only time when the return lines need to be connected to the line going to the SCS, is during defuel-refuel mode. The configuration is shown in Figure 118a, except that the redistribution portion will not be connected.

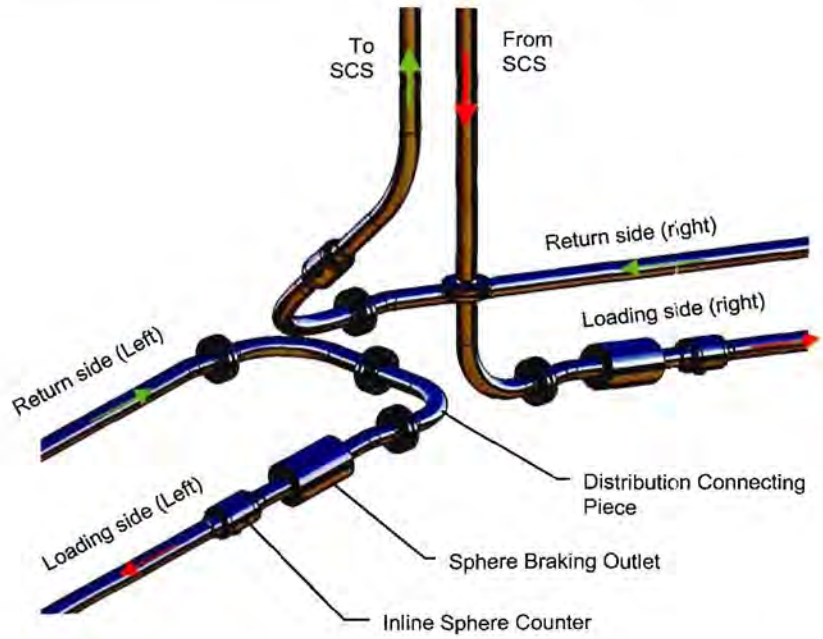

a) Loading from SCS to right side; Redistribute from left side to left side; Return from right side to SCS

b) Loading from SCS to left side only.

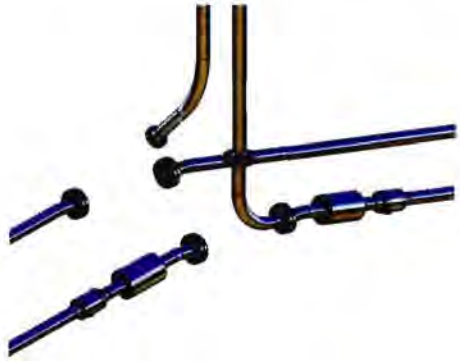

c) Loading from SCS to right side only.

d) Redistribute from right side to left side only.

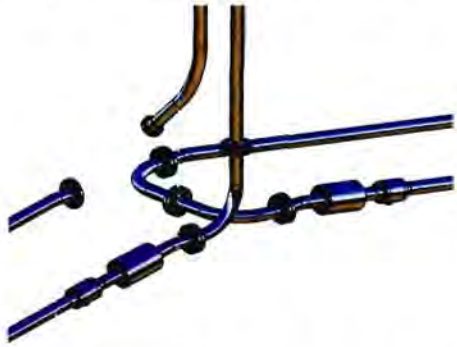

e) Loading from SCS to left side; Re-distribute from right side to right side.

Figure 118: Typical routing combinations at the cross over region.

4.3 UF & GR TRANSFER DEVICE

The Used Fuel & Graphite Transfer Device is a component used to connect two sphere lines simultaneously to the UFSU or the GRSU. This device is located at the loading and return sides of the SSS Sphere Piping. Figure 119a shows the orientation of the device in order to connect the UFSU's two lines to the required SCS lines. By rotating the device 180°, the connection is changed to the GRSU's two lines, as shown in Figure 119b. The additional two lines of the UFSU and GRSU are only needed during defuel-refuel. When spent fuel is discharged, the device will be removed, and blind flanges will blank off the UFSU and GRSU.

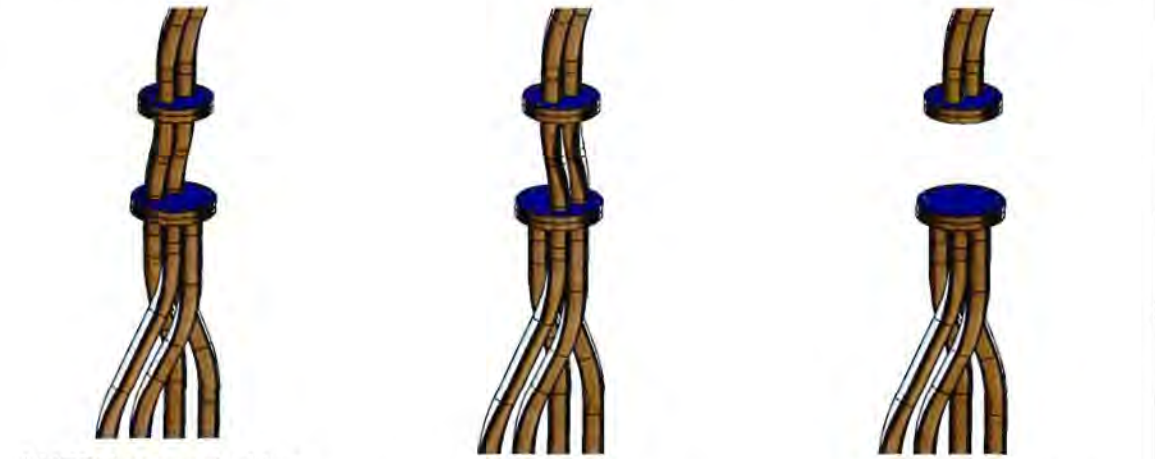

a) UFSU connected two lines

b) GRSU connected two lines

c) UFSU & GRSU blanked off

Figure 119: UF & GR Transfer Device configurations.

4.4 PIPE ROUTING TOWARDS SFSU

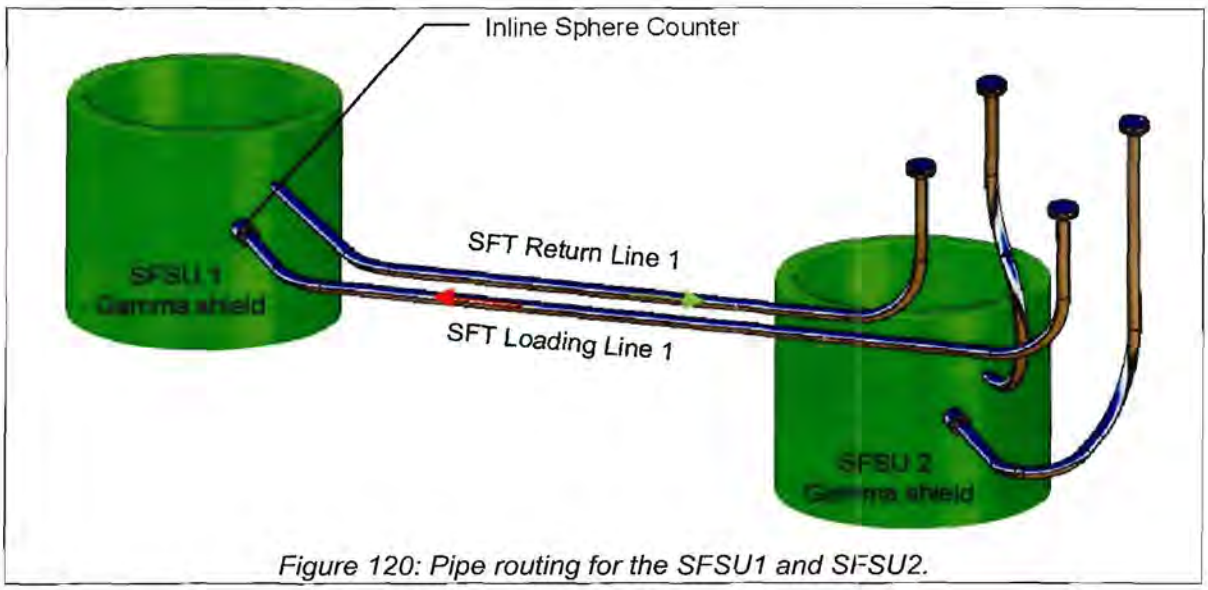

Figure 120: Pipe routing for the SFSU1 and SFSU2.

As was discussed in paragraph 4.1, the loading and return lines going to the storage units are also fixed components. Figure 120 shows the loading and return lines for SFSU1 and SFSU2. This layout looks the same for all other SFSU pairs.

The Loading Line ends at the Gamma Shield by means of an inline sphere counter. This is the last point where the spheres can be detected. Any blockage further down will not be known until the spheres have built up beyond the sphere counter. However, the pipe beyond the counter is not more than 2m long, and there are no other process elements in the pipe. The probability of a blockage is thus regarded as extremely low. When the tank is not in use, the sphere counter is replaced by a straight spool piece. Therefore, only one sphere counter is needed, which is moved along as the tanks are being filled.

The return line also comes from the Gamma Shield. However, it is not flanged via a sphere counter, rather, it is welded directly onto the Gamma Shield.

The orientation and position of the entry and exit points at the Gamma Shield is the same for all SFSU's. This simplifies the design and documentation, especially in terms of maintenance procedures of the tanks.

4.5 PIPE ROUTING TOWARDS UFSU OR GRSU

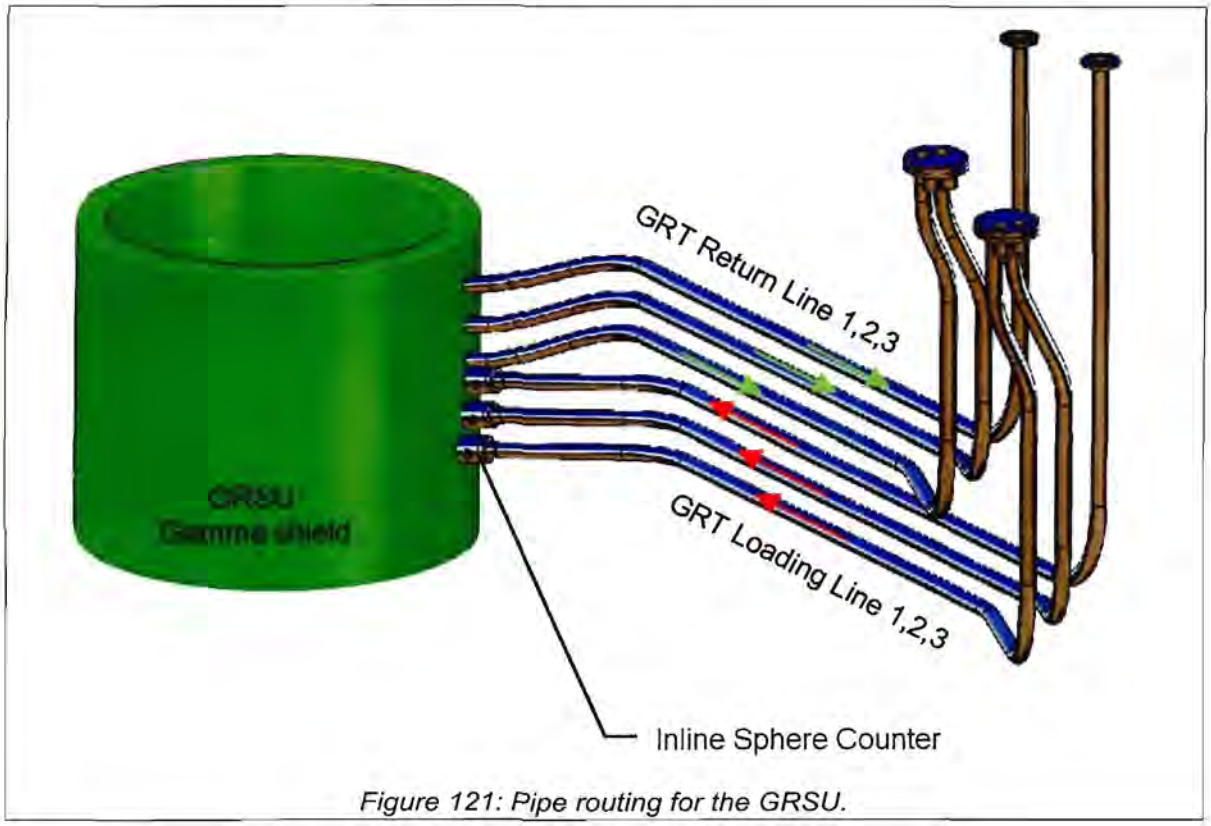

Figure 121: Pipe routing for the GRSU.

The pipe routing towards the UFSU and GRSU is, in principle, the same as for the SFSU's, except that there are three loading and three return lines for each. The loading lines are also flanged to the Gamma Shield via inline sphere counters, and the return lines are welded to the Gamma Shield.

Figure 121 shows the routing for the GRSU. It is essentially the same as for the UFSU, except that the UFSU's pipes are longer, and there are small differences due to layout constraints.

5. PROCESS AND OPERATION

5.1 STORAGE UNIT ALLOCATION AND READINESS

Before a storage unit can receive spheres, it needs to be put into a state of readiness. This is predominantly a manual action.

The first action would be to ensure that the Thermal Shield and the TUD Housing and Blank Plugs are installed. This should be done well in advance, as it takes several days to install the shield. Also, a thermal shield installation schedule should be set up that will determine the order in which tanks are filled. This is because the walls between the tanks are not thick enough to allow personnel to enter the lower tank cavity if the adjacent tank contains "fresh" spent fuel. The loading schedule shown in Figure 122 ensures that the adjacent tank's contents is always at least 3.5 years "old" (it take 3.5 years to fill a tank), or the tank is empty. It is assumed that the UFSU and the GRSU will be fitted with thermal shields from day one. Shielding calculations still have to be performed to confirm whether this loading sequence will result in sufficient shielding or not. Refer to paragraph 7.2 for the maintenance actions involved in installing the thermal shield panels.

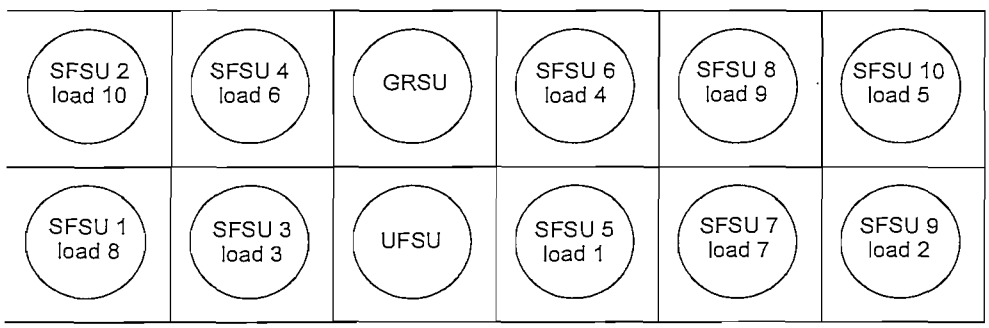

Seq.	SFSU
1	5
2	9
3	3
4	6
5	10
6	4
7	7
8	1
9	8
10	2

Figure 122: Spent Fuel Storage Unit loading sequence to be able to install the thermal shield only before loading commences.

Once the thermal shield is in place, the CCUs need to be configured for the required cooling configuration (see Chapter 10 section 5 for the list of possible flow configurations). Normally, the Storage Unit will initially be in a closed loop conditioning mode in order to protect the tank against corrosion. Configuring the CCUs for the correct cooling configuration involves, for example, the installation of the heat exchanger, fans and orientation of the louvres. The required cooling configuration and its related CCU configuration is described in detail in Chapter 10. Configuring a CCU should not take longer than 3 days if all the components are ready for installation.

The next step in bringing the Storage Unit into a state to receive spheres is to connect the sphere pipes and install the required sphere counter/s at the inlet to the gamma shield. Refer to paragraph 4 for a discussion on the different pipe connections possible, and paragraph 7.3 for the maintenance actions involved.

The operator now performs a total system check to ensure that the newly allocated Storage Unit is ready to receive spheres. The check involves as a minimum the following:

a. A pressure test;

b. Verify that the correct sphere path has been set and that the sphere counters are all operational;

c. Verify that the CCUs work properly;

d. Verify that the thermal shield and TUD housing and spindle are in place.

It might also be required that a quick commissioning test, using a few manually inserted graphite spheres, be done. The operation of the TUD and sphere counter can hereby be tested. This is however not defined as a requirement, and should be considered during Detail Design.

Only after all the required tests and verifications are completed successfully, will the Licensing Authority grant a permit to start loading fuel spheres into the tank.

5.2 RECEIVING SPHERES FROM THE SPHERE CIRCULATING SYSTEM

The dominant mode of operation of the SSS during the operational life of the reactor will be to receive spent fuel from the SCS. This will be done on a daily basis after the required quota of spent fuel was removed from the core by the SCS. Based upon the power levels, the fuel composition and the fuel target burn-up value, the number of spent fuel spheres entering the tank per day varies from about 330 to 500.

Spent fuel discharge occurs at a pressure just above atmosphere. This is because the tank is kept at a slight over pressure to indicate any leakage (refer to section 9 for a discussion on the purpose of the over pressure). However, the rest of the SCS is at the Main Power System pressure of 9MPa. A discharge pressure lock is used to create the pressure boundary (see the process flow diagram in Appendix H). This discharge lock is part of the SCS and is not controlled by the SSS.

Spheres are indexed one by one to the connected SFSU. Only when the sphere counter at the Gamma Shield has indicated that the sphere had passed, would the next sphere be indexed from the SCS. The time interval between spheres is estimated at 10 seconds, giving a total time of about 1.4 hours to discharge 500 spheres.

Spheres will also be discharged to the SSS when the reactor needs to be emptied. This operation should be done as fast as possible in order to reduce the down time of the reactor. For this reason, the SCS and the SSS are then both pressurized to 1MPa. The discharge lock is then kept open with three lines connected to either the UFSU or the GRSU. Spheres are again discharged one by one, per sphere line, into the tank.

To prevent the spheres from impacting the brake pillar inside the tank too hard and thus sustaining unacceptable damage, the spheres are decelerated using reverse gas flow. The gas enters at the pressure relief assembly that is directly connected to the tank. Inside the tank, the gas moves up into the sphere pipe (in reverse direction to the sphere movement) to the top at the SSS Sphere Piping cross over. At this point the gas is extracted using the Sphere Braking Outlet.

5.3 REDISTRIBUTING SPHERES

The TUD at the bottom of the storage tank enables one to discharge the contents of the tank into a sphere line. The spheres are then transported pneumatically using atmospheric air to the SSS Sphere Piping located in the service floor corridor. The TUD can control the time interval between successive spheres thereby ensuring that there is only one sphere per line at a time. By using the cross-over (refer to paragraph 4.2), the spheres can be loaded into

another storage tank. The counter at the cross over indicates to the TUD if the sphere has indeed reached the top or not. It takes approximately 6 seconds for a sphere to reach the top. It will therefore take about 2.5 months to move 530 000 spheres from one tank to another using 12 hour shift days.

Redistribution can be done from any tank into any other tank (including the UFT & GRT) during and after plant operation, except during defuel, refuel or core unload. However, during plant operation, the spent fuel discharge takes precedence.

A movable air-conveying unit is used to supply the redistribution air. Redistribution is performed with a closed loop (see Figure 123). The conveying gas is injected into the TUD and extracted at the Sphere Braking Outlet located in the cross over area. Reverse gas is supplied into the receiving tank and is also extracted at the Sphere Braking Outlet. This outlet has a fine screen to prevent any particles from entering the blower. It does not prevent the dust from entering the blower. The dust is simply transported through the blower and eventually into the receiving tank.

The three-way valves allow one to introduce gas at the Sphere Braking Outlet, and extract it at the receiving tank. In this way, the screen can be cleaned now and then, and the debris is transferred to the receiving tank.

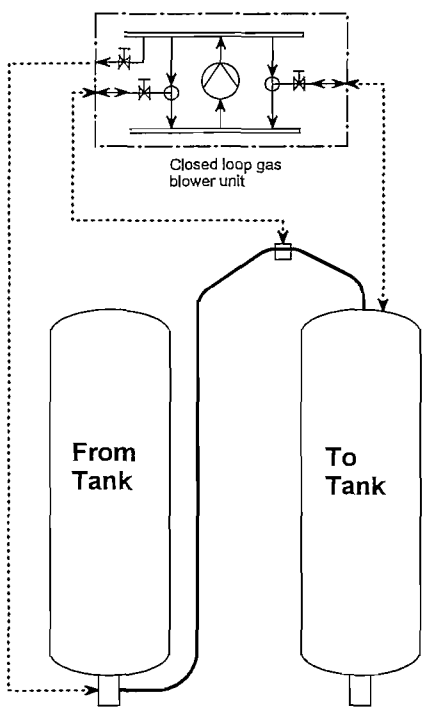

Figure 123: Schematic diagram of the air redistribution.

5.4 RETURNING SPHERES TO THE SPHERE CIRCULATING SYSTEM

Once the maintenance on the core is complete, the used fuel that was stored in the UFSU needs to be returned to the core. This operation is done in Helium at 1MPa system pressure with three sphere lines. The process is similar to sphere redistribution, except that the spheres go up further to the Charge Lock Outlet Block of the SCS.

In special instances (defuel-refuel), the core contents will be replaced by graphite, coming from the GRSU. This is done in exactly the same manner as returning used fuel.

5.5 INTERRIM STORAGE – 40 YEARS AFTER PLANT OPERATION

During the 40 years storage after plant operation, no more spent fuel is discharged and spheres need not be returned to the SCS. The only functions left is that of redistribution (which will only be done if really necessary), and to store the spheres. It is assumed that most other systems around the SSS are not operational, and that it should rely on its own capabilities to perform maintenance and redistribution. The only active components required to work during this period are the CCUs.

5.6 DECOMMISSIONING

Decommissioning of the SSS involves the removal of the spheres from the storage tanks and loading them into transport casks for final disposal. A new system will be built and installed after the 40-year storage period to perform the loading of the transport casks.

The removal of the spheres from the tanks for decommissioning is similar to the redistribution operation. The major difference is that instead of connecting a receiving tank, the pipes are connected to a line going out of the module building. Currently, the design makes provision for an exit point at both sides of the service floor corridor. However, the spheres can be discharged at any position because of the assumption that major construction will be allowed during the decommissioning phase. Any debris remaining in the tank after decommissioning has to be removed by a remote-control vacuum device.

The cask loading described in this thesis is only a conceptual design. Technology can change dramatically in 80 years, and it may well be that a different loading scheme will be used. It is also not unlikely that the spheres may be transferred directly into a processing plant before being loaded into transport containers for disposal (see Chapter 2 section 5).

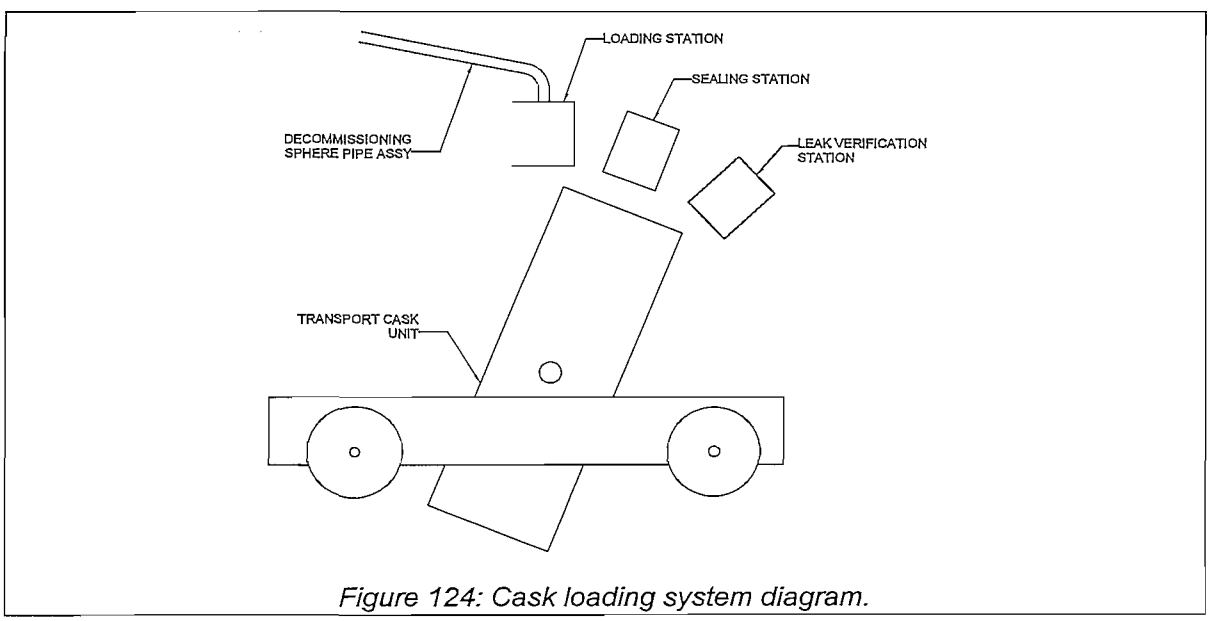

Figure 124: Cask loading system diagram.

The process of decommissioning is a repetitive operation, since there are more spheres stored in the SSS than a single transport cask can hold. The number of repetitions will depend upon the capacity of the transport cask.

In principle, the Transport Cask Unit is positioned below the filling station and locked into place. The cask is then tilted upright and the filling station locks onto the cask. The number of spheres received at the loading station and the number of spheres discharged into the cask is closely logged. Once the cask has reached capacity, the loading station disconnects and the cask is tilted to the sealing station.

The sealing station presses a lid into the neck of the cask. The lid is deformed plastically during the press operation, thereby ensuring a proper seal contact, and it is fixed in place. No bolts are thus needed. A similar method was used to seal the THTR casks [19].

The cask is now tilted to the leak verification station, where the air is extracted and replaced with helium, and pressurized. A helium sniffer is then used to verify the leak tightness of the seal. If the seal leaks too much, the cask is tilted back to the sealing station and a second lid is placed above the first lid. Leak verification is again performed. If the leak is still too much, human intervention may be required by means of remote manual operations.

Once properly sealed, the cask is lowered down, where it fits into a shielding door and gets locked in place. The Transport Cask Unit can now be moved away from the loading station area to make room for the next unit.

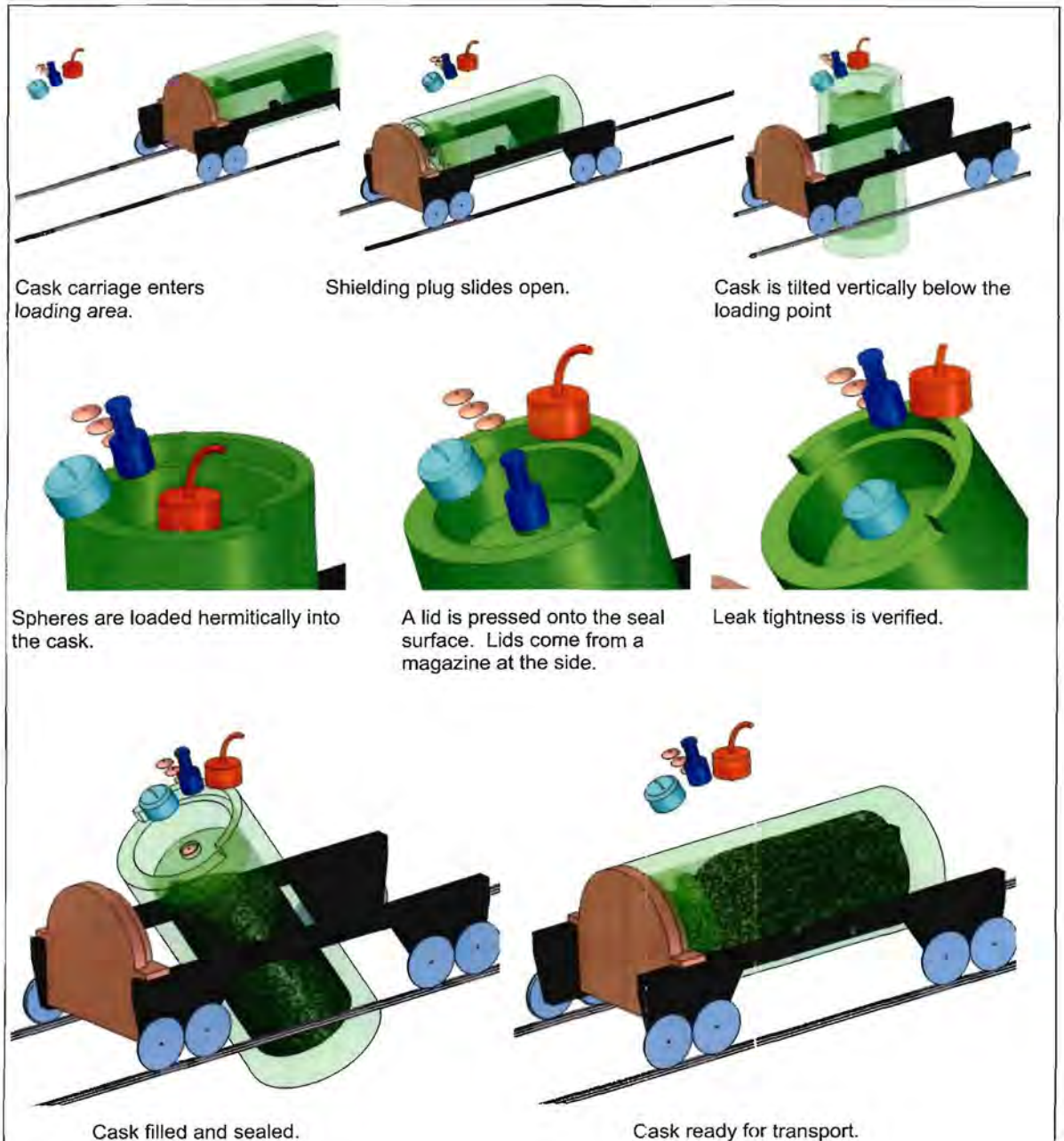

Figure 125: Graphical presentation of the cask loading process.

6. BUILDING INTERFACE AND INSTALLATION

6.1 INTERFACES

The storage unit design is specifically tailored to simplify the interface with the civil structure of the building. This is achieved by having special interface components that get cast into the concrete during wet construction. There are three major building interfaces: where the TUD penetrates the floor, where the tank is supported and the top service floor where the cooling inlets and outlets are. For each of these interfaces, a component is defined below.

TUD Floor Penetration: This penetration allows the TUD to penetrate the lower service floor. It consists of a cast-in frame and a bucket for shielding material. Radiation coming from the tank is thereby prevented from passing through the thinner region where the penetration cut-out is. There is also a bellow that connects to the TUD thereby sealing the interface but still allowing the tank to move axially. It also supports the tank in the lateral direction during a seismic event.

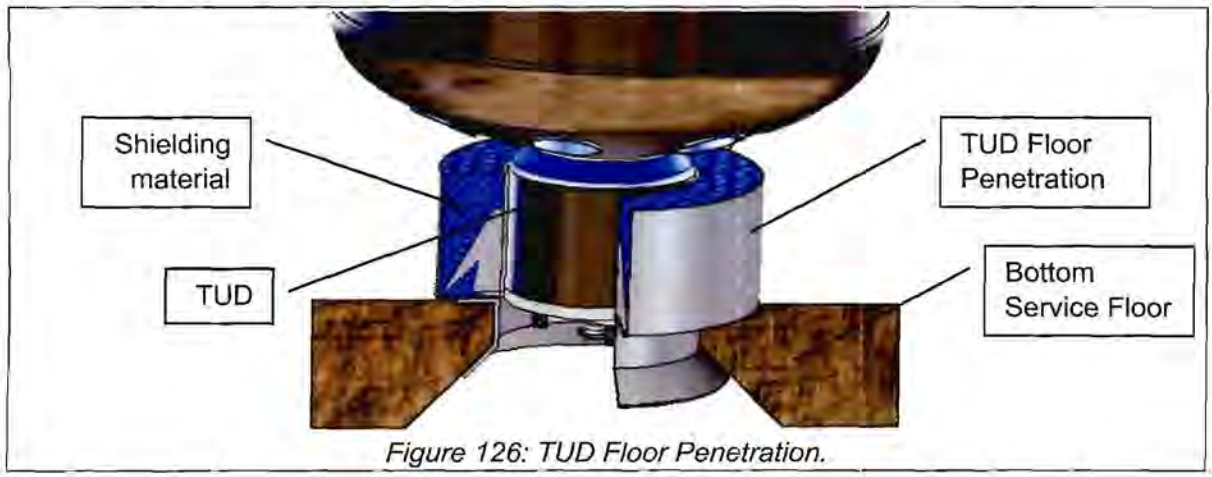

Figure 126: TUD Floor Penetration.

Tank Support Frame: The Tank Support Frame forms the physical interface between the storage tank ring support and the module building. This frame is cast into the support floor and is also welded onto the re-enforcement of the floor. The frame has a number of support pads, which can be adjusted vertically. During installation, these pads are first aligned on the same plane before the tank is lowered onto it. The pads have a slip material to allow the tank to expand radially due to temperature variations. After positioning of the tank, three clamps are placed over the ring support to retain the tank. The clamps still allow radial movement, but prevent the tank from shifting from its original centre position or to lift vertically upward.

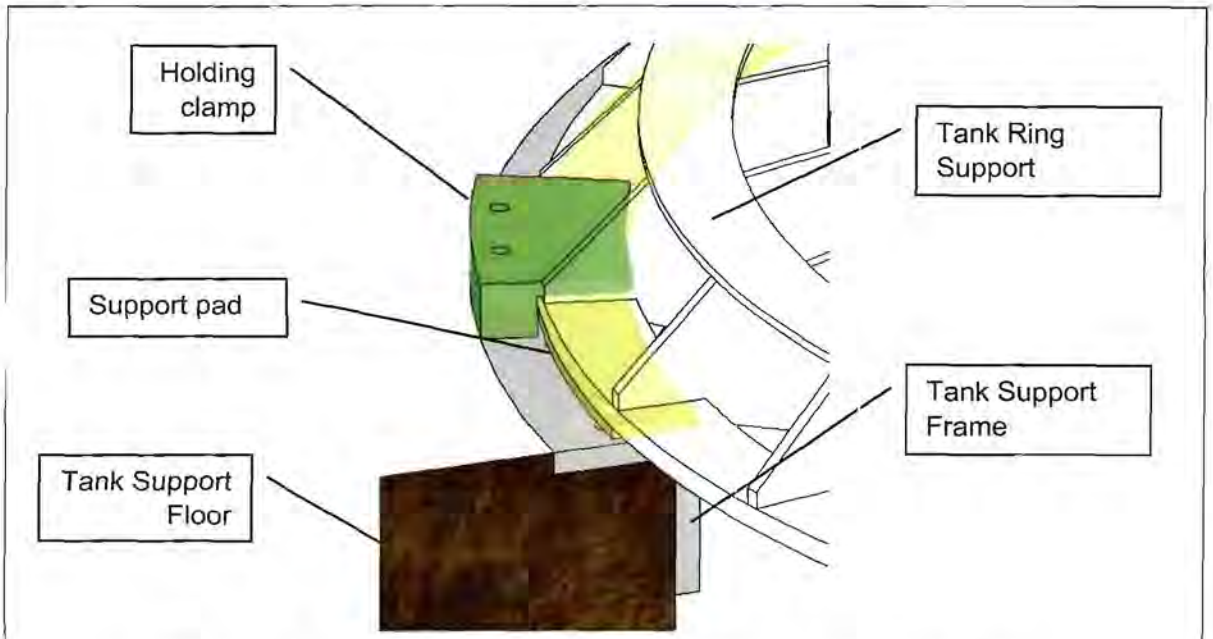

Figure 127: Tank Support Frame with support pads and holding clamp.

Top Service Floor Frame: This frame acts as the physical interface between the building and the cooling units. It contains all the mechanical interfaces required for connection of the components above the floor. The frame is a sheet metal assembly which is cast into the Top Service Floor. It thus forms permanent shuttering for the concrete during wet construction. The frame defines the inlet and outlet openings, as well as a man way to access the upper tank cavity. The frame also contains lugs that help to bond the concrete to the steel. Before installation, an initial layer of concrete will be poured onto the frame. This is to increase its stiffness so that it will not need vertical supports when the rest of the concrete is cast. Lifting lugs are provided on the frame to handle it with the initial concrete layer.

There is a crawl beam underneath the frame running around the perimeter. This beam is to assist in the installation of components and the inspection device below the floor.

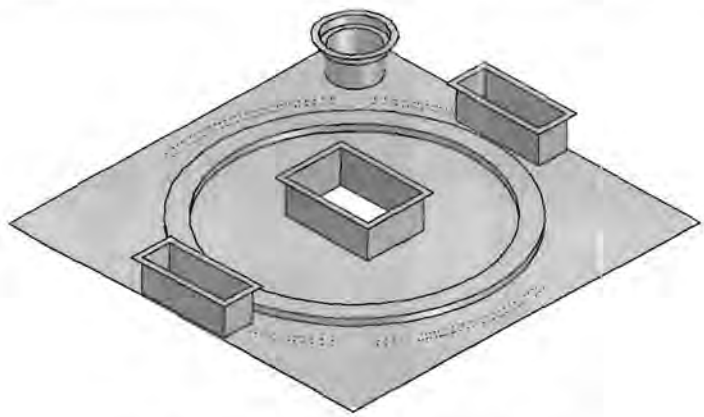

Figure 128: Top Service Floor Frame.

6.2 INSTALLATION

The principle that will be followed for the construction of the PBMR plant is that all the civil construction work has to be completed before installation of the mechanical equipment can begin. Only the significantly large components such as the storage tanks that cannot be installed afterwards will be installed during the wet construction.

The civil works will be done up to the floor above ground level. The TUD floor penetration and tank support frame should then also be installed. In the mean time, the tanks will be delivered to site at the rate that the manufacturer can supply. This means that the tanks has to be kept in storage for a period until all the tanks are delivered, and the civil construction is at the required level (Figure 129 a).

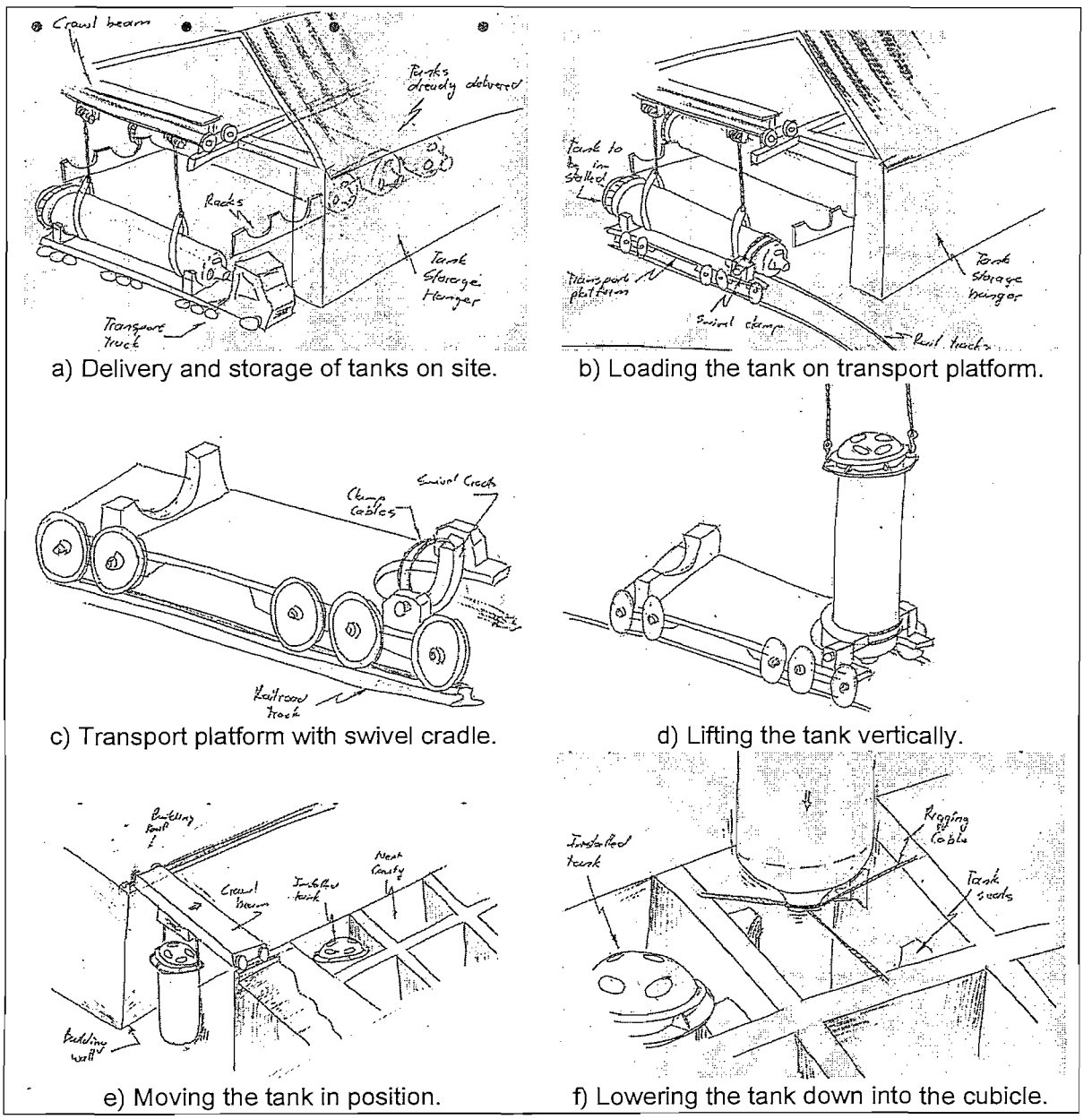

a) Delivery and storage of tanks on site.

b) Loading the tank on transport platform.

c) Transport platform with swivel cradle.

d) Lifting the tank vertically.

e) Moving the tank in position.

f) Lowering the tank down into the cubicle.

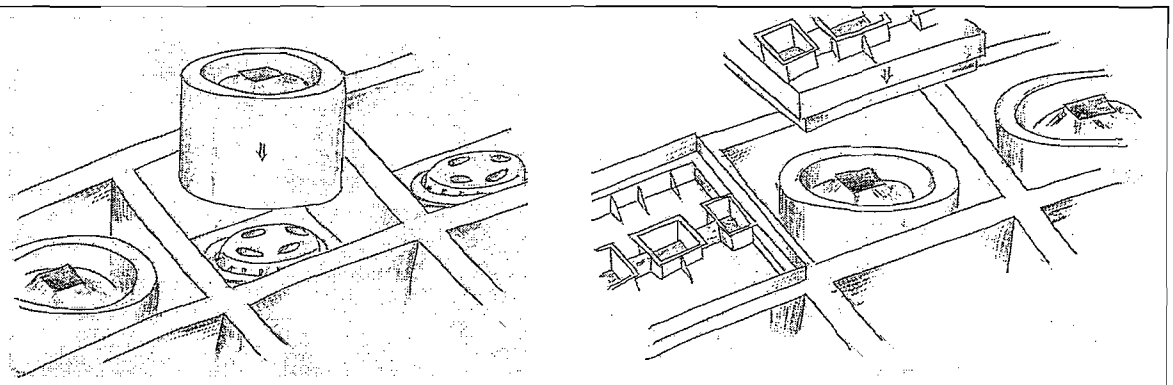

g) Installing the gamma shield. h) Installing the top service floor frame.

Figure 129: Installation sequence of the large storage unit components.

When it is time to install the tanks, they are removed one by one from the storage area and placed on a special transport platform (Figure 129 b and c) and moved next to the building. The tank is then lifted vertical from the ring support by using a crane (Figure 129 d). The transport platform has a special swivel cradle to support the tank during the lifting. The tank is then moved to the desired position above the building, and lowered into the cavity and onto the support frame (Figure 129 e and f).

After all the tanks are installed, the gamma shields are installed in a similar manner (Figure 129 g). Finally the top service floor frames are placed onto the cubicle walls (Figure 129 h). The floor re-enforcement steel is placed over the frames and the concrete floor is cast in a continuous process. The civil construction of the rest of the building can then continue.

After all the civil construction is competed, the CCUs, sphere pipes, cabling and exhaust ducts are installed.

7. MAINTENANCE AND LOGISTICS

7.1 ACCESSIBILITY

The access to the different building regions shown in Figure 114 is described below. Also refer to Figure 115 for a pictorial view of the SSS.

7.1.1 Top Service Floor

Access to the top service floor is achieved via the passage in the centre of the building on the floor above ground level. There is a door at both sides of the passage, creating an air lock that prevents the air in the service floor (which is unconditioned coastal air), from being drawn into the building, since the adjacent rooms are at a negative pressure relative to the atmosphere. Only when large equipment such as the heat exchanger is transported into the room will both doors be open.

The room is properly shielded from the radiation of the tanks and the sphere pipes, thus allowing free access to any component. Also, none of the components to be maintained in this room will be contaminated or activated. Maintenance actions at this level are no more complex than as for a standard HVAC plant room.

Because the cubicle of the UFSU and GRSU is wider than the rest, it creates a space between the CCUs. This space lines up with the passage to the room. The CCUs are placed in two rows, allowing access through the middle where a fork-lift can move.

Above the CCUs, suspended from the roof, is a crawl beam that can be used to position heavy equipment, such as the heat exchanger, during installation.

7.1.2 Shielded Corridor

Access to the shielded corridor is via doors on both sides of the passage to the top service floor. These doors will have IAEA seals in order to ensure that no unauthorised access takes place.

The corridor is 1.4m wide, and fairly crowded with sphere and gas pipes. It is therefore not possible to use large maintenance equipment in this area. For this reason the most complex maintenance action required is that of connecting/disconnecting flanges using bolts. There are also platforms and fixed ladders in order to access all the flanges.

Before a person may enter the room, the radiation inside the room is measured. If the radiation levels are too high, the pipe system will be flushed to remove any remaining debris or excessive dust. Also, both isolation valves of the spent fuel discharge lock and the valves of the reverse gas supply have to be closed.

There is a continuous supply of HVAC air to the shielded corridor that will vent out any airborne contaminants that may be released during a flange disconnection.

Access to this area is highly restricted and will be accompanied by a proper human safety assessment. One would need to enter the room every 3.5 years to move to the next storage tank, three times during the planned core unload and refuel, whenever the sphere counters fail, and if sphere redistribution is required.

7.1.3 Upper Tank Cavity

Access to the upper tank cavity is achieved via the man way located in the top service floor. This man way may also be sealed with an IAEA seal. The only portion accessible in this cavity is the region around the gamma shield. There is a walkway grid above the tank ring support to prevent a person from entering the radiation shine path coming through the ring support. No access is allowed inside the gamma shield when the tank contains fuel, nor below the walkway grid. There is however a man way in the side of the gamma shield in order to install the pipes during construction phase, as well as to insert an inspection device during operation.

Access to this cavity follows the same rules as for the shielded corridor in terms of measured activity and closed valves. It is therefore also a restricted access area, but will be accessed more frequently than the corridor due to regular inspections of the tank.

When a tank containing fuel is inspected, the CCU will remain in its current flow configuration, which would probably be closed loop active cooling. The man way will be open, and it may happen that un-conditioned air from outside is drawn into the cavity. Because of the expected short duration that the inspection will last, this leakage is felt to be acceptable. The air-conditioner will be able to restore the environment within a very short period.

7.1.4 Lower Tank Cavity

Access to the lower tank cavity is by means of an access hatch through the bottom shielding floor, in one corner of each cubicle. This hatch is large enough to be able to introduce the thermal shield panels and the installation platform. It also has sufficient shielding thickness. Removal of the hatch still needs to be clarified, as it will be a heavy component. Because the hatch only needs to be opened once or twice during the 80 years, removal could be done using a forklift.

Access to the cavity is only allowed when the tank is empty, and when residual radiation remaining in the tank is low enough. Also, radiation from adjacent cubicles should be taken into account. This can be verified by means of an activity sensor lowered down from the gamma shield above. The hatch will be locked to prevent unauthorised opening, and will have a gas tight seat to limit leakage of the purified air.

7.1.5 Lower Service Floor

The lower service floor is a large empty hall below the storage tanks. There are no dividing walls or large fixed components on the floor. Access to this floor is achieved via an opening on the reactor side of the room, in the centre at the basement level.

Maintenance on the TUD of the storage tanks is performed at this level by means of the standard FHSS maintenance equipment. It is for this reason that the floor should remain as open as possible. The connection of the movable air blower and TUD drive to the required tank is also performed at this floor.

7.2 MAINTENENACE ON EMPTY STORAGE UNITS

The only maintenance foreseen on an empty storage unit, is to make the tank ready to receive spheres (refer to paragraph 5.1).

The majority of the work entails the installation of the thermal shield panels. It is envisaged that a removable platform be installed in the tank cubicle. This platform is similar to what is used to wash large building windows. The platform covers a quarter of the cubicle, and thus needs to be moved around to complete the installation.

A batch of thermal panels will be loaded onto the platform from the access hatch in the bottom shielding floor. The platform is then hoisted to the correct position, and all the panels are installed. The platform is then lowered down, and the next batch of panels is loaded. This process is repeated until all the panels are in place.

Due to the confined space in which the installation takes place, it is being contemplated to rather install the shield before the tank is installed. This means that all the tanks will be fitted with thermal shields from the beginning. This option still needs further attention.

7.3 CONNECTING / DISCONNECTING SPHERE PIPES

In order to change the loading from one tank to the next, the pipes in the shielded corridor needs to be re-arranged (see paragraph 4). This involves the disconnection of the currently connected tank's flanges, moving the tank connection piece to its new position and reconnecting the flanges. All open flanges also receive a blind flange to close the pipe section. It might be necessary to fill the closed pipe section with helium from a bottled supply in order to protect it from internal corrosion. This operation should not take longer than 2 hours, once every 3.5 years.

During de-fuel, re-fuel or core unload operations, more actions are required to orient the transfer device, install the additional sphere counters and link the additional two pipe lines. This operation may take 8 hours, but is foreseen to happen only three times during the plant life (unloading, loading, and return to original configuration). Maintenance in this area will happen according to rigid procedures and may be monitored by the IAEA.

7.4 MAINTENANCE ON STORAGE UNITS CONTAINING FUEL

No maintenance will be done in the lower tank cavity when the storage tank contains fuel. Maintenance on the inline counter at the gamma shield and the TUD below the tank is however envisaged. All maintenance will be done using similar tools and techniques as for the rest of the FHSS.

If maintenance is required in the lower tank cavity (for example, a failure of the thermal shield panels), the storage tank needs to be emptied and its contents redistributed to another storage unit. This is not a scheduled action.

7.5 STORAGE TANK INTEGRITY MONITORING

The integrity of the storage tank will be regularly monitored with a structured monitoring programme and schedule. The monitoring will focus predominantly on corrosion but is not limited to these actions.

An inspection gantry is located below the horizontal part of the gamma shield. This gantry forms the platform for various inspection devices that will enable the operator to view or even measure more than 90% of the tank surface. Procedures to open the hatch in the gamma shield and the installation of the inspection device onto the gantry will be defined during the detail design.

The inspection may be done remotely from the upper service floor if the radiation levels around the gamma shield are above the ALARA targets. Human access is therefore only needed to install and to remove the device. There may be a stage where the radiation levels around the gamma shield are above limits for human access. This could happen during the last few months before the tank is completely full and for a duration thereafter. Detailed shielding analyses will determine the actual window during which the area will be inaccessible, or whether more shielding is required.

8. IAEA INSPECTION

The International Atomic Energy Association (IAEA) has indicated a need to have an independent inspection access to the storage tanks. This is to independently verify that the declaration of the power plant operator regarding the amount of nuclear fuel is correct. If there is a large difference, it may mean that someone has diverted some of the fuel to extract the plutonium for a nuclear weapon. It is the primary purpose of the IAEA to ensure that nuclear material is used for peaceful purposes and does not fall into malicious hands [85].

The Storage Unit design allows for four methods to verify the contents of the tank. Firstly, there are the sphere counters at the gamma shield and at the TUD. By keeping track of the amount of spheres that has entered and exited the tank, one can accurately determine the amount of spheres in the tank. However, this does not mean that the spheres actually contain nuclear material. To verify that the contents of the tank do contain nuclear material, there is an IAEA activity sensor access pipe running inside the cubicle. This pipe is 110mm in diameter, and is open at the tank's end. The fill level and gamma radiation can be

measured to determine the contents of the tank.

Thirdly, it is possible to hook up to the temperature sensor in the storage tank. An independent estimate can be made of the fill level of the tank by looking at the temperature gradient along the tank's length. The fourth option is to make use of the inspection gantry. A device can be connected to the gantry that will allow inspection of the exterior of the tank. A typical measurement would be the gamma radiation or neutron flux as a function of height at different positions around the tank and inside the tubes. This will be a good representation of the contents and volume of the tank.

9. CONTAMINATION CONTROL

The PBMR fuel spheres have a very good contamination retention ability. It was proven through several tests that significant contamination release only occurs at temperatures above 1600°C [24]. Below this temperature, very low releases occur due to small failures in the fuel kernels and diffusion.

A preliminary estimate was done by PBMR to quantify the accumulated airborne activity inside a storage tank for the 80-year storage period. The estimate showed that the maximum ^{85}Kr release that could occur would be 0.011% of the Annually Authorized Discharge Quantity [86]. Anything below 1% need not be reported, therefore a gas leak of a storage tank will not present a contamination release of note.

The major contamination is actually situated in the graphite dust inside the tank. To release significant amounts of dust into the air requires a large break in the storage tank. In order to identify a leak before break at an early stage, the tanks are stored with helium at a pressure of maximum 10kPa above atmosphere. The pressure difference due to temperature fluctuations is not important and thus no active pressure control will be done. More helium will however be added to the tank should the pressure drop too much. This helium originates from a helium bottle. Any leakage of the helium will be noted by the CCU's instruments and the origin can thus be found.

10. CONCLUSION

The twelve storage units are connected to each other and the SCS by using sphere pipes. The pipes are arranged such that all the functional requirements of loading, redistribution and returning of spheres are fulfilled. The layout of the building separates the SSS into four regions. The tanks occupy the middle two regions. Above and below these are service rooms containing all equipment that requires maintenance.

Spent fuel spheres are loaded into a tank at atmospheric pressure via a pressure lock. Used fuel spheres are loaded at 1MPa system pressure to eliminate the need for a pressure lock. The spheres can be redistributed from one tank to any other tank using air in a closed loop circulation. The same process is followed for decommissioning after the 80-years of storage, except that the spheres are loaded into a transport cask. This cask is sealed and its leak tightness verified before the next cask is loaded.

All interfaces between the storage units and the building have been captured in mechanical structures that are cast into the concrete. This allows for accurate alignment during the installation process. The storage tanks and gamma shields will be installed half-way during the wet construction of the building. All other components will be installed after the civil works are completed.

Maintenance on empty tanks entails the installation of the thermal shield and other

components to get the tank ready to receive spheres. Once it contains spheres, only the region around the gamma shield in the upper tank cavity is accessible from where the tank can be fully inspected. All other maintenance intensive components are placed either above or below the tanks where radiation shielding is provided by the concrete floors.

There are four ways is which the IAEA can verify the tank contents: by making use of the sphere counters of the FHSS, by checking an external tube in the tank cubicle, from the temperature measurement, or lastly from the inspection gantry below the gamma shield.

The tanks are kept at a slight pressure above atmosphere in order to sense a small leakage of the tank. Preventative action can then be taken to ensure that no contamination release to the atmosphere will occur.

Overall the Sphere Storage System performs all the nuclear and functional requirements. It is an integrated, modular and optimised design solution for interim storage of nuclear fuel.

Chapter 12 : Closure and Recommendations

1. NUCLEAR SAFETY

This section is a summary of the aspects driving nuclear safety of the SSS. In each case, an indication is given whether it is a Defence-in-Depth (DiD) aspect, As Low As Reasonably Achievable (ALARA), a conservative safety margin (SM), or a passive safety feature (Passive).

1.1 CONTAINMENT

- The storage tanks are pressure vessels, thus preventing any radioactive elements from escaping the SSS (DiD).
- The low fuel temperature (< 400°) ensures that minimal contamination diffuses through the kernels (ALARA).
- Spheres can be redistributed from any tank to another tank, or even removed at an early stage should there be a problem on the storage tanks (DiD).
- The GRT can be used as an additional SFT if more storage capacity is required (DiD).

1.2 CRITICALITY

- Criticality under optimum water moderation of the tank is 0.85, which is well below the 0.95 requirement (SM).
- Burn-up credit is taken as 40GWd/tu for all storage tanks, which is 20% below the average burn-up of the core (SM).
- Criticality is maintained by means of the geometry of the tank only (Passive).

1.3 MAINTAINING SPHERE INTEGRITY

- The tanks are in a closed loop conditioned air environment, minimising corrosion and thus protecting the fuel from being exposed to oxygen (ALARA).
- Although the tank is made from 16mm steel, only 13.5mm is required to withstand the internal pressure. This leaves a 2.5mm inherent corrosion allowance on the tank (SM).
- The mechanical brake, TUD and sphere pie bends are all designed to minimize sphere damage (ALARA).

1.4 DECAY HEAT REMOVAL

- The active cooling system can be switched to passive mode during a power or

component failure. Cooling is thus guaranteed at all times (Passive and DiD).

- The CCUs are semi-redundant, and one can operate even when the other has failed (DiD).
- The maximum fuel temperature is below 350°C during normal conditions, which is 50°C below the specification (SM).

1.5 RADIATION PROTECTION

- The gamma shield around the top of each tank allows access to the tank cubicle without excessive exposure (ALARA).
- The service floors above and below the tanks are properly shielded to such an extent that it can be accessed without any time constraint (ALARA).
- Maintenance actions required to connect/disconnect the pipe flanges are minimal and not very frequent (ALARA).

2. FUNCTIONAL PERFORMANCE

The SSS is designed to perform all the necessary functions. This is mainly achieved through a novel pipe distribution layout. It allows a large range of sphere routes to be defined, and can even perform some functions simultaneously. The closed loop air conveying ensures that the SSS can redistribute spheres during the last forty years of storage when all other support systems of the FHSS are shut down.

3. OVERALL COST EFFICIENCY

Several formal manufacturing quotes were obtained for the different components of the SSS, but due to the sensitivity of the commercial plan of the PBMR, the actual costs may not be given in this document. However, the cost efficiency of the design can still be described using qualitative arguments.

To minimise cost was a major driver in all the design aspects of the SSS. Not only capital cost, but also operating and decommissioning costs were taken into account. As a result, the SSS is a life cycle cost optimised system. This can be seen in the choice of a closed loop cooling instead of using very exotic and expensive materials for the tanks. Also, by having a passive fallback ability, the CCU is not safety-related, hence much cheaper.

The total capital cost can also be kept at a minimum by only installing the TUD's major components and thermal shields when needed. Also, the option to down-grade the cooling ability of the CCUs by replacing the heat exchangers results in a minimum capital cost.

When compared with a traditional "spent fuel pool" and an interim storage facility, the SSS is certainly the most cost-effective storage system for nuclear fuel.

4. DESIGN MATURITY

The basic design of the SSS presented in this thesis addresses all design drivers applicable to a spent fuel storage system of a nuclear plant. Sufficient attention has been given to the design drivers in order to verify the feasibility of the integrated system.

The design therefore has sufficient maturity so that detail design of the main components can continue. There are still a few of outstanding issues that need to be addressed by means of detail analyses or tests. The basic design of the major components has sufficient margins for improvement should these analyses show a problem. It is therefore not foreseen that major obstacles, causing a return to concept phase, will be encountered during the detail phase.

5. RISK STATUS

The following paragraphs discusses issues that may be perceived by the reader as a potential risk, meaning the level of uncertainty is such that there is a high probability that it may significantly influence the project cost, timescales or feasibility.

Public acceptance of the SSS: The question whether the public and the nuclear industry will accept the SSS design is raised frequently. Storage of spent fuel is and always will be a big argument against nuclear power. The philosophy followed for the PBMR spent fuel storage is unique in the world. This means that the industry looks upon the design with an uncertain frown, regardless of the amount of proof presented for its safety. This uncertainty is mainly due to a fear of the unknown, and it is the responsibility of PBMR to change the public, and industry's perception as to what entails safe storage of PBMR-type spent fuel.

Guaranteed passive cooling: Passive cooling of the storage tanks has up to now been calculated by StarCD, Fluent and FlowNex. These are all numerical analysis software, which implies that the results are directly coupled to the analysis model and method of solving. The question is whether one can base the safety case on computer simulations alone. It is a known fact that passive cooling by means of natural convection is not a simple calculation, and computer codes may present inaccurate results. However, natural convection is widely used in industry for passive cooling, and there are a number of design principles to follow if one wants to rely on passive cooling. These principles have been fully incorporated in the cooling design of the storage units and were demonstrated with the passive cooling demonstrator model. The other cooling tests such as the tank convection tests and storage unit micro model are thus aimed to validate the computer software, and to increase the accuracy of the analysis.

Guaranteed storage life of 80 years: Very few mechanical components are designed for a service life of 80 years. It is therefore reasonable for someone to question if it is actually possible to guarantee the life of the storage tanks for 80 years, especially in the harsh coastal environment at Koeberg. With the closed loop cooling design, one could eliminate the corrosive elements from the air. The corrosion tests already showed favourable results although there is still a large amount of tests to be done. It is felt that the design has the capability to maintain the tank integrity for 80 years. The only risk remaining is that the operating cost may be more than initially expected if the corrosion tests indicate that impurities other than water and NO_x needs to be removed, or if the tanks should be cooled by an inert gas like pure nitrogen for example.

Maintenance and accessibility of the storage tanks: There is the perception amongst some circles that the maintenance and accessibility of the storage tanks may not be feasible, or could result in unacceptable exposure to workers. This is to an extent true, since maintenance on the tank will not be easy. However, it was attempted to arrange the storage unit such that maintenance will be possible. Also, components requiring frequent maintenance have been placed in accessible areas. There is the possibility that workers may be exposed to unacceptable dose rates if cognisance is not taken of the contents of a storage tank and its adjacent tanks. A correct loading sequence for example, will ensure that radiation from adjacent cubicles does not affect the accessibility to the tank. Detailed

shielding calculations, still outstanding, will determine the allowable time and duration to access the area around the gamma shield.

6. SUMMARY OF THE CONTRIBUTIONS OF THIS STUDY

This study has made a large number of contributions to the PBMR project as a whole. The contributions are summarized below:

1. This study presents the first bulk storage design for spherical nuclear fuel elements. It is unique in the world, but still performs all the nuclear and functional requirements. A patent has been registered by PBMR Company titled "Storage of Nuclear Fuel" [87]. This is an indication of the uniqueness and value of the design.
2. A unique design is presented for the spent fuel tanks, which is the first bulk storage container design for spent fuel. The tank can hold about 530 000 spheres, and forms the final containment barrier of harmful fission products.
3. A new device called the mechanical brake was developed and tested to load the spheres into the tank. The device has no moving components, yet has the ability to reliably load the tank from the bottom without allowing the spheres to drop more than 1m before impacting the bed.
4. Another unique device was developed and tested to remove the spheres from the tank when needed. The device has a highly controllable and reliable discharge characteristic without damaging the spheres. This is a feature that has not been possible with any other unloading concept investigated in the past for unloading tanks containing spherical material.
5. A novel algorithm has been developed to calculate the optimum spacing of absorber rods in a storage tank. Although it was not used for the final criticality design, it is still a valuable tool for other storage designs.
6. The tank's unique geometry with tubes on the inside creates a passive way to keep the fuel sub-critical. The burn-up credit is taken such that the full contents of the core can be stored in any tank. It is thus not necessary anymore to have two types of tanks, one for the spent fuel and one for the used fuel. This reduces the licensing, qualification and manufacturing exercises to one storage tank design only.
7. The cooling tubes inside the tank and the thermal shield around the tank create well-defined cooling flow paths. With this geometry it was possible to develop a new and very fast method to calculate the temperatures inside the tank. The method is a combination of finite element analysis techniques and analytical equations. Without the technique, it would not have been possible to perform the vast amount of sensitivity calculations with CFD alone within the time frame of the study. The method is thus a valuable tool for thermal analysis, and can be extended to many other applications where the external flow can be described using analytical calculations.
8. The corrosion protection design of the tank is a highly cost-effective solution for 80-years storage. Most other storage systems make use of very thick stainless steel or concrete containers. Instead, a low cost, thin carbon steel tank is proposed, without any coating. The cooling air is conditioned such that minimal corrosion occurs on the tank. The preliminary corrosion tests have indicated that this is a valid solution.
9. The storage unit layout presents a way to automatically change from a closed loop active cooling mode to an open loop passive cooling mode. This way there is no need to have a safety-related active cooling system. It has been shown to be highly

reliable, and the principles could be expanded to other active cooling systems as well.

10. A new method was developed to calculate the passive cooling flow at a fraction of the time it takes CFD analysis. The method approximates the storage tanks and other flow paths as a pipe network system. This enables one to also include flow characteristics of the heat exchangers and blowers of the storage unit in order to calculate actual mass flows for the system. This is not easily done using CFD analyses. The method can also be linked to the FEA method to determine tank temperatures during transients.
11. A highly integrated, yet modular design is presented for the total storage system. It contains twelve storage units that are able to operate autonomously from one another. All aspects such as accessibility, maintainability, process operation, decommissioning, contamination control and IAEA access are provided for. Future PBMR designs can make use of the storage unit design as-is and simply add the required number of storage units based upon the expected fuel consumption.
12. The unique sphere pipe routing design provides a high level of functional flexibility to the SSS. It is possible to load spheres to any tank, extract it from any tank and transfer it to any other tank or even back to the reactor. This is achieved by simply moving pipe segments from one place to another.
13. This study presents a cost-effective solution for initial and interim storage of spent fuel for the PBMR.

7. RECOMMENDATIONS AND FUTURE WORK

It is recommended that the design as it is presented in this thesis be used for the storage of the spent and used fuel of the PBMR demontration module. Detail design of the main components should continue, and the few uncertainties and outstanding issues should be resolved. This includes full-scale tests of some of the mechanical components such as the TUD and mechanical brake to obtain more reliable performance characteristics. Also, the corrosion tests should be continued, and the effect of radiolysis should be quantified. Thorough radiation shielding analyses are also required to verify the accessibility to the tanks and maintenance intensive components.

The pipe convection tests should also be done to validate the CFD analysis, and to add more accuracy to the FEA technique. If the budget permits, the proposed storage unit micro model should also be built.

Future research should investigate the feasibility to store water reactor fuel in a similar manner by making use of the principles and philosophies followed in this design. The concept of rectangular storage tanks should also be re-investigated as it presents a more compact storage than the cylindrical tanks. Most of the components and analysis techniques developed in this study can still be used.

It is also suggested that the design be advertised to other countries currently involved in the development of a pebble bed-type nuclear reactor. This design can be used as-is for any reactor design, due to its modularity and standardised components. The more reactors there are that make use of this design, the lower the cost will be for components such as the storage tank and CCU.

REFERENCES

Due to the nature of the PBMR project, some references listed below are not available in the public domain. These include internal documents generated by the PBMR company and IST Nuclear, as well as reports obtained through a technology transfer transaction with Germany. The reader may request these documents from the document control centre of PBMR. Note that PBMR may decline the request based upon the confidentiality of the information contained therein.

The address of PBMR's Document Control Centre and other primary sources of references are provided in the table below:

PBMR (Pty) Ltd. Document Control Centre PO Box 9396 Centurion 0046 South Africa	**IST Nuclear, a Division of IST Holdings** PO Box 95355 Waterkloof 0145 South Africa	**Manufacturing and Materials Technology Division, CSIR** PO Box 395 Pretoria 0001 South Africa
M-Tech Industrial (Pty) Ltd PO Box 19855 Noordbrug 2522 South Africa	**Forschungszentrum GmbH Jülich** D-52425 Jülich Germany	**Westinghouse Reaktor GmbH** PO Box 105063 D-68140 Mannheim Germany

[1] *Website of PBMR company*; https://www.pbmr.co.za/; October 2004

[2] *Press statement by the Minister of Public Enterprises*, Mr Alec Erwin; Sunday Times; 24 October 2004.

[3] *PBMR Demonstration Power Plant Development Specification;* PBMR (Pty) Ltd. Internal document; PP100-000554-4325; Rev 3.

[4] *PBMR Main Power System Development Specification;* PBMR (Pty) Ltd. Internal document; MS000-013473-4325; Rev B.

[5] *IAEA Safety Standard Series : Design of Fuel Handling and Storage Systems for Nuclear Power Plants*; IAEA; VIENNA; NS-G-1.4; 2003.

[6] *IAEA Safety Standard Series : Design of Spent Fuel Storage Facilities*; IAEA; VIENNA; STI/PUB/976; 1994.

[7] *FHSS Development Specification*; PBMR (Pty) Ltd. Internal document; MF000-016062-4325; Revision 1.

[8] *Basic Licensing Requirements for the Pebble Bed Modular Reactor*; National Nuclear Regulator; South Africa; LG-1037; Rev 2.

[9] *ALARA Safety Philosophy Document*; PBMR (Pty) Ltd. Internal document; 012364-34; Rev. 4.

[10] *PBMR Defence-in-depth Guidance Document*; PBMR (Pty) Ltd. Internal document; LC120-017062-4635; Rev 1.

[11] *Nuclear Technology Review*; International Atomic Energy Agency General Conference; GC(48)/INF/4; 16 July 2004.

[12] *Long term storage of spent nuclear fuel - Survey and recommendations*; IAEA; VIENNA; IAEA-TECDOC-1293; May 2002;

[13] *Introduction to Nuclear Engineering*; John R. Lamarsh; Third Edition; Prentice Hall; 2001

[14] *The problem of used nuclear fuel: lessons for interim solutions from a comparative cost analysis*; Allison Macfarlane; Energy Policy vol. 29 (2001); pp 1379-1389;

[15] *GNB Castor brochures*; Gesellschaft für Nuklear-Behälter mbH; Holle Street 7A; D-45127; Essen.

[16] *Japan's first High Temperature Engineering Test Reactor of JAERI*; Nuclear Engineering and Design; Vol. 233; 2004.

[17] *IAEA Power Reactor Information System (PRIS) web site*; http://www.iaea.org/programmes/a2/index.html; November 2004.

[18] *The Chinese High Temperature Reactor HTR-10, The First Inherently Safe Generation IV Nuclear Power System*; Nuclear Engineering and Design; Vol. 218 (2002); October 2002.

[19] *THTR 300 Data pack*; IST Nuclear Document Control Centre; South Africa;

[20] *The Long Term Storage of Radioactive Waste: Safety and Sustainability*; IAEA; VIENNA; IAEA-LTS/RW; 2003.

[21] *Half Life – The lethal legacy of America's nuclear waste*; National Geographic; pp 2-33; July 2002;

[22] *Deep-Burn: making nuclear waste transmutation practical*; C. Rodriguez et al.; Nuclear Engineering and Design; vol. 222 (2003); pp 299–317.

[23] *A Cost effective bulk storage design for the PBMR spent fuel*; W. F. Fuls; Potchefstroomse Universiteit vir Christelike Hoër Onderwys; Potchefstroom; August 2004.

[24] *Performance of HTR Fuel Samples under High-Irradiation and Accident Simulation Conditions, with Emphasis on Test Capsules HFR-P4 and SL-P1*; W. Schenk, R. Gontard, N. Nabilek; Forschungszentrum Jülich GmbH.

[25] *Fuel Performance and Fission Product Behaviour in Gas Cooled Reactors;* IAEA; VIENNA; IAEA-TECDOC-978; November 1997.

[26] *Release of Noble Gases and Halogens from the PBMR Core*; K. Röllig, a Westinghouse Reaktor GmbH report; GBRA 052 336; 2001.

[27] *Decommissioning graphite cores containing significant amounts of stored energy*; B. J. Marsden; C504/003/95; AIMechE; 1995.

[28] *ASME Boiler and Pressure Vessel Code*; Section VIII; 1998.

[29] *ASME Boiler and Pressure Vessel Code*; Section III; 1998.

[30] *Studies in the geometry of random packing*; JD Bernal & JL Finney; University of London; UK.

[31] *Investigation on the friction coefficient of graphite in the presence of different lubricants, measured on a single sphere;* Prof. Schulten et al.; a THTR 300 research report; 750-230 BE 1916; Jülich; 27 February 1969.

[32] *Self-Welding Results Database in a Helium Environment*; PBMR (Pty) Ltd. Internal document; 008264-34; Rev A.

[33] *Measurement of the friction coefficient of graphite on graphite*; Dr. Lange, Dr. Pfeiffer; a THTR 300 research report; 750-210 BE 1088;Jülich; 10 October 1967.

[34] *Friction coefficient of 9mm steatite spheres*; Mergler; a THTR 300 research report; 422-211 BE 2724;Jülich;14 August 1989.

[35] *LabVIEW 7 Express*; National Instruments; www.ni.com/labview

[36] *Mechanical Measurements*; Beckwith et al.; Fifth Edition; Addison-Wesley Publishing Company, Inc.; July 1993.

[37] *Dimensional analysis for engineers;* E.S. Taylor; Claredon Press; Oxford; 1974.

[38] *Practices and developments in spent fuel burn-up credit applications*; Proceedings of an Technical Committee meeting held in Madrid; IAEA; VIENNA; IAEA-TECDOC-1378; October 2003.

[39] *Spent Fuel Tank Criticality Results*; PBMR (Pty) Ltd. Internal document; MF000-DIT000292-4585; 2003/10/16.

[40] *Confirmation of the UFT criticality using the latest geometry and burn-up credit specification*; PBMR (Pty) Ltd. Internal document; PP350-DIT-000426-4585; March 2004.

[41] *Comments on the Materials Selection for Spent Fuel Storage Vessels for the proposed PBMR Power plant at the Koeberg Site*; a CSIR contracted report; Manufacturing and Materials

Technology Division; number 010150; August 2002.

[42] *Excitation in the Radiation Chemistry of Inorganic Gasses*; C. Willis and A. W. Boyd; International Journal of Radiation Physics Chemistry; 1976; Vol. 8; pp 71-111.

[43] *Low Dose-rate Radiolysis of Nitrogen : Yield of Nitrogen Atoms, N(4S) and N(2D,2P)*; R. Glen Macdonald and O.A. Miller; International Journal of Radiation Physics Chemistry; 1985; Vol 26; No. 1; pp 63-72.

[44] *Literature Review of the Effect of Radiation on Corrosion Processes in Air and Calculations of Nitric Acid Radiolysis Yields*; a CSIR contracted report; Manufacturing and Materials Technology Division; number 020216; December 2002.

[45] *Spent fuel storage vessel material selection*; IST Nuclear internal document; FH-B-000000-189/5; Revision A.

[46] *Principles of Materials Science and Engineering*; WF Smith; 2nd Edition; McGraw-Hill; 1990.

[47] *ASHRAE Handbook : Fundamentals;* American Society of Heating, Refrigerating and air-Conditioning Engineers; 1997.

[48] *Growth of Salt and Acid Aerosol Particles in Humid Air*; A. Schenkel and K. Schaber; Journal of Aerosol Science; Vol. 26; No. 7; pp. 1029-1039; 1995.

[49] *Calculation of the Dew Point of Nitric Acid*; a CSIR contracted report; Manufacturing and Materials Technology Division; number 68DB / HT522; November 2002.

[50] *Environmental Conditions for Process Measurement and Control Systems : Airborne Contaminants*; IEEE Specification; ISA-S71.04-1985.

[51] *Corrosion protection Guidelines for Mechanical and Civil Works*; PBMR (Pty) Ltd. Intemal document; PP100-008212-4410; Revision 1.

[52] *Progress Report on: Corrosion Tests on Potential Fuel Storage Vessel Materials*; IST Nuclear internal document; FHD1-000005-34/3; Revision B.

[53] *ASME Boiler and Pressure Vessel Code*; Section IID; Subpart 1; Table 1A; 1998.

[54] *Code Requirements for Nuclear Safety-Related Concrete Structures*; ACI 349; 1990.

[55] *The Finite Element Method in Mechanical Design*; C.E. Knight; PWS-KENT Publishing Company; 1993;

[56] *Strand7 finite element analysis system*; G+D Computing; Version 2.3.2; www.strand7.com; 2004.

[57] *Star-CD*; Prostar v3.150.012 and STAR v3.150A.011; CD Adapco Group; www.cd-adapco.com; 2004.

[58] Fluent; v6.1.18; Fluent Inc.; www.fluent.com; 2004.

[59] *VDI-Warmeatlas: Berechnungsblatter fur den warmeubergang*; Verein Deutscher Ingenieure; Dusseldorf; 4th Print; 1984.

[60] *Basic Heat and Mass Transfer*; A.F. Mills; Irwin; 1995.

[61] *Convective heat transfer*; L.C. Burmeister; John Wiley & Sons; 1983;

[62] *Convective heat and mass transfer;* Second Edition; W.M. Kays, M.E. Crawford; McGraw-Hill Publishing Company; 1980.

[63] *Convection heat transfer;* A. Bejan; John Wiley & Sons; 1984.

[64] *Heat transfer;* J. Taine, J. Petit; Prentice Hall; 1993.

[65] *Heat transfer;* M. Jakob; John Wiley & Sons; Volume 1.

[66] *Heat transfer in turbulent mixed convection;* B.S. Petukhov, A.F. Polyakov; Hemisphere Publishing Corporation; 1988.

[67] *Fluid Mechanics*; F.M. White; 2nd Edition; McGraw-Hill; 1988.

[68] *A CFD evaluation investigating the effect of thermal radiation from the fuel spheres to the tank inner wall;* PBMR (Pty) Ltd. Internal document; 00353; October 2001.

[69] *UFT : CFD thermo-hydraulic report*; PBMR (Pty) Ltd. Internal document; 015867/2A; Rev 1A.

[70] *Sphere Storage Area CFD Result Report*; PBMR (Pty) Ltd. Internal document; MF000015106-3130; Rev A.

[71] *UFT : CFD thermo-hydraulic report*; PBMR (Pty) Ltd. Internal document; 015867/1; Rev A.

[72] *Aluminium Plate Heat Exchangers for Heat Recovery in Ventilation Systems*; Hoval PWT; Handbook for Design, Installation and Operation; Hw99aE3; June 2001.

[73] *Z Duct Plate Heat Exchangers*; Des Champs Laboratories Inc.; www.deschamps.com; 2002.

[74] *Heat Exchanger Quote*; Des Champs Technologies; 0207139-B.MF; August 2002.

[75] *Koeberg Site Safety Report*; Chapter 7 Meteorology; Rev 0; Eskom; 1997.

[76] *ASHRAE Handbook : HVAC Systems and Equipment*; American Society of Heating, Refrigerating and air-Conditioning Engineers; 2000.

[77] *Honeycomb wheels and desiccant options*; Munters Corporation – Dehumidification Division; www.muntersamerica.com; 2000.

[78] *PBMR Plant Building External Effect of Wind on Pressure Distribution*; PBMR (Pty) Ltd. Internal document; T000029; Rev A.

[79] *FHSS Storage Tanks Pressure Drop Optimization CFD Report*; PBMR (Pty) Ltd. Internal document; MF000-025850-3130; Rev A.

[80] *Flownex*; V6.5; M-Tech Industrial (Pty) Ltd; www.flownex.com; March 2004;

[81] *Heat and fluid flow resulting from the chimney effect in a symmetrically heated vertical channel with adiabatic extensions*; A. Auletta, O. Manca; International Journal of Thermal Sciences; Vol. 41; 2002.

[82] *RS Components SA*; www.rssouthafrica.com; April 2004 – March 2005.

[83] *Measuring stick for velocity*; Testo 405-V1.

[84] *Fuel Storage Tanks Transient CFD Analysis*; PBMR (Pty) Ltd. Internal document; T000088; Rev A.

[85] *Statute of the IAEA*; www.iaea.org/About/statute_text.html#A1.12; As amended on 28 December 1989.

[86] *Spent Fuel Tank Fission Product Content: First Estimate*; PBMR (Pty) Ltd. Internal document; MF100-015585-3340; Rev 1.

[87] *Storage of Nuclear Fuel*; Dry Bulk Storage of Spent Fuel – Case 71; V16453; Adams & Adams Patent Attorneys; Pretoria; South Africa; September 2004.

[88] *Studies of Mixed Convection in Vertical Tubes*; JD Jackson et al; International Journal of Heat and Fluid Flow, Vol. 10, No. 1; March 1989.

[89] *Local heat transfer in a vertical gas-cooled tube with turbulent mixed convection and different heat fluxes*; JV Vilemas et al; International Journal of Heat and Mass Transfer; Vol. 35, No. 10, pp 2421-2428; 1992.

[90] *New correlations for mixed turbulent natural and forced heat transfer in vertical tubes*; T. Aicher, M. Martin; International Journal of Heat and Mass Transfer; Vol. 40, No. 15, pp 3617-3626; 1997.

[91] *Effects of buoyancy and of acceleration owing to thermal expansion on forced turbulent convection in vertical circular tubes* – criteria of the effects, velocity and temperature profiles, and reverse transition from turbulent to laminar flow; H. Tanaka et al.; International Journal of Heat and Mass Transfer; Vol. 16, pp 1267-1288; 1973.

[92] *Laminarization of turbulent gas flow inside a strongly heated tube*; S. Torii; International Journal of Heat and Mass Transfer; Vol. 40, No. 13, pp 3105-3117; 1997.

[93] CFD modelling of heat transfer in turbulent pipe flows; S.S. Thakre, J.B. Joshi; AIChE Journal, Vol. 46, No 9; September 2000.

[94] *Decay Heat for the PBMR Used and Spent Fuel Tanks*: A Second Study; Atomic Energy Corporation of South Africa internal document; RRT-FMR-99014 (R/B); April 2000.

[95] *Decay Heat for PBMR 400MW Design Using DIN-25485 Standard*; PBMR (Pty) Ltd. Internal document; MR100-013836-3240; Rev 1.

[96] *Flownex 6.5 User Manual*; M-Tech Industrial (Pty) Ltd; March 2004.

Appendix A : Overview of the Fuel Handling and Storage System

The Fuel Handling and Storage System (FHSS) is in essence a material handling system supporting the PBMR reactor fuel scheme for the on-line multi-pass fuel movement through the core to obtain a high burn-up over all fuel spheres. The FHSS is required to operate over the module lifetime, which includes commissioning, refurbishment and decommissioning functions.

The main functions required from the FHSS can be summarized as follows:

- Load and circulate the start-up core;
- Circulate and replenish the equilibrium core by discharging Spent Fuel and introducing Fresh Fuel;
- Store and decommission Spent Fuel;
- Unload, de-fuel and re-fuel of the equilibrium core to allow reactor maintenance activities;
- Perform the required control, support, maintenance and High Level Waste handling functions to ensure an integrated operation;

The FHSS is divided into a number of subsystems, inter alia the Sphere Storage System (SSS), the Sphere Circulation System (SCS) and the Logistics System. The FHSS comprises of three duplicate process lines primarily because the reactor has three sphere outlets. Except for spent fuel discharge, all operations are performed in triplex format.

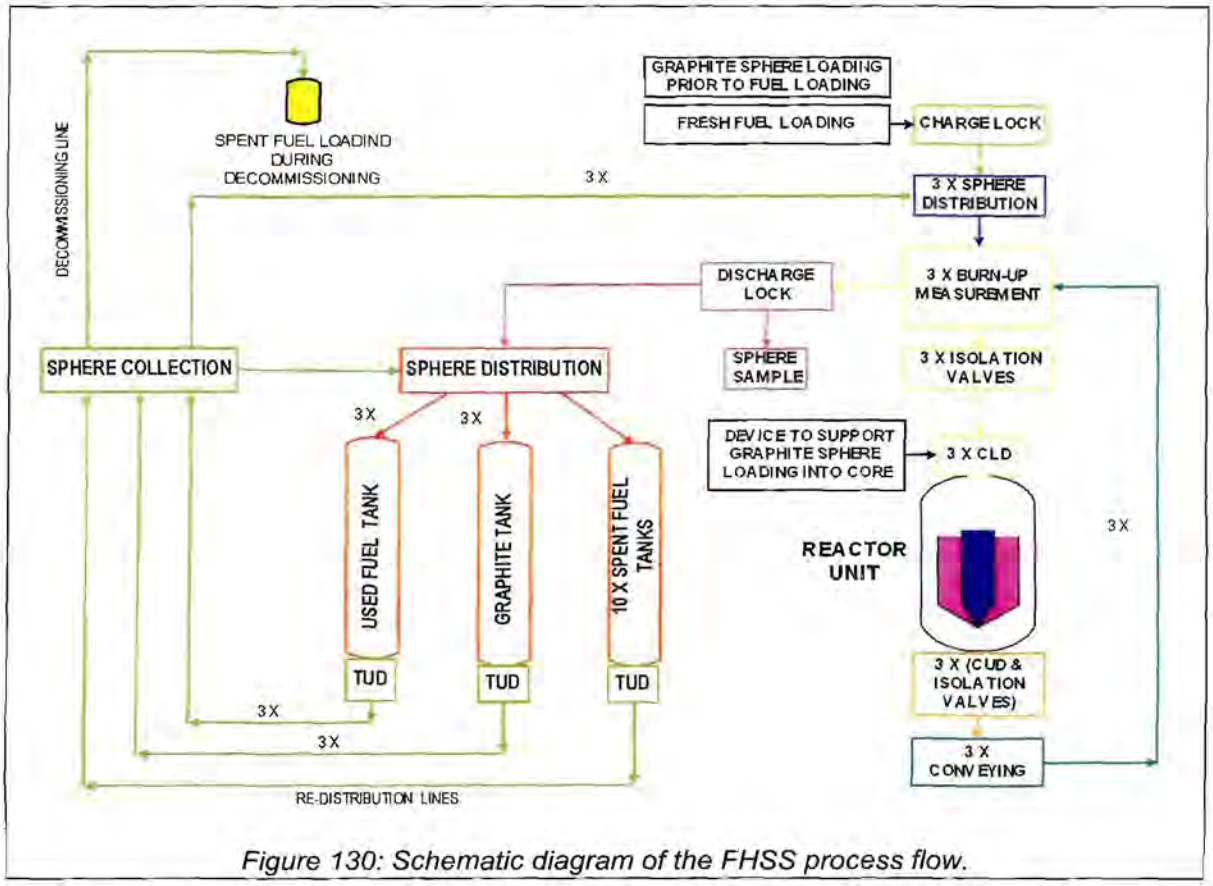

Figure 130: Schematic diagram of the FHSS process flow.

Figure 130 shows the schematic process flow diagram. The spheres are removed from the reactor by three Core Unloading Devices (CUD) and stored in a buffer in the conveying block. From there, they are pneumatically lifted to the top of the FHSS where a burn-up measurement is performed on the individual spheres. If the sphere has reached its target burn-up, it is classified as "spent" and diverted to the discharge lock. A sphere can also be extracted from the discharge lock for laboratory analysis. If the sphere is not "spent", it is returned to the top of the reactor via a Core Loading Device (CLD). For each spent fuel sphere discharged, a fresh fuel sphere is loaded from the charge lock via the distribution block to the reactor.

Each day the Main Power System of the PBMR will request that the FHSS replace a certain amount of spent fuel spheres with fresh fuel. This is determined based upon the previous day's power consumption. The FHSS will then circulate the spheres through the core until the required amount of spent fuel has been discharged in the discharge lock. The discharge lock is then isolated and depressurised, and the spent fuel is loaded into a single tank. At the same time, a new batch of fresh fuel is loaded into the charge lock.

During mid-life of the reactor, all of the spheres inside the core must be transferred to a storage tank. This allows maintenance on the reactor's internal structures. It is required that the reactor be unloaded as fast as possible, since each day's down time means a loss of income. The FHSS achieves this fast unloading by depressurizing to 1MPa, and opening the discharge lock. Spheres are than transferred with three lines directly into the used fuel tank. This fast unloading still takes about 20 days to perform.

Once maintenance on the reactor is complete, graphite spheres are introduced from the graphite tank into the core. After the core is filled, used fuel from the used fuel tank is returned to the core, and at the same time, the graphite spheres are returned to the graphite tank.

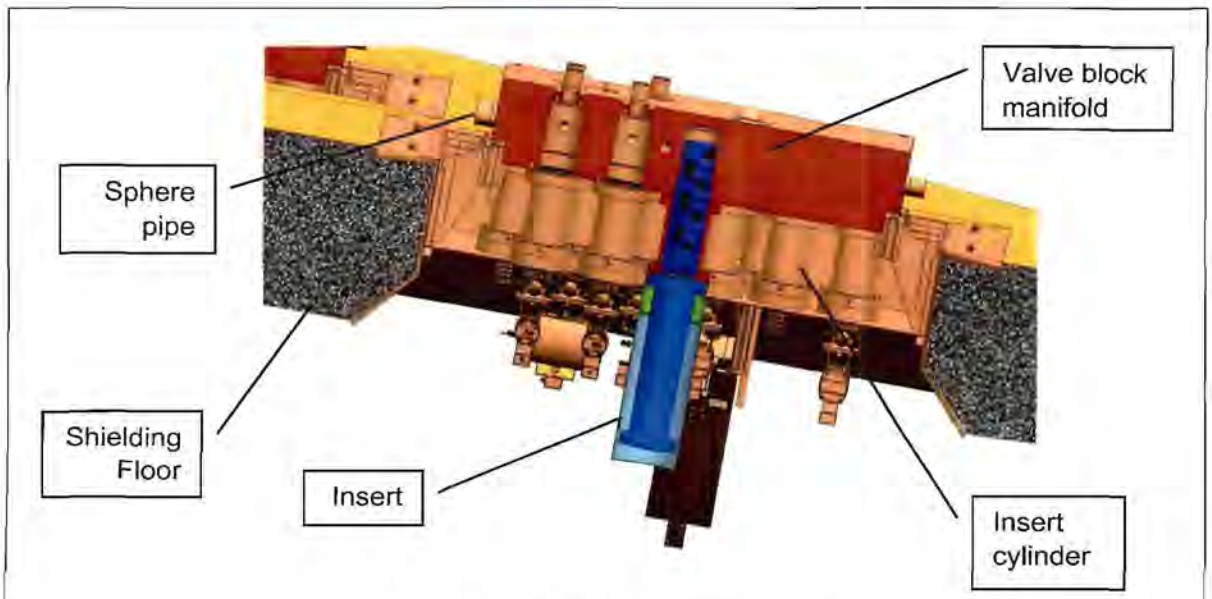

Figure 131: Valve block with inserts.

Each "block" shown in the diagram represents a position where equipment is needed to handle the spheres. These equipment are all in the form of an insert that fits into a steel manifold. This manifold is called a valve block. The valve block is mounted above the floor, with cylinders for the inserts protruding downward through the floor. The sphere pipes are welded to the block itself, and the inserts are installed from below (see Figure 131). The floor in which the block is mounted performs the radiation shielding for personnel when a sphere is in the pipe. There is also shielding material between the cylinders such that a person may touch the bottom of the cylinder even if there is a sphere inside the insert.

The interface between the insert and the valve block cylinder is identical throughout the FHSS. This standardisation and modularity allows for one maintenance procedure to remove any insert. In principle, the insert is un-bolted manually, but does not fall out because of an internal locking mechanism. A remote tool is then used to unlock the insert and pull it from the valve block into a shielded cask. The reverse process is used to install the new insert. The FHSS maintenance concept makes use of a remove-and-replace principle and minimal on site repair is performed.

Appendix B : Study on the Choice of Natural Convection for the FEA Thermal Analysis

1. PURPOSE

The purpose of this study was to determine the sensitivity of the convection coefficient on the Used Fuel Tank fuel temperatures. The heat transfer properties, and hence the convection coefficient around the tank is not exactly known. Several empirical correlations exist but it is not certain which is the most applicable.

This study aims to highlight the importance or insignificance of using the correct convection coefficients for thermal analysis of the UFT.

2. PROBLEM DEFINITION

A method is described in Chapter 9 for calculating the fuel temperatures inside a storage tank using FEA software, coupled with empirical equations for the heat transfer. The question is which empirical equation to use. The literature is overwhelmed with research work relating to all kinds of heat transfer problems in ducts, however, none of them describes the flow phenomena inside the tank precisely. An approximate equation has to be chosen. This equation should include effects such as mixed convection, turbulent flow and developing flow.

The following paragraphs present the results of analyses done for a 20% filled UFT, cooled by 6 kg/s at 35°C inlet temperature. The purpose of the different analyses was to investigate how sensitive the fuel temperatures are for the choice of convection coefficient, and to help choose the most applicable equation. It is certainly not fully comprehensive, and several other equations could have been included, but there was limited time to perform the study.

3. DITTUS-BOELTER EQUATION

A very well known equation for the heat transfer (Nusselt number) inside a tube is given by the Dittus-Boelter equation (taken from reference [60]).

$$Nu_T = 0.023 \cdot Re^{0.8} \cdot Pr^{0.4}$$

$$hc = Nu_T \cdot \frac{k}{D}$$

This equation is valid for fully developed turbulent forced flow inside a duct with hydraulic diameter **D**. It does not include any buoyancy or natural convection effects, and is an average result. By using this equation, the following convection coefficients are calculated for the individual flow regions:

Centre tube	4.770	[W/m^{2}K]
Outer tubes	8.451	[W/m^{2}K]
Thermal shield channels	6.945	[W/m^{2}K]

These coefficients were applied as constants on the FEA model. The temperature distribution for the upper portion of the tank is shown below. It represents a 1/16th section of the fuel volume. The maximum temperature is 458.23°C.

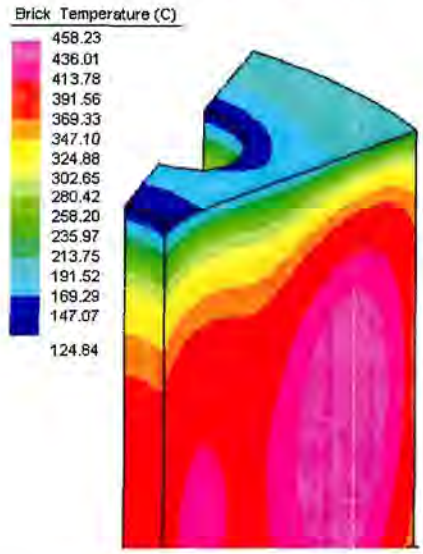

4. ENTRANCE EFFECT INCLUDED

The Dittus-Boelter equation is valid only if the flow is fully developed. This occurs at a distance between 15 to 40 pipe diameters from the entrance. For the pipes of the storage tank, a large portion of the heat transfer occurs in the entrance region (the centre pipe is for example only about 23 diameters long). In this region, the heat transfer can increase to 2.5 times of the fully developed flow due to the high shear forces associated with flow development.

In reference [66] an adjustment equation is given to calculate the local heat transfer Nusselt number in the entrance region. The equation looks as follows:

$$Ax = 1 + 2.35 \cdot Re^{-0.15} \cdot Pr^{0.4} \cdot \left(\frac{x}{D}\right)^{-0.6} \cdot \exp\left(\frac{-0.39}{Re} \cdot \frac{x}{D}\right)$$

$$Nu_x = Nu_T \cdot Ax$$

This equation becomes singular in regions close to x/D = 0. From test results of various researchers, it can be seen that the heat transfer reaches a peak between x/D = 0 to x/D = 0.3. This was used as a cut-off value for calculating the heat transfer along the full length of the tube. The resultant convection profile looks as follows:

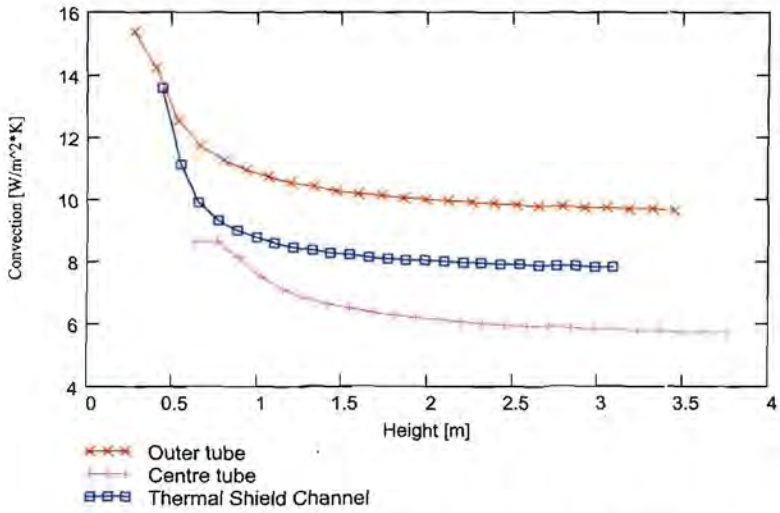

The fuel temperatures are shown below, with the maximum temperature now 417.27°C.

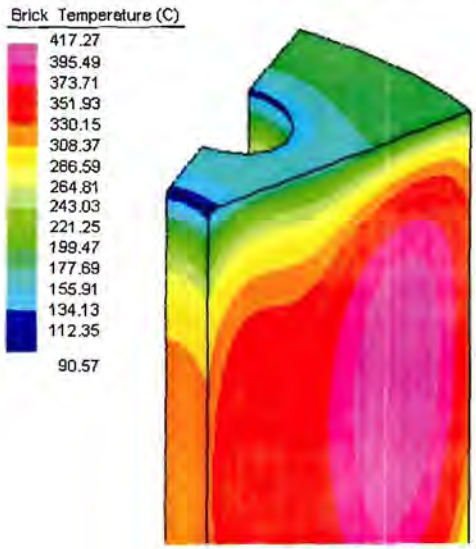

5. EQUATION FROM JAKOB

In the book from Jakob [65] an equation is proposed for the average Nusselt number which introduces the entrance effect by a D/L ratio. It also includes the effect of property changes of the fluid along the pipe. Although the equation describes the total average Nusselt number, it was found that substituting **L** for the local position **x** gives very realistic results.

$$Nu_x = 0.036 \cdot Re^{0.8} \cdot Pr^{0.3} \cdot \left(\frac{\mu_x}{\mu_{in}} \right)^{0.14} \cdot \left(\frac{D}{x} \right)^{\frac{1}{18}}$$

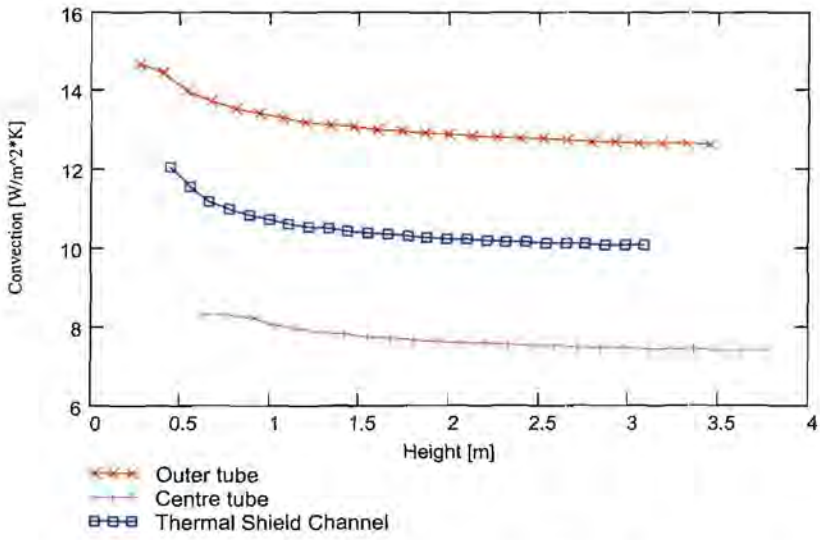

The resulting temperature profile is shown below. The maximum temperature is now 371.94°C.

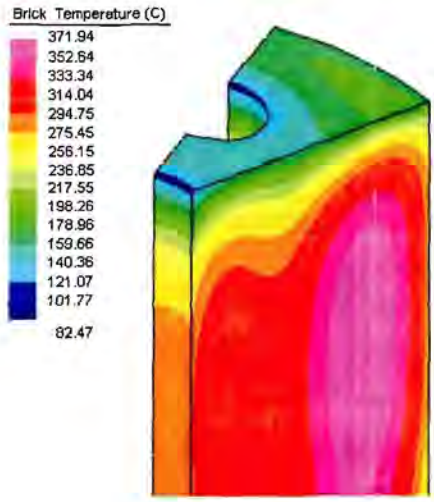

6. MIXED CONVECTION FROM VILEMAS

All of the previous equations assume pure forced flow, i.e. they do not include the effect of buoyancy-induced flow. For the tank with its long vertical pipes, this effect is what gives the tank a passive cooling ability. The actual flow inside the tubes is thus a combination of forced flow and natural convection, called mixed convection.

Several researchers have found that for turbulent aiding mixed convection (flow where the buoyancy flow is in the same direction as the bulk fluid flow), the heat transfer can be reduced at certain scenarios [88]-[92]. This is due to the high local fluid temperature in the boundary layer that reduces the ability of the wall to transfer the heat to the bulk fluid.

It was also found that the heat transfer experiences a significant drop for fluids close to its critical point (the point where the density changes rapidly as a function of temperature). This critical point is often associated with pressurized gasses or liquid metals. However, this phenomenon was also found for atmospheric gasses at very high buoyancy parameters, and is called re-laminarization.

In reference [89] Vilemas proposes three regimes for mixed convection based upon the buoyancy parameter **K**, with **K** defined as:

$$K = \frac{Gr_A}{Re^2} \qquad \text{with} \qquad Gr_A = \frac{Gr}{4 \cdot Re \cdot Pr} \qquad \text{and} \qquad Gr = \frac{g \cdot q \cdot D^4}{T_{gas} \cdot \nu^2 \cdot k}$$

The value $\mathbf{Gr_A}$ is a Grashof number based upon temperature gradient, and **Gr** the Grashof number based upon the specific heat flux **q** in [W/m^2]. The regimes were defined as weak, intermediate and strong effect of natural convection.

For the weak region, the traditional equations that include the entrance effect can be used. For the intermediate regime, the authors could not obtain a suitable correlation, however, this regime is relatively small. For the strong regime, the authors define correlation equations for the value and position of the local maximum and minimum heat transfer. They also propose smooth equations for joining these local maximum and minimum points. Reference [89] is the only text that could be found relating directly to mixed convection in vertical tubes.

For the maximum temperature calculations, the buoyancy parameter for the storage tanks falls within the strong regime. Below are the resultant convection coefficients for the tubes. Note that it is not always possible to see the local minimum or maximum points. This is because they occur at an x/D distance above the 20% fill level of the tank.

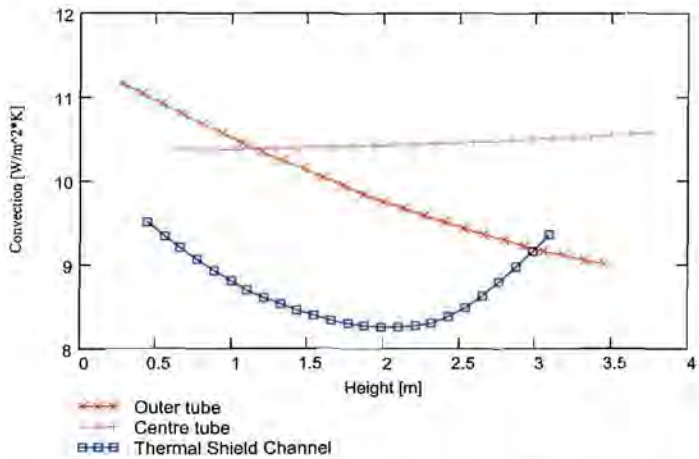

The next figure shows the convection coefficients for a tank filled to 100% capacity. The local minimum and maximum points can now be seen.

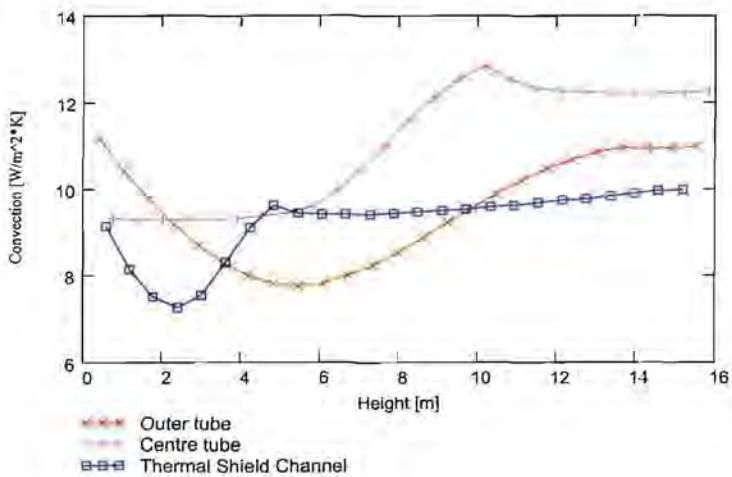

The temperature profile for the 20% filled case is shown below. The maximum temperature is 413.83°C.

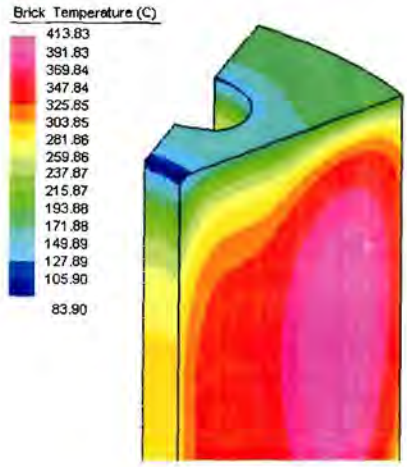

7. CFD RESULT

PBMR uses Star CD software as the primary CFD analysis tool. The results from CFD analyses are supposed to be the most accurate since it does not make the large assumptions as needed for the FEA method. However, the result is still based upon the choice of turbulence model and mesh refinement. Although it is attempted to define the CFD model as accurately as possible, it is not certain what the error may be. Also, it is suggested that some CFD techniques do not properly predict the effect of buoyancy [88][93].

The convection coefficients calculated for the 20% fill level by CFD are shown below, as well as the temperature profile. The maximum temperature is 365.9°C.

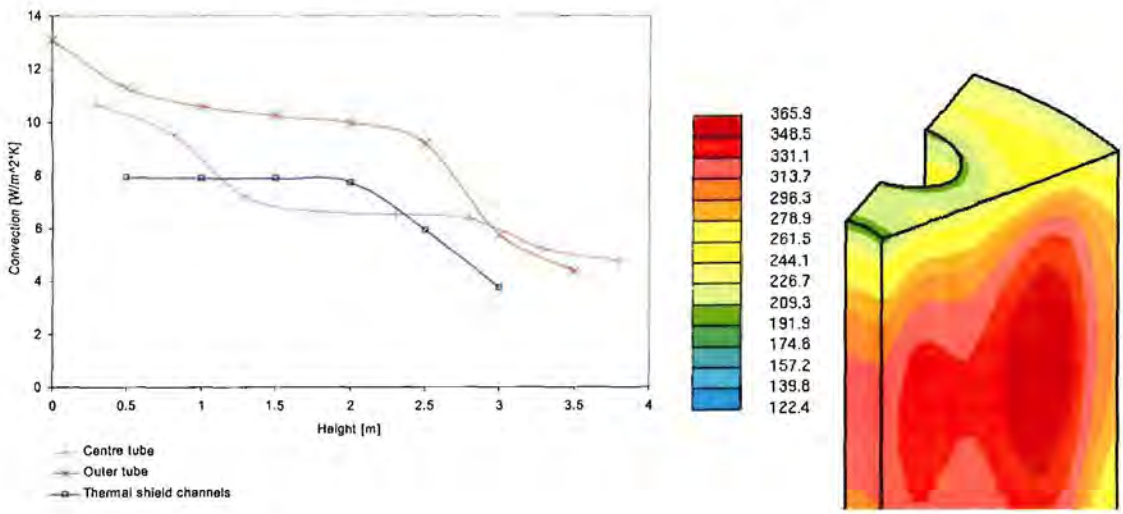

8. SUMMARY OF RESULTS

All of the analyses resulted in similar temperature distributions as compared to the CFD result. The correlation that gave the most accurate results is that of Jakob. This is strange as one would expect that the equation from Vilemas, which includes all the flow characteristics present, to be the most accurate. Also, the equation from Jakob was not derived for local convection but rather average convection over the length of the tube.

Another important aspect to note is that the maximum temperature is significantly sensitive to the actual local heat transfer coefficients. The convection for the outer tube for example, varied from 8.5 to 15.5, with resulting temperature variations from 372°C to 458°C. It is therefore important that an accurate convection coefficient equation be used in the FEA analysis method.

The convection coefficient profile calculated by CFD has a strange drop at around 2.5m. The only explanation thus far for the drop is due to the lower heat flux at the upper region. This is because heat flows axially upward to the top of the pebble bed hence reducing the radial flux through the pipes. However, convection coefficient is rarely a function of heat flux (only for very high buoyancy effects), and certainly does not necessarily drop as the heat flux drops. It could be that the method of convection coefficient extraction done in the CFD has a different definition than for analytical calculations, though all attempts have been made to have the results comparable.

The average values for the CFD results compare reasonably with those from the Jakob equation. This may explain the correlation with the temperatures. However, the convection profiles differ significantly. It is thus more coincidental that the equation from Jakob gives reasonable answers.

9. CONCLUSIONS

It is evident that an accurate correlation for the local convection coefficient be used for thermal analyses of the storage tanks using the FEA method. Several equations have been investigated, but only one produces results similar to that of the CFD analyses. However this specific equation is actually valid for average convection, not local convection. This implies that the most accurate equation should rather be chosen based upon CFD results for the expected range of application than for its initial origin.

Unless improvement and better understanding of the equations presented by Vilemas is made, the equation of Jakob is to be used for analyses. It is then important to bench-mark the FEA results with some representative CFD results before a large number of analyses are done. Better understanding can be achieved through representative convection tests. This will also verify the CFD results, and is therefore a very important activity to be done.

Appendix C : Storage Tank Volumetric Calculations

1. INTRODUCTION

This appendix contains the algorithm used to calculate the storage tank capacity. The total tank weight and gas volumes are also calculated. The algorithm was written as an active worksheet in MathCAD. The worksheet was then used as an input document for further analyses.

2. CALCULATION METHODOLOGY

The fuel volume is approximated by a cylinder with a conical top and bottom, and hollow regions running at certain positions through the volume. The geometry of the bottom region where the centre tube splits into four smaller tubes is not included. The error made by ignoring this part has been verified by 3D CAD modelling to be acceptably small.

It can be shown mathematically that the volume of the semi-ellipsoidal dish end of the bottom of the tank can be approximated by a conical region of horizontal angle of 14.784° and a straight section.

From tests performed previously, it was found that the top of the sphere volume forms a cone with horizontal angle of 30°. In order to calculate the height of the pebble bed's conical apex (theoretical tip if no centre tube were present), the number of spheres occupying the top and bottom cones is calculated first. The remaining spheres fit in the middle portion, which is a cylinder with constant cross section. The total capacity can thus be calculated as follows:

$$N_{tot} = \frac{H_{mid} \cdot A_{fuel} \cdot PF}{V_s} + N_{up} + N_{low}$$

A free height above the pebble bed is added for uncertainties of the filling ability of the mechanical brake, as well as to prevent the spheres to fill to the top of the dish-end. The height of the mid section can thus be calculated as follows:

$$H_{mid} = H_{tank} - (H_{up} + H_{low} + H_{free})$$

By using the conical approximation of the dish end, the internal gas volume can be calculated. The tank mass is calculated from the total surface area, for a given material thickness. A constant mass is added for other components such as the ring support and TUD. These masses were obtained from the CAD model.

3. INPUTS

Sphere volume: $V_s := \frac{1}{6} \cdot \pi \cdot (60mm)^3$

Tank dome to dome height: $H_{tank} := 18.0 \cdot m$

Tank inner diameter: $D_{tank} := 3.1m$

Cooling tubes OD:

$$d := \begin{pmatrix} 762 \\ 406 \\ 406 \\ 406 \\ 406 \\ 406 \\ 406 \\ 406 \\ 406 \end{pmatrix} \cdot mm$$

Cooling tubes PCD:

$$PCD := \begin{pmatrix} 0 \\ 1800 \\ 1800 \\ 1800 \\ 1800 \\ 1800 \\ 1800 \\ 1800 \\ 1800 \end{pmatrix} \cdot mm$$

Packing Factor of spheres: $PF := 0.60$

Upper cone angle: $\theta_{up} := 30 \cdot deg$

Lower cone angle: $\theta_{low} := 14.784 \cdot deg$

Free height between pebble bed and tank top: $H_{free} := 500 \cdot mm$

Material density: $\rho_{steel} := 7850 \cdot kg \cdot m^{-3}$

Sphere mass: $m_s := 0.210 \cdot kg$

Tank shell thickness: $t_{tank} := 16 \cdot mm$

Tube wall thickness: $t_{tube} := 16 \cdot mm$

Ring support mass: $m_{ring} := 1733 \cdot kg$

TUD mass: $m_{TUD} := 4240 \cdot kg + 2000kg$

4. STORAGE TANK CAPACITY

Number of tubes: $tubes := 0 .. length(d) - 1$

Tube cross sections: $A_{tubes} := \frac{1}{4} \cdot \pi \cdot \left(d_{tubes}\right)^2$

Tank cross section: $A_{tank} := \frac{1}{4} \cdot \pi \cdot D_{tank}^{\ 2}$

Fuel volume cross section: $A_{fuel} := A_{tank} - \sum_{tubes} A_{tubes}$

Volume of upper cone:

$$V_{up} := \frac{1}{3} \cdot \pi \cdot \left(\frac{D_{tank}}{2}\right)^3 \cdot \tan\left(\theta_{up}\right) - \sum_{tubes} \left[A_{tubes} \cdot \tan\left(\theta_{up}\right) \cdot \frac{\left(D_{tank} - PCD_{tubes}\right)}{2} \right]$$

Spheres in upper cone: $N_{up} := \frac{V_{up} \cdot PF}{V_s}$ $H_{up} := \frac{1}{2} \cdot D_{tank} \cdot \tan\left(\theta_{up}\right)$

Volume of lower cone:

$$V_{low} := \frac{1}{3} \cdot \pi \cdot \left(\frac{D_{tank}}{2}\right)^3 \cdot \tan\left(\theta_{low}\right) - \sum_{tubes} \left[A_{tubes} \cdot \tan\left(\theta_{low}\right) \cdot \frac{\left(D_{tank} - PCD_{tubes}\right)}{2} \right]$$

Spheres in lower cone: $N_{low} := \frac{V_{low} \cdot PF}{V_s}$ $H_{low} := \frac{1}{2} \cdot D_{tank} \cdot \tan\left(\theta_{low}\right)$

Mid section height: $H_{mid} := H_{tank} - \left(H_{up} + H_{low} + H_{free}\right)$

Total sphere capacity: $N_{max} := \frac{H_{mid} \cdot PF \cdot A_{fuel}}{V_s} + N_{up} + N_{low}$ $N_{max} = 531588$

Fill height vs. fill percentage: $H_{fill}(fill, N_{tot}) := H_{low} + H_{up} + \frac{V_s \cdot \left(N_{tot} \cdot fill - N_{up} - N_{low}\right)}{PF \cdot A_{fuel}}$

5. GAS VOLUMES

Conical height: $H_c := \frac{D_{tank}}{2} \cdot \tan(\theta_{low})$ $H_c = 0.409\ m$

Conical dish end volume: $V_{dish} := \frac{1}{3} \cdot \pi \cdot \left(\frac{D_{tank}}{2}\right)^3 \cdot \tan(\theta_{low})$ $V_{dish} = 1.029\ m^3$

Straight section volume: $V_{straight} := A_{tank} \cdot (H_{tank} - 2 \cdot H_c)$ $V_{straight} = 129.683\ m^3$

Volume occupied by tubes:

$$V_{tubes} := \sum_{tubes} \left[\left(A_{tubes}\right) \cdot \left[H_{tank} - \tan(\theta_{low}) \cdot \left(D_{tank} - PCD_{tubes}\right) \right] \right]$$

$V_{tubes} = 26.123\ m^3$

Total empty volume: $V_{empty} := V_{straight} + 2 \cdot V_{dish} - V_{tubes}$

$V_{empty} = 105.619\ m^3$

Volume of gas of a full tank: $V_{full} := V_{empty} - N_{max} \cdot V_s$

$V_{full} = 45.498\ m^3$

6. TANK MASS

Shell outer surface:

$$A_{shell} := \pi \cdot D_{tank} \cdot \left(H_{tank} - 2 \cdot H_c\right) + 2 \cdot \frac{A_{tank}}{\cos\left(\theta_{low}\right)} \qquad A_{shell} = 182.945\ m^2$$

Tubes total surface:

$$A_{c.tubes} := \sum_{tubes} \left[d_{tubes} \cdot \pi \cdot \left[H_{tank} - \tan\left(\theta_{low}\right) \cdot \left(D_{tank} - PCD_{tubes}\right) \right] \right]$$

$$A_{c.tubes} = 221.301\ m^2$$

Total surface: $A_{shell} + A_{c.tubes} = 404.246\ m^2$

Total empty mass:

$$M_{empty} := \rho_{steel} \cdot \left(A_{shell} \cdot t_{tank} + A_{c.tubes} \cdot t_{tube}\right) + m_{ring} + m_{TUD}$$

$$M_{empty} = 58.746 \times 10^3\ kg$$

Total full mass: $M_{full} := M_{empty} + m_s \cdot N_{max} \qquad M_{full} = 170.38 \times 10^3\ kg$

Appendix D : Spent and Used Fuel Decay Heat Calculations

1. INTRODUCTION

This appendix contains the algorithm used to generate a smooth function for the decay heat of a single spent and used fuel sphere. The algorithm was written as an active worksheet in MathCAD. The worksheet was then used as an input document for further analyses.

All data are curve-fitted using a built in spline fit algorithm. The curve is thus not mathematically definable, but rather a smooth interpolation. This approach gives the highest accuracy, especially for the long-term decay values.

The units for time is in seconds, measured from the moment when the nuclear reaction stopped. However, the spent fuel spheres always decay approximately 100 hours inside the reactor de-fuelling tube before it can enter the FHSS. For this reason, all spent fuel decay heat calculations should include a time offset. For example, a spent fuel sphere which was diverted at the start of the day, would have a decay "age" of 100 hours + 8 hours when it is discharged to a spent fuel tank at the end of the day.

The heat is given in Watt per sphere. A portion of this heat (47% for short term and 30% for the long term [94]) is actually Gamma radiation escaping the sphere, and not thermal heat. This energy will be deposited on the sphere's surroundings. In the case of a sphere inside a pebble bed, much of this heat is deposited on neighbouring spheres. Therefore in the combined case, most of the Gamma radiation is converted to thermal heat inside the tank. For this reason, no differentiation will be made for heat lost due to radiation. This assumption will only give more conservative results (higher temperatures) for the regions close to the tank wall.

The data supplied in reference [95] is for the pilot plant fuel as well as the commercial plant fuel. In order to stay conservative, the maximum value of either fuel type is used to define the decay heat.

2. SPENT FUEL

$$\begin{pmatrix} time_{spent} \\ HeatPilot_{spent} \\ HeatComm_{spent} \end{pmatrix} :=$$

$$i := 0 .. length(time_{spent}) - 1$$

$$Heat_{spent_i} := max(HeatPilot_{spent_i}, HeatComm_{spent_i})$$

Spline fit:

$$C_{spent} := lspline(time_{spent}, Heat_{spent})$$

$$Q_{spent}(t) := interp(C_{spent}, time_{spent}, Heat_{spent}, t)$$

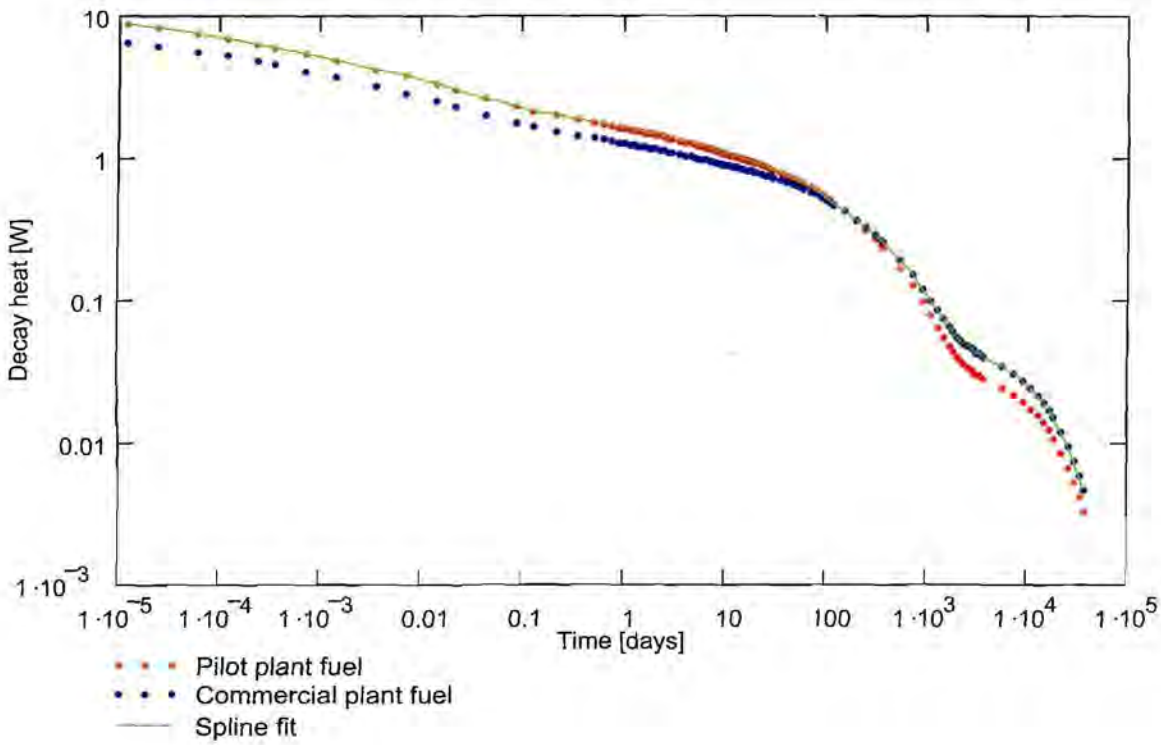

3. USED FUEL

$$\begin{pmatrix} time_{used} \\ HeatPilot_{used} \\ HeatComm_{used} \end{pmatrix} := \quad i := 0 .. length(time_{used}) - 1$$

$$Heat_{used_i} := \max\left(HeatPilot_{used_i}, HeatComm_{used_i}\right)$$

Spline fit:

$$C_{used} := lspline(time_{used}, Heat_{used})$$

$$Q_{used}(t) := interp(C_{used}, time_{used}, Heat_{used}, t)$$

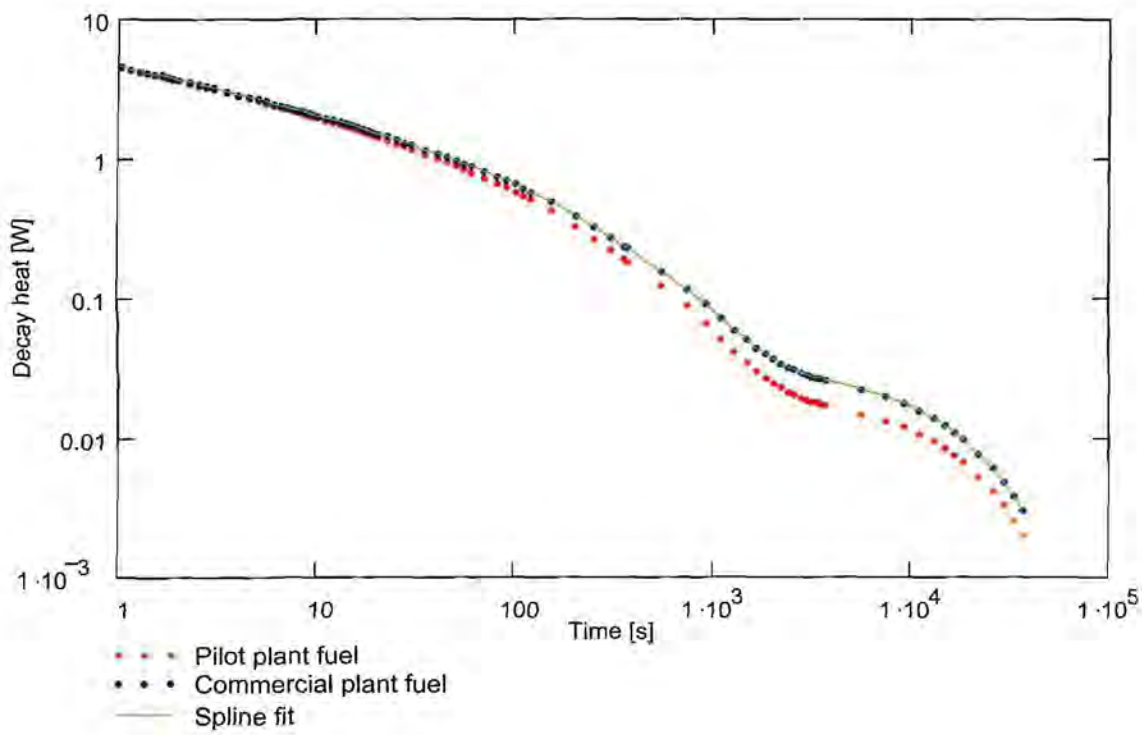

4. GRAPHICAL REPRESENTATION

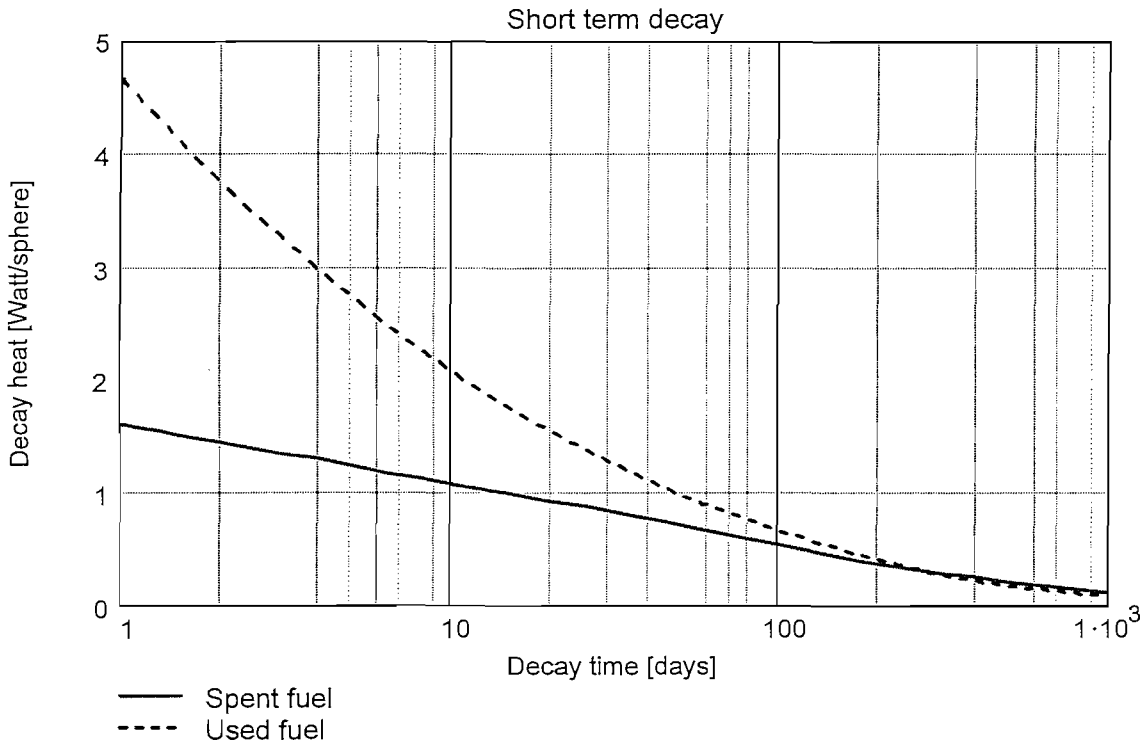

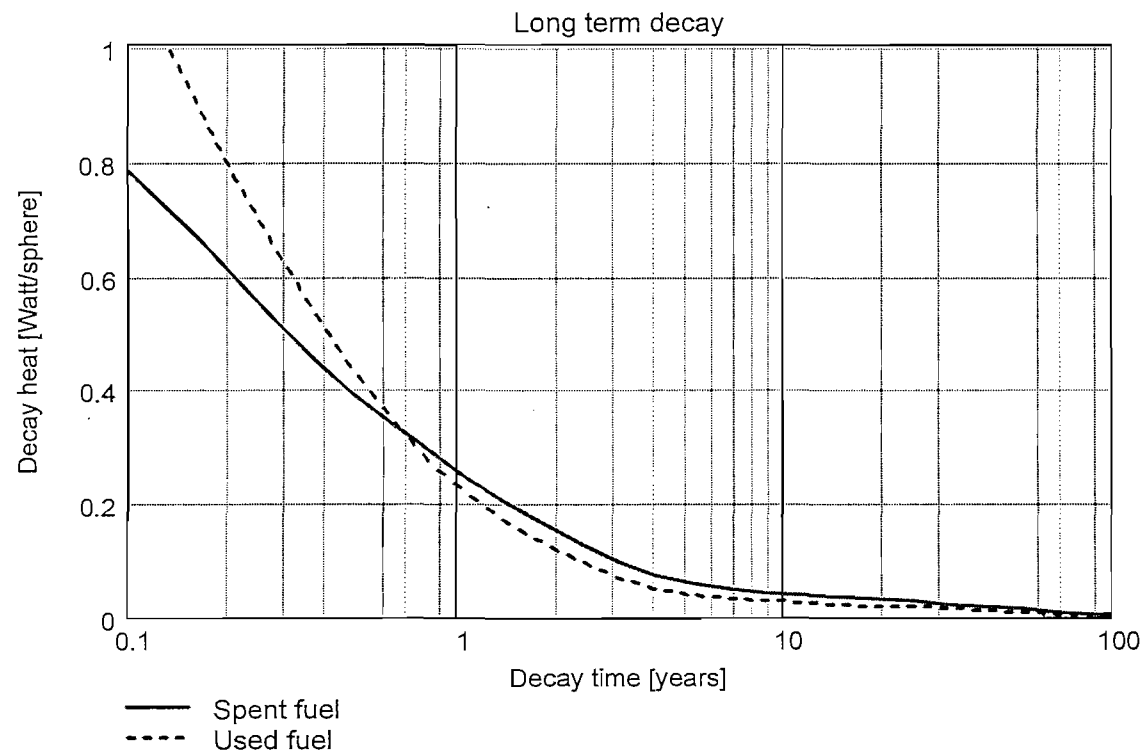

Appendix E : Spent Fuel Tank Heat Load Calculations

1. INTRODUCTION

This appendix contains the algorithm used to calculate the decay heat density in the SFT as a function of height. The algorithm was written as an active worksheet in MathCAD. The worksheet was then used as an input document for further analyses. It also makes use of the decay heat calculation of Appendix D.

2. ANALYSIS METHODOLOGY AND ASSUMPTIONS

It is assumed that the rate of filling V' (number of spheres per day) is constant over time. This assumption is not valid between successive days due to variations in the power output of the reactor. However, based upon a successful continuous operation over the time span to fill a tank, the assumption is valid. Even so, as long as the rate of filling is chosen as the fastest rate probable, the results will be conservative.

Now consider a cylinder of cross section Ac. To determine the time it takes to fill the cylinder to height H, one simply calculates the volume V=Ac*H, and divides this with the rate of volume increase, t=V/V'. However, If the cross section changes with height, one needs to integrate the area with respect to height in order to calculate the actual volume.

The equation then looks as follows: $t_{fill}(z) = \frac{1}{V'} \cdot \int_0^H Ac(z)\, dz$

Due to the dished shape bottom, conical shaped top and tubes running through the tank, the fuel volume does not have a constant cross section, especially at low fill levels. Instead of attempting to derive a mathematical equation for the fuel cross section, a 3D CAD model was used to extract the cross section area at different heights for different fill levels. The cross section of the bottom and top dish areas were extracted. The middle portion is constant. By entering a specific fill level percentage, the complete cross section profile can be defined by calculating the distance of the middle portion. This is then placed into a linear interpolation function.

The time vs. height is simply a numerical integration of the area interpolated function, as shown above. This time is the time it took to fill the tank to the specific height. However, the decay age of the spheres at a certain height is the time it took to fill the tank to the fill level, subtracted by the time to fill to the certain height, plus the initial decay time of the spheres inside the de-fuel chute.

Thus: $t_{age}(z) = t_{init} + t_{max} - t_{fill}(z)$

The heat density can be calculated by getting the decay heat of a sphere at the specific age, divided by the sphere volume. To relate the density to a pebble bed volume, the packing density PF should be incorporated.

The heat density is thus: $Q'''(z) = \frac{Q_{spent}(t_{age}(z))}{V_s} \cdot PF$

To calculate the total heat load, one simply integrate the heat per unit height over the full height, giving $Q_{total} = \int_0^{H_{fill}} Q'''(z) \cdot Ac(z)\, dz$

Finally, the heat density is approximated by a high order polynomial to be used as input for thermal calculations.

It should be noted that it is assumed that the heat density is constant at a certain height. Another assumption could be that it is constant in conical layers. This means that each day's load of spheres distributes evenly over the conical bed. From tests it was found that the newly added spheres tend to stay at the top, and pushes the other spheres down. The constant heat approximation is thus deemed to be more representative.

3. INPUTS

Max number of spheres: $N_{tot} := 530000$

Fill level: Fill :=

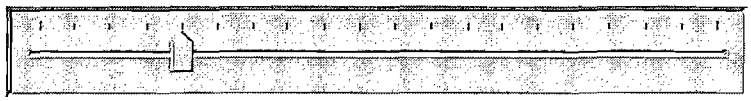

Fill = 25 %

Sphere diameter: $d := 0.060$ m

Packing Factor: $PF := 60\%$

Rate of sphere discharge into tank: $n_s := \frac{484}{day}$ $\frac{spheres}{day}$

Initial decay time: $t_{init} := 98 \cdot hour$

4. GEOMETRY

Cross sections extracted from 3D CAD model.

Sphere volume: $V_s := \frac{\pi \cdot d^3}{6}$

Volume of bottom dish:

$$\begin{pmatrix} Height \\ Area \end{pmatrix} :=$$

Height	Area
[m]	[m^2]
0.02	0.31039
0.05	0.77126
0.1	1.34073
0.2	2.41175
0.3	2.94352
0.4	4.21953
0.5	5.27422
0.6	5.8893
0.7	5.9749
0.8	6.05594

$Ac_{bottom}(z) := linterp(Height, Area, z)$

$$V_{bottom} := \int_0^{max(Height)} Ac_{bottom}(z)\, dz$$

$V_{bottom} = 3.113$

$N_{bottom} := \frac{V_{bottom} \cdot PF}{V_s}$ $N_{bottom} = 16517$

Volume of upper cone:

$$\begin{pmatrix} \text{Height} \\ \text{Area} \end{pmatrix} :=$$

Height	Area
[m]	[m^2]
0.85	6.05594
0.9	5.77368
1	4.21294
1.1	2.84069
1.2	1.87621
1.3	1.42932
1.4	0.89061
1.5	0.27235
1.558	0

$$Ac_{top}(z) := \text{linterp}(\text{Height}, \text{Area}, z)$$

$$V_{top} := \int_{\min(\text{Height})}^{\max(\text{Height})} Ac_{top}(z)\, dz$$

$V_{top} = 1.731$

$$N_{top} := \frac{V_{top} \cdot PF}{V_s} \qquad N_{top} = 9183$$

Mid volume : $$V_{mid} := \frac{(N_{tot} \cdot Fill - N_{bottom} - N_{top}) \cdot V_s}{PF} \qquad V_{mid} = 20.131$$

Mid length : $$L_{mid} := \frac{V_{mid}}{Area_0} \qquad L_{mid} = 3.324$$

Fill height : $$H_{fill} := \max(\text{Height}) + L_{mid} \qquad H_{fill} = 4.882$$

Area function : $$Ac(z) := \begin{cases} Ac_{bottom}(z) & \text{if } z < \min(\text{Height}) \\ Ac_{top}(z - L_{mid}) & \text{if } z > \min(\text{Height}) + L_{mid} \\ Area_0 & \text{otherwise} \end{cases}$$

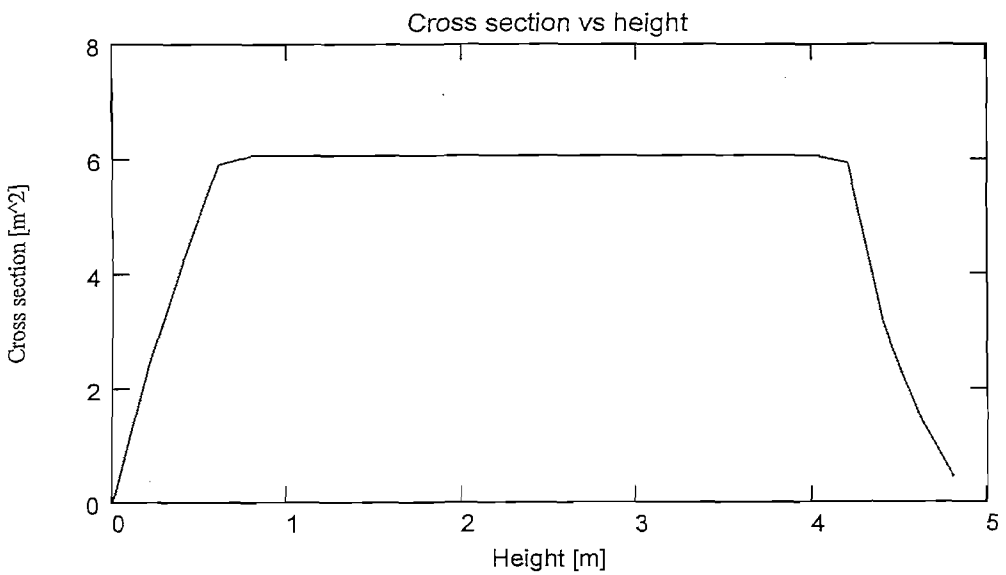

5. DECAY AGE CALCULATION

Rate of volume increase in the tank: $V' := \frac{n_s \cdot V_s}{PF}$ $V' = 1.056 \times 10^{-6}\ m^3 \cdot s^{-1}$

Integral equation: $t_{fill}(z) := \frac{1}{V'} \cdot \int_0^z Ac(z)\, dz$

Max time: $t_{max} := t_{fill}(H_{fill})$ $t_{max} = 0.759\ year$

Sphere decay age: $t_{age}(z) := t_{init} + t_{max} - t_{fill}(z)$

6. HEAT LOAD CALCULATION

Decay heat referenced from Appendix D algorithm.

Heat density: $Q'''(z) := \frac{Q_{spent}(t_{age}(z))}{V_s} \cdot PF$

Total heat load: $Q_{total}(Fill) := \int_0^{Hfill} Q'''(z) \cdot Ac(z)\, dz$

$Q_{total}(Fill) = 69.01\ kW$

7. POLYNOMIAL APPROXIMATION

Analysis increments: $i := 0 .. 100$ $H_i := \frac{H_{fill}}{100} \cdot i$

Heat density: $Heat_i := Q'''(H_i)$

Polynomial order: $PolyOrder := 9$

Polynomial coefficients:

$C := submatrix(regress(H, Heat, PolyOrder), 3, PolyOrder + 3, 0, 0)$

Polynomial curve fit: $Heat'''_{fit}(z) := \sum_{k=0}^{PolyOrder} \left[C_k \cdot (z)^k \right]$

Export text polynomial: $HeatPoly := TextPoly(C)$

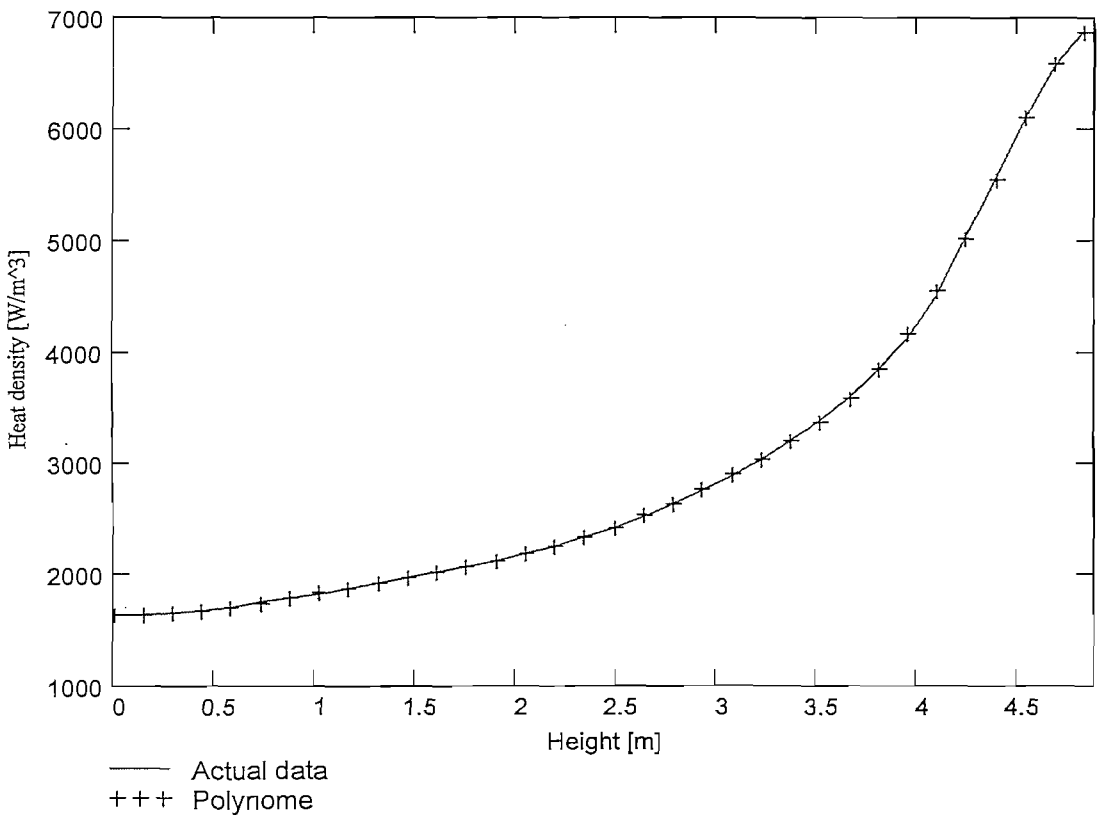

HeatPoly = "+512.712840065541*z^0 + -296.666646348315*z^1 + 471.714652960961*z^2 + -278.39500475636*z^3 + 84.5570430705458*z^4 + -14.5338408495778*z^5 + 1.46933402803559*z^6 + -0.0863422061715477*z^7 + 0.00272057239892539*z^8 + -3.54026519972653e-005*z^9"

$$C = \begin{bmatrix} 1.6219908302 \cdot 10^{3} \\ 8.5808179712 \cdot 10^{1} \\ -1.5852765782 \cdot 10^{2} \\ 6.2522902708 \cdot 10^{2} \\ -4.6120175414 \cdot 10^{2} \\ 3.718050721 \cdot 10^{1} \\ 9.8981878171 \cdot 10^{1} \\ -4.7582825328 \cdot 10^{1} \\ 8.6882425482 \cdot 10^{0} \\ -5.7375901216 \cdot 10^{-1} \end{bmatrix}$$

Actual heat load: $Qact := \int_0^{H_{fill}} Q'''(z) \cdot Ac(z)\, dz$

Approximated heat load: $Qappr := \int_0^{H_{fill}} Heat'''_{fit}(z) \cdot Ac(z)\, dz$

Error: $\frac{Qact - Qappr}{Qact} = -0.005\ \%$

Appendix F : Used Fuel Tank Heat Load Calculations

1. INTRODUCTION

This appendix contains the algorithm used to calculate the decay heat density in the UFT as a function of the fill level. The algorithm was written as an active worksheet in MathCAD. The worksheet was then used as an input document for further analyses. It makes use of the decay heat calculation given in Appendix D.

2. ANALYSIS METHODOLOGY

The decay heat of the Used Fuel Tank is much simpler than that of the Spent Fuel Tank. This is because the decay age of all the spheres is the same, because the nuclear reaction has stopped for all the spheres at the same time. For this reason, the tank geometry does not play a role in the decay heat distribution. The only parameter needed is the total number of fuel spheres. From there, the decay heat for different fill levels can be calculated.

A factor which plays a major role in the decay heat inside the tank is the delay time before core unloading starts, as well as the time it takes to completely empty the core. These two factors are used to calculate the decay age of a sphere as follows:

$$t_{age} = t_{delay} + t_{unload} \cdot Fill$$

The heat load at a certain fill level is the number of spheres for that fill level, multiplied by the decay heat of a single sphere at that stage.

$$Q_{uft}(Fill) = N_{tot} \cdot Fill \cdot Q_{used}(t_{age})$$

The heat density for the specific fill level is the decay heat of a single sphere at that stage, divided by the sphere volume, and multiplied with the packing factor in order to account for the empty spaces between spheres.

$$Q'''(Fill) = \frac{Q_{used}(t_{age})}{V_s} \cdot PF$$

3. LOADING SEQUENCE

Initial delay time of spheres: $t_{delay} := 10 \cdot Day$

Time to unload spheres: $t_{unload} := 20 \cdot Day$

Total number of spheres: $N_{tot} := 500000$

4. HEAT LOAD CALCULATIONS

Decay heat referenced from Appendix D algorithm.

Maximum heat load: $Q_{max} := N_{tot} \cdot Q_{used}(t_{unload} + t_{delay})$

$Q_{max} = 640\ kW$

Fill level: $Fill := 100\ \%$

Sphere volume: $V_s := \frac{1}{6} \cdot \pi \cdot (0.06)^3$

Packing density: $PF := 0.60$

Sphere decay age: $t_{age}(Fill) := t_{delay} + t_{unload} \cdot Fill$

$t_{age}(Fill) = 30\ days$

Total heat load: $Q_{total}(Fill) := N_{tot} \cdot Fill \cdot Q_{used}(t_{age}(Fill))$

$Q_{total}(Fill) = 640 \times 10^3 \quad W$

Heat density: $Q'''(z) := \frac{Q_{used}(t_{age}(Fill))}{V_s} \cdot PF$

$Q'''(0) = 6.79061 \times 10^3 \quad \frac{W}{m^3}$

Heat polynomial: $HeatPoly := num2str(Q'''(Fill))$

$HeatPoly = "6790.6109052542"$

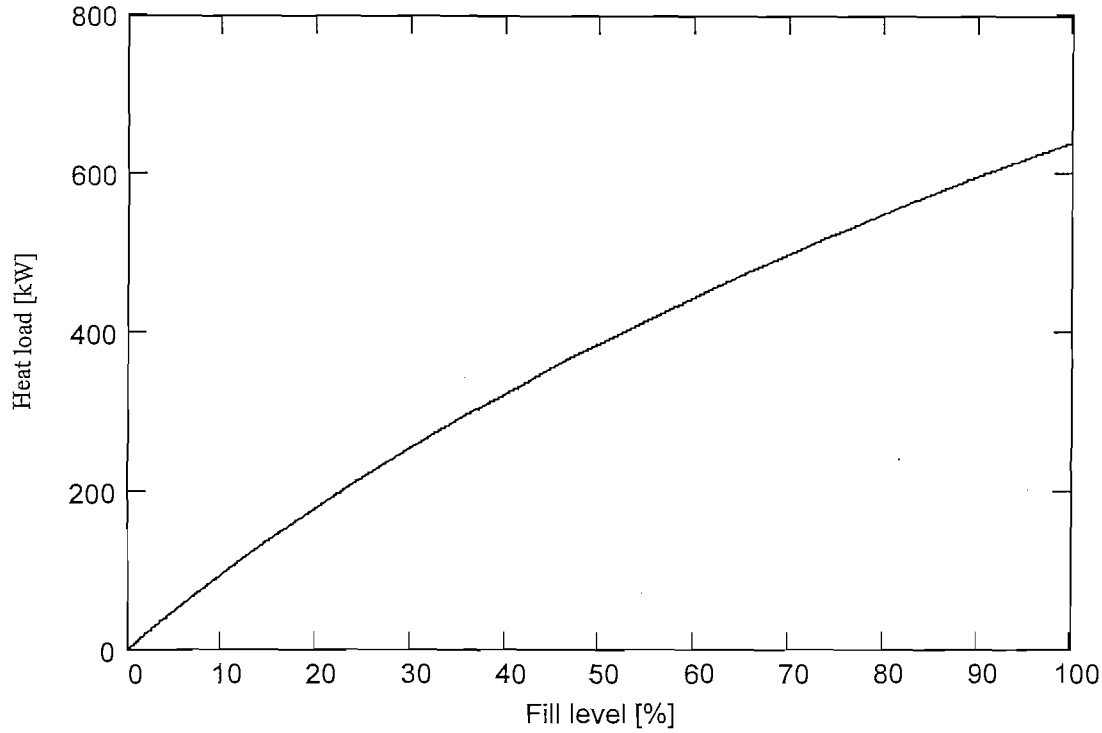
800
600
400
200
0
Heat load [kW]
0
10
20
30
40
50
60
70
80
90
100
Fill level [%]

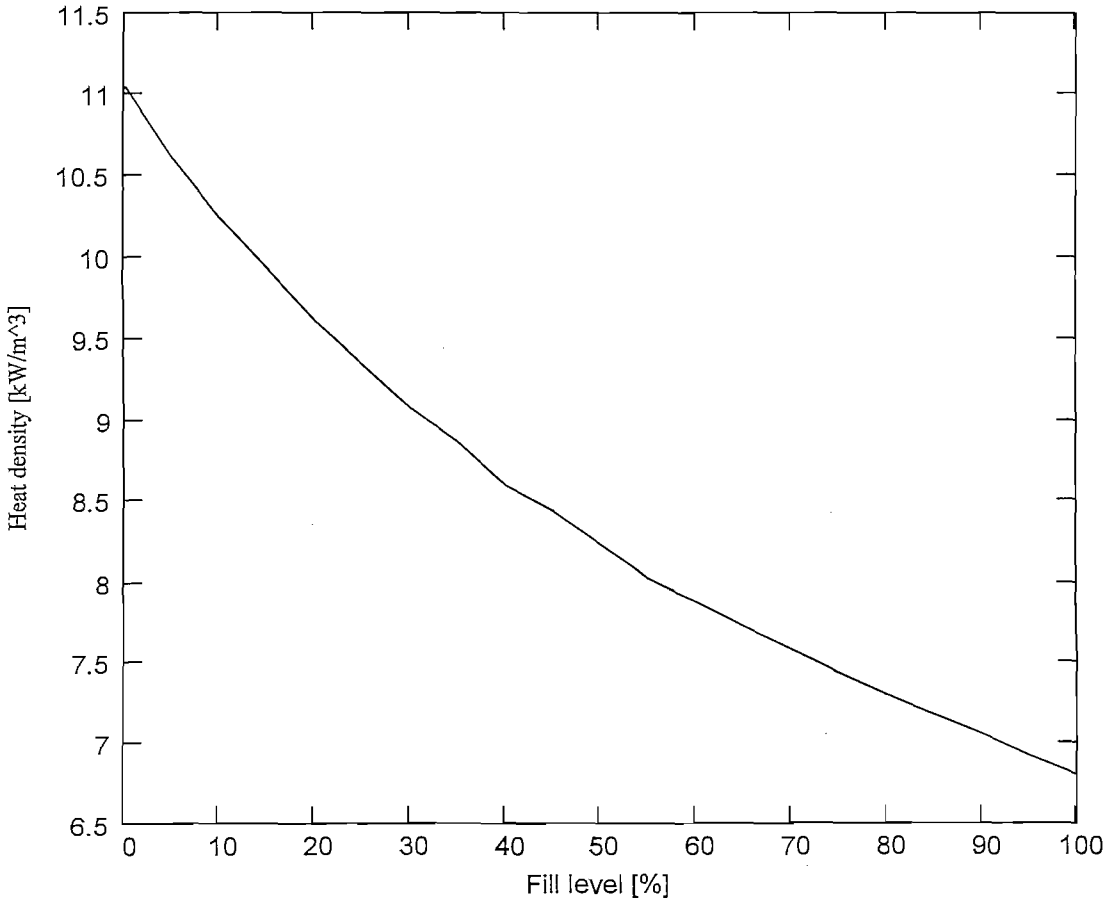
11.5
11
10.5
10
9.5
9
8.5
8
7.5
7
6.5
Heat density [kW/m^3]
0
10
20
30
40
50
60
70
80
90
100
Fill level [%]

Appendix G : Tank Convection Coefficient and Air Temperature Calculations

1. INTRODUCTION

This appendix contains the algorithm used to calculate the convection coefficients and air temperatures for use in the FEA analysis described in Chapter 9. The algorithm was written as an active worksheet in MathCAD. It also makes use of several other worksheets that define the tank geometry and heat load.

2. ANALYSIS METHODOLOGY

The analysis starts off by referencing heat load and volumetric calculations done in other documents for the Used or Spent Fuel Tank.

The fill level is first defined and then additional information not defined in the referenced documents, such as the geometry of the bottom collection tubes and thermal shield geometry. The region between the tank and shield is defined as a number of flow channels.

All calculations are based upon an inlet temperature, pressure and total cooling mass flow. These are specified by the user.

Firstly, a number of geometry calculations are performed. These are for example, tube cross section areas; actual tube lengths, based upon tank geometry; and heat transfer surfaces.

Next the mass flow distribution through the individual tubes and channels are calculated. It is assumed that the total pressure drop between the top and bottom of the tank is the same for each air inlet and outlet. Buoyancy effects are not included. The pressure drop due to flow friction and inlet losses is therefore the same for each tube / channel, as well as for the combination of centre tube and collection tubes. The sum of all the mass flows should also equal the total given mass flow. The pressures and mass flows can all be written in terms of flow velocity equations, and solved simultaneously. The equations look as follows:

$$\Delta P = \left[\left(K_{inlet} + \frac{f \cdot L}{D}\right) \cdot \frac{\rho \cdot v^2}{2}\right]_{outer}$$

$$\Delta P = \left[\left(K_{inlet} + \frac{f \cdot L}{D}\right) \cdot \frac{\rho \cdot v^2}{2}\right]_{channel}$$

$$\Delta P = \left[\left(K_{inlet} + \frac{f \cdot L}{D}\right) \cdot \frac{\rho \cdot v^2}{2}\right]_{centre} + \left[\left(K_{inlet} + \frac{f \cdot L}{D}\right) \cdot \frac{\rho \cdot v^2}{2}\right]_{collection}$$

$$(\rho \cdot A \cdot v)_{centre} = (N \cdot \rho \cdot A \cdot v)_{collection}$$

$$m'_{tot} = (N \cdot \rho \cdot A \cdot v)_{outer} + (N \cdot \rho \cdot A \cdot v)_{channel} + (\rho \cdot A \cdot v)_{centre}$$

The friction factor is calculated from D'Arcy friction factor correlations for different flow regimes. The inlet loss factors are estimated and adjusted to obtain similar flow distributions as was obtained with CFD analyses. The effect of the collection of the small tubes into one large tube is hereby incorporated.

Each tube / channel is divided into a number of small increments. The heat per section is then calculated, based upon the assumption that the heat flux through all heat transfer surfaces are the same for a given height. The heat is calculated using the following equation:

$$Q_{pipe}(z) = \frac{Q'''(z) \cdot A_{fuel} \cdot \pi \cdot D_{pipe} \cdot \Delta z_{pipe}}{Perimeter_{total}}$$

For each pipe / channel increment, the temperature, local flow velocity and convection coefficient can then be calculated. The air temperature is calculated as follows:

$$T_j = T_{j-1} + \frac{Q_j}{m' \cdot Cp}$$

The local velocity changes due to the temperature and effectively the density change, thus:

$$v_j = \frac{m'}{A \cdot \rho(T)}$$

The convection coefficient is calculated using an empirical equation. An equation that was found to best fit the results obtained from detail CFD analyses (see Appendix B) are used. The equation includes the entrance effect as well as the change in thermal properties as the air heats up.

Finally, a polynomial is fitted to the temperature and convection results. The order of the polynomial can be changed, depending upon the nature of the results. The polynomial coefficients are transferred into a text string polynomial, and exported to text files "Temperature.dat" and "Convection.dat". These text polynomials can be used as inputs for the FEA thermal analyses.

3. GEOMETRY INPUTS

Fill level : Fill :=

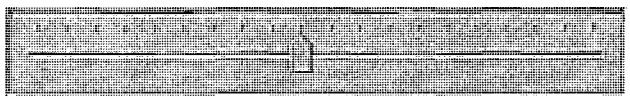

Fill = 50 %

Tank geometry

TankType = "Spent Fuel Tank"

Total number of spheres: $N_{tot} = 530000$

Tank diameter: $D_{tank} = 3.1$ m

Tank height: $H_{tank} := 18$ m

Fill level: Fill = 50 %

Fuel fill height: $H_{top} := H_{fill}(Fill, N_{tot})$ $H_{top} = 9.202$ m

Collection tube geometry

Collection tube diameter: $D_{col} := 0.273$ m

Number of collection tubes: $N_{col} := 4$

Collection tube length: $L_{col} := 0.7$ m

Collection tube height: $H_{col} := 0.6$ m

Inlet loss factor: $K_{col.i} := 0.5$ $K_{col.e} := 2$

Centre tube geometry

Centre tube diameter: $D_{cen} = 0.762$ m

Inlet loss factor: $K_{cen.i} := 0$ $K_{cen.e} := 1$

Outer tube geometry

Outer tube diameter: $D_{out} = 0.406$ m

Number of outer pipes: $N_{out} := \text{length}(d) - 1$ $N_{out} = 8$

Outer tubes PCD: $PCD = 1.8$ m

Inlet loss factor: $K_{out.i} := 0.5$ $K_{out.e} := 1$

Cooling channels of thermal shield

Thermal shield width: $w_{ch} := 0.15$ m

Number of shield channels: $N_{ch} := 27$

Channel breath: $b_{ch} := \frac{\pi \cdot D_{tank}}{N_{ch}}$ $b_{ch} = 0.361$ m

Surface roughness: $\varepsilon := 100 \cdot 10^{-6}$ m

Inlet loss factor: $K_{ch.i} := 0.1$ $K_{ch.e} := 0.5$

4. THERMAL AND COOLING INPUTS

Atmospheric pressure: $P_{atm} := 101.3 \cdot 10^{3}$ Pa

Inlet temperature: $T_{in} := 35 + 273$ K

Cooling air mass flow: $m'_{tot} := 3$ $kg \cdot s^{-1}$

Gravity: $g := 9.81$ $m \cdot s^{-2}$

Pebble bed emissivity: $\varepsilon_b := 0.88$ $\sigma := 5.67 \cdot 10^{-8}$

Outer wall emissivity: $\varepsilon_e := 0.29$

5. GEOMETRY CALCULATIONS

Centre tube length: $L_{cen} := H_{tank} - H_{col}$ $L_{cen} = 17.4$ m

Outer tubes length: $L_{out} := H_{tank} - \frac{PCD}{2} \cdot (\tan(\theta_{up}) + \tan(\theta_{low}))$ $L_{out} = 17.243$ m

Channel length: $L_{ch} := H_{tank} - \frac{D_{tank}}{2} \cdot (\tan(\theta_{up}) + \tan(\theta_{low}))$ $L_{ch} = 16.696$ m

Height of centre tube heat input end: $h_{cen} := H_{top} - \frac{D_{cen}}{2} \cdot \tan(\theta_{up})$

Height of outer tube heat input start: $h_{p1} := \frac{PCD}{2} \cdot \tan(\theta_{low})$

Height of outer pipe heat input end: $h_{p3} := H_{top} - \frac{PCD}{2} \cdot \tan(\theta_{up})$

Height of channel heat input start: $h_1 := \frac{D_{tank}}{2} \cdot \tan(\theta_{low})$

Height of channel heat input end: $h_2 := H_{top} - \frac{D_{tank}}{2} \cdot \tan(\theta_{up})$

Tube cross sections: $A_{out} := \frac{\pi \cdot D_{out}^{2}}{4}$ $A_{cen} := \frac{\pi \cdot D_{cen}^{2}}{4}$

$A_{col} := \frac{\pi \cdot D_{col}^{2}}{4}$

Channel cross section: $A_{ch} := b_{ch} \cdot w_{ch}$

Fuel cross section above collection: $A_{fuel1} := \frac{\pi \cdot D_{tank}^2}{4} - N_{out} \cdot A_{out} - A_{cen}$

Fuel cross section below collection: $A_{fuel2} := \frac{\pi \cdot D_{tank}^2}{4} - N_{out} \cdot A_{out} - N_{col} \cdot A_{col}$

Heat transfer perimeter above collection: $Ptr1 := \pi \cdot D_{tank} + N_{out} \cdot \pi \cdot D_{out} + \pi \cdot D_{cen}$

Heat transfer perimeter below collection: $Ptr2 := \pi \cdot D_{tank} + N_{out} \cdot \pi \cdot D_{out} + N_{col} \cdot \pi \cdot D_{col}$

Channel flow hydraulic diameter: $D_{ch} := \frac{2 \cdot b_{ch} \cdot w_{ch}}{b_{ch} + w_{ch}}$

6. FLOW DISTRIBUTION CALCULATIONS

Inlet air density: $\rho_{in} := \rho_{air}(T_{in}, P_{atm})$ $\rho_{in} = 1.146$

D'Arcy friction factor

Compiled from reference [96]

Laminar flow: $f_{lam}(Re) := \frac{64}{Re}$

Turbulent flow: $f_{turb}(D, Re) := \frac{0.25}{\left(\log\left(\frac{\varepsilon}{3.7 \cdot D} + \frac{5.74}{Re^{0.9}}\right)\right)^2}$

Combined:

$$friction(D, v, T) := \left| \begin{array}{l} Re \leftarrow \frac{v \cdot D}{\nu_{air}(T, P_{atm})} \\ f_{up} \leftarrow f_{turb}(D, 5000) \\ f_{low} \leftarrow f_{lam}(2300) \\ f \leftarrow \left| \begin{array}{ll} f_{lam}(Re) & \text{if } Re < 2300 \\ \left[\frac{f_{up} - f_{low}}{5000 - 2300} \cdot (Re - 2300) + f_{low}\right] & \text{if } 2300 \le Re \le 5000 \\ f_{turb}(D, Re) & \text{otherwise} \end{array} \right. \end{array} \right.$$

$friction(D_{out}, 1, 300) = 0.025$

7. ANALYSIS INCREMENTS

Analysis increments: $n := 100 \quad i := 0..n \quad j := 1..n$

Tube height increments:

$$\Delta zout := \frac{(h_{p3} - h_{p1})}{n} \qquad zout_i := h_{p1} + \Delta zout \cdot i$$

$$\Delta zcen := \frac{h_{cen} - H_{col}}{n} \qquad zcen_i := \Delta zcen \cdot i + H_{col}$$

$$\Delta zcol := \frac{H_{col}}{n} \qquad zcol_i := \frac{H_{col}}{n} \cdot i$$

Channel height increments:

$$\Delta zch := \frac{(h_2 - h_1)}{n} \qquad zch_i := h_1 + \Delta zch \cdot i$$

Minimum length ratio: $Dx_{cut} := 0.3$

8. CONVECTION COEFFICIENT EQUATION

Convection coefficient:

e.q. 26-13 from reference [65]

$$hc(v, D, T_g, x) := \left| \begin{array}{l} Re \leftarrow \dfrac{v \cdot D}{\nu_{air}(T_g, P_{atm})} \\ R \leftarrow \left| \begin{array}{ll} \dfrac{D}{x} & \text{if } x > Dx_{cut} \cdot D \\ \dfrac{1}{Dx_{cut}} & \text{otherwise} \end{array} \right. \\ \dfrac{k_{air}(T_g)}{D} \cdot 0.036 \cdot Re^{0.8} \cdot Pr_{air}(T_g)^{0.3} \cdot \left(\dfrac{\mu_{air}(T_g)}{\mu_{air}(T_{in})} \right)^{0.14} \cdot (R)^{\frac{1}{18}} \end{array} \right.$$

9. HEAT LOAD PER SECTION

$$Q_{out_i} := \frac{Q'''\left(zout_i\right)\cdot A_{fuel1}\cdot\pi\cdot D_{out}\cdot\Delta zout}{Ptr1} \qquad Q_{col_i} := \frac{Q'''\left(zcol_i\right)\cdot A_{fuel2}\cdot\pi\cdot D_{col}\cdot\Delta zcol}{Ptr2}$$

$$Q_{cen_i} := \frac{Q'''\left(zcen_i\right)\cdot A_{fuel1}\cdot\pi\cdot D_{cen}\cdot\Delta zcen}{Ptr1} \qquad Q_{ch_i} := \frac{Q'''\left(zch_i\right)\cdot A_{fuel1}\cdot b_{ch}\cdot\Delta zch}{Ptr1}$$

10. PRESSURE LOSS EQUATIONS

$\Delta P_{out}(m) :=$

$T_0 \leftarrow T_{in}$

$\rho_0 \leftarrow \rho_{air}\left(T_{in}, P_{atm}\right)$

for $i \in 1..n$

$\quad T_i \leftarrow T_{i-1} + \dfrac{Q_{out_i}}{m\cdot Cp_{air}\left(T_{i-1}\right)}$

$\quad \rho_i \leftarrow \rho_{air}\left(T_i, P_{atm}\right)$

$\quad v_i \leftarrow \dfrac{m}{\rho_i\cdot A_{out}}$

$\quad f_i \leftarrow friction\left(D_{out}, v_i, T_i\right)$

$\Delta P_{fric} \leftarrow K_{out.i}\cdot\dfrac{\rho_0}{2}\cdot\left(v_0\right)^2 + K_{out.e}\cdot\dfrac{\rho_n}{2}\cdot\left(v_n\right)^2$

$\Delta P_{fric} \leftarrow \Delta P_{fric} + \sum_{i=0}^{n-1}\left[\dfrac{f_i}{2\cdot D_{out}}\cdot\rho_i\cdot\left(v_i\right)^2\cdot\Delta zout\right]$

$\Delta P_{fric} \leftarrow \Delta P_{fric} + \dfrac{f_n}{2\cdot D_{out}}\cdot\rho_n\cdot\left(v_n\right)^2\cdot\left(L_{out} - \Delta zout\cdot n\right)$

$\Delta P_{boy} \leftarrow \sum_{i=0}^{n-1}\left[g\cdot\left(\rho_0 - \rho_i\right)\cdot\Delta zout\right]$

$\Delta P_{boy} \leftarrow \Delta P_{boy} + g\cdot\left(\rho_0 - \rho_n\right)\cdot\left(L_{out} - \Delta zout\cdot n\right)$

$\Delta P \leftarrow \Delta P_{boy} - \Delta P_{fric}$

$$
\begin{aligned}
\Delta P_{ch}(m) := \;& T_0 \leftarrow T_{in} \\
& \rho_0 \leftarrow \rho_{air}(T_{in}, P_{atm}) \\
& \text{for } i \in 1..n \\
& \quad T_i \leftarrow T_{i-1} + \frac{Q_{ch_i}}{m \cdot Cp_{air}(T_{i-1})} \\
& \quad \rho_i \leftarrow \rho_{air}(T_i, P_{atm}) \\
& \quad v_i \leftarrow \frac{m}{\rho_i \cdot A_{ch}} \\
& \quad f_i \leftarrow \text{friction}(D_{ch}, v_i, T_i) \\
& \Delta P_{fric} \leftarrow K_{ch.i} \cdot \frac{\rho_0}{2} \cdot (v_0)^2 + K_{ch.e} \cdot \frac{\rho_n}{2} \cdot (v_n)^2 \\
& \Delta P_{fric} \leftarrow \Delta P_{fric} + \sum_{i=0}^{n-1} \left[\frac{f_i}{2 \cdot D_{ch}} \cdot \rho_i \cdot (v_i)^2 \cdot \Delta zch \right] \\
& \Delta P_{fric} \leftarrow \Delta P_{fric} + \frac{f_n}{2 \cdot D_{ch}} \cdot \rho_n \cdot (v_n)^2 \cdot (L_{ch} - \Delta zch \cdot n) \\
& \Delta P_{boy} \leftarrow \sum_{i=0}^{n-1} \left[g \cdot (\rho_0 - \rho_i) \cdot \Delta zch \right] \\
& \Delta P_{boy} \leftarrow \Delta P_{boy} + g \cdot (\rho_0 - \rho_n) \cdot (L_{ch} - \Delta zch \cdot n) \\
& \Delta P \leftarrow \Delta P_{boy} - \Delta P_{fric}
\end{aligned}
$$

$$\Delta P_{cen}(m) := \left| \begin{array}{l} Qcol \leftarrow \sum_{i=1}^{n} Q_{col_i} \cdot N_{col} \\ T_0 \leftarrow T_{in} + \frac{Qcol}{(m \cdot Cp_{air}(T_{in}))} \\ \rho_0 \leftarrow \rho_{air}(T_{in}, P_{atm}) \\ \text{for } i \in 1..n \\ \quad \left| \begin{array}{l} T_i \leftarrow T_{i-1} + \frac{Q_{cen_i}}{m \cdot Cp_{air}(T_{i-1})} \\ \rho_i \leftarrow \rho_{air}(T_i, P_{atm}) \\ v_i \leftarrow \frac{m}{\rho_i \cdot A_{cen}} \\ f_i \leftarrow friction(D_{cen}, v_i, T_i) \end{array} \right. \\ \Delta P_{fric} \leftarrow K_{cen.i} \cdot \frac{\rho_0}{2} \cdot (v_0)^2 + K_{cen.e} \cdot \frac{\rho_n}{2} \cdot (v_n)^2 \\ \Delta P_{fric} \leftarrow \Delta P_{fric} + \sum_{i=0}^{n-1} \left[\frac{f_i}{2 \cdot D_{cen}} \cdot \rho_i \cdot (v_i)^2 \cdot \Delta zcen \right] \\ \Delta P_{fric} \leftarrow \Delta P_{fric} + \frac{f_n}{2 \cdot D_{cen}} \cdot \rho_n \cdot (v_n)^2 \cdot (L_{cen} - \Delta zcen \cdot n) \\ \Delta P_{boy} \leftarrow \sum_{i=0}^{n-1} [g \cdot (\rho_0 - \rho_i) \cdot \Delta zcen] \\ \Delta P_{boy} \leftarrow \Delta P_{boy} + g \cdot (\rho_0 - \rho_n) \cdot (L_{cen} - \Delta zcen \cdot n) \\ \Delta P \leftarrow \Delta P_{boy} - \Delta P_{fric} \end{array} \right.$$

$$\Delta P_{col}(m) := \left| \begin{array}{l} T_0 \leftarrow T_{in} \\ \rho 0 \leftarrow \rho air(T_{in}, P_{atm}) \\ \text{for } i \in 1..n \\ \quad \left| \begin{array}{l} T_i \leftarrow T_{i-1} + \dfrac{Q_{col_i}}{m \cdot Cp_{air}(T_{i-1})} \\ \rho i \leftarrow \rho air(T_i, P_{atm}) \\ v_i \leftarrow \dfrac{m}{\rho i \cdot A_{col}} \\ f_i \leftarrow friction(D_{col}, v_i, T_i) \end{array} \right. \\ \Delta P_{fric} \leftarrow K_{col.i} \cdot \dfrac{\rho 0}{2} \cdot (v_0)^2 + K_{col.e} \cdot \dfrac{\rho n}{2} \cdot (v_n)^2 \\ \Delta P_{fric} \leftarrow \Delta P_{fric} + \sum_{i=0}^{n-1} \left[\dfrac{f_i}{2 \cdot D_{col}} \cdot \rho i \cdot (v_i)^2 \cdot \Delta zcol \right] \\ \Delta P_{boy} \leftarrow \sum_{i=0}^{n-1} \left[g \cdot (\rho 0 - \rho i) \cdot \Delta zcol \right] \\ \Delta P \leftarrow \Delta P_{boy} - \Delta P_{fric} \end{array} \right.$$

11. SOLVE MASS FLOWS

Initial guess : $m'_{out} := \frac{m'_{tot}}{N_{ch} + N_{out} + 1}$ $m'_{out} = 0.083$

$m'_{cen} := m'_{out}$ $m'_{cen} = 0.083$

$m'_{col} := \frac{m'_{cen}}{N_{col}}$ $m'_{col} = 0.021$

$m'_{ch} := m'_{out}$ $m'_{ch} = 0.083$

$\Delta P := 10$

Given

$m'_{tot} = m'_{out} \cdot N_{out} + m'_{cen} + m'_{ch} \cdot N_{ch}$

$m'_{cen} = m'_{col} \cdot N_{col}$

$\Delta P = \Delta P_{out}(m'_{out})$

$\Delta P = \Delta P_{ch}(m'_{ch})$

$\Delta P = \Delta P_{cen}(m'_{cen}) + \Delta P_{col}(m'_{col})$

Solve for mass flows:

$$\begin{pmatrix} m'_{out} \\ m'_{cen} \\ m'_{col} \\ m'_{ch} \\ \Delta P \end{pmatrix} := \text{Find}(m'_{out}, m'_{cen}, m'_{col}, m'_{ch}, \Delta P)$$

$$\begin{pmatrix} m'_{out} \\ m'_{cen} \\ m'_{col} \\ m'_{ch} \\ \Delta P \end{pmatrix} = \begin{pmatrix} 0.175 \\ 0.363 \\ 0.091 \\ 0.046 \\ 11.624 \end{pmatrix}$$

Check: $m'_{out} \cdot N_{out} + m'_{cen} + m'_{ch} \cdot N_{ch} = 3$ $m'_{tot} = 3$

Inlet flow velocities:

$v_{out} := \frac{m'_{out}}{A_{out} \cdot \rho_{in}}$ $v_{out} = 1.183$

$v_{cen} := \frac{m'_{cen}}{A_{cen} \cdot \rho_{in}}$ $v_{cen} = 0.694$

$v_{ch} := \frac{m'_{ch}}{A_{ch} \cdot \rho_{in}}$ $v_{ch} = 0.737$

12. LOCAL TEMPERATURE AND CONVECTION

Outer tube conditions:

$Tgout_0 := T_{in}$

$Tgout_j := Tgout_{j-1} + \frac{Q_{out_j}}{m'_{out} \cdot Cp_{air}(T_{in})}$ $\quad Tgout_n - 273 = 69.175$

$vout_i := \frac{m'_{out}}{A_{out} \cdot \rho_{air}(Tgout_i, P_{atm})}$

$hout_i := hc(vout_i, D_{out}, Tgout_i, \Delta zout \cdot i)$ $\quad hout_1 = 8.567$

$hout_n = 7.022$

Collection tubes:

$Tgcol_0 := T_{in}$

$Tgcol_j := Tgcol_{j-1} + \frac{Q_{col_j}}{m'_{col} \cdot Cp_{air}(T_{in})}$ $\quad Tgcol_n - 273 = 36.565$

$vcol_i := \frac{m'_{col}}{A_{col} \cdot \rho_{air}(Tgcol_i, P_{atm})}$

$hcol_i := hc(vcol_i, D_{col}, Tgcol_i, \Delta zcol \cdot i)$ $\quad hcol_1 = 10.324$

$hcol_n = 9.259$

Centre tube conditions:

$Tgcen_0 := Tgcol_n$

$Tgcen_j := Tgcen_{j-1} + \frac{Q_{cen_j}}{m'_{cen} \cdot Cp_{air}(T_{in})}$ $\quad Tgcen_n - 273 = 70.433$

$vcen_i := \frac{m'_{cen}}{A_{cen} \cdot \rho_{air}(Tgcen_i, P_{atm})}$

Turbulence adjustment factor : $\quad tx := 1.0$

$hcen_i := hc(vcen_i, D_{cen}, Tgcen_i, \Delta zcen \cdot i) \cdot tx$ $\quad hcen_1 = 4.942$

$hcen_n = 4.195$

Channel conditions:

$$Tgch_0 := T_{in}$$

$$Tgch_j := Tgch_{j-1} + \frac{Q_{ch_j}}{m'_{ch} \cdot Cp_{air}(T_{in})} \qquad Tgch_n - 273 = 67.192$$

$$vch_i := \frac{m'_{ch}}{A_{ch} \cdot \rho_{air}(Tgch_i, P_{atm})}$$

$$hch_i := hc(vch_i, D_{ch}, Tgch_i, \Delta zch \cdot i) \qquad hch_1 = 6.606$$

$$hch_n = 5.295$$

Mixed air exit temperature:

$$Q_{tot} := Q_{total}(Fill) \qquad Q_{tot} = 100.912 \text{ kW}$$

$$T_{out} := T_{in} + \frac{Q_{tot}}{m'_{tot} \cdot Cp_{air}(T_{in})} \qquad T_{out} - 273 = 68 \quad °C$$

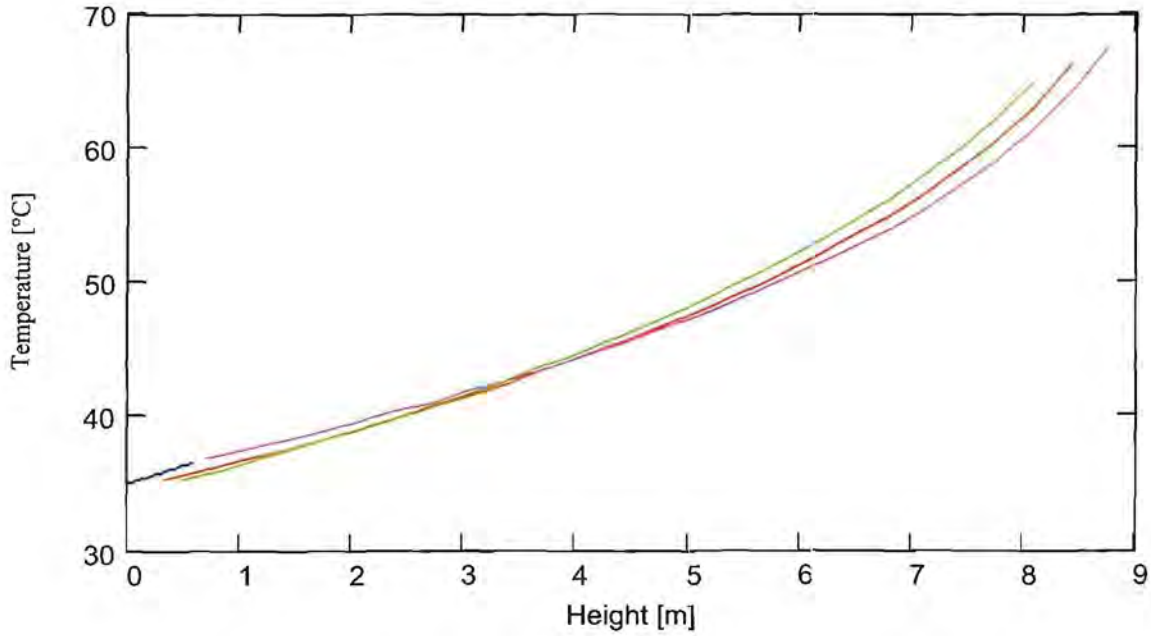
Temperature [°C]
70
60
50
40
30
0
1
2
3
4
5
6
7
8
9
Height [m]

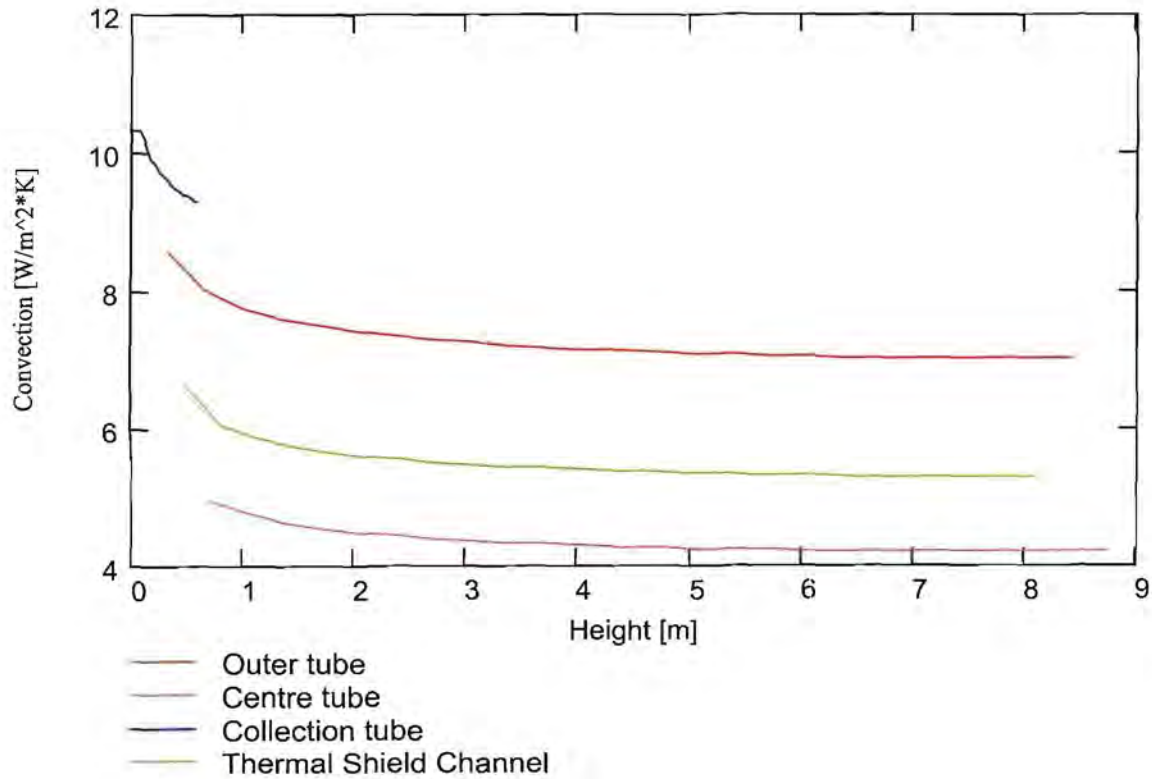
Convection [W/m^2*K]
12
10
8
6
4
0
1
2
3
4
5
6
7
8
9
Height [m]
Outer tube
Centre tube
Collection tube
Thermal Shield Channel

13. POLYNOMIAL APPROXIMATION

Centre tube

Convection:

PolyOrderC := 9

C := submatrix(regress(zout, hout, PolyOrderC), 3, PolyOrderC + 3, 0, 0)

Polynomial curve fit: $hf(z) := \sum_{k=0}^{PolyOrderC} \left(C_k \cdot z^k \right)$

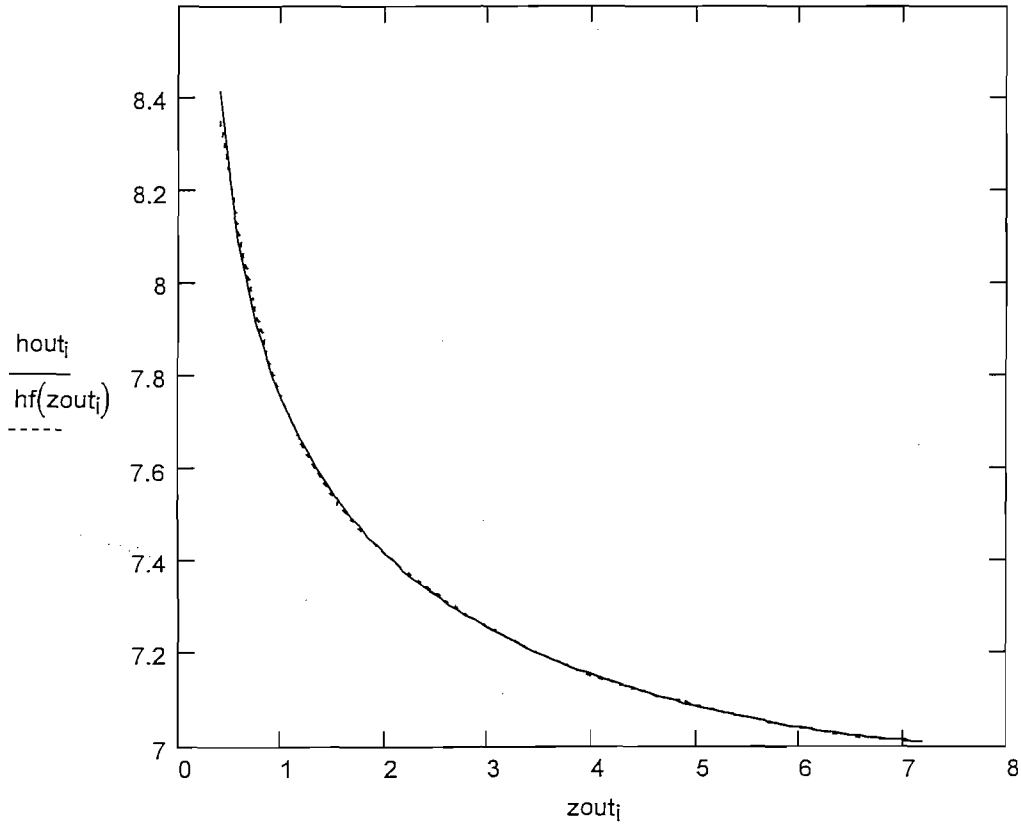

Temperature:

PolyOrderT := 7

C := submatrix(regress(zcen, Tgcen, PolyOrderT), 3, PolyOrderT + 3, 0, 0)

Polynomial curve fit: $Tf(z) := \sum_{k=0}^{PolyOrderT} \left(C_k \cdot z^k \right)$

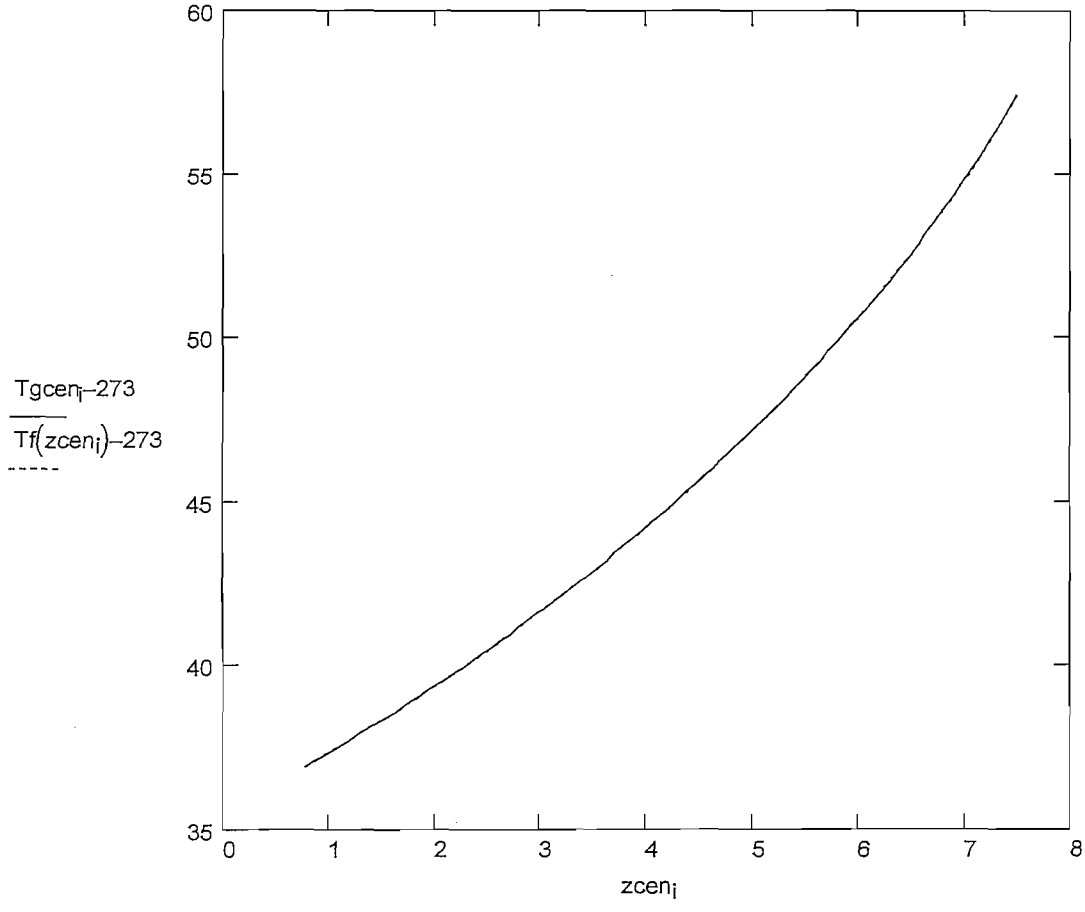

14. SAVE RESULTS IN TEXT FILE

All convection coefficients polynomial fit

$$Convect := \begin{pmatrix} \text{"Outer tube"} \\ FitPoly(zout, hout, PolyOrderC) \\ \text{"Center tube"} \\ FitPoly(zcen, hcen, PolyOrderC) \\ \text{"Collection tube"} \\ FitPoly(zcol, hcol, PolyOrderC) \\ \text{"Channel"} \\ FitPoly(zch, hch, PolyOrderC) \end{pmatrix}$$

Convec

Convect

All temperatures polynomial fit

$$Temperature := \begin{pmatrix} \text{"Outer tube"} \\ FitPoly(zout, Tgout - 273, PolyOrderT) \\ \text{"Center tube"} \\ FitPoly(zcen, Tgcen - 273, PolyOrderT) \\ \text{"Collection tube"} \\ FitPoly(zcol, Tgcol - 273, PolyOrderT) \\ \text{"Channel"} \\ FitPoly(zch, Tgch - 273, PolyOrderT) \end{pmatrix}$$

Temper

Temperature

Heat load polynomial fit

Heat.da

HeatPoly

Sample of the output files

Heat.dat

```
+591.104491702713*z^0 +-204.050960491474*z^1 +365.126083785151*z^2 +-226.035604196537*z^3
+72.2475389493915*z^4 +-13.0520933590069*z^5 +1.38422310162111*z^6 +-0.0851335456607556*z^7
+0.00280036981298612*z^8+-3.79192178246695e-05*z^9
```

Convect.dat

Outer tube

```
+9.63635999465454*z^0 +-2.56997312423525*z^1 +1.59908149069182*z^2 +-0.584262121263745*z^3
+0.129609591169634*z^4 +-0.0179730859429095*z^5 +0.00156463884982868*z^6 +-8.29803432131425e-05*z^7
+2.44800322136792e-06*z^8 +-3.07763912828551e-08*z^9
```

Center tube

```
+5.27817884173493*z^0 +-1.0207016862356*z^1 +0.416441297904125*z^2 +-0.100263987260555*z^3
+0.0145797661765536*z^4 +-0.00128133506796282*z^5 +6.47544365046289e-05*z^6 +-1.56751773021035e-06*z^7
+3.49576047119168e-09*z^8 +3.8579337160736e-10*z^9
```

Collection tube

```
+11.5009749362155*z^0 +-0.40333779335872*z^1 +105.928541255949*z^2 +-2892.24539846247*z^3
+26652.3641661192*z^4 +-126532.532968402*z^5 +344811.404800498*z^6 +-545168.866852041*z^7
+465575.777785852*z^8 +-166266.205218847*z^9
```

Channel

```
+7.67569185331125*z^0 +-3.14036748481B1*z^1 +2.1284151664555*z^2 +-0.815953579344325*z^3
+0.187650151943647*z^4 +-0.0268477028492147*z^5 +0.0024059942183942*z^6 +-0.000131208206697654*z^7
+3.97791866803835e-06*z^8 +-5.13825890718745e-08*z^9
```

Temperature.dat

Outer tube

```
+39.4988327427991*z^0 +1.86943245606121*z^1 +-0.533163426749508*z^2 +0.216003778882049*z^3
+-0.0402428461982092*z^4 +0.00400471542758676*z^5 +-0.000200973836439524*z^6 +4.03285218209713e-06*z^7
```

Center tube

```
+39.5990947669285*z^0 +2.586145420203O6*z^1 +-0.984855613794686*z^2 +0.345352395938023*z^3
+-0.0599950519585101*z^4 +0.00564890568048161*z^5 +-0.000271335632985243*z^6 +5.242242754837B4e-06*z^7
```

Collection tube

```
+39.9999986652211*z^0 +1.59158639613668*z^1 +-0.0026378684719681*z^2 +0.070077184791045*z^3
+-0.110667471954958*z^4 +0.0703434742340527*z^5 +0.121776556560379*z^6 +-0.137962219701926*z^7
```

Channel

```
+39.3690651841203*z^0 +1.55558844581022*z^1 +-0.339059387655736*z^2 +0.136944293134084*z^3
+-0.0250303045025305*z^4 +0.00248515110528734*z^5 +-0.000125410029057989*z^6 +2.55129437095522e-06*z^7
```

Appendix H : FHSS Process Flow Diagram

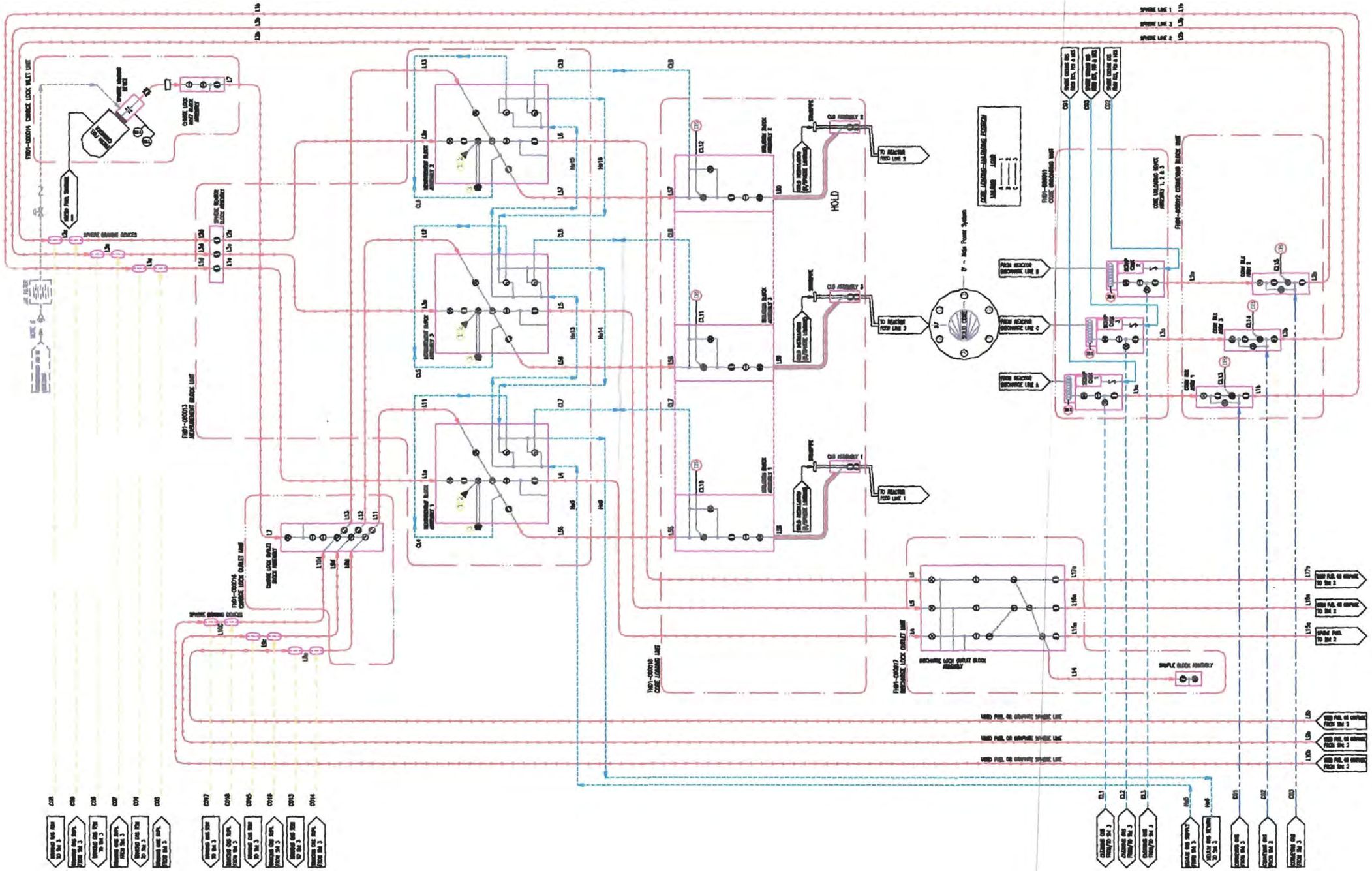

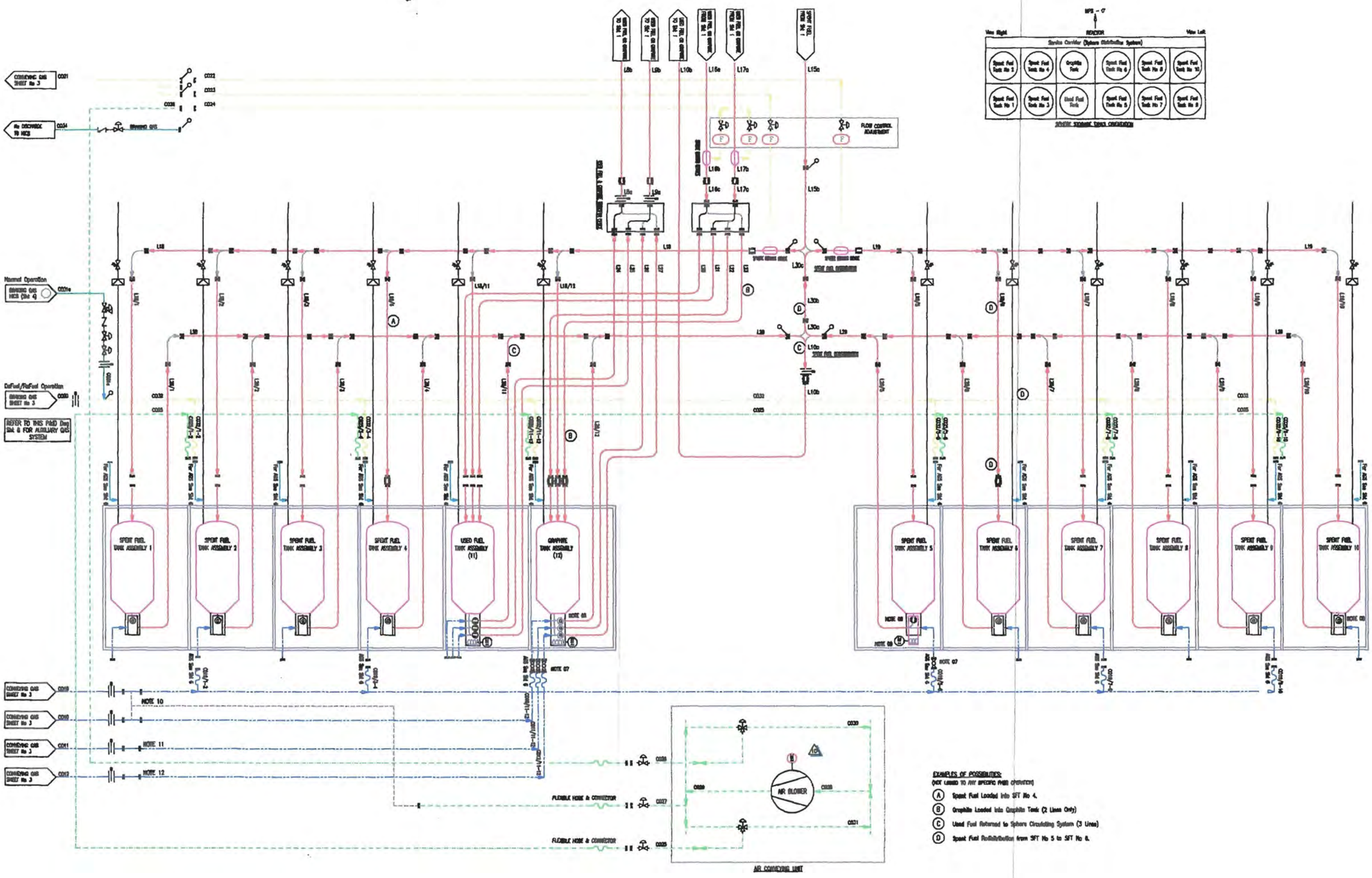
Normal Operation
DeFuel/ReFuel Operation
REFER TO THIS P&ID Dwg
No. 6 FOR AUXILIARY GAS
SYSTEM
SPENT FUEL TANK ASSEMBLY 1
SPENT FUEL TANK ASSEMBLY 2
SPENT FUEL TANK ASSEMBLY 3
SPENT FUEL TANK ASSEMBLY 4
USED FUEL TANK ASSEMBLY (#1)
GRAPHITE TANK ASSEMBLY (#2)
SPENT FUEL TANK ASSEMBLY 5
SPENT FUEL TANK ASSEMBLY 6
SPENT FUEL TANK ASSEMBLY 7
SPENT FUEL TANK ASSEMBLY 8
SPENT FUEL TANK ASSEMBLY 9
SPENT FUEL TANK ASSEMBLY 10
FLOW CONTROL ADJUSTMENT
NOTE 10
NOTE 11
NOTE 12
NOTE 07
NOTE 08
FLEXIBLE HOSE & CONNECTOR
FLEXIBLE HOSE & CONNECTOR
AIR BLOWER
AIR CONVEYING UNIT
EXAMPLES OF POSSIBILITIES:
(NOT LIMITED TO ANY SPECIFIC FHSS OPERATION)
(A) Spent Fuel Loaded into SFT No 4.
(B) Graphite Loaded into Graphite Tank (2 Lines Only)
(C) Used Fuel Returned to Sphere Circulating System (3 Lines)
(D) Spent Fuel Redistribution from SFT No 5 to SFT No 6.